with retarded mining trainees who fell within prescribed chronological ages and IQ range.

Here again in the 'Rate of Learning' study with the mini entrants, the results significantly disproved the 'null hypothesis', but in the remainder of the research studie significant results were established. Possibilities of work in these areaswere opened up, however.

Concurrent with this part of the enquiry, using the libr the University of Sheffield, research was made into rele studies made elsewhere and these are critically discusse the text of the thesis.

In conclusior, the enquiry did establish that regular employment of programmed material accelerated the rate o learning to read of ESN pupils beyond that which can be expected from their mental ages. Nevertheless, and in s the large amount of literature surveyed in this study, m more research is indicated to establish which variables, combination of variables, are the most potent factors in material and method employed.

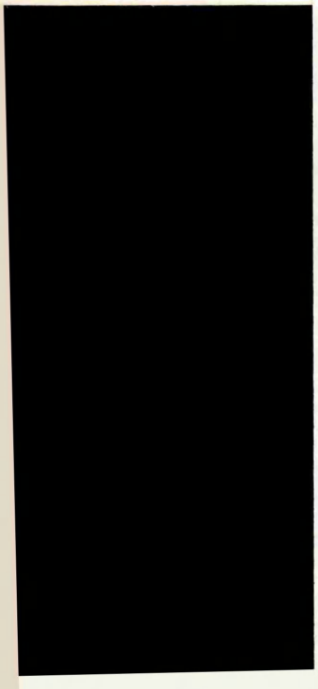

Fatigue Properties of Dissimilar Metal Laser Welded Lap Joints

Christopher Paul Dinsley

A thesis submitted in partial fulfilment of the requirements of

Sheffield Hallam University

for the degree of Doctor of Philosophy

November 2004

Collaborating Organisation

Outokumpu Stainless Research Foundation

Abstract

This thesis describes work conducted at the Materials Research Institute at Sheffield Hallam University from August 2000 to August 2003.
The work involves laser welding austenitic and duplex stainless steel to zinc-coated mild steel, more specifically 1.2mm V1437, which is a Volvo Truck Corporation rephosphorised mild steel. The work investigates both tensile and lap shear properties of similar and dissimilar metal laser welded butt and lap joints, with the majority of the investigation concentrating on the fatigue properties of dissimilar metal laser welded lap joints. The problems encountered when laser welding zinc-coated steel are addressed and overcome with regard to dissimilar metal lap joints with stainless steel. The result being the production of a set of guidelines for laser welding stainless steel to zinc-coated mild steel. The stages of laser welded lap joint fatigue life are defined and the factors affecting dissimilar metal laser welded lap joint fatigue properties are analysed and determined; the findings suggesting that dissimilar metal lap joint fatigue properties are primarily controlled by the local stress at the internal lap face and the early crack growth rate of the material at the internal lap face. The lap joint rotation, in turn, is controlled by sheet thickness, weld width and interfacial gap. Laser welded lap joint fatigue properties are found to be independent of base material properties, allowing dissimilar metal lap joints to be produced without fatigue failure occurring preferentially in the weaker parent material, irrespective of large base material property differences. The effects of Marangoni flow on the compositions of the laser weld beads are experimentally characterised. The results providing definite proof of the stirring mechanism within the weld pool through the use of speeds maps for chromium and nickel.

Keywords: Laser welding, dissimilar metal, Zinc-coated mild steel, Austenitic stainless steel, Duplex stainless steel, Fatigue, Lap joint rotation, Automotive.

Acknowledgements

The author would like to thank the Welsh Technology Centre (Port Talbot) for the use of the Trumpf 5kW CO_2 industrial laser welder and Coventry University for the use of the Rofin 2kW CO_2 industrial laser welder, which allowed the course of research to proceed on schedule.

The author would like thank the technical staff at Sheffield Hallam University, Materials Research Institute for fabrication and analytical support throughout the course of research; also the research staff at the Avesta Research Centre for the use of numerous fatigue testing machines.

The author would like to thank Rebecca Milsom for both support and guidance during the start of the authors' academic career and the authors' family and friends for their continual support during the course of research.

Special thanks to my partner Jackie Green, and both Professor Hans Nordberg and Dr Alan Smith for their personal support, guidance and patience during the course of research.

Advanced Studies

The following section contains the list of advanced studies undertaken in connection with the course of research.

Publications/Posters

- Laser Welding Of Austenitic and Duplex Stainless Steel to Zinc Coated Mils Steel, Poster Presentation, IOMMM Materials Congress 2002, London

Presentations

- AvestaPolarit Research Foundation Annual Presentation, Avesta, Sweden (2001/02)
- AvestaPolarit Research Foundation Annual Presentation, Sheffield, UK (2001/02)

Conferences

- Attendance at BSSA Stainless Steel Conference, NMC Birmingham
- Attendance at SMEA Lectures, Sheffield

Training

- Institute of Materials Project Management and Presentation Skills Workshop, IOMMM London
- Internal Scanning Electron Microscopy training, MRI
- Internal Finite Element Modelling Short Course, SHU

Secondments

- Seven week research secondment to AvestaPolarit R&D, Sweden 2001
- Seven week research secondment to AvestaPolarit R&D, Sweden 2002

Table of Contents

Table of Figures

Table of Graphs

Table of Images

Tables

1 Introduction

The automotive industry is one of the most competitive industries in the world. Continuous research is being carried out by automotive material suppliers and manufacturers to develop existing materials and integrate new materials into automotive design. This research has included extensive evaluation of the use of lightweight structures, aluminium alloys, and the integration of plastics and composite materials into vehicle body assembly[1].

The driving force for the development and integration of new materials, apart from the competitive nature of the automotive industry, is the implementation of new legislation. More specifically, in July 1998 the European Association of Car Makers agreed to gradually reduce the emissions rate from new vehicles sold in Europe by its members, the aim being to reduce CO_2 emissions to 140g/km by 2008 and to develop and market vehicles emitting only 120 g of CO_2 per km by the same date[2].

Areas identified to allow the reduction of CO_2 emissions were:

1. New engine technologies to reduce fuel consumption
2. Friction and aerodynamic resistance are to be reduced
3. Vehicle weight to be reduced

Calculations made by PSA Peugeot Citroen revealed that the CO_2 emission reduction brought about by new engine technologies, friction and aerodynamic reduction would not be enough; therefore, car weight reduction, including "body in white" lightening must be intensified[2].

---

[1] Powell, H.J. Wiemer, K. Joining Technology for High Volume Manufacturing of Lightweight Vehicle Structures, Part 1: Joining Technology Implications for Lightweight Vehicles, TWI, Cambridge, UK, June 96

[2] Lozach, G. The Future of Galvanised Steel Sheets as a Material for the Automotive Body in White, Galvanised Steel Sheet Forum-Automotive, 15-16 May 2000, The Institute of Materials, London, UK

Current trends in automotive manufacture are to utilise high strength steels, which allow weight reductions whilst maintaining component strength and rigidity. Hence, the steels that are currently used in automotive manufacture are:

1. HSLA or micro-alloyed steels
2. Rephosphorised steels
3. Bake hardening steels
4. Dual phase steels
5. Trip steels
6. High strength Interstitial Free (IF) steels

The major disadvantage of these steels is their corrosion resistance, however, steel can be protected in a number of ways to improve the corrosion properties, e.g. painting, galvanising, coating with PVC or concrete, or, for wet applications, cathodic protection. However, these all add an additional cost to that of the basic steel production figure. In the case of automotive steel grades, coating the steel with zinc is the preferred and most widely used method. Mild steel can be hot dip galvanised or electro-galvanised to achieve the requisite corrosion resistance. The main difference between these two methods is the thickness of the deposited coating. Hot dip galvanising provides a thicker coating and consequently better corrosion resistance; thus, it is the most widely used.

One material that has seemingly been overlooked for potential integration into lightweight automobile construction is stainless steel. This is, more than likely, due to the higher cost of stainless steel compared to high strength steel on a weight basis.

It has been estimated that the integration of austenitic and duplex stainless steel into 'lightweight' automobile construction could achieve a weight saving of up to 40% when compared to carbon steel[3]. This is primarily through the elimination of corrosion allowances; but also by utilising the superior mechanical properties of stainless steel (especially duplex stainless steel), thinner gauges may be used.

The ability to join dissimilar metals allows further development of many existing products and components and allows specific material properties to be exploited.

It is often too expensive to design and build prototypes solely for the purpose of testing a new materials' suitability for a particular application. Therefore, the most common route is to introduce a material into specific areas of the existing design.

The welding process most commonly used in large-scale automotive production is resistance spot welding (RSW). This welding process has been used successfully to join many different materials including some dissimilar metal joints[4]. The disadvantage of the RSW process is its inherent inflexibility in adapting to new vehicle program changes without significant modifications to the equipment, for example a program change may result in the RSW equipment having to be moved to a new jig position to allow successful completion of the welding sequence. Recent trends toward economically fabricating vehicle structures whilst ensuring quality have led to the implementation of lasers in the automobile industry[5],[6],[7], which can be incorporated in the production line as a substitute for the conventional resistance spot welding process.

---

[3] Northart, J. F. Utility Chromium Stainless Steels in the Transportation Industry, Corrosion, 98

[4] Marples, M. Investigation into the Resistance Spot Welding of Stainless Steel to Coated Ferritic Steel, Mphil/PhD Transfer Report, Materials Research Institute, Sheffield Hallam University, 2001

[5] Heston, T. Remote Laser Beam Welding shows Potential in the Body Shop, Welding Journal, June 2000

[6] Irving, B. Lasers continue to Penetrate Automotive Production Lines, Welding Journal, June 2000

[7] Yang, Y.S. Lee, S.H. A Study on the Joining Strength of Laser Spot Welding for Automotive Applications, Journal of Materials Processing Technology 94 (1999), pp 151-156

The use of lasers in the automotive industry has seen a dramatic increase in recent years to a position where approximately 15% of all industrial processing lasers are installed in automotive production[8]. Although most of these lasers are devoted to cutting applications, a significant and increasing proportion of lasers are being applied to welding. Surveys conducted in 1992 by Rossler, D. et al reported about 20% of the lasers installed in the automotive industry were used in welding applications[9].

Since the survey was conducted, the automotive industry has seen a significant growth in laser welding applications, particularly involving steel manufacturers, for tailored blank manufacture and in body-in-white welding applications. Today, this technology is widespread through the automotive industries of America and Europe[9]. Figure 1 shows a 5kW CO_2 industrial laser welder from the Welsh Technology Centre, Port Talbot.

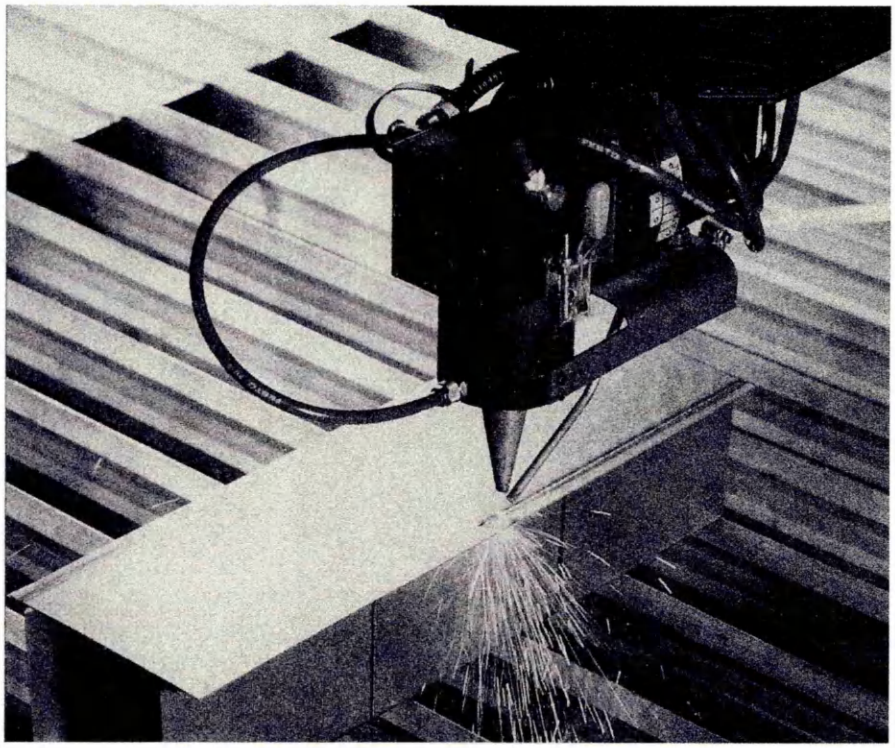

Figure 1 Welsh Technology Centre Trumpf 5kW CO_2 Laser Welder

[8] Riches, S. T. Lasers in the Automotive Industry, Make It With Lasers Workshop, Nissan Motor Manufacturing (UK), 22 October 1998

[9] Roessler D. Laser Materials Processing in General Motors Corporation, Proc ISATA 92, June 1992, pp37-51

Laser welders are currently used in the production lines of General Motors, BMW and Volvo to name but a few. The current BMW 5-series contains approximately eleven metres of laser weld on each car body[10].

Laser welding tailored blanks allow manufacturers to provide the material properties in the areas where they will be used to their best effect, where material utilisation is maximised or where the total number of build operations are minimised – whichever is chosen.

Owing to the high formability levels of laser welds, the desired combinations of steel strength, thickness and/or coating type can be laser welded together as flat sheets and then pressed into the required panel shape. The rear inner door panel shown in Figure 2 contains three different steels. The lower part of the door contains an area of hot-dip galvanised steel, which protects against corrosion in the most vulnerable spot. The right hand side contains an area of high strength, un-coated steel, which replaces many of the reinforcement parts that are currently welded-on after pressing. This steel also provides the necessary strength for the door hinges and door mirrors. The rest of the door is made from iron-zinc coated steel.

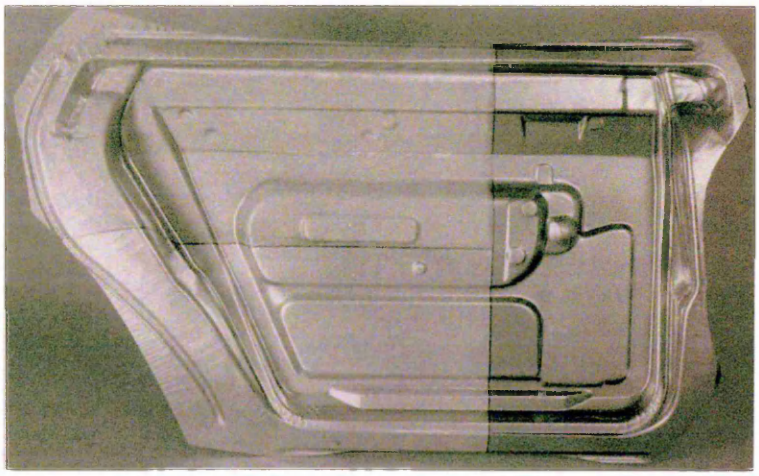

Figure 2 Picture showing an inner door panel that is made up of three different steels that have been laser welded together[11]

[10] Larsson, J.K. Automotive Laser World – The Use of Lasers in Car Body Manufacturing. Proceedings of the 6th Nordic Laser Materials Processing Conference, NOLAMP 6. Aug. 27-29, 1997, Lulea, Sweden. pp 76-94

Another current laser welded application is the use of composite blanks for chassis members, for example structural areas within the body shell that are conventionally made from single thickness steel and strengthened in critical areas by welding on stiffening assemblies after the forming operations. By laser welding together areas of thicker or higher strength steels with thinner gauge steels, a lighter structure (with the higher strength areas only where required) can be produced in one pressing operation. This negates additional stamping and forming to make the reinforcement parts and the resistance welding together of the various parts.

The formability of laser welds is the key to the success or failure of a part. Due to the small HAZ, the welds are extremely formable, as long as joint quality is good and in cupping tests generally give between 80 and 100% of the fracture height of the base material.[11]

There still remain, however, a number of areas that have yet to be examined in-order to improve the confidence of automotive manufacturers in the exploitation of these joining technologies and for the integration of new materials in lightweight automotive design, these include:

- Weldability of dissimilar material combinations
  (zinc-coated mild steel/stainless steel)
- Performance knowledge for structural and non structural components (including long term prediction)
- Modelling of fatigue performance and fatigue life prediction for dissimilar metal, dissimilar thickness joints

[11] Lalley, M. Laser welding provides tailored properties, Welsh Technology Centre, Materials world, Nov 1994, no. 11, vol. 2, Page 576.

2 *Literature Review*

2.1 Solid State and Gas Lasers

There are four types of laser that prevail in metalworking. These are:

1. Gas laser, the so-called CO_2 (mixture of CO_2, N_2 and He is used)
2. Ruby laser
3. Solid state laser, the neodymium-doped yttrium-aluminium-garnet (Nd:YAG) or simply YAG laser
4. Neodymium-doped glass (Nd Glass) or simply glass laser

It should be noted that approximately 90% of metalworking is done using (1) and (3)[12], these being the two main types of laser, the gas laser and the solid-state laser.

The solid state laser, in this case, Neodymium-doped Yttrium-aluminium-garnet (Nd:YAG), does not encompass semiconductor devices. The neodymium atoms, which when held in a suitable host, can be excited by light from an external source, to produce laser action. Continuous arc lamps, pulsed flashlamps and more recently diode lasers are used commercially (a typical schematic diagram can be seen in Figure 3). Thus, solid-state lasers can generate continuous beams of a few milli-watts to several kW, short pulses with peak powers in the giga-watt range, or pulsed beams with average powers in the kW range. The wavelength of the Nd:YAG laser is 1.06μm.

[12] Ghosh, S. K. & Ericsson, T. Laser welding, IITT International, ISBN 2-907-669-04-4

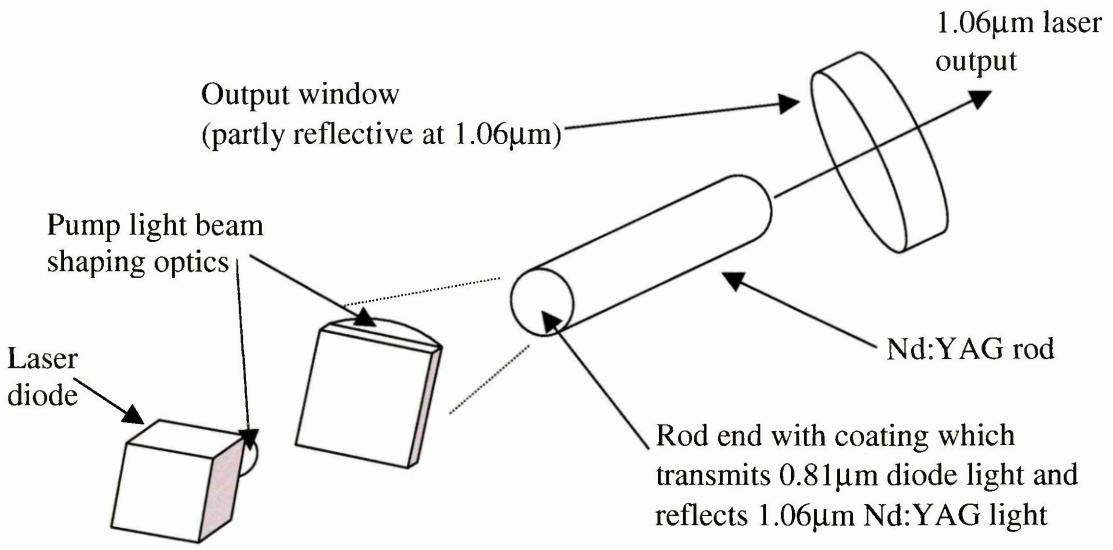

Figure 3 Schematic diagram showing a typical diode (end) pumped Nd:YAG laser set up

The carbon dioxide (CO_2) gas laser is one of the most versatile for materials processing applications. Of the several types of CO_2 laser that are available, the waveguide, the low power sealed tube and the transversely excited atmospheric (TEA) lasers are used for small-scale materials processing applications. The fast axial flow CO_2 laser and the less widely used slow flow laser are used for thick section cutting 1-15mm and deep penetration welding.

The active medium in a CO_2 laser is a mixture of carbon dioxide, nitrogen and (generally) helium. The carbon dioxide produces the laser light, while the nitrogen molecules help excite the CO_2 molecules and increase the efficiency of the light generation processes. The helium plays a dual role in assisting heat transfer from the gas caused by the electric discharge used to excite the gas, and also helps the CO_2 molecules to return to the ground state. The CO_2 laser has a wavelength of 10.6μm.

A schematic diagram of the 'waveguide' CO_2 laser can be seen in Figure 4 below.

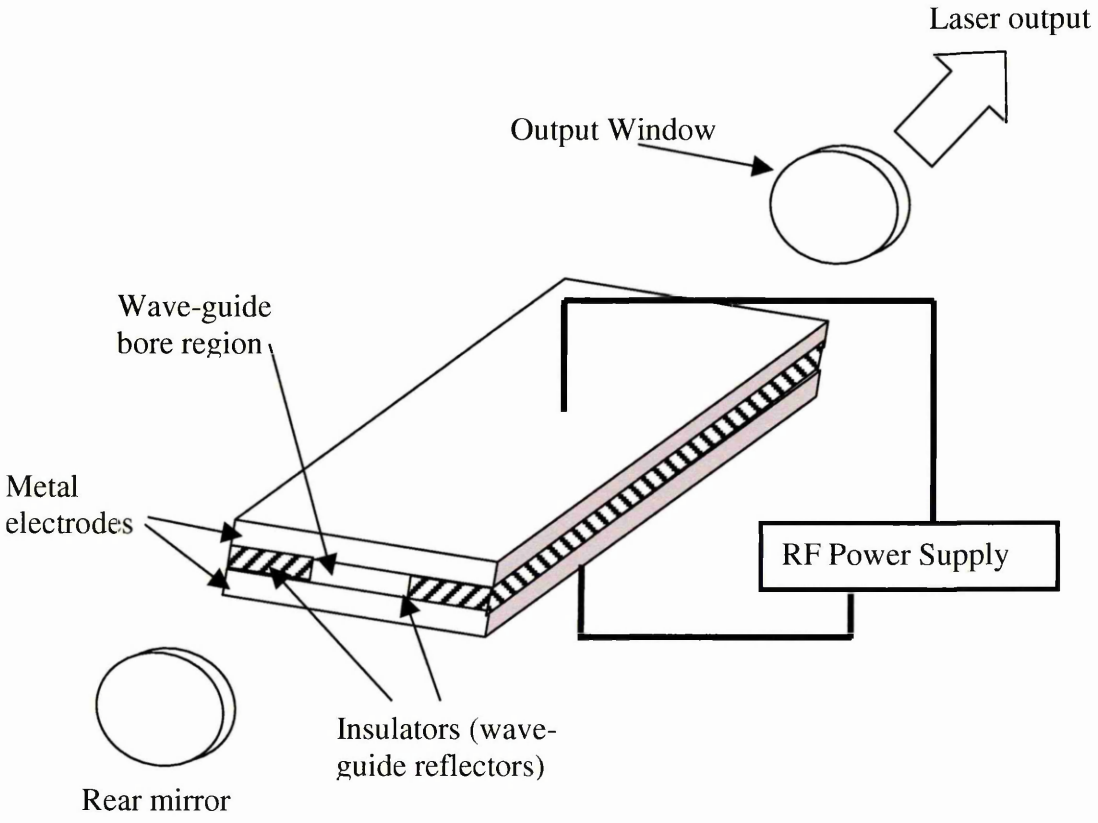

Figure 4 Schematic diagram showing a typical Wave-guide CO_2 laser set up

2.2 Basic Mechanisms of Laser Welding

Both solid state and gas lasers operate on the principle that photons of light emitted from excited atoms can be amplified to produce an intense beam of coherent, uniquely directional, mono-chromatic light.

Stimulated emission requires more atoms at high energy levels and this is achieved by external excitation of the laser medium by optical or electrical means. External excitation is applied either at a constant energy level to produce continuous wave (CW) laser beams or in a series of bursts to produce pulsed laser beams. Gas lasers are typically CW whilst solid-state lasers are typically pulsed.

Laser beam welding (LBW) uses a moving high-density (10^5 to 10^7 W/cm²) coherent optical energy source called a laser as the source of heat. The coherent nature of the laser beam allows it to be focused to a small spot, leading to high energy densities. The typical focal spot diameter for a laser beam ranges from 100 to 1000μm. The capability of the laser to generate a power density greater than 10^6 W/cm² is the primary factor in establishing its potential for welding. Numerous experiments have shown that the laser permits precision and high quality weld joints rivalled only by those made with an electron beam[13].

The localised heating obtained with laser sources was soon realised to be an important advantage. Anderson and Jackson[14] reported an interesting comparison between heating effects produced with a conventional arc source and those occurring with a pulsed laser for an iron substrate. They show that not only is the laser-produced HAZ small, but also that the laser source is more efficient because it requires only 37.8J/cm² (0.229 Btu/in.²) to produce melting to the required depth, while the arc source must deliver 246

[13] Mazumber, J. Laser Beam Welding, ASM handbook 1, page 262 - 269
[14] Anderson, J. E. & Jackson, J. E. Welding Journal, vol. 44, 1965, page 1018

J/cm² (1.49Btu/in.²) to the work-piece. This shows the high energy densities achieved with the laser beam welding process.

Table 1 shows the energy consumption and efficiency of laser-beam welding in comparison to other common welding processes[15].

Welding process	Intensity of energy source		Joining efficiency mm^2/kJ	Fusion Profile
	W/cm^2	W/in^3		
Oxyacetylene (OAW)	$10^2 - 10^3$	$6x10^2 - 6x10^3$	0.2 – 0.5	Shallow for single pass
Arc welding	$5x10^2 - 10^4$	$3x10^3 - 6x10^4$	0.8 – 2 (a) 2 – 3 (b) 4 – 10 (c)	Shallow for single pass
Plasma arc (PAW)	$10^3 - 10^6$	$6x10^3 - 6x10^6$	5 – 10	Shallow at low-energy end Deep penetration at high-energy end
Laser beam	$10^5 - 10^7$	$6x10^5 - 6x10^7$	15 – 25	Shallow at low-energy density range Deep penetration at high-energy density range
Electron beam	$10^5 - 10^8$	$6x10^5 - 6x10^8$	20 – 30	Deep penetration
(a) Gas – tungsten arc welding (GTAW), (b) Gas – metal arc welding (GMAW), (c) Submerged arc welding (SAW)				

Table 1 Energy consumption and efficiency of LBW relative to other selected welding processes

It can be seen that the joining efficiency of laser-beam welding is far greater than most other joining processes with the exception of electron beam welding. As well as being much more efficient, the laser welding process has a large number of advantages that allow it to compete with many well-established techniques such as soldering, arc welding, electron beam welding and, the most commonly used automotive welding process, resistance spot welding[12, 16, 17].

[15] Mazumber, J. Procedure Development and Practice Considerations for Laser Beam Welding, ASM handbook 3, page 874 - 880

[16] Wilson, J. & Hawkes, J. F. B. Laser Principles and Applications, Prentice hall, international series in optoelectronics, ISBN 0-13-523705-X

[17] Lampa, C. Laser Welding, Energy Redistribution and Weld Geometry, Doctoral Thesis, 1997:33, Luleå university of technology, ISSN: 1402 - 1544

Advantages include:

1. There is no physical contact with external components; this can be compared to resistance spot welding where contact occurs between the work-piece and the electrode tip.
2. Single sided access only is required; again this can be compared with resistance spot welding which requires double sided access
3. The heating is very localised
4. Dissimilar metals can be welded
5. Welding can be carried out in a controlled atmosphere with the work-piece sealed if necessary within optically transparent materials
6. Use of inert gas (argon or helium) for shielding to eliminate oxidation
7. Use of both continuous wave and pulsed lasers
8. Use of numerical control (NC) / digital numerical control (DNC) / Robotics devices for accuracy and complex jobs
9. The ability to carry out laser weld simulations using a low density laser spot prior to completing the weld

These advantages alone make the laser a very attractive alternative to many existing welding processes.

As with all welding processes there are some disadvantages to the laser welding process. These include[18]:

1. Work-piece 'fit up'; close fitting joints are required to ensure high quality welding when making autogenous welds. Alternatively special tooling can be used to force parts together.

[18] Dawes, C. J. CO_2 Laser Welding Low Carbon Steel Sheet, The Welding Institute Research Bulletin, August 1983, pp260-265

2. Work-handling; precision work or beam handling equipment is necessary to ensure good alignment of the laser beam with the work-piece and to control weld energy input.
3. Consumables; CO_2 lasers consume He, N_2 and CO_2 gases in their operation and He shielding gas is usually necessary.
4. Beam focusing; High power lasers use beam focusing lenses or mirrors, these optics are expensive and may have limited service life.
5. The initial cost of a laser system is expensive in comparison to resistance spot welding, for example.

2.3 Laser Welding Mode

Laser welding can be carried out in two modes. These are conduction mode laser welding, and for relatively thick sheets, keyhole laser welding. Keyhole laser welding requires higher power densities to produce the keyhole and results in a weld with a higher depth to width ratio.

2.3.1 Conduction Mode Laser Welding

The laser welding of thin steel sheets generally involves conduction mode laser welding. The laser beam irradiates the material surface and heat is conducted radially away from the laser-material interaction zone[19]. The molten weld pool produced generally has a semi-circular type cross section as shown in Figure 5 below.

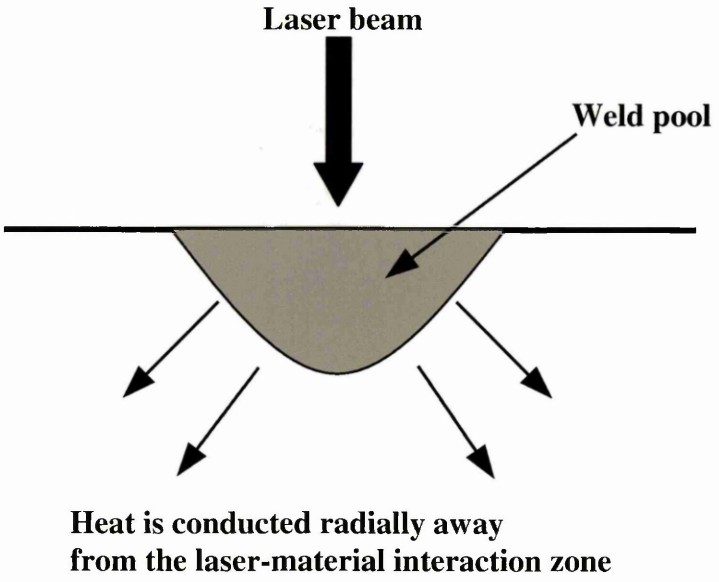

Figure 5 Heat dissipation in a conduction mode laser weld[19]

[19] Lampa, C. Laser Welding – Energy Redistribution and Weld Geometry, Doctoral Thesis, Lulea University of Technology, 1997, ISSN: 1402 - 1544

The depth to width ratio of conduction mode laser welds provides a greater tolerance to poor fit than keyhole type laser welds. However, conduction mode laser welding is far less efficient than keyhole laser welding in terms of energy consumed per unit area of join[17].

The surface condition of the sheets to be welded greatly affects the absorption of the laser beam. The surface reflectivity of cold rolled thin sheet can be as high as 65-80% in CO_2 laser welding[20], with the reflectivity of highly polished surfaces such as bright annealed stainless steel being as high as 98% at room temperature. However, the surface reflectivity reduces as the temperature of the surface rises.

Nath et al investigated the laser power coupling efficiency in conduction and keyhole mode welding of austenitic stainless steel. The estimated coupling efficiencies in conduction and keyhole mode welding were found to be 16% and 65% respectively[21].

[20] Xie, J. Kar, A. Laser Welding of Thin Steel Sheet with Surface Oxidation, Welding Journal, 78: (10) 343S-348S OCT 1999

[21] Nath, A. K. Sridarhar, R. Ganesh, P. & Kaul, R. Laser Power Coupling Efficiency in Conduction and Keyhole Welding of Austenitic Stainless Steel, Sadhana, Vol.27, Part 3, June 2002, pp. 383-392

2.3.1.1 Dilution/Stirring Mechanism

The high-power density (10^5 to 10^7 W/cm²) in laser welding produces a temperature gradient in the order of 10^6 K/cm which, in turn, leads to thermo-capillary flow (Marangoni convection) with surface velocities in the order of 1m/s.

The driving forces for thermo-capillary flow in weld pools can be described by three phenomena[22].

1. Surface tension flow
2. Buoyancy force
3. Electromagnetic force

Laser welding uses no electrical current; consequently the electromagnetic force can be neglected[17].

Generally, surface tension of a melt decreases with temperature[17]. For laser welding; surface tension is at a maximum at the edges of weld pool and at a minimum in the centre (see Figure 6). This surface tension gradient produces a stirring action which acts outwards from the centre of the weld pool. It should be noted, that this flow pattern can be reversed in some cases by the presence of surface active agents such as sulphur or oxygen in steel[23].

The buoyancy force reinforces the surface tension stirring effect and is produced by the density of liquid metals decreasing with increasing temperature. Thus, the hotter (less dense) material towards the centre of the melt pool will tend to rise whilst the cooler (more dense) material at the edges will tend to sink.

---

[22] Wang, Y.H. Kou, S Driving Forces for Convection in Weld Pools. Proceedings of the international Conference on Trends in Welding Research. May 18-22, 1986, Galinburg, TE, USA, pp. 65-69..
[23] Kou, S. Welding Metallurgy. New York: Wiley. 1987

The convection stirring induced by these two forces is the single most important factor affecting the geometry of the laser melt pool (that is, pool shape, aspect ratio, and surface ripples) and can result in defects such as variable penetration, porosity, and lack of fusion.

As stated, convection is also responsible for mixing and therefore affects the composition of the melt pool during laser welding because pool configuration in conduction-mode laser welding is a function of the Prandtl number (kinematic viscosity/molecular diffusivity), Pr_m, of the materials.

The following image shows the surface flow, stirring and dilution produced with materials with a high and low Prandlt numbers. It should be noted that laser beam spatial distribution is of the Gaussian distribution type.

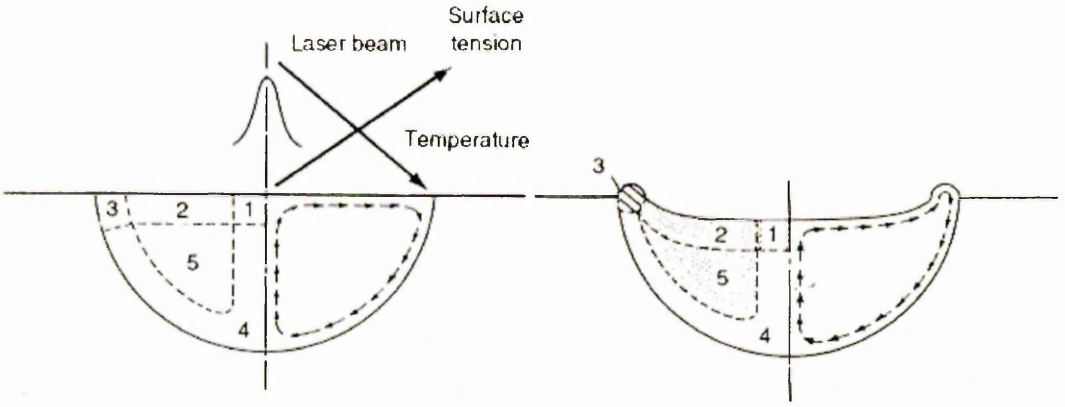

Figure 6 Laser weld surface flow for materials with low (left) and high (right) Prandlt numbers

Research conducted by Yang et al, investigated the characteristics of a 304 laser weld pool. The numerical model produced predicted the effects of Marangoni force, buoyancy force and thermal conduction[24]. The model shows that the molten liquid at the free surface flows from the weld centre outwards to the solid-liquid interface where

[24] Yang, L.X. Peng, X. F. Wang, B.X. Numerical Modelling and Experimental Investigation on the Characteristics of Molten Pool during Laser Processing, International Journal of Heat and Mass Transfer, 44, 2001, 4465-4473

two vortexes are formed. The numerically predicted stirring mechanism can be seen in Figure 7.

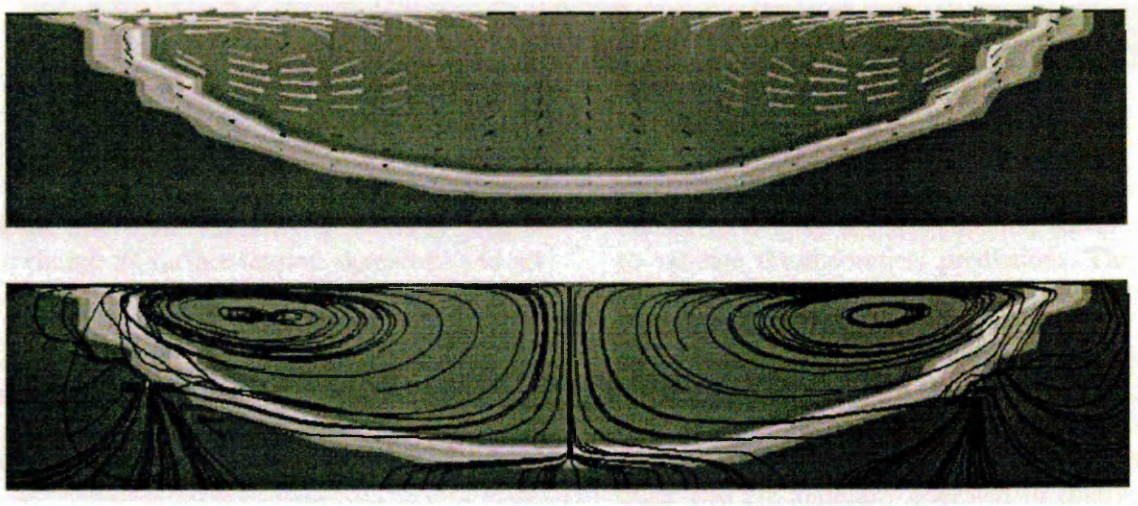

Figure 7 Velocity distribution at the X-Y central plane of the laser beam, (a) vector plot, (b) streamline plot[24]

The figure shows that the material at the edges of the weld flows down (depicted by the arrows), and flows up at the centre of the weld bead.

2.3.2 Keyhole Laser Welding Mode

Increasing the intensity of the laser beam to values in the order of $1x10^6$ W/cm^2 (for metals) leads to boiling and the formation of a vapour hole approximately the size of the focussed laser beam known as a 'keyhole', surrounded by a hollow column of molten material. The metal vapour in the keyhole now efficiently absorbs the laser light as it is subjected to many reflections from the keyhole walls; hence, the increased coupling efficiency of keyhole welding (65%) compared to conduction mode (16%). Consequently, the absorptivity and hence the laser wavelength becomes less important the deeper the hole. Conduction and convection in the liquid transfer heat to the material increasing the molten volume. A schematic of the laser 'keyhole' and its components can be seen below in Figure 8.

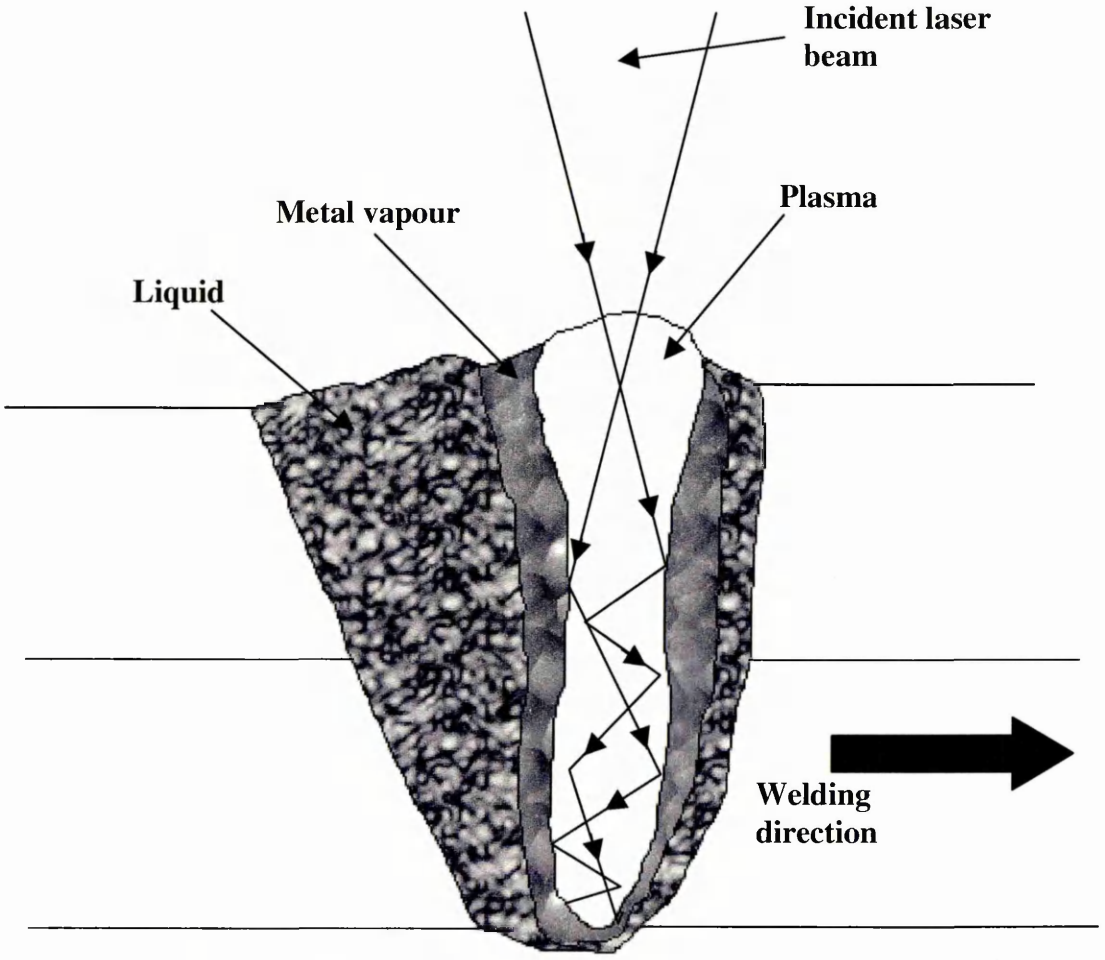

Figure 8 Schematic showing the components of a laser 'keyhole'

In keyhole welding, relative motion of the beam sends the keyhole through the work-piece leaving a fused zone behind. The vapour column is of great importance because this is the medium that transfers energy from the laser beam to the work-piece. Its vapour pressure keeps the keyhole open allowing the beam to penetrate deeply into the material being welded.

2.4 Laser Welding Parameters

The key factor for weldability is the selection of optimum independent and dependent process variables. The independent process variables for laser welding include:

1. Incident laser-beam power
2. Incident laser-beam diameter
3. Traverse speed
4. Absorptivity
5. Shielding gas
6. Depth of focus and focal position
7. Design and aperture size

These in turn will affect the dependent process variables having an important affect on heat flow and fluid flow in the weld pool. This in turn will affect penetration depth, shape and final solidification structure of the fusion zone. Both the shape and microstructure of the fusion zone will considerably influence the properties of the laser weld[25].

The independent laser welding variables, as defined by Yih-Fong Tzeng [26] can be seen in Figure 9.

[25] Naeem, M. Nd:YAG Laser Welding of Thin Sheet, Welding and Fabrication, June 2000, page 6 - 10
[26] Yih – Fong Tzeng, Parametric Analysis of the Pulsed Nd:YAG Laser Seam – Welding Process, Journal of Materials Processing Technology, 102, 2000, page 40 - 47

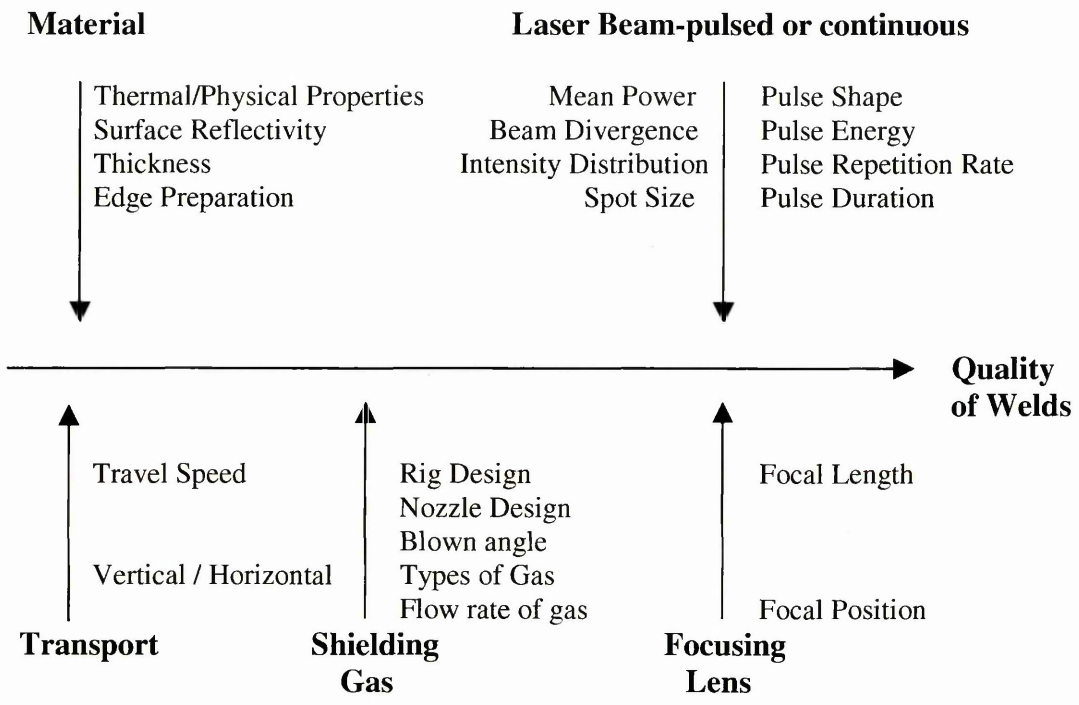

Figure 9 Independent process variables that can be controlled to aid in the production of high quality laser welds

2.4.1 Power Density

Power density is defined as the incident power per unit area[15]. In any welding process it is the power density that determines the depth of penetration and joining rate for the process, not the total power of the source. Therefore, beam diameter and spatial distribution of the laser-beam energy play an extremely important role as they determine the area of incidence.

Two other variables affecting the ultimate power density driving the welding process are absorptivity and plasma-beam interaction, such as refraction. Position of focus with respect to the substrate and depth of focus of the beam also affects the power density and penetration depth.

2.4.1.1 Absorptivity

As mentioned in section 2.3.1, the efficiency of laser beam welding depends on the absorption of light energy by the work-piece. The infrared absorption of metals largely depends on the conductive absorption by free electrons. Therefore, absorbtivity is a function of the electrical resistivity of the substrate material. Arata and Miyamoto[27] measured the absorptivity of polished surfaces of various materials and concluded that absorptivity is proportional to the square root of the electrical resistivity. This agreed closely with the following equation:

$$A := 112.2 \cdot \sqrt{\rho r}$$

Equation 1 **Absorptivity of laser beam**

For reflective materials such as aluminium, Nd: YAG has better coupling, especially for conduction mode welding, due to their shorter wavelength (1.06μm, as opposed to the CO_2 wavelength 10.6μm).

However, it has been shown that this coupling advantage quickly diminishes as the material temperature increases and once the material has reached a molten state there is no great advantage from the shorter wavelength Nd: YAG laser[16].

[27] Arata, Y. & Miyamoto, Laser Focus, vol 3, 1977

2.4.1.1.1 Plasma Beam Interaction

At power densities ~10^7 W/cm^2 (in metals) and higher, some of the electrons in the vapour become ionised. These free electrons can also absorb energy directly from the incoming laser beam, resulting in higher temperatures, more increased ionisation and absorption. Plasma of ionised metal vapour, which can absorb laser light and emit 'black body' radiation, is formed. Providing the power density is sufficient to sustain it, the plasma will be a net contributor to the process. At even higher power densities, the vapour column leaves the keyhole, forming a 'cloud' over its opening. This plasma cloud (or plume) absorbs light, decreasing the energy entering the keyhole.

The plasma that is formed directly over the molten weld pool can seriously affect penetration depth. Rockstroh, et al.[28] found that during high-power laser welding, free electrons in the plasma column cause absorption and refraction. When welding aluminium with a CO_2 laser, as much as 30 % of the energy is lost in the plasma and the refracted beam diameter is 8% larger.

Generally, when welding zinc coated steel there is a very strong plasma formation (even in conduction mode laser welding) owing to the low boiling point of zinc (906°C) and its high vapour pressure, which is about eight orders of magnitude greater than that of Fe. The high vaporisation rate of zinc increases the pressure of the vapour, which is transformed to plasma in the laser beam, and expands further into the free space above the metal surface. This affects the absorption and fluctuation of the plasma and in practice this is shown as increased spattering and porosity in the weld[29]. See section 2.5 for a comprehensive analysis of the problems associated with laser welding zinc coated steel, including potential solution to these problems.

---

[28] Rockstroh, T. & Mazunder, J. Applied Physics, vol 61 (no.3), 1987, page 917 - 923

[29] Matsunawa, A. Monem, A. El-Batahgy and Zaghoul, B. Laser Beam Welding of Lap Joints of Dissimilar Metals, Incomplete source information

2.4.1.2 Focal Position

The focal position is the point where the beam is focused in respect to the surface. The focal position can be controlled to 0.1mm and range from several millimetres above the surface, the material surface itself (0mm), or several millimetres below. As well as controlling the depth of penetration by altering power density, it can also (to a lesser extent) be selected to control the weld bead shape. These effects can be seen in Figure 10 and Figure 11 respectively.

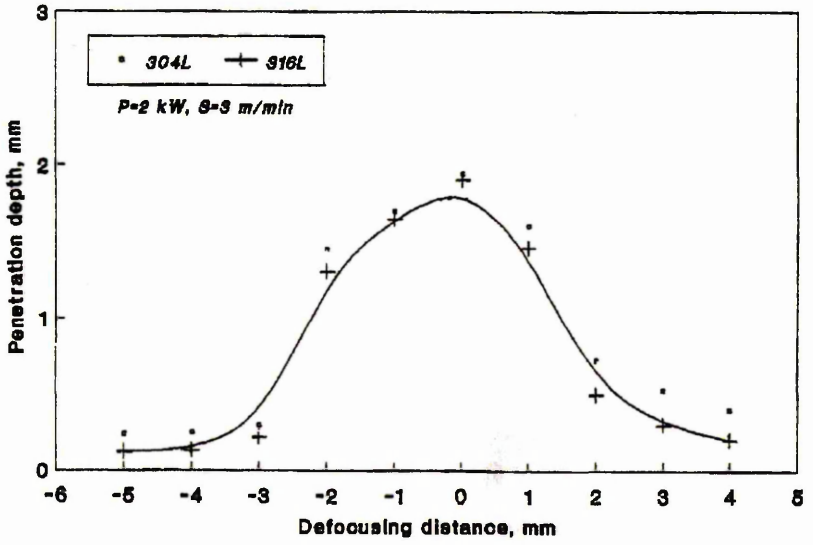

Figure 10 The relationship between the focal position and the depth of penetration for 304 & 316 stainless steel[30]

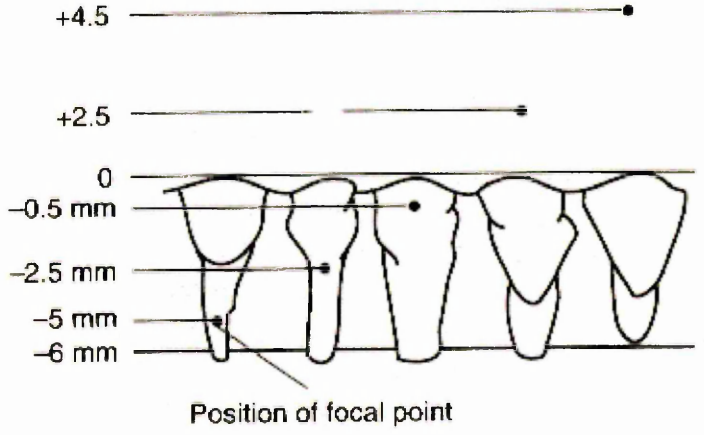

Figure 11 Transverse profiles as a function of focus position for a laser-beam welded type 310 stainless steel. Negative and positive numbers indicate position of focal point below and above, respectively, the surface of the plate. Beam power, 5kW, Traverse welding speed, 16mm/s[15]

[30] Monem, A & El-Batahgy, Effect of Laser Welding Parameters on Fusion Zone Shape and Solidification Structure of Austenitic Stainless Steel, Materials Letters 32 (1997), page 155 - 163

2.4.1.3 Depth of Focus

Depth of focus is extremely important for welding thin-section materials as for a shallow depth of focus the substrate comes in and out of the focal position due to thermal distortion. Depth of focus is defined as the distance over which the focus beam has approximately the same intensity. It is usually defined as the range over which the focused spot radius is increased by no more than 5%.

As the f-number of the focusing optics increases, depth of focus increases (the f-number is defined as the effective focal length divided by the incoming raw beam diameter). However this is also accompanied with an increase in beam diameter and decreased power density. As a result, focal point and depth of focus must be optimised for each particular application.

2.4.1.4 Interaction Time

Interaction time is defined as the time a particular point on the substrate spends under the laser beam[15]. In simple terms, it is the ratio of the beam diameter to the traverse speed. On the basis of heat transfer, the total time of heating and cooling at the point above the ambient temperature should be accounted for. This is, however, a much more difficult quantity to keep track of compared to the ratio of the traverse speed and beam diameter. It is the interaction time that controls the weld pool profile, not the traverse speed alone.

2.4.2 Laser Beam Power

Laser-beam power is one of the primary variables in determining the penetration depth in laser welding. The relationship between welding power and penetration depth was investigated by Yih-Fong Tzeng, who found that penetration depth was proportional to welding power. This can be seen Figure 12. It should be noted that the sample thickness was 3mm.

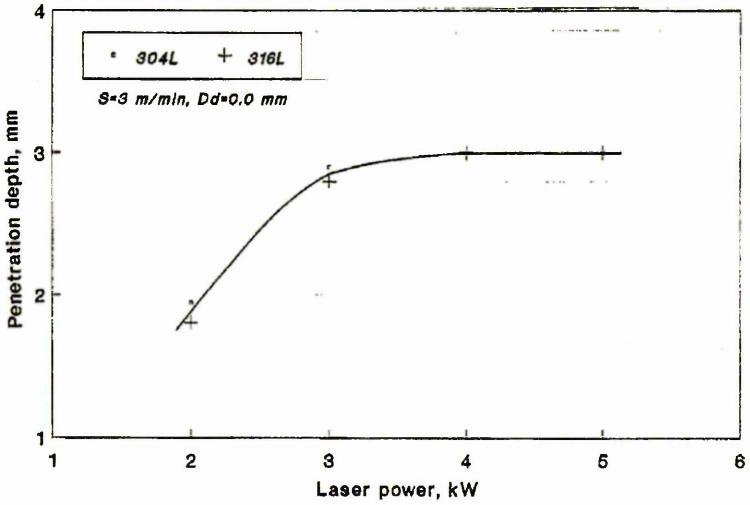

Figure 12 The relationship between laser power and the penetration depth achieved[30]

In addition to the absolute power measurement, the beam mode (that is, the spatial distribution of energy) and beam diameter should be monitored since they also strongly affect the power density.

2.4.3 Laser-Beam Diameter

Laser beam diameter is one of the most important variables since it determines the power density for a given total power. The spatial distribution of energy in the beam affects the focusing characteristics of the beam. For a Gaussian beam, the diameter is defined as the $1/e^2$ of the central value; see Figure 13, and it contains almost 86% of the total power[15].

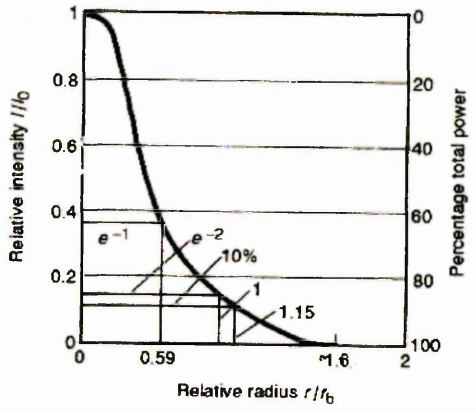

Figure 13 Variation of relative intensity and percentage of total power with radius for a gaussian beam[15]

2.4.4 Traverse Speed

Generally welding speed increases with increasing laser power. It can be seen from Figure 14 and Figure 15 that a range of speeds can be used for a given thickness and power to produce successful welds. It can also be seen that the envelope becomes larger when welding thinner material. It should be noted, however, that the fusion zone size increases with decreased speed within the welding range. This can be seen in Figure 16.

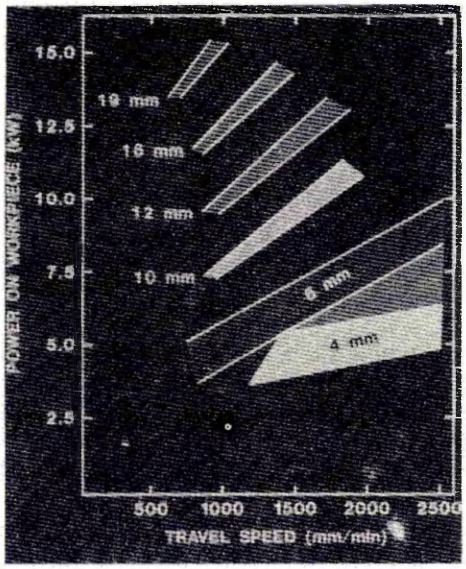

Figure 14 The welding envelope for a variety of materials thickness[40]

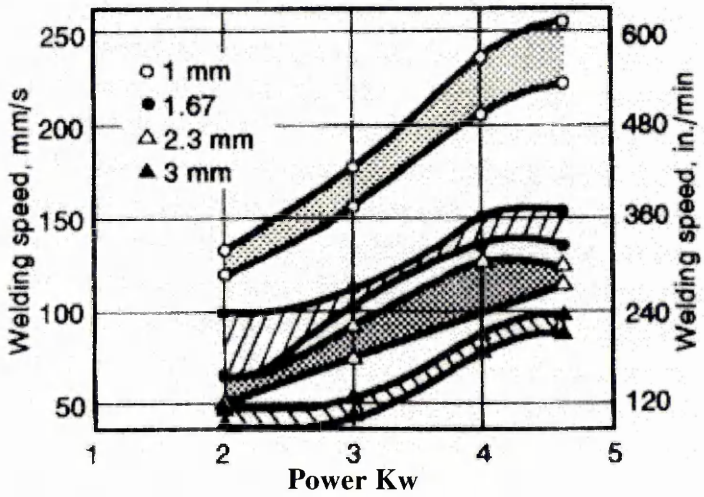

Figure 15 Welding speed versus laser power for a 5 kW CO_2 laser. These welding envelopes were produced for a Ti-6Al-4V[15]

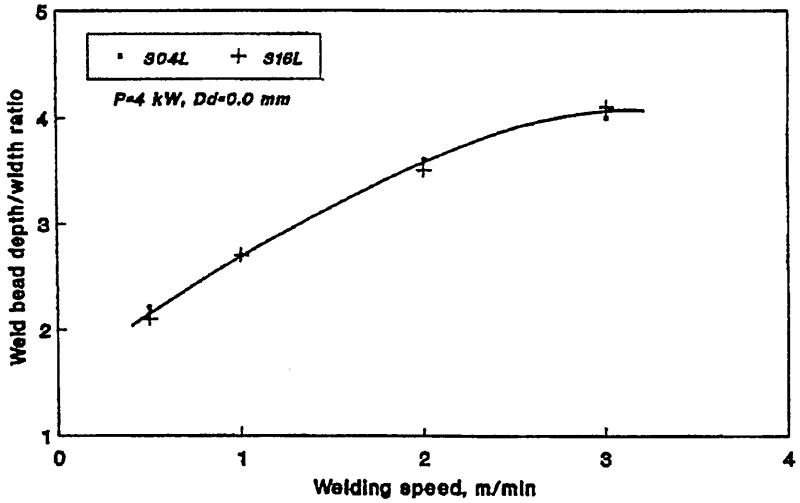

Figure 16 The relationship between the traverse speed and the weld bead depth to width ratio[30]

2.4.5 Shielding Gas

Shielding gas is used to suppress plasma formation as well as provide a controlled atmosphere around the weld to prevent oxidation etc[31] [32]. Successful plasma suppression results in high quality welds with consistent shape and penetration depth. The type and flow rate of the shielding gas are the most commonly controlled aspects of this variable. However, the direction of the shielding gas can also be controlled; for example, the gas can be directed from behind the laser (trailing gas) or can be incorporated around the laser beam (coaxial). A combination of the two can also be used. The most common types of shielding gas are Argon and Helium. Studies have shown, however, that Helium is more successful at suppressing plasma and seems to improve beam transmission whereas Argon can cause severe blockage of the laser power by not suppressing plasma formation, see Figure 17. It is thought that this is due to the fact that argon has a lower ionisation potential (15 eV) compared to that of helium (25 eV)[32]. Matsunawa *et al.*[29] found that during laser welding of stainless steel to zinc coated steel the numbers of pores obtained when using helium as a shielding gas was much less than when Argon was used as the shielding gas.

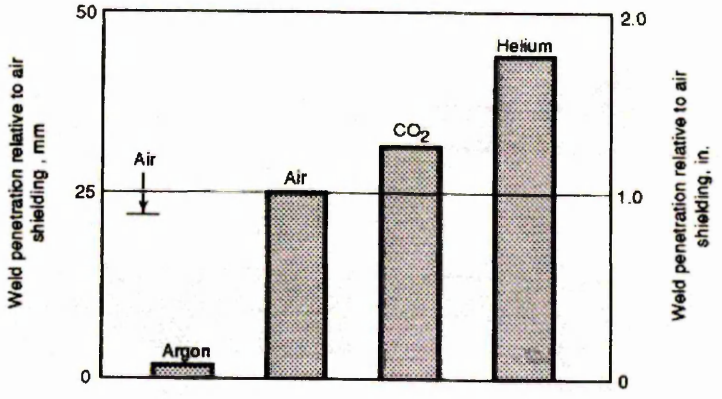

Figure 17 The penetration depth achieved from various shielding gases in comparison to air[15]

[31] Metzbower, E.A. Moon, D.W. & Denney, P.E. Laser Beam Welding of HSLA Steels, ASM conference proceedings, 8 – 12 October 1990
[32] Seaman, F. Role of Shielding Gas in Laser Welding, Technical paper no. MR77-982, 1977

2.4.6 Focussing System

The laser welding process involves focusing a laser beam, using either a lens or a mirror, to a small spot, which has sufficient power density to melt the surface of the substrate or to produce a keyhole type laser weld. The focusing system is generally defined by its focal length. However, the critical factors that determine the selection of the lens are the focused spot diameter and the depth of focus. The depth of focus is the effective distance over which satisfactory welding can be achieved. It can be defined as the distance over which the focused spot size does not increases beyond 5%. For a given beam diameter, as the focal length becomes shorter the focused spot diameter and the depth of focus also become smaller. The size of the actual spot size is also dependent on the raw beam diameter. As the raw beam diameter increases, for a given focussing system, the focused spot size will decrease. To allow comparison between lasers with different beam diameters the f-number is used. As it is not feasible to control the raw beam diameter, it is usual to select the correct focussing system to give a focused beam of the required type. The only other consideration is that the shorter the focal length, the closer the focusing optics are to the work piece, and therefore more likely to be damaged by spatter from the welding process.

Thus when welding thicker section materials the requirements would be a high power density and therefore a small focused spot size but with a long depth of focus, hence an ability to process thicker materials with a reasonable tolerance to focus position variation, see section 2.4.1.2.

2.5 Current Automotive Steel Grades

Automotive manufacturers use a range of 'high strength' steels in the production of lightweight automotive structures. As stated in section 1, the steels currently used in automotive manufacture are:

7. HSLA or micro-alloyed steels
8. Rephosphorised steels
9. Bake hardening steels
10. Dual phase steels
11. Trip steels
12. High strength IF steels

The materials that have received the most attention as potential new materials for lightweight automotive construction are aluminium alloys. As well as the initiatives stated in section 1 from the European Association of Car Makers to reduce CO_2 emissions; the US automotive industry also face demands to simultaneously increase its average fuel economy and reduce green house gas emissions, with the use of lightweight aluminium alloys being identified as an effective way to meet these new standards[33].

[33] Brown, K. R. Venie, M. S. & Woods, R. A. Journal of Metals, July 1995, pp20-23

2.5.1 High Strength Low Alloy (Micro-Alloyed Steels)

These steels have yield strengths in the range of 300-350 MPa for cold rolled production and typically 550 MPa for hot rolled produce. As the name suggest, micro-alloying additions of titanium, niobium or vanadium are added to low carbon, aluminium killed steel. This produces high yield strength by precipitation hardening through the combination of alloying effects and thermo-mechanical treatment received during the hot strip mill.

2.5.2 Rephosphorised Steels

Rephosphorised steels (currently used by Volvo Truck Corporation) have yield strengths in the range of 190-269 MPa. These steels achieve their strength with the additions of phosphorous (typically 0.1%) to an aluminium killed base steel. These phosphorous additions provide increased strength by the means of solid solution strengthening and have yield strengths up to 30% higher than plain carbon steels, with an increase in cost of less than 10%[34]. A welding problem associated with these steels, which are due to the increased phosphorous content, is the potential increase in susceptibility to solidification cracking during laser welding. Microhardness measurements in the heat affected zones (HAZs) have also indicated that rephosphorised steel is harder, even with reduced carbon content, compared to plain carbon steel[35]. These problems would be exacerbated at higher welding speeds; thus, laser-welding speeds are usually reduced slightly in practice to eliminate this effect.

---

[34] Hoult, S.H. Kerr, H.W. Spot Weldability of Rephosphorised Steels, Metal Construction, August 1982, pp426-432

[35] Sawhill, J.M. Jr Baker, J.C.: Welding Journal, 1980, 59, 19s

2.5.3 Bake Hardening Steels

This group of steels have a yield strength ranging from 160-260 MPa. These are produced by vacuum degassing low carbon aluminium killed steels, and achieve higher strength by ageing during the paint stoving operation. An increase in yield strength of up to 40% can be achieved from the bake hardening process. This increase is known as the 'bake-hardening factor' and is dependent on the specific steel grade and ageing conditions.

2.5.4 High Strength Interstitial-Free (IF) Steels

High strength interstitial free steels have yield strengths in the order of 190-300 MPa. Similar to Bake Hardening steels, these steels are vacuum degassed. This reduces the carbon and nitrogen levels within the steels. The end result is a carbon content of <0.0003%, which with strengthening from niobium, vanadium and titanium additions results in a pearlite-free base metal structure.

2.6 Current Automotive Painting Systems

Continual research is being carried out to improve existing paint systems and to develop more resilient paint systems. Although current automotive grades are galvanised to achieve the requisite corrosion resistance, increasing demands for quality from the customers, changes in the environment and more stringent legal requirements for less harmful products and processes has led to the development of paint systems which can meet very complex requirements. These systems must also provide a coating that is acceptable for gloss, colour durability, cracking resistance, adhesion throughout all layers, acid, chemical and scratch resistance[36].

Even more important perhaps, is the surface condition and keying afforded by the base material prior to the application of the paint system. This has led to a number of pre-treatments for zinc-coated automotive grades. A 'general' zinc-coated automotive steel pre-treatment can be split into the following processes[37].

2.6.1 Pre-cleaning

The purpose of pre-cleaning is the removal of contamination from the surface to be painted. These contaminants include, oil, grease, scale, weld spatter and lubricants that can be present due to previous manufacturing processes. In extreme cases the pre-cleaning may include blasting, polishing, pickling and solvent degassing. It should be noted that the pre-cleaning stage does not provide any protection to the surface.

[36] Jurgetz, A. Automotive Paint Performance, Bayerische Motoren Werke AG, Germany, Metal Finishing, October 1995, pp 53-55

[37] Murphy, M. Joseph, R. Introduction to Paint Application Systems, Application Methods, pp161-166

2.6.2 Pre-treatment

Surface pre-treatments can include a combination of chemical cleaning and a conversion coating. The purpose of a conversion coating is to improve the corrosion resistance and to provide a surface with enhanced adhesion and acceptance of the organic coating.

2.6.3 Dry-Off

After pre-treatment the 'wet' parts are immediately transferred to a high-temperature dry-off oven. For small, lightweight, metal parts the oven temperature can be as low as 121°C. For larger, heavy parts or bulky constructions, the oven temperature may be as high 204°C. The sole purpose of this 'dry-off' period is to evaporate the water as quickly as possible to prevent flash rusting. It should be noted that in coating operations where the parts are immersed into a dip tank containing a waterborne coating, this 'dry-off' period might be eliminated.

2.6.4 Coating Application Methods

There is a wide choice of application methods available for both primers and topcoats. The most extensively used coating deposition methods in automotive applications are spray, dip, electro-deposition or electro-coating.

2.6.5 Curing Process

Drying is the process by which the solvents and/or water in the coating evaporates to allow the film to achieve a 'dry-to-touch' or 'dry-to-recoat state. Curing on the other hand implies that the coating resin undergoes a chemical reaction, rendering the cured film hard, abrasion resistant, and relatively inert to the environment (chemicals, solvents, sunlight etc).

Hence, the integration of a new material into current automotive design will require analysis of the materials' paint ability and determination of the systems required to produce a coating which meets the current standards for paint appearance and durability testing.

In the case of dissimilar metal joints between stainless steel and zinc coated mild steel, the presence of the passive film on the stainless steel surface may produce problems with paint adhesion. Stainless steel may also require the use of different chemical cleaning processes during the pre-treatment stage, which is required to produce suitable adhesion of the organic coats.

Thus, to allow integration of stainless steel into automotive construction, the suitability of current painting systems for coating stainless steel would need to be investigated; more specifically, the performance of the pre-treatments and chemical cleaning prior to the standard automotive scratch and durability tests.

2.7 Stainless Steel Paint Adhesion

Research conducted by Marples investigated the resistance spot welding of austenitic stainless steel (1mm 304) to zinc-coated mild steel (1.2mm V1437)[38]. A number of dissimilar metal spot welded samples were subjected to Volvo Truck Corporations' current painting system and durability testing.

Dissimilar metal spot welded joints with vertical and horizontal joint orientation were compared with 1.2mm V1437 similar metal spot welded joints as the reference.

The dry and wet adhesion was tested using the cross-cut test method and the corrosion resistance of the joints was tested using VICT (accelerated indoor corrosion test) and scab (accelerated outdoor corrosion test)[39].

The investigation resulted in the 1mm 304 stainless steel being approved for both wet and dry adhesion. However, the accelerated corrosion tests revealed that increased corrosion was evident on the dissimilar metal scab tested samples when compared with the V1437 similar metal reference samples. This was attributed to increased galvanic corrosion of the dissimilar metal joints, the zinc being consumed more quickly when joined to stainless steel[39]. The following images show the VICT exposed 1mm 304 – 1.2mm V1437 dissimilar metal joints and scab exposed tests compared to the similar metal 1.2mm V1437 joints respectively.

---

[38] Marples, M. Resistance Spot Welding of Autstenitic Stainless Steel to Galvanised Mild Steel, Unpublished Work, Sheffield Hallam Univeristy, 2003

[39] Hedlund, J. Corrosion Test of Spot Welded Joints of Stainless Steel and Hot Dip Galvanised Steel, VTC. Engineering Report ER-511811, 16th Oct, 2001, pp 1-6

It can be seen in the VICT exposed dissimilar and similar metal corrosion comparison that more corrosion is present on the surface of the dissimilar metal joint.

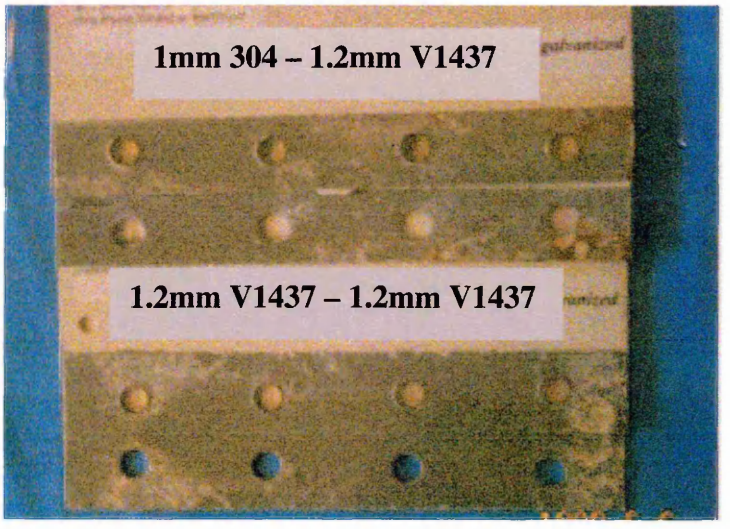

Image 1 1mm 304 – 1.2mm V1437 at the top and the 1.2mm V1437 similar metal joint at the bottom – both VICT exposed

It can also be seen in the scab exposed dissimilar and similar metal corrosion comparison that more corrosion is present on the surface of the dissimilar metal joint.

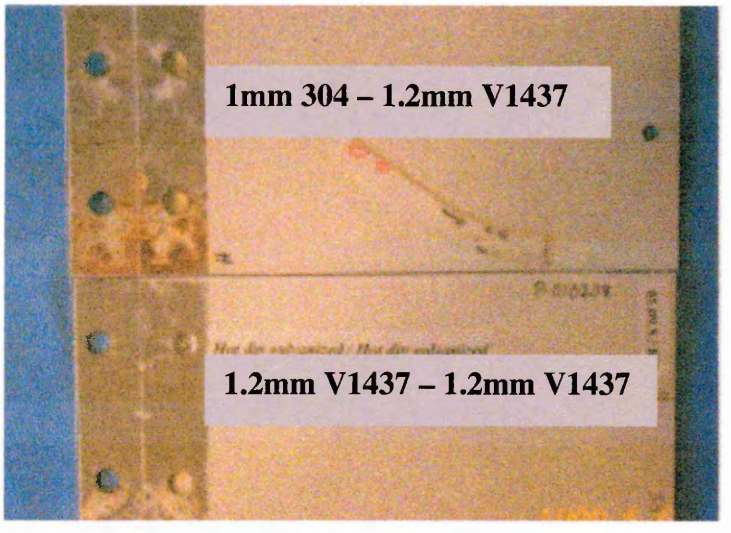

Image 2 1mm 304 – 1.2mm V1437 at the top and the 1.2mm V1437 similar metal joint at the bottom – both scab exposed

Hence, it was concluded that a dissimilar metal lap joint between stainless steel and zinc-coated mild steel would corrode at a higher rate than a zinc-coated mild steel similar metal joint.

2.8 Stainless Steel

Stainless steels were initially developed to improve the wear resistance of gun barrels and were later developed to obtain resistance to corrosion[40]. However, stainless steels also exhibit excellent mechanical properties, and in some applications, these mechanical properties are as important as corrosion resistance in determining the life or utility of a given structural component. Within the stainless steel family there are many different types of stainless steels including martensitic, ferritic, austenitic, duplex and precipitation-hardenable steels. Thus, with so many types of stainless steel, a wide variety of mechanical properties can be achieved.

2.8.1 Austenitic Stainless Steel

Austenitic stainless steel has sufficient γ-stabiliser, in the form of Ni, added to a Fe-Cr alloy to produce a microstructure that consists entirely of f.c.c. austenite at room temperature. The f.c.c. structure provides a tough, very ductile steel which work-hardens rapidly when machined or cold formed. The f.c.c. structure provides the steel with no impact transition temperature and thus can be used for cryogenic applications.

The austenitic stainless steels do exhibit a wide range of mechanical properties. These steels, as stated, have an austenitic microstructure at room temperature and cannot be hardened to any great extent by heat treatment, although they can be appreciably strengthened by cold working. These steels exhibit good ductility and toughness even at high strength levels. Austenitic stainless steels have lower melting points, higher electrical resistance, lower coefficients of thermal conductivity, and higher coefficients of thermal expansion than mild steels[41 42].

---

[40] Brickner, K. G. Stainless Steels for Room and Cryogenic Temperatures, Selection of Stainless Steel, American Society for Metals, 1968

[41] Leffler, B. Stainless Steels their Properties, 2nd revised edition

[42] Holmberg, B. Stainless Steels: Their Properties and their Suitability for Welding

2.8.2 Duplex Stainless Steel

Duplex stainless steel consists of two phases, austenite and ferrite, both about 50%. The primary structure is ferrite and the secondary structure is austenite. The combination of these two phases results in a very high yield and tensile strength as well as an excellent resistance to chloride-induced stress corrosion and pitting[41].

The structure of duplex stainless steel strongly depends on its chemical composition and thermal history such as heat-treatment or heat input from welding.

The production of the duplex stainless steel microstructure (austenite/ferrite structure) is formed as follows.

When the composition cools down from the liquid phase it starts to solidify as ferrite at 1450°C. Below 1300°C the austenite phase starts to form by nucleating at the grain boundaries of the ferritic phase. An amount of austenite will be formed which is dependent on the cooling rate. When the cooling rate is low there is a lot of time hence a large amount of austenite will be formed. Alternatively when the cooling is high there is very little time, hence only a small amount of austenite will be formed.

To obtain the best possible structure the material is eventually homogenised at about 1050°C and water quenched to maintain the optimum structure (about 50% ferrite and 50% austenite) and to suppress uncontrolled precipitation.

Duplex stainless steels have high resistance to hot cracking during welding, compared with fully stable austenitic stainless steels.

2.8.2.1 Lean Duplex Stainless Steel

Lean duplex or more specifically, 2101 is a relatively new grade of stainless steel. It possesses the same two phases, austenite and ferrite, again both about 50%. The main difference of this steel when compared to standard duplex grades is, as the name suggests, in the composition. The lean duplex grade has a lower nickel content which reduces cost. The manganese content of this steel is increased, which in turn increases the amount of soluble nitrogen. Hence, a balance is again struck between the austenite and ferrite formers/stabilisers and the 50% ferrite and austenite structure can be achieved.

2.9 Laser Welding Zinc Coated Steel

Many problems can occur when laser-welding zinc coated steels, especially in the lap joint configuration. This is due to the low vaporisation temperature of zinc (906°C).

2.9.1 Butt joints

As explained in section 1, laser welding has been successfully used in the production of tailor welded blank manufacture and in body-in-white welding applications, an example of the former can be seen in Figure 2. The joint configuration used for laser welded tailored blanks is the butt joint. Thus, the effect of the zinc coating is minimal. The only impact on laser weldability is a slight reduction in welding speed compared to uncoated steel of the same thickness. This is to allow for adequate suppression of the plasma formed. Some consideration should be made towards preventing damage to the focusing optics caused by the slight increase in spatter and potential of fume condensation on the focusing optics. No other problems are associated with laser welding zinc-coated steels in the butt joint configuration apart from the removal of the zinc coating adjacent to the weld. The uncoated area of zinc-coated laser welded butt joint is ~3-5mm; hence, the weld is cathodically protected by the sacrificial zinc adjacent to the weld. As the tailored blank is painted, the reduction in corrosion is minimal.

2.9.2 Lap joints

Research has shown that the presence of zinc at the interface of lap and hem joints causes disruption to the laser welding process[2543]. If the sheets are intimately clamped, the zinc vapour at the internal lap face has no means of escape other than through the molten weld pool. As stated in section 2.4.1.1.1, the vapour pressure of zinc is very high, thus, ejection of the molten weld metal occurs.

In practice this disruption is manifested as increased spatter during the welding process, which causes blow holes and porosity in the laser weld bead. It can also reduce the power absorbed by the work piece due to the formation of a dense plasma cloud, also explained in section 2.4.1.1.1, which results in variable or reduced penetration.

Current automotive grades are zinc-coated to achieve the requisite corrosion resistance. The two most commonly used zinc-coating types are:

- Electro-galvanised
- Hot-dipped galvanised

The main difference between these two zinc-coating types, besides deposition method, is the thickness of the deposited zinc coating. Generally, hot-dipped galvanised coatings are thicker (≥5μm) than electro-galvanised (<5μm) and galvannealed coatings. These thicker coatings exacerbate the problems mentioned above and consequently, have provided the driving force to find potential solutions. These proposed solutions can be split into the following categories:

- Introduction of novel clamping techniques
- Modification of sheets to be clamped
- Control of the welding process/parameters

---

[43] Park, H. Rhee, S. Analysis of Mechanism of Plasma and Spatter in CO_2 Laser Welding of Galvanised Steel. Optics and Laser Technolgy, 31, 1999, pp 119-126

One proposed solution is with the use of modified clamping systems. The purpose is to introduce a gap between the sheets to allow the zinc vapour to escape from the internal lap face. This could be achieved by reducing the clamping force or the use of intermittent point clamps along the length of the weld. The use of shims has also been tried, although, this solution may produce problems with reproduction and does not lend itself to automation.

A more novel approach to sheet clamping has been with the use of a spring-loaded roller positioned adjacent to the weld. Volvo currently uses this system in the production of a roof joint to create a gap on one side of the lap joint, thus allowing the zinc vapour to escape the internal lap face in front of the laser beam.

Modification to the pre-welded sheets may also provide a solution with the introduction of 'dimples' by mechanical stamping. This system, aims to provide a gap between the sheets whilst allowing clamping along the entire length of the lap joint. Again, the gap introduced allows the zinc vapour to escape from the internal lap face.

One disadvantage of these potential solutions is the cost of the additional equipment (spring-loaded roller) or the cost of introducing a further manufacturing step (sheet dimple stamping) to introduce the gap.

Perhaps, the simplest and most cost effective method to overcome the problems associated by welding zinc-coated lap joints lies with the inherent flexibility and control of the laser welding system. It should be noted that the control of the laser welding parameters, or manipulation of the optic beam delivery aim to overcome the problems of porosity, blow holes and spatter by increasing the solidification time of the weld bead, thus, providing sufficient time for the zinc vapour to escape through the weld bead in its molten state.

The huge range of laser welding process variables, explained in section 2.3, may hold the key to solving the problems of zinc-vapour evacuation. This may lie with

development of special welding parameters, perhaps involving pulsing of the laser energy or the use of propriety gas mixtures. There have been investigations into the development and use of energy dispersive laser optics capable of producing a twin-spot laser output to permit additional venting (by slightly elongating the weld pool) of zinc vapour from the weld pool, see Figure 18. This system may also have the potential to be used to deliver a post-weld heat treatment in one welding operation.

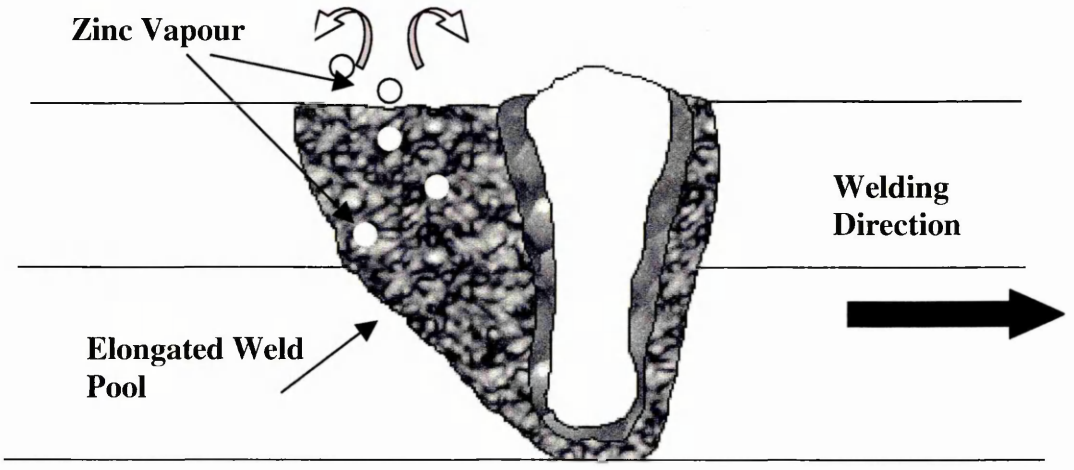

Figure 18 Additional venting permitted by elongating the weld pool with the use of a 'Twin spot' laser beam

The problems of laser welding zinc-coated steels in the lap joint configuration are well known. Hence, a set of guidelines has been generally accepted to aid the production of high quality laser welds with zinc-coated steels. If the zinc-coating of the sheet is <5μm, the sheets can be clamped with no gap at the interface; however, should the zinc coating thickness be ≥5μm (hot-dipped galvanised automotive grades), it is advisable to introduce a gap to allow for the evacuation of zinc vapour from the internal lap face.

2.9.3 Damage to the Focusing Optics by Spatter

Owing to the low vaporisation temperature of zinc (906°C), laser welding zinc-coated steel produces more spatter than uncoated steel. One way to overcome potential damage to the focusing mirror or lens is to increase the focal length of the laser welding system when welding zinc-coated steel[44][45]. This system for reducing damage to the focusing optics has been employed by the Welsh Technology Centre, which currently uses a focal length of 250mm for laser welding zinc coated steel. This reduces the chance of damage to the focusing mirror or lens. The laser can also be reflected from the mirror/lens through a nozzle to the work piece. The nozzle reduces the area below the focusing optics and thus reduces the chance of spatter hitting and damaging the mirror or lens. This is illustrated in Figure19.

[44] Naeem, M. YAG Laser Welding of Thin Sheet,Welding Metal and Fabrication, June 2000, pp 6-10
[45] Bratt, C. Discussions, Laser Welder Project Leader, Welsh Technology Centre, 2000 - 2002

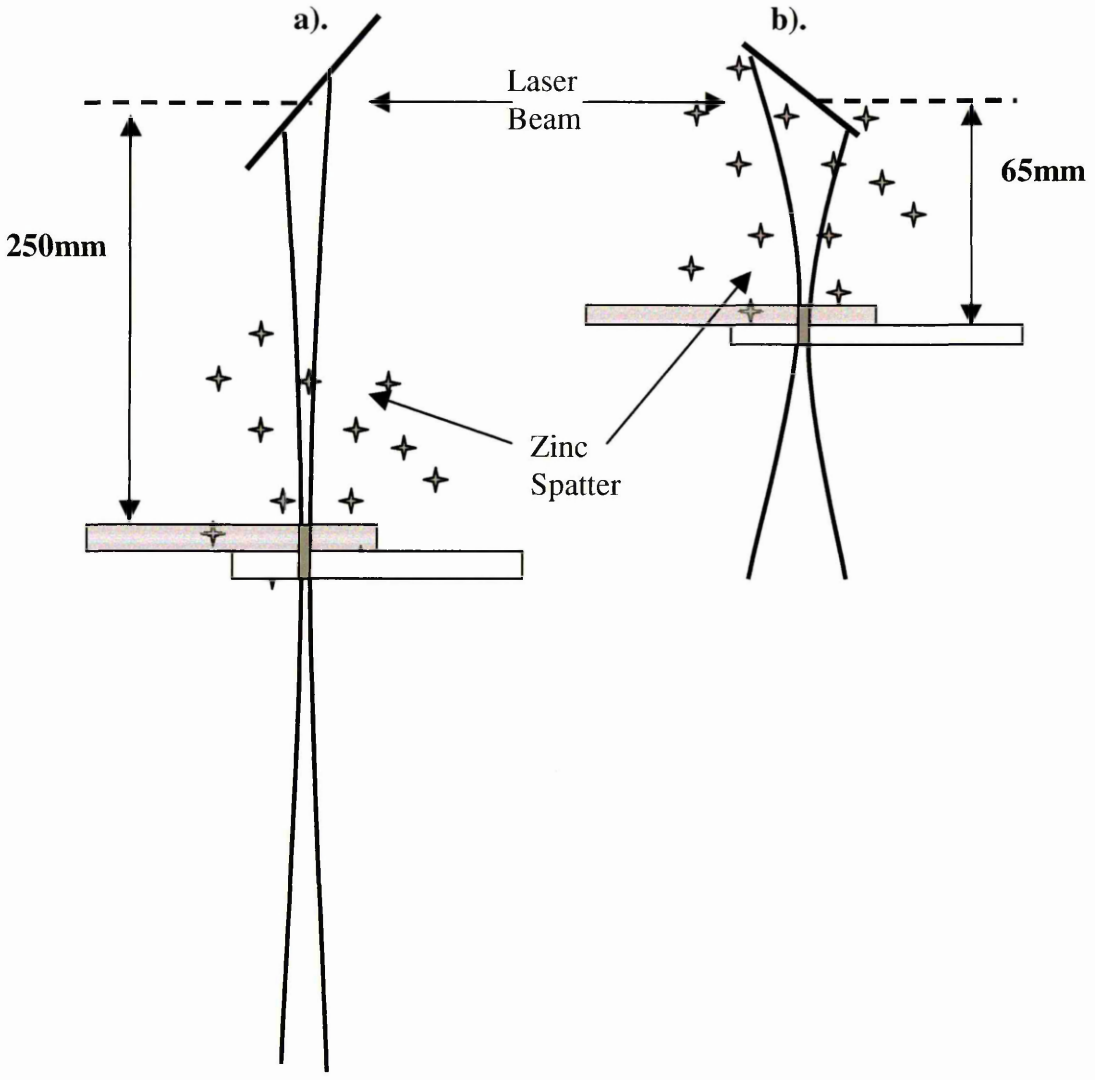

Figure 19 Schematic showing two laser welding 'set-ups', a) shows a laser set-up with a high focal length and b) with a reduced focal length, both systems have a mirror optic beam delivery and show the effects of spatter

It should be noted that the focal lengths shown in the above figure, are currently used by the Welsh Technology Centre Trumpf 5kW CO_2 Laser and Coventry Universities' Rofin-Sinar 2kW CO_2 laser.

Another way to use mirror optics without a nozzle and a short focal length is to use an optically transparent system that protects the focusing mirror from the spatter. One such system is the 'Air Knife'.

2.9.3.1 Air Knife

It is possible to use a reduced focal length with a mirror beam delivery whilst removing any possibility of damage to the focusing mirror. The air knife attachment is placed at the bottom of the aperture below the focusing mirror and blows compressed gas, usually air, across the face of the aperture. This jet or 'knife' of compressed air allows the laser beam to pass through uninhibited (optically transparent) whilst blasting any spatter that may come into contact with the gas, thus, protecting the focusing mirror. This system is currently used with Coventry University's Rofin-Sinar 2kW CO_2 laser welder which uses a focal length of 65mm.

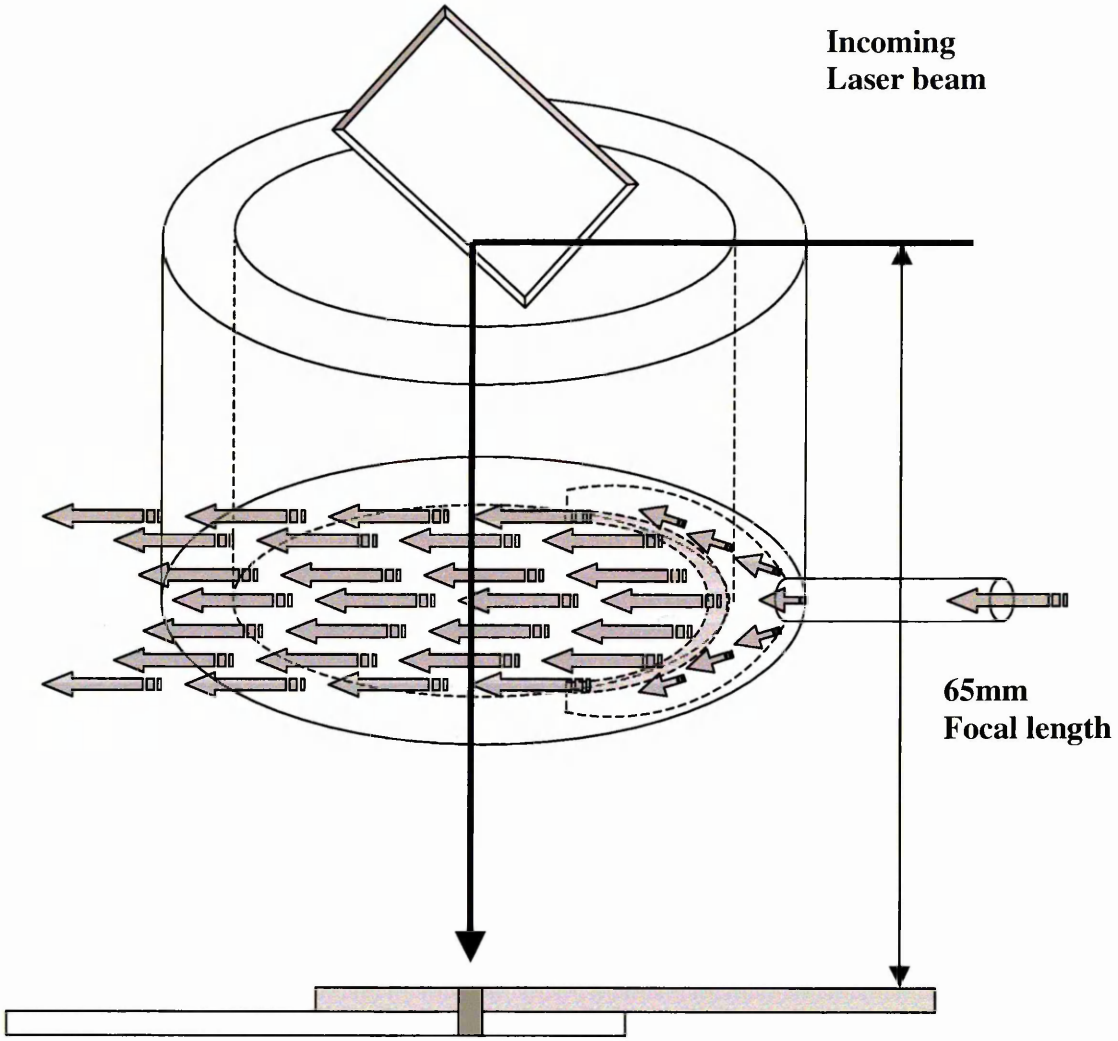

Figure 20 Schematic diagram showing a typical air knife assembly used to protect the focusing mirror when welding zinc-coated steel with a small focal length

Figure 20 shows that the open aperture below the focusing mirror is much closer to the sample than the stated focal length of the system. Without protection from the 'air knife' the spatter would be channelled up through the open aperture and onto the focusing mirror.

2.10 Laser Welding Stainless Steel

As explained in section 2.6, there are a number of different types of stainless steel. Laser welding has been successfully used to produce joints incorporating most of these steel types. Each type of stainless steel however, presents different welding problems, some of which have been characterised.

2.10.1 Austenitic Stainless Steels

Austenitic stainless steels are generally suitable for laser welding. Lower thermal conductivity of these steels grades allows slightly higher welding speeds to be achieved for the same laser welding parameters, e.g. welding power, focusing system etc, in comparison to mild steels. These higher welding speeds result in higher cooling rates due to the lower general heat input and are consequently advantageous in reducing the susceptibility to corrosion caused by the precipitation of chromium carbides at grain boundaries.

2.10.2 Duplex Stainless Steels

Laser welding of duplex and super-duplex stainless steels is also possible. The steel composition, laser parameters and shielding gas type can influence phase distribution in the weld metal. The low general heat input (higher cooling rate) associated with laser welds can reduce the proportion of austenite present in the weld metal and heat affected zone, which may impair the corrosion properties of the joint. One potential solution to increase the austenite content in the weld metal is to use nitrogen as a shielding gas, as this may increase the stability of the austenite phase during welding.

2.11 Laser Welding Aluminium

As stated in sections 1 and 2.5, the aluminium alloys are currently the most researched alternative material for integration into existing automotive design; and as laser welding has been identified as a key technology (which offers distinct advantages over conventional joining technologies) the laser welding of aluminium has been extensively researched.

In general, aluminium alloys possess poor laser weldability[4647], the main problems associated with laser welding aluminium alloys being high surface reflectivity, high thermal conductivity and volatilisation of lower boiling point constituents[25].

The use of Nd:YAG lasers are generally employed to weld aluminium alloys as the shorter wavelength of these lasers (1.06μm) compared to that of the CO_2 lasers (10.6μm) provides better coupling efficiency.

Research conducted by Pastor et al, revealed that the main problems with volatilisation of lower boiling point constituents were associated with Mg loss during laser welding of automotive aluminium grades. More specifically, Al-5xxx and Al-6xxx aluminium alloys, which are solid solution strengthened with Mg and precipitation strengthened with Mg_2Si respectively. The volatilisation of Mg during laser welding of both these alloy series affected the respective strengthening mechanism, which caused degradation of mechanical properties.

These and other material related problems have led to weld bead and heat affected zone cracking, degradation in mechanical properties and a general inconsistent welding performance.

In extreme cases, the laser weld can possess lower hardness and strength than the base material[47].

---

[46] Starzer, T. Ebner, R. Glatz, W. Ellermann, F. Kuhlein, W. Ellermann, W. Symposium on Automotive Technology and Automation, Proc. 26th, Aachen, 131, 1993

2.12 Laser Weld Solidification

The solidification process exerts a great influence on the microstructure and performance of welds[48]. The type of weld fracture and corrosion behaviour is closely related with phase chemistry, solute segregation and grain structure which is developed during weld solidification[49].

2.12.1 Austenitic Stainless Steel Solidification

Most austenitic stainless steels solidify as ferrite and transform to austenite on cooling to room temperature. This mode of solidification with 'primary ferrite' has a superior resistance to solidification cracking than primary austenite. This is attributed to reduced wetting of boundaries by liquid films and the complicated crack paths these boundaries form[49].

The solidification mode is primarily determined by chemical composition, and is quite insensitive to welding conditions (solidification conditions) unless the welding speed becomes extremely high (laser welding).

The primary phase is either ferrite or austenite, and is associated with the equilibrium primary phase as long as the solidification rate is within a range that conventional welding practices employ. The compositional boundary between the primary ferrite and the primary austenite should be at the equilibrium eutectic trough in the multi-component system of interest. This boundary, however, shifts to higher Cr side as the solidification rate increases, for example, in laser welding and electron beam welding[48].

---

[47] Ebner, R. Karaaslan, A. & Brandstotter, E. Laser Welding of Structual Components Made of Dissimilar Materials, pp 215 – 220.
[48] Koseki, T. Inoue, H. Ichikawa, K. Nogami, A. Prediction and Control of Weld Solidification in Steels and Ni-base Alloys. Keynote Adress, pp51-60
[49] Brooks, J.A. Thompson, A.W. Int'l Material. Rev, 36, pp 16, 1991

Consequently, the selection of the primary phase becomes non-equilibrium, where the austenite as the primary phase is favoured over the ferrite at high cooling rates of solidification[50].

The solidification modes of austenitic stainless steel can be seen in Figure 21, where the primary phase and the subsequent formation of secondary phases are major concerns.

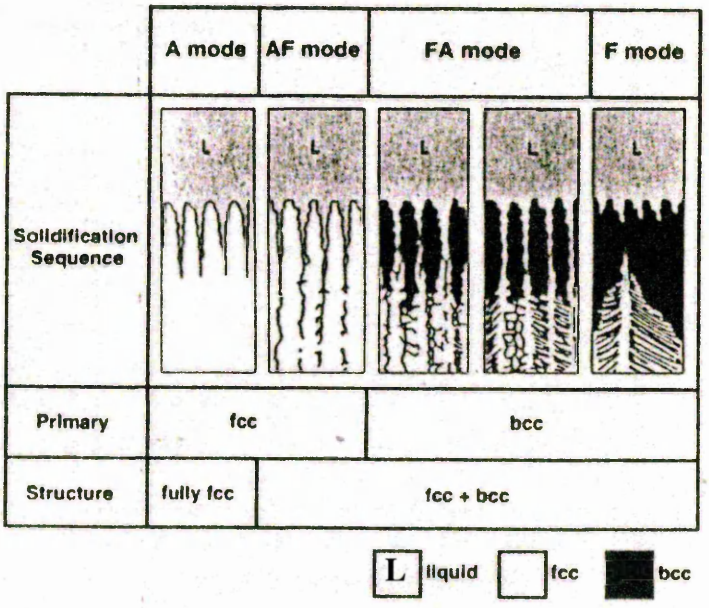

Figure 21 Schematics of Solidification Modes of Austenitic Stainless Steel Welds[48]

The effect of various laser-welding process parameters on the solidifying microstructures and associated cracking susceptibility were reported to be limited when compared to the influence of composition[51].

Prediction of the primary phase has been carried out using the Cr and Ni equivalents to take into account the effects of multiple components during solidification[52].

[50] David, S.A Vitek, J.M. Int'l Material. Rev, 34, pp213, 1989
[51] Pacary, G.M. Moline, M. Lippold, J.C. EWI Research Brief. B008, 1990
[52] Suutala, N. Metall. Trans. A, 13A, pp2121, 1982

Further research has since been carried out to produce a diagram (Figure 23) where values of %Fe and Cr-Ni equivalent ratios are compared with the eutectic compositions taken from the Fe-Ni-Cr ternary liquidus diagram, see Figure 22[53].

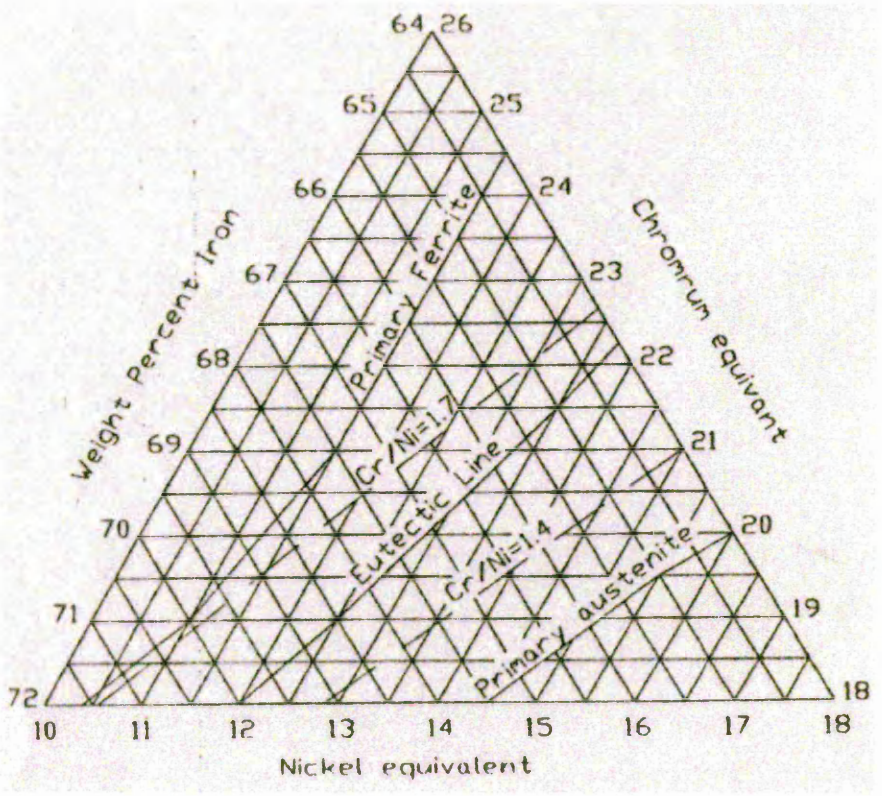

Figure 22 Relevant part of the Fe-Cr_{eq}-Ni_{eq} ternary liquidus diagram for austenitic stainless steels with eutectic and solidus lines[53]

[53] Yardy, J.W. Laursen, B.N. Microstructural Predictions for Laser Welded Austenitic Stainless Steels, pp89-92

Figure 23 predicts the primary solidifying phase for an alloy together with a rough estimate of the laser welding speed necessary to avoid primary phase shift from ferrite to austenite solidification.

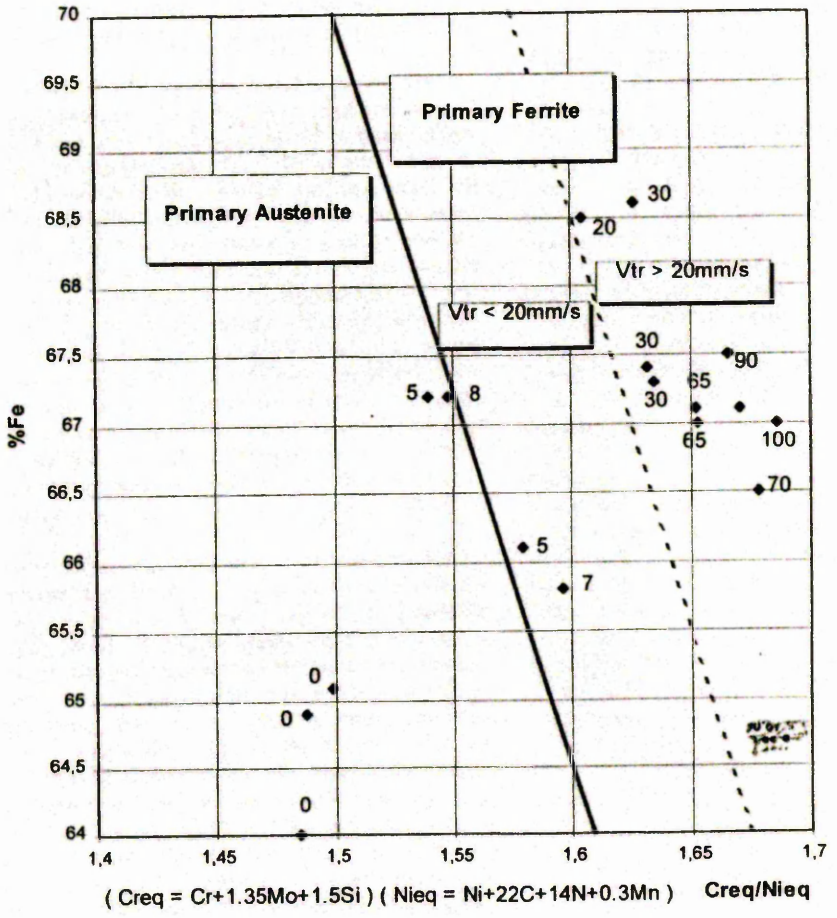

Figure 23 Diagram for predicting solidification mode from alloy composition for laser welded austenitic stainless steels. Values of solidification velocity for the transition from ferritic to austenitic primary solidification, Vtr, are shown for the alloys studies – 304 & 316[53]

Hence, it can be seen that alloys positioned above and to the right of the eutectic line solidify as primary ferrite, and those below and to the left, as primary austenite. The approximate welding speeds can also be seen.

Thus, the relationship found between solidification mode, transition velocity, and composition was that an increase in either the %Fe content or Cr_{eq}/Ni_{eq} ratio strengthens the tendency towards primary ferrite solidification and also increases the laser welding speed at which this occurs[53].

2.12.2 Duplex Stainless Steel Solidification

The low general heat input of the laser welding system produces very high cooling rates of approximately 1004°C/sec at the weld centre line. These high cooling rates, when laser welding duplex stainless steels, lead to high ferrite levels in the solidified weld bead[54]. Research conducted by Gooch et al, investigated the properties of resistance and laser welds in 2304 duplex stainless steel. It was found that autogenous 1mm 2304 laser welds contained approximately 90% ferrite, compared to the 30-40% ferrite contained in the 'as received' condition. Similarly, the ferrite contents in the HAZ were substantially ferritic[55]. The high ferrite content resulted in an increase in weld and HAZ hardness from 276Hv to 304 and 286-290 respectively, also a reduction in the corrosion resistance of the laser welded joints[55].

Image 3 shows localised pitting in the HAZ of a 1mm 2304 laser weld tested in 150ppm NaCl solution at 90°C.

There have been a number of techniques used to increase the austenite content of duplex stainless steel laser welds. These include:

1. The use of a nitrogen assist shielding gas to increase the austenite content of the weld metal[56].
2. The addition of a high alloy filler (22Cr, 9Ni, 3Mo) to increase the austenite content[55].

Optimisation of process conditions has been seen to increase austenite content, although, the use of a post weld heat treatment was required to produce a significant increase[54].

---

[54] Bonolio, F. Giordano, L. Tiziani, A. Zambon, A. Microstructural Optimisation of Laser Beam Welded Duplex Stainless Steel, Florence, Associazone Italiana Di Metallurgia, Milan, Italy, ISBN:88-85298-15-X, 1993, pp 3.251-3.257

[55] Gooch, T.G. Gin, B.J. Properties of Resistance and Laser Welds in UNS S32304 Duplex Stainless Steel. Duplex Stainless Steels 97, 5th World Conference, D97-024, pp 311-319

[56] Lawn, P. Deans, W.F. Shannon, G.J. Watson, J. Preliminary Investigation into the Laser Welding of Duplex Stainless Steel, Proc. Duplex Stainless Steels 94, Glasgow, UK, TWI Abington, 1994, paper

One recommendation made by Gooch et al, is that the high nitrogen duplex stainless steels are the preferred choice for laser welding, the welds produced being suitable for mildly aggressive media[55].

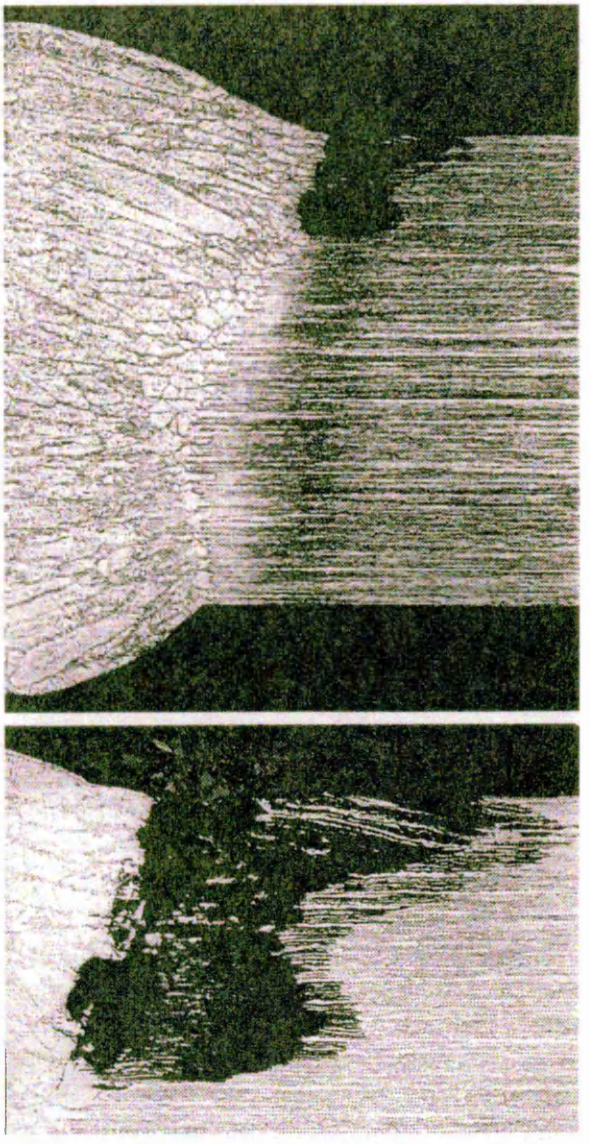

Image 3 Pitting in the HAZ of a laser weld tested in 150ppm NaCl solution at 90°C (top image x 35 & bottom x 130)[55]

Research conducted by Wray investigated the austenite contents of a number of resistance spot welded duplex stainless steels. The results revealed that higher austenite contents were present for the leanest grade of duplex stainless steel 2101 in comparison with the higher alloyed duplex stainless steels (2304, 2205, 2507). This was attributed to the increase in nitrogen content of the 2101 which had a greater mobility during the solidification process and thus provided the highest spot weld austenite content. As a consequence of the increased austenite content, the 2101 spot weld possessed the lowest hardness of the four duplex grades tested[57].

[57] Wray, T. Resistance Spot Welding of Duplex Stainless Steel, Transfer Report, Sheffield Hallam University, 2002

2.12.3 Low Alloyed Steel Solidification

The main feature of laser welds in plain carbon or low alloyed steels is the pronounced hardness increase in the melt zone and the heat affected zone (HAZ)[47].

This increase in hardness is attributed to the phase transformation to martensite during the rapid melt zone solidification subsequent to laser welding.

The properties of low alloyed carbon steels, for example, depend on the cooling rate in the critical temperature range from 800 - 500°C. In the case of laser welding this temperature range is usually passed within 0.5 – 2 seconds, which results in martensitic transformation[4758].

The hardness of martensitic microstructures generally depends on the carbon content[59], which is also true of laser welds[47]. The relationship between the weld metal hardness of low alloyed carbon steels as a function of the carbon content can be seen in Figure 24. This figure shows that for a martensitic structure, increasing the carbon content gave a pronounced increase in hardness.

[58] Ebner, R.E. Brandstatter, H. Klampf. Proceedings 26th Int Synopsium on Automotive Technology and Automation, Aachen, 349, 1993

[59] Pickering, F.B. Pysical Metallurgy and the Design of Steels, Applied Science Publishers Limited London, 1978

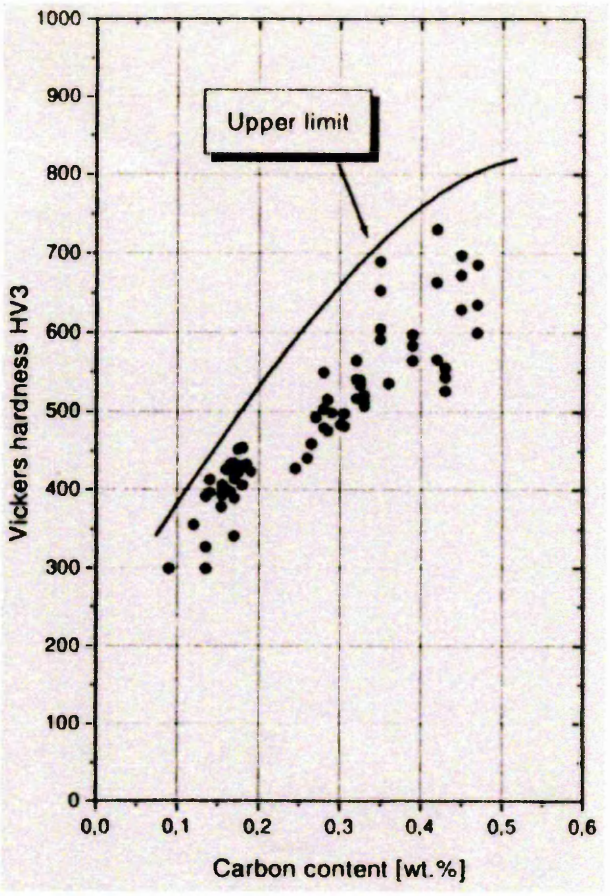

Figure 24 Hardness of the weld metal of low alloyed carbon steels as a function of the carbon content[47]

The result of the high weld and HAZ hardness is that the tensile strength of laser welded butt joints in low alloyed carbon steels usually equals that of the parent material or that of the softer material in a dissimilar metal butt joint[47]. However, the elongation to fracture is reduced as the hard weld does not contribute to the plastic deformation[47].

Similar trends have also been seen for the fatigue properties of low alloyed carbon steel laser welds, which usually show no loss in fatigue strength compared to the parent material[4760], if the welds are free of large defects.

It should be noted that exceptions are found in laser welded materials which can exhibit a pronounced hardness loss in the heat affect zone, for example, quenched and tempered steels with a high hardness level, also some aluminium alloys[47].

[60] Schutz, H. Szinjur, K. M. Radlmayr, H. Mildner, W. Schiefermuller: BHM 136, 430, 1999

2.13 Factors Affecting Weldability

As well as the laser welding process variables, there are a large number of other factors that affect weldability. When dissimilar metal welding austenitic or duplex stainless steel to zinc coated mild steel, these factors, outlined below, become even more critical and compromises are often necessary.

2.13.1 Thermal Conductivity

When welding dissimilar metals differences in thermal conductivity can have a profound effect on the shape and structure of the weld bead. Due to the nature of the laser welding process, the heat is applied to a small area on the surface of the material and then transferred through the material by conduction[17]. In a lap joint configuration the thermal conductivity properties of the material on the top and the bottom of the lap joint will affect the size, shape and thickness of the weld bead produced and, to a lesser extent, the penetration achieved for a given power and welding speed. The typical thermal and electrical properties of AISI 304, 2205, 2101 and mild steel can be seen in Table 2 [41 42 61].

[61] Bolton, W. Engineering Materials Pocket Book, Butterworth-Heinemann, 1989

2.13.2 Thermal Expansion Coefficient

With any welding process residual stresses can pose great problems. This is especially true when welding dissimilar metals with different coefficients of thermal expansion. Austenitic stainless steel has a higher expansion coefficient compared to that of mild steel. Thus, in any welded joint comprising these two materials, the stainless steel will be more prone to buckling and warping and will contract more than the mild steel on cooling. This greater contraction will result in higher residual stresses and increase the possibility of distortion and solidification cracking. High tensile residual stresses may severely reduce properties such as fatigue life. The thermal and electrical properties of austenitic and duplex stainless steel and mild steel can be seen in Table 2 [41 42 61]. The thermal and electrical properties of 2101 can also be seen in this table. This grade of duplex stainless steel is considered in section 2.8.2.1.

Steel	**Thermal expansion ($x10^{-6}$/°C) 200 –600°C**	**Thermal conductivity (W/m°C) 20°C**	**Resistivity (μΩ.m) 20°C**
304	17 – 19	12 – 15	0.60 – 0.75
2205	13	20	0.70 – 0.85
2101		16	0.75
Mild steel	12	64	0.16

Table 2 Thermal and electrical properties of 304, 2205 and mild steel.

2.13.3 Metallurgical Characteristics

Laser welding is characterised by its low specific heat input and high welding speeds; thus, the cooling rate is very high. Recent modelling studies indicate that the cooling rate from 800°C to 500°C in the HAZ of a HSLA steel is more than 100°C/s[31]. High cooling rate may result in deleterious phase transformation in the HAZ. Post weld heat treatments are seldom used with the laser welding process and add additional cost and time to fabrication.

When welding stainless steel, it is preferable to cool the material quickly to avoid the precipitation of $Cr_{23}C_6$, i.e. chromium carbide, as high cooling rates help to avoid sensitisation. Precipitation of chromium occurs at grain boundaries during cooling from 800 – 550°C and will produce areas denuded in chromium or "sensitised" adjacent to the weld[41]. These denuded areas will be susceptible to intergranular corrosion, as no passive film will form. On the other hand, high cooling rates may cause problems in many ferrous alloys by promoting martensite transformations which may produce higher residual stresses and be susceptible to hydrogen-induced cold cracking; however this also results in a smaller HAZ size.

Thus, there are a number of considerations to be taken into account when welding materials with such different properties and characteristics. There is also the potential of deleterious phases being present in the weld when dilution of austenitic stainless steel and mild steel occurs. The susceptibility of the duplex stainless steel to heat treatment may further exacerbate this problem when welded to mild steel. The dilution of the stainless steel will result in lower chromium and nickel content in the weld bead. As these elements stabilise ferrite and austenite phases (respectively) in the steel, they have a direct effect on the structure and phases produced, see Figure 25.

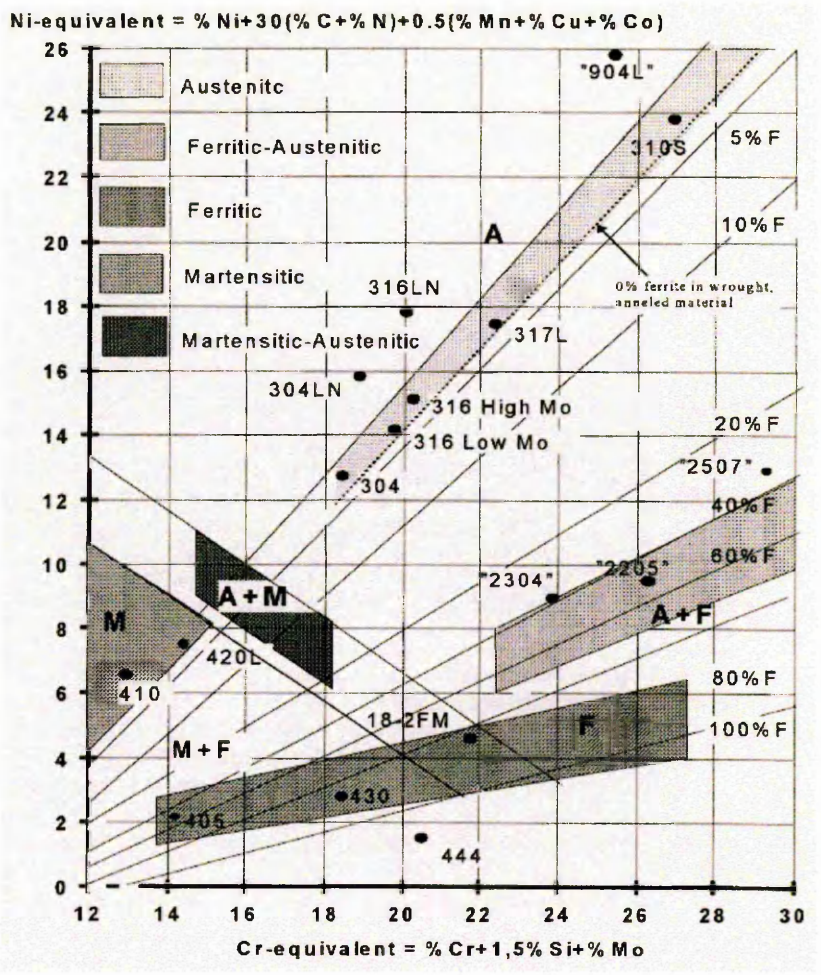

Figure 25 The Schaeffler Delong diagram[41]

2.13.3.1Liquid Metal Embrittlement

The intimate surface contact between the stainless steel and zinc coated mild steel may produce problems associated with environmentally assisted cracking. Liquid metal embrittlement (LME) cracking of austenitic stainless steels by molten zinc has been seen in many dissimilar metal joints when austenitic stainless steel is welded to galvanised steel[62].

There are at least four distinct forms of liquid metal embrittlement:

Type 1 Instantaneous fracture of a metal under an applied or residual tensile stress when in contact with certain liquid metals. This is the most common type of LME.

Type 2 Delayed failure of a metal when in contact with a specific liquid metal after a certain time interval at a static load below the ultimate tensile stress of the metal. This form involves grain-boundary penetration by the liquid metal and is less common than type one.

Type 3 Grain-boundary penetration of a solid metal by a specific liquid metal, which causes the solid metal to eventually disintegrate. Stress does not appear to be a prerequisite for this type of LME in all observed cases.

Type 4 High-temperature corrosion of a solid metal by a liquid metal, causing embrittlement, an entirely different problem from types 1 to 3.

---

[62] Bruscato, R. M. Liquid Metal Embrittlement of Austenitic Stainless Steel when Welded to Galvanised Steel, Welding Research Supplement, December 1992, page 455 - 459

There are two types of interactions between molten zinc and austenitic stainless steel that have been reported[63].

Molten zinc slowly erodes unstressed 300 series stainless steel at 419°C to 570°C penetrating (diffusing) primarily along the grain boundaries in a relatively slow manner. This phenomenon has been designated 'Type I' embrittlement.

'Type II' embrittlement occurs in stainless steel above 750°C when it is stressed and exposed to molten zinc. It is characterised by extremely rapid crack propagation perpendicular to the applied stress. This phenomenon is described as classic liquid metal embrittlement (LME).

Important microstructural factors that affect environment sensitive cracking of austenitic stainless steels are grain size, cold work (dislocation substructure, martensite formation), sensitisation, segregation, δ-ferrite and radiation damage.

The only way to completely prevent this phenomena when dissimilar metal laser welding austenitic stainless steel and zinc coated mild steel is to remove the zinc from the surface of the mild steel prior to welding.

[63] Metals Handbook, ninth edition, vol.11, Failure Analysis and Prevention, ASM page.236 - 237

2.14 Weld Geometry

The inherent flexibility of the laser system coupled with the ability to use NC/CNC/Robotics devices allows many welding patterns to be used[64]. As well as complex weld patterns; complex weld configurations can also be produced. This provides the ability to weld pre-formed sheets. The lap joint configuration is usually utilised due to the increased fit-up flexibility afforded from the overlap. Complex weld configurations utilise robotic laser control with up to six degrees of freedom axis. These systems, when coupled to a computer program can complete a 'trial weld' to allow a fine adjustment of the focal length and weld position etc. These systems can be used for mass production runs with very high accuracy and reproduction.

Figure 26 and Figure 27 show that the use of more complex welding geometries can improve fatigue properties[64]. However, in existing large-scale operations, where fit-up, reproduction and time are important factors; the single straight-line laser weld has the greater potential for integration[65].

	STRESS RANGE (MPa)				
PATTERN	200	170	150	120	100
Single straight-line	22,700		48,000	169,300	169,400
	19,600				265,000
Double straight-line	48,700		68,200	103,700	569,700
Triple straight-line			162,900		
Sawtooth	20,800	41,600	109,800	159,300	686,800
Double circular-arc	19,800		109,800	91,900	531,000
LLSG (7.6 mm)*	162,000	160,400	184,200		2,010,100**
	123,800				
LLSG (12.5 mm)*	179,100	333,200	571,800	2,283,200**	
Ladder			1,026,400		

*Weld length
**Did not fail in 2,000,000 cycles

Figure 26 Cycles to failure of different weld patterns in 0.61mm carbon steel[64]

[64] Albright, C. E. Hsu, C. Lund, R. O. Fatigue Strength of Laser Welded Lap Joints, Materials Joining Technology, July 1989, MR8905

[65] Smith, A. J. Nordberg, H. Cawely, J. Discussions with Supervisory Team, Sheffield Hallam University, 2000

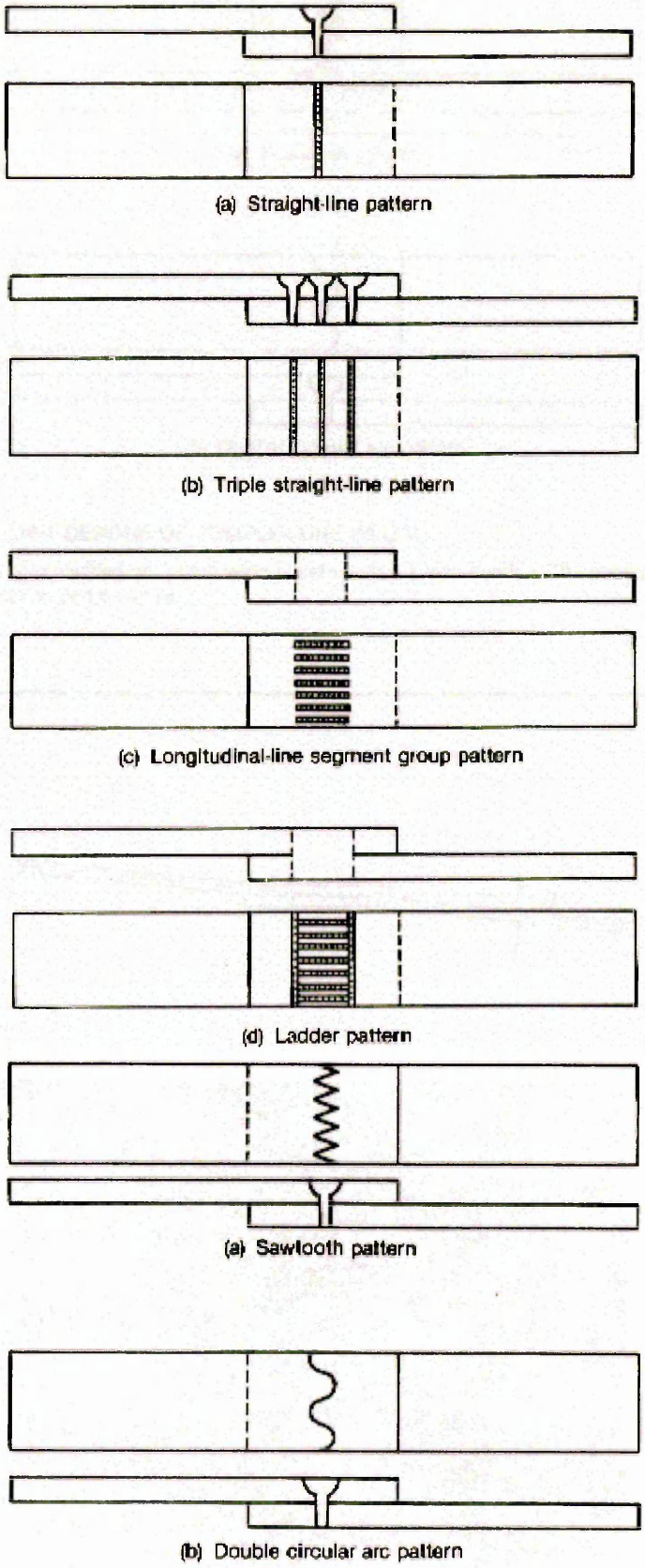

Figure 27 Visual key for the fatigue properties in Figure 26[64]

2.15 Joint Geometry

The flexibility of the laser welding system allows both butt and lap joints to be successfully welded.

2.15.1 Butt Joint

Tailored blanks have made a great impact on pressed sheet components in the automotive industry. Larger pressings can be made than with standard sized sheets, and dissimilar steel types or thickness can be joined. The resulting benefits are improved material use, potential weight savings and a reduction in subsequent assembly operations.

Currently, resistance and CO_2 laser welding are major welding processes used for tailored blanks. Typical welding speeds are 7m/min for 6kW CO_2 lasers.

In many applications where resistance spot welding has been traditionally used, laser welding can offer many advantages, including single side access and reductions in weight and costs by removing the overlap needed in resistance spot welding. It has been estimated that up to 60 kg (130 lb) of steel can be saved from an automobile by replacing resistance spot welding with laser welding and taking advantage of the design flexibility[66].

One problem associated with welding very thin sheets in the butt weld configuration is edge preparation and fit up. Tests have shown that if the gap between 1.50mm plates can be maintained at 0.2mm or less (which is possible with, for example, precision sheared edges) then it is possible to achieve welds at speeds of 10m/min in a typical tailored blank configuration using a 0.6mm spot size[67]. However, if the edges are not

---

[66] DiPietro, F. A. Robotic Laser Welding Systems in the Automotive Proceedings of Laser Systems Application in Industry, Italy, 1990, page103 - 119

[67] Sundnik, W. Radaj, D. & Erofeew, W. Computerised Simulation of Laser Beam Welding Formation Comprising Joint Gaps, J. Phys. D:Appl. Phys. 31 (1998), 3457-3480

precision sheared the gap between the plates can grow to at least 0.5mm or more over a length of weld. This can result in concavity of the weld bead, see Figure 28, which increases the stress ultimately reducing the tensile and fatigue properties of the weld.

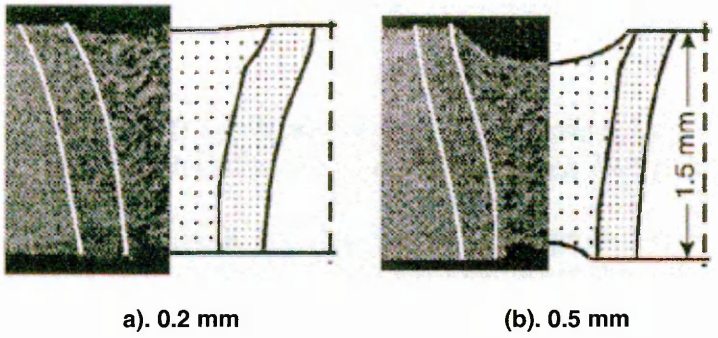

Figure 28 Weld cross sections in butt joints with smaller (a) and larger (b) gap widths[67]

2.15.2 Lap Joint

The lap joint configuration removes the problems associated with edge preparation and is the preferred configuration for laser welding; however, the configuration has some inherent problems of its own.

2.15.2.1Joint Rotation

When lap joints loaded in tension, or tested either in lap-shear tests or in fatigue tests, the eccentricity of the applied load introduced by the lap joint configuration results in rotation of the lap joint. It can be seen from Figure 29 below that increasing sheet thickness in the lap joint configuration would increase the eccentricity of the applied load.

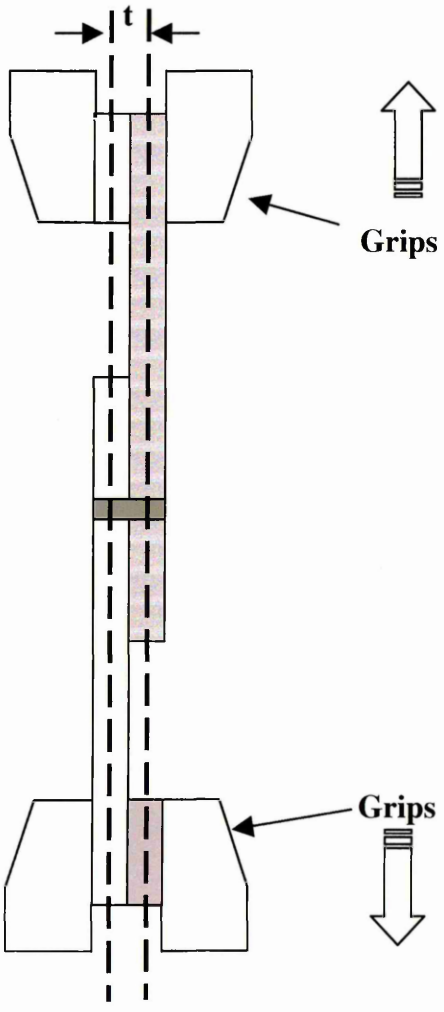

Figure 29 Lap joint schematic showing the increase of misalignment of the applied load with increasing sheet thickness

Lap joint rotation, seen in Figure 29, is larger for thicker materials and has been seen to reduce fatigue life[68]. The greater the eccentricity of the applied load, the more rotation has to occur to align the applied load. This can be seen from Figure 30, which shows the angle of rotation the lap joint is subjected to in order to align the applied load.

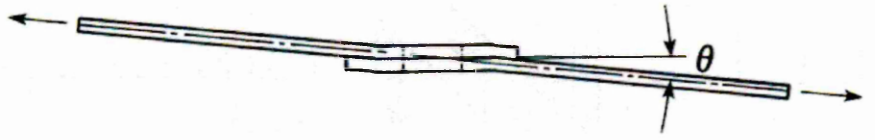

Figure 30 The rotation resulting from a lap joint loaded in tension[69]

[68] Albright,C. E. Hsu, C. & Lund, R. O. Fatigue Strength of Laser-Welded Lap Joints, Materials Joining Technology, July 1989, MR8905

[69] Dieter, G. E. Mechanical Metallurgy SI Metric Edition,McGraw-Hill Book Co (UK) Limited, ISBN 0-07-100406-8

This lap joint rotation results in an applied bending moment to the joint[70] [71]. The applied bending moment of the lap can be explained by analysing the reaction forces and moments that occur in the laser welded lap joint specimen[70].

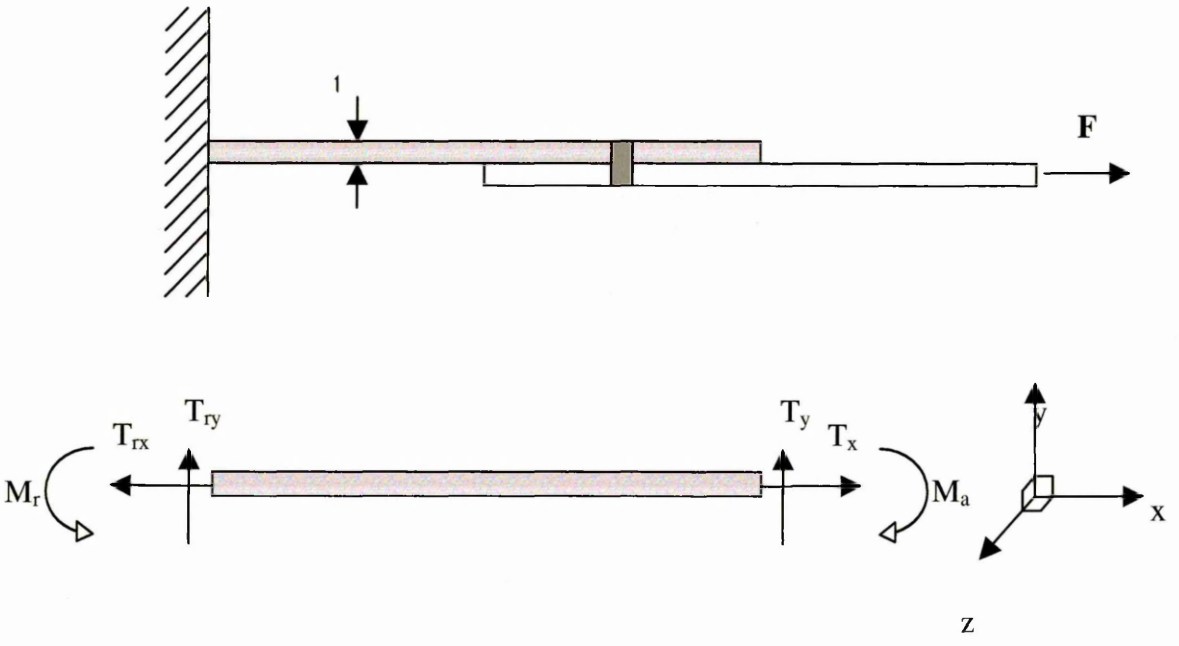

Figure 31 schematic diagram of reaction forces and moments that occur in a laser-welded lap joint[70]

It should be noted that M_r and T_r are reaction moment and force which develops for rigid loading of the specimen[70].

[70] Linder, J. Nilsson, K*. Meurling, F. Engstrom, H*. Larsson, M. Fatigue Strength of Laser welded Stainless Steel sheets, Swedish Institute for Metals Research, Sweden, *Lulea University of Technology, report no: IM-2000-529, ISSN: 1403-848/X

[71] Kaitanov, A. Investigation of Static and Fatigue Strengths of Stainless Steel Laser Welded Over-Lap Joints with Controlled Penetration, Experimental and Theoretical Study, St. Petersburg State Marine Technical University of Ocean Technology, 2001

The applied bending moment can be calculated from the following equation.

$$Ma := F \cdot \frac{(t + g)}{2} \quad (Nmm)$$

Equation 2 Applied bending moment

where:

Ma = applied bending moment

F = applied force

t = sheet thickness

g = interfacial gap

Equation 2 assumes a similar sheet thickness. Where dissimilar sheet thickness is present *t* is replaced with the following equation.

$$t := \frac{(t1 + t2)}{2} \quad (mm)$$

Equation 3 Average sheet thickness

Where:

t1 = sheet 1 thickness

t2 = sheet 2 thickness

The rotation and resulting bending moment change the mode of loading applied to the lap joint from a mode-II to a mode-I. As it can be seen from Figure 32, mode-I is an opening mode and is more detrimental to lap joint fatigue properties than mode-II.

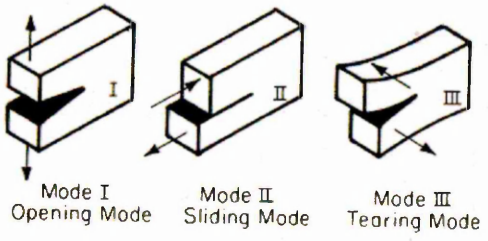

Figure 32 Modes of loading which involve crack surface displacement[69]

2.16 Fatigue Properties

Fatigue testing has been conducted by numerous researchers on similar metal laser welded lap joints[7071]. There are two main types of stress life fatigue data that can be produced to assess a joint's fatigue properties. These are high stress-low cycle fatigue and low stress-high cycle fatigue. The selection of the type of testing required depends on the level of stress the joint will be subjected to in service. However, if time (test frequency at resolvable load) and money are critical factors, high stress-low cycle fatigue can be conducted to produce a series of results that can be extrapolated to give an indication of the joint fatigue properties at lower stress and higher cycles. In some situations this may be feasible, as the scatter of cycles to failure increases at higher fatigue lives, but, obviously, there is no substitute for conducting the tests and generating the results at these lower load levels and higher cycles.

Although research has been conducted to determine the fatigue properties of laser welds in excess of $2x10^6$ cycles (spot welds fatigue properties have been produced at $10x10^6$ cycles) there is very little data for the statistically valid mean fatigue strength of laser welds at pre-assigned cycle lives, for example, $2x10^6$ cycles.

If the joint fatigue property of interest is the mean fatigue strength at a pre-assigned cycle life, for example $2x10^6$ cycles then a test method must be employed to generate the results and determine the mean fatigue strength whilst accounting for the test scatter. One method which allows the determination of a joint's mean fatigue properties is the staircase method. This method also allows the mean fatigue properties to be validated statistically.

There is no current literature on similar metal laser welded lap joint mean fatigue properties. Research to determine the statistically valid mean fatigue properties ($2x10^6$ cycles) of spot welded joints has been conducted by Marples and Wray, who investigated dissimilar metal joints between stainless steel and zinc coated mild and similar metal duplex stainless steel joints respectively[38][72].

The majority of similar metal laser welded lap joint fatigue properties are characterised by three or more load or stress ranges, with three or four tests at each load or stress range. These results are then used to insert trend lines and thus, indicate the fatigue properties at higher cycle lives.

The following fatigue results from previous work, here, are presented using the line load range unit (unless otherwise stated). This is simply the applied load range per unit length and allows comparison of dissimilar thickness joints on a line load bearing basis. See section 4.6 for a comprehensive explanation of the line load range unit.

[72] Wray, T. Resistance Spot Welding of Duplex Stainless Steel, Doctoral Thesis, Sheffield Hallam University, 2004

2.16.1 Similar Metal Laser Welded Stainless Steel Fatigue Properties

Research conducted by Linder et al, investigated factors affecting laser welded stainless steel (cold rolled SS2333 austenitic stainless steel) lap joint fatigue properties[70]. The welds were produced using an Nd:YAG laser producing a maximum power of 3kW at the work piece. The results were presented using P_{max} (kN)/cycles to failure.

The following graph shows the effects of weld width on the fatigue properties of similar metal stainless steel laser welded lap joints.

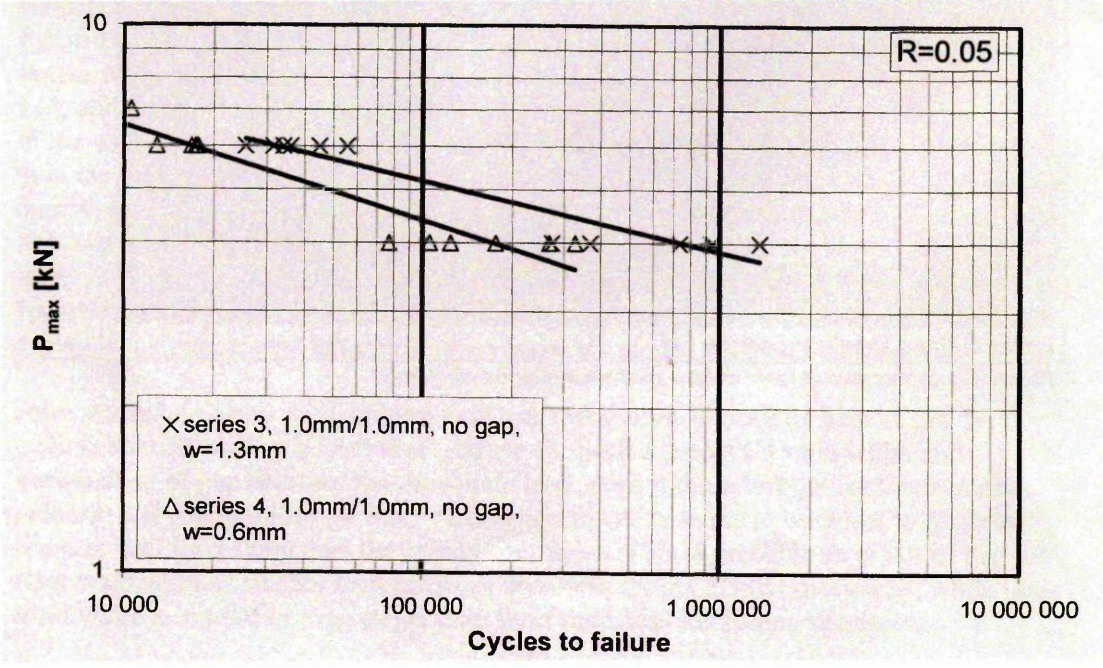

Graph 1 Effect of weld width on laser welded stainless steel lap joint fatigue properties[70]

It can be seen that for the same sheet thickness and no interfacial gap, increasing the weld width (between the sheets), increases the fatigue properties of the lap joints.

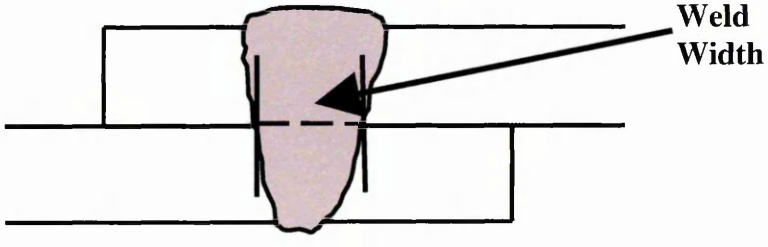

The following graph shows the effect of interfacial gap on the fatigue properties of similar metal stainless steel laser welded lap joints.

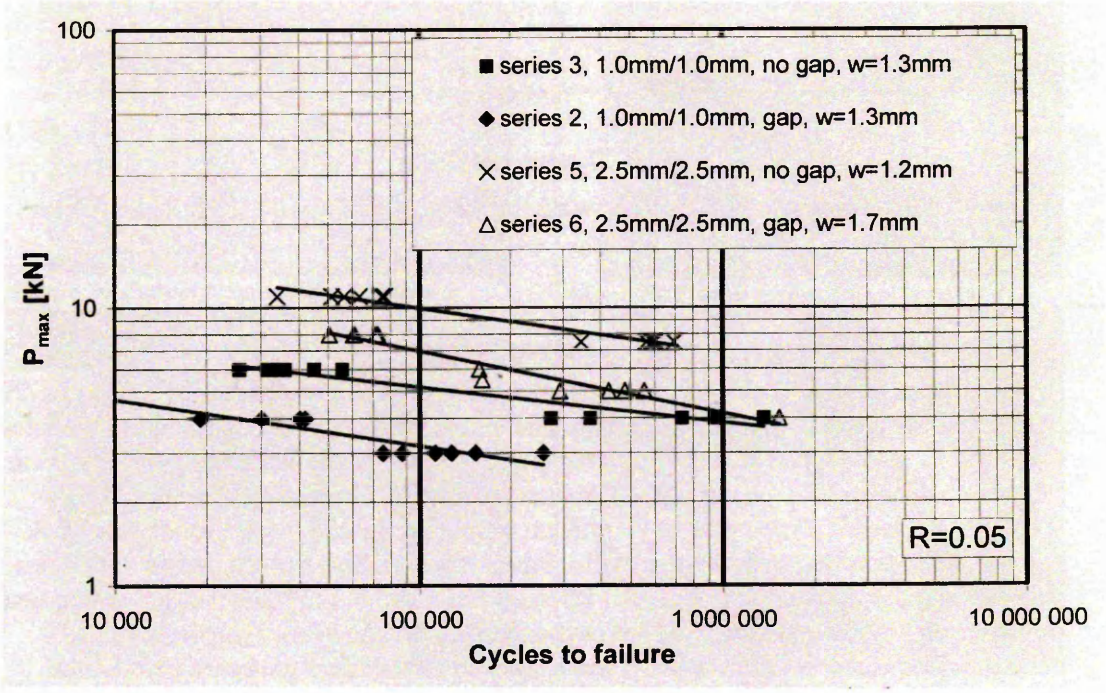

Graph 2 Effect of interfacial gap on laser welded stainless steel lap joint fatigue properties[70]

Graph 2 shows that the presence of an interfacial gap between the sheets reduces the fatigue properties of the respective lap joint configuration. It can also be seen that the trend lines for the 1mm/1mm, no gap, w=1.3mm and 2.5mm/2.5mm, gap, w=1.7mm appear to diverge at approximately 1.6 x 10^6 cycles. This illustrates the large influence of sheet gap on the high cycle fatigue properties. Linder et al concluded that increasing the gap from ~0mm to 40% of the sheet thickness reduced the allowable fatigue load by ~40% to obtain a similar number of cycles to failure[70].

The following graph shows the effect of sheet thickness on the fatigue properties of similar metal stainless steel laser welded lap joints.

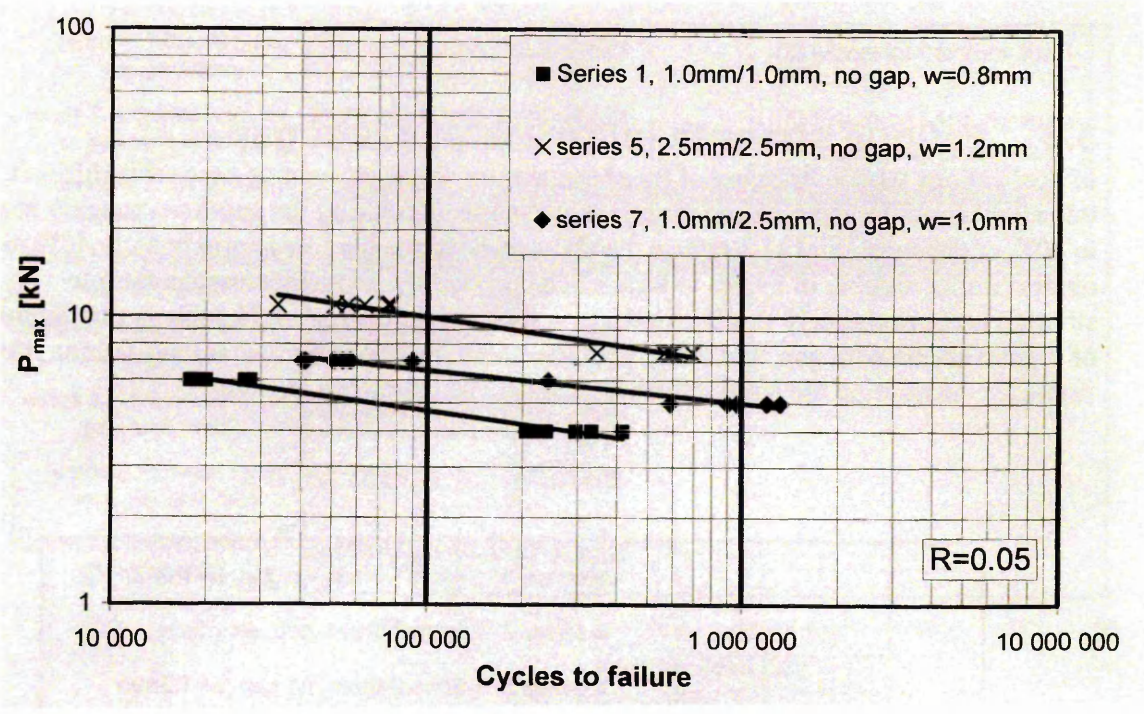

Graph 3 Effect of sheet thickness on laser welded stainless steel lap joint fatigue properties[70]

Graph 3 indicates that increasing the sheet thickness of even one of the sheets improves the fatigue properties of the similar metal stainless steel lap joint. Linder et al stated that the amount of rotation depended primarily upon the sheet thickness, since the resistance to bending of a sheet is proportional to the thickness squared[70]. It should be noted that Graph 3 not only shows the fatigue strength influence of sheet thickness, but also the affect of weld width.

Similarly, research conducted by Kaitanov revealed that improved 3mm 304 similar metal laser welded lap joint fatigue properties were achieved with a wide (as opposed to a narrow) weld width, see Graph 4[87].

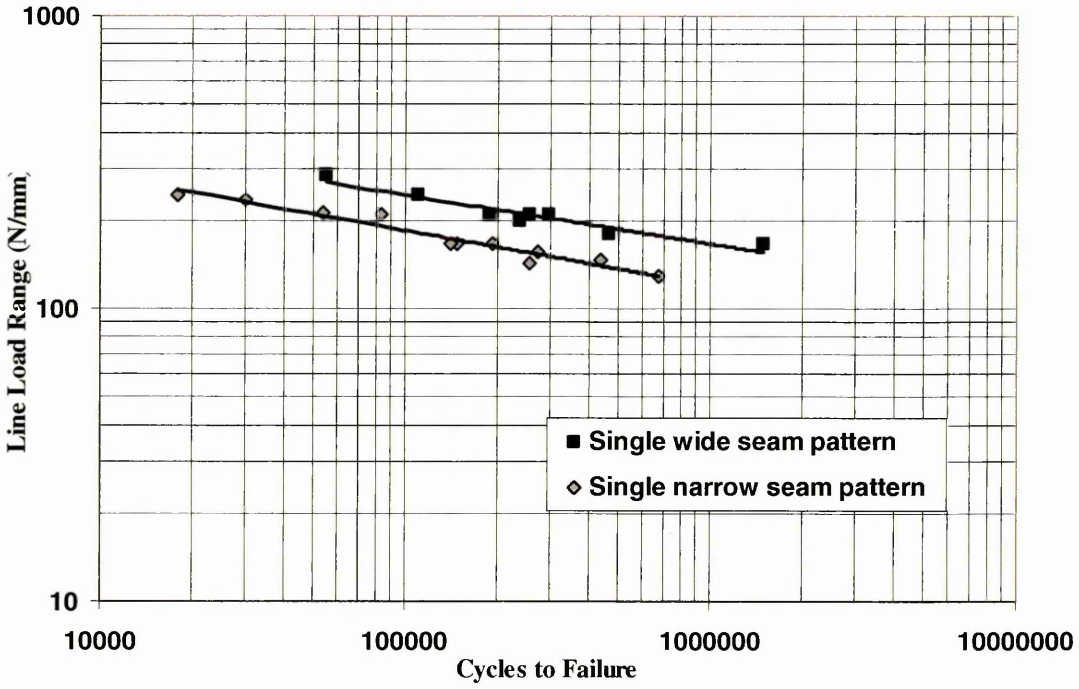

Graph 4 3mm 304 lap joint fatigue property comparison with a wide and narrow weld width[87]

Kaitanov also investigated the effects of a double narrow weld seam pattern on the lap joint fatigue properties of 3mm 304 austenitic stainless steel[87]. The results showed higher fatigue properties were achieved with the double narrow weld seam pattern as opposed to the single narrow weld seam pattern, see Graph 5. A similar trend can be seen in section 2.14, through the research conducted by Albright et al, which shows higher lap joint fatigue lives were achieved at the same stress level for the double weld seam when compared to the single weld seam configuration.

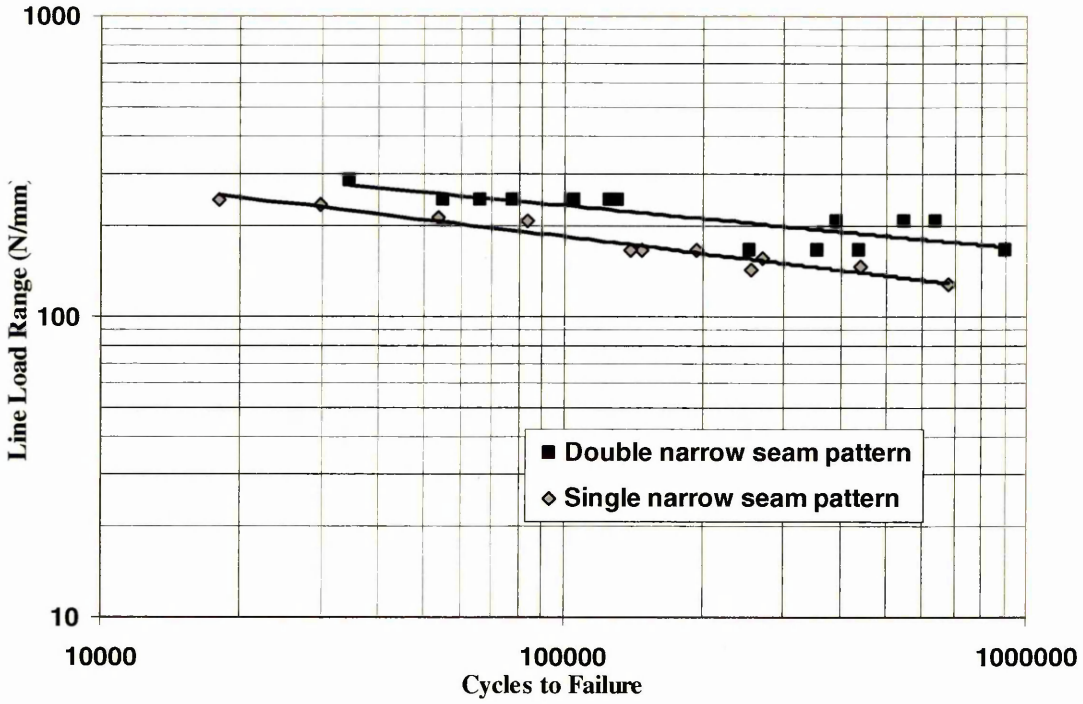

Graph 5 3mm 304 laser welded lap joint fatigue comparison for double and single narrow weld seam patterns[87]

Thus, it can be seen that higher fatigue properties were achieved with the double weld configuration.

Kaitanov also found that similar fatigue properties were achieved with both the double narrow seam penetration and the single wide seam pattern. However, the weld widths were not characterised during this investigation.

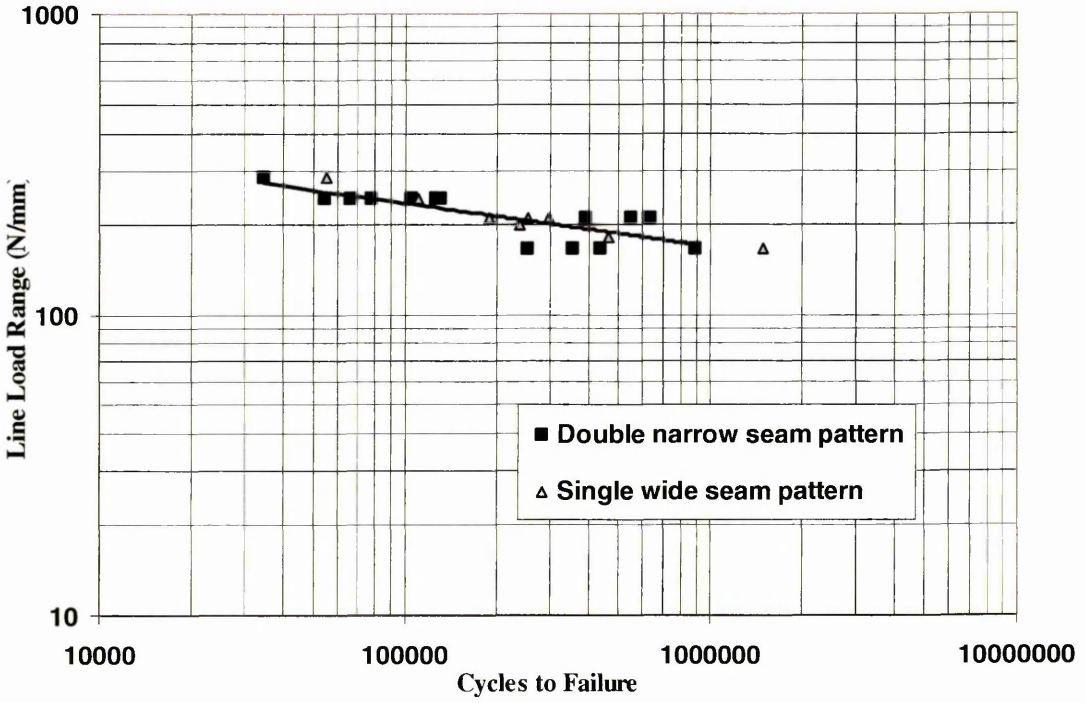

Graph 6 3mm 304 lap joint fatigue comparison between a double narrow and single wide seam pattern

2.16.1.1Laser Welded Lap Joint Fatigue Failure Criteria

The fatigue failure criterion has to be selected carefully to provide reproduction of tests to allow comparison of the fatigue data produced. For resistance spot-welds, the fatigue failure criterion is usually determined by a pre-assigned cyclic elongation, for example, 2mm. This is due to the nature of spot weld fatigue failures, where fatigue crack initiation at the periphery of the nugget causes plastic deformation, rotation and appreciable elongation prior to sheet separation.[73].

Similarly a fatigue failure criterion has been assigned to laser welded lap joints. Tests have been carried out to determine the fatigue test specimen stiffness over the duration of a fatigue test. These tests show that the lap joint stiffness dramatically decreases prior to failure and sheet separation, see Figure 33. Thus, the fatigue failure criterion has been defined as total sheet separation[70].

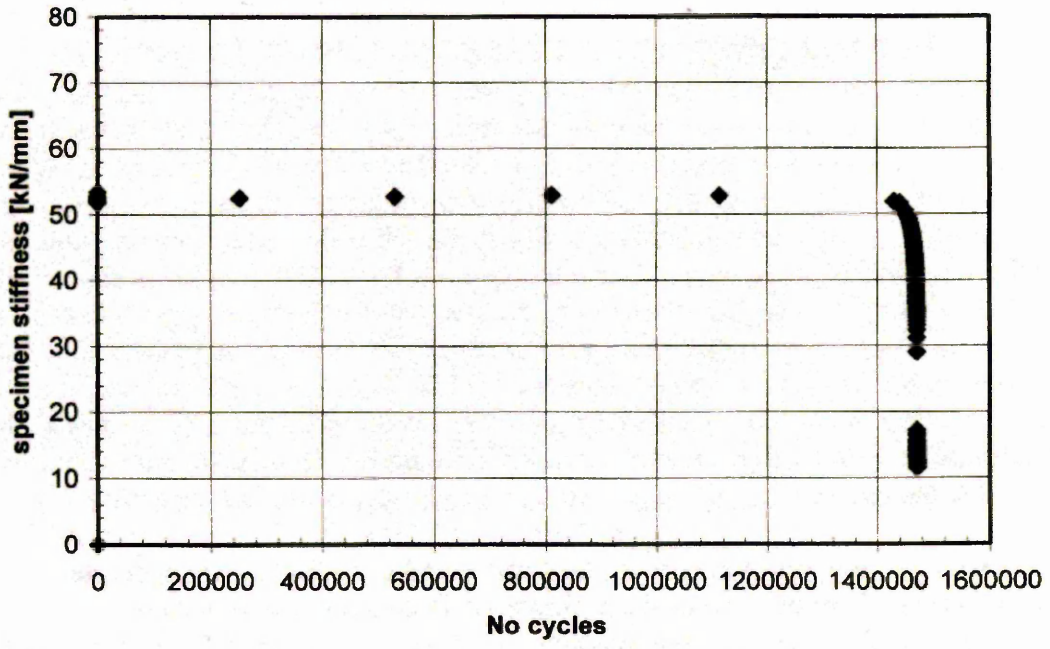

Figure 33 Graph showing the reduction of lap joint specimen stiffness prior to fatigue failure

[73] Marples, M. Resistance Spot Welding of Autstenitic Stainless Steel to Galvanised Mild Steel, Unpublished Work, Sheffield Hallam Univeristy, 2003

2.16.2 Similar Metal Laser Welded Mild Steel Fatigue Properties

Linder et al compared the fatigue properties of similar metal stainless steel laser welded lap joints with similar metal carbon steel laser welded lap joints[74]. In order to normalise the results to allow fatigue comparison of dissimilar thickness joints with and without interfacial gaps, the results were presented using nominal sheet stress and the calculated applied bending moment (Equation 2). The use of the applied bending moment allows the interfacial gap to be used as a damage parameter; however, the disadvantage is that sheet thickness has to be considered separately.

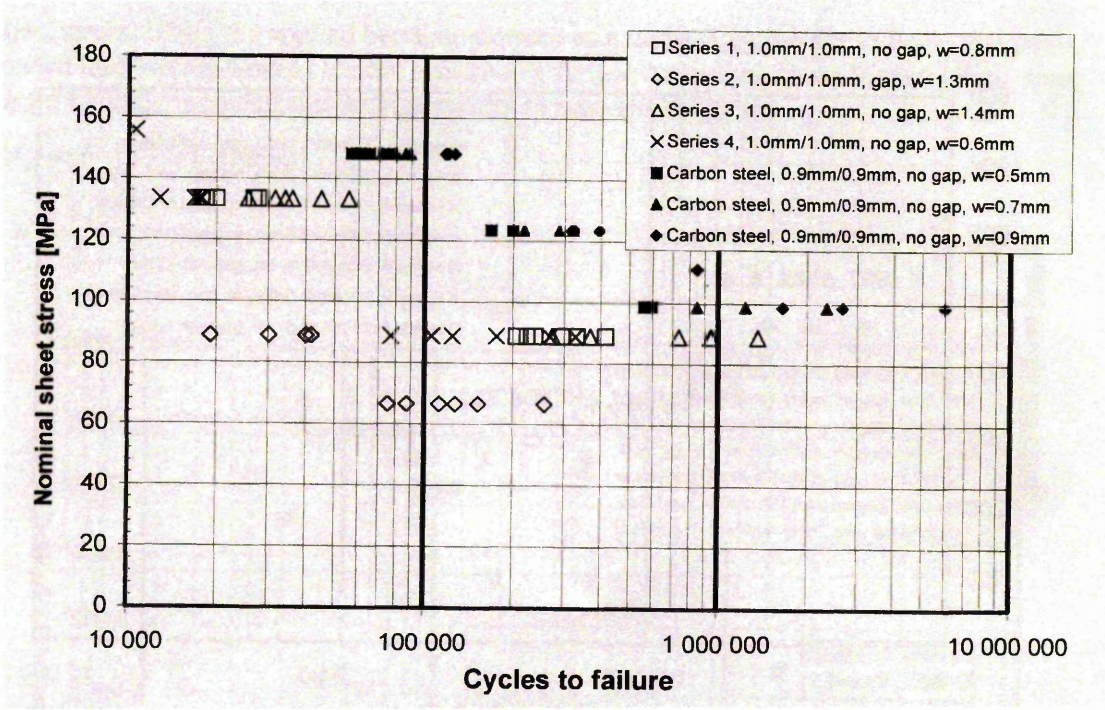

Graph 7 Nominal sheet stress stainless steel/carbon steel laser welded lap joint fatigue comparison[70]

Thus, it can be seen that higher fatigue properties were achieved by the carbon steel laser welded lap joints in comparison to the stainless steel lap joints. Even with a wider weld between the sheets, the 1mm/1mm, no gap, w=1.4mm stainless steel fatigue properties were lower than the carbon steel grades, which all possessed lower weld widths.

---

[74] Larsson, J.K. Abdulwahab, F. Meurling, F. Fatigue Properties and FE-Simulation of Laser-Welds, Proc. 7th Nordic Conference in Laser Processing of Materials (NOLAMP), eds Kujanpaa, K. and Ion, J. vol 1, pp 55-61, 1999

It should be noted however, that the use of the nominal sheet stress increased the carbon steel similar metal joint fatigue properties, as the sheet thickness was 0.9mm in comparison to the 1mm stainless steel fatigue properties.

The applied bending moment fatigue comparison can be seen in Graph 8 below.

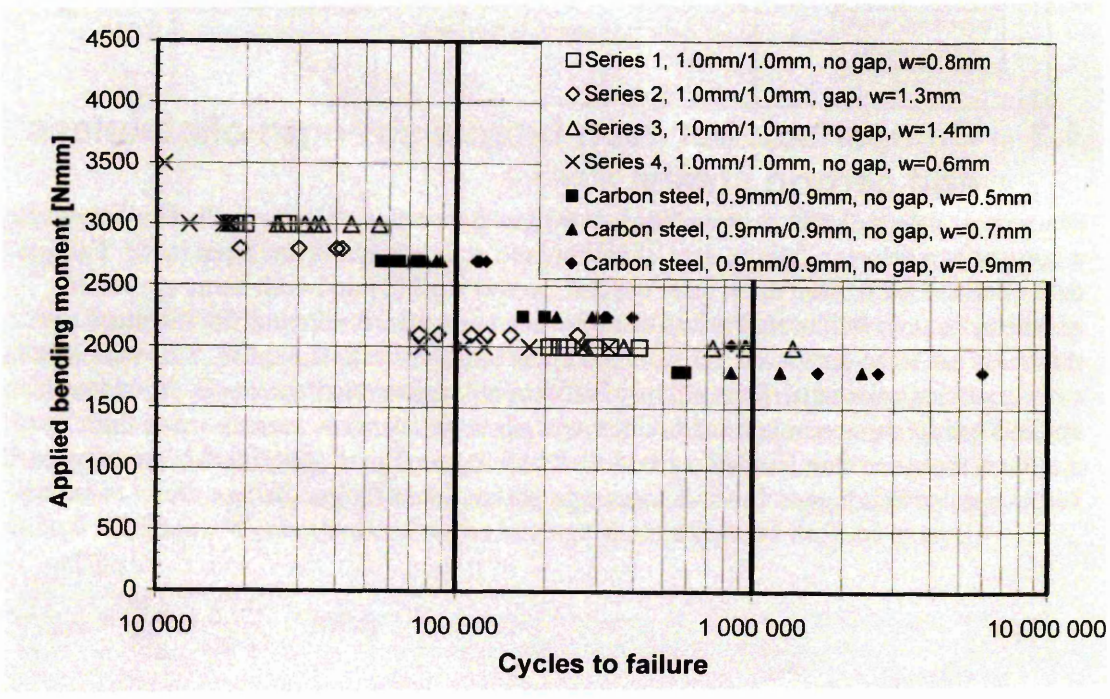

Graph 8 Applied bending moment stainless steel/carbon steel laser welded lap joint fatigue comparison[70]

It can be seen that when the applied bending moment is used as a damage parameter, the scatter decreases and the similarity between stainless steels and carbon steels increases. The conclusion drawn was that the applied bending moment could be used as a damage parameter for the assessment of lap joint fatigue properties[70].

2.16.3 Similar Metal Laser Weld Fatigue Failure

Similar metal laser welded lap joint fatigue failure was found to occur at the weld edge fusion line at the internal lap face. This was found for both similar metal stainless steel and carbon steel lap joints and was insensitive to microstructure, with fatigue failure being observed in the parent material, heat affected zone and in the laser weld[70,71,74]. Research by Linder et al revealed that fatigue failure occurred at the weld edge (fusion line) between the sheets and propagated through the sheet approximately perpendicular to the applied load[70]. The initiation angle was observed to be approximately 75 - 80° from the centre of the specimen and is illustrated in the following image.

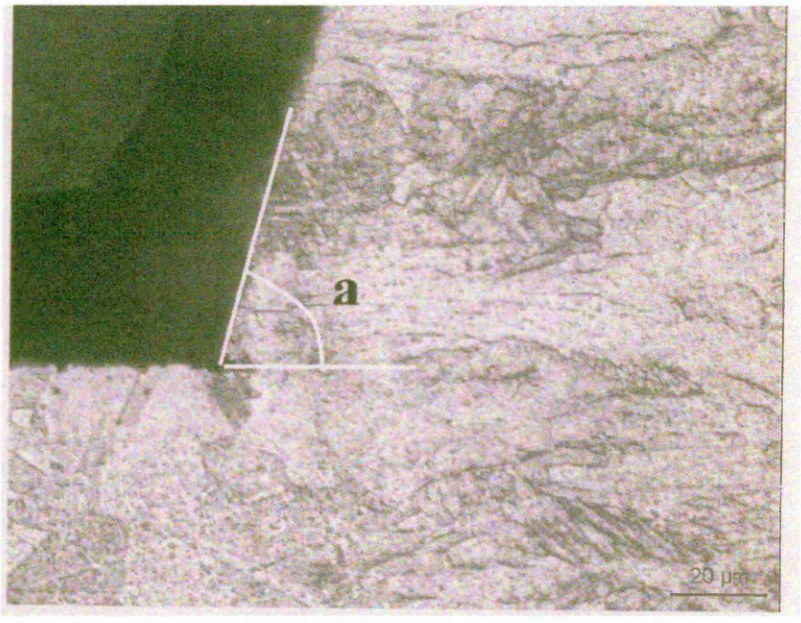

Image 4 Fatigue crack initiation angle of a similar metal laser welded stainless steel lap joint

2.16.4 Finite Element Analysis – Similar Metal Lap Joints

In order to understand how sheet thickness, interfacial gap and weld width can affect the fatigue properties of laser welded lap joints, research using FE analysis has been conducted to determine the effect joint rotation has on the stress distribution during similar metal, similar thickness lap shear or lap joint fatigue loading.

Finite element analysis of lap joints under a static load has been conducted by Kaitanov[71]. Figure 34 is an FE stress analysis of a laser welded lap joint, which shows the stress distribution present in the lap joint under an applied static load of 15kN. The simulated laser weld is in 3mm 304 and has a width of 0.86mm[71].

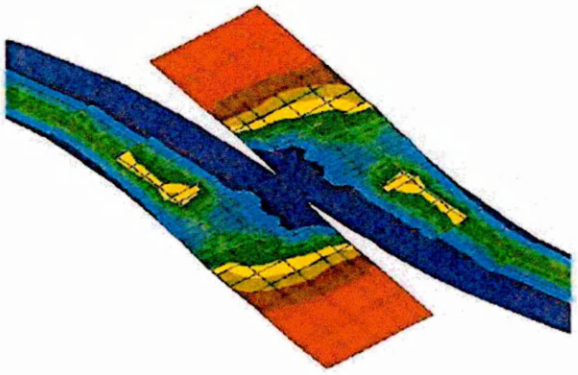

Figure 34 FEA stress concentration distribution in a statically loaded 3mm laser welded lap joint[71]

It can be seen that the greatest stress, depicted by the area in purple, runs along the internal lap face of the two sheets and across the weld width between the two sheets.

Finite element simulation of laser welds during crash testing also showed the greatest stress was present at the internal lap face[75]. This can be seen from the FEA plots in Figure 35, which show the effective plastic strain and von Mises effective stress at 2mm displacement for a 1mm DDQ steel similar metal laser welded lap joint subjected to a 10m/s impact velocity.

---

[75] Melander, A. Finite element simulation of crash testing of laser welded joints, Swedish institute for metals research, IM-2000-062, ISSN: 1403-848/X

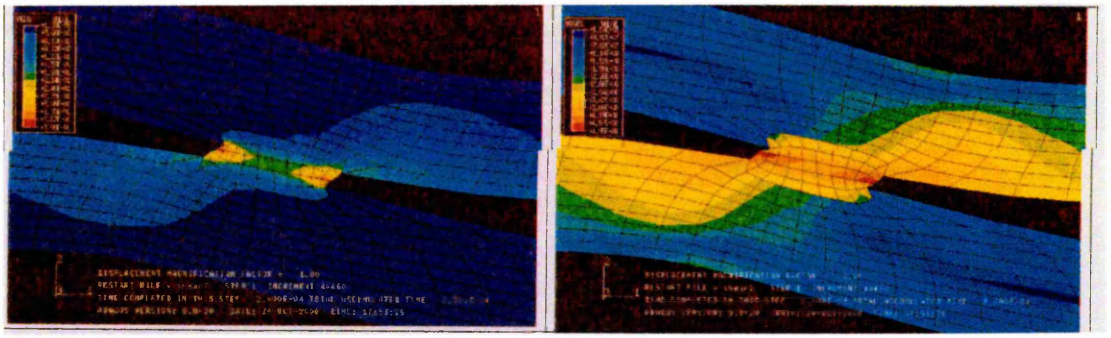

Figure 35 **Effective plastic strain** **von Mises effective stress**

for a 1mm similar metal laser welder lap joint at 2mm displacement when subjected to a 10m/s impact load[71]

Similarly, it was found that the greatest von Mises stress occurred at the internal lap face at the edge of the weld.

These FE analyses correlate with the similar metal fatigue failures positions characterised by Linder et al.

Increasing the sheet thickness increases the stress concentration at the internal lap face. This is the single most important lap joint fatigue property controlling factor as it directly affects the applied bending moment.

There are two schools of thought for the effect of weld width on the fatigue properties of laser welded lap joints. The first is that the weld width should equal the sheet thickness or average sheet thickness for dissimilar thickness lap joints. This was corroborated by Helin[76], who carried out solid element analysis of the stress intensity versus weld width for a 0.9mm laser welded lap joint. Figure 36 below shows the graph of stress intensity versus weld width.

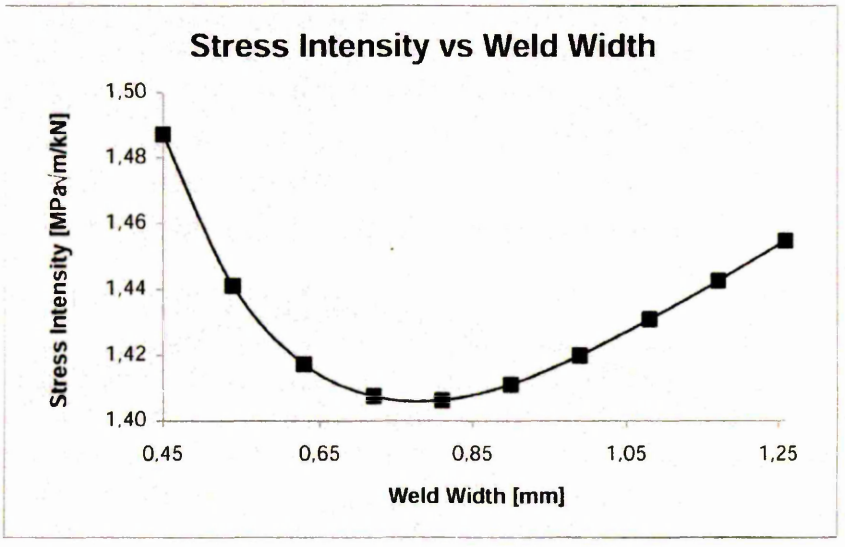

Figure 36 Solid element analysis of stress intensity versus weld width for a 0.9mm laser welded lap joint

It can be seen that the lowest stress intensity was achieved with a weld width (between the sheets) of 0.8mm, which was approximately 90% of the sheet thickness.

[76] Helin, W. Finite element analysis of fatigue loaded laser welded lap joints, Swedish institute for metals research, Stockholm, Aug 2000, ISSN: 1403-848/X

The second school of thought, corroborated by the fatigue results of Linder et al states, the wider the weld the higher the lap joint fatigue properties[70]. This is due to the increase in weld width decreasing the average stress within the weld. This is shown in Figure 37 below[70].

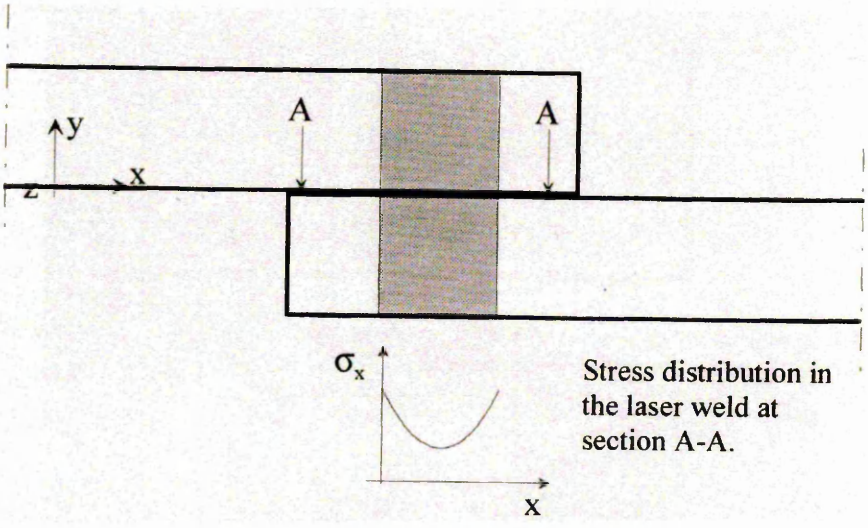

Figure 37 Schematic representation of the stress distribution for a shear loaded lap joint

As can be seen, the stress is highest at the weld edge in comparison to the weld centre, thus, although increasing the weld width would reduce the average stress within the weld; the effects are less pronounced when compared with sheet thickness and applied bending moment.

Solid element analysis was conducted by Helin to find the critical angle of laser weld fatigue initiation. The following graph shows the stress intensity versus crack angle for a 0.9mm weld width and sheet thickness laser welded lap joint subjected to a 1kN applied load.

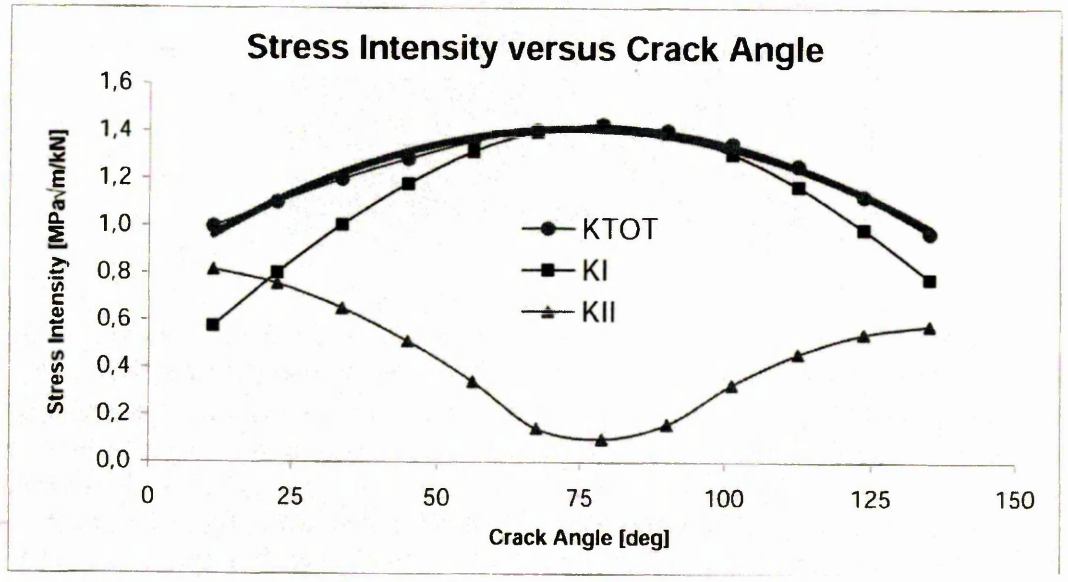

Figure 38 Solid element analysis showing stress intensity versus crack angle

Thus, it can be seen that the stress intensity reaches its maximum at approximately 75 - 80°; this being the preferred angle of fatigue crack initiation and corroborates the experimentally measured fatigue crack angles by Linder (Image 4).

It should be noted that the research conducted by Linder et al was on similar metal stainless steel laser welded lap joints. The factors identified as affecting the stainless steel similar metal lap joint fatigue properties were observed to have the same effect on mild steel similar metal laser welded lap joints.

There is, however, no current literature on laser welded lap joint mean fatigue properties, high cycle fatigue properties of dissimilar metal lap joints or the factors affecting dissimilar metal lap joint fatigue properties.

2.16.5 Analytical Modelling of Joint Rotation

Nordberg and McCann developed a simple analytical model using beam-bending theory[77]. The model was used to evaluate the effect of different joint parameters on joint rotation and the resulting development of the opening mode tensile load and or peel stresses.

The load, P, was divided into a shear force, P*cosθ , and a peel force, T*P where θ is the angle of joint rotation. For small θ, P*cosθ = P

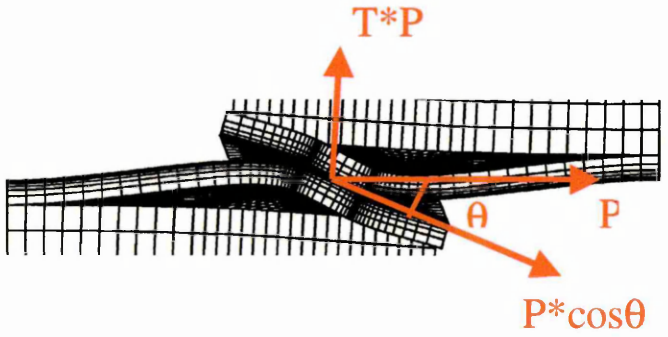

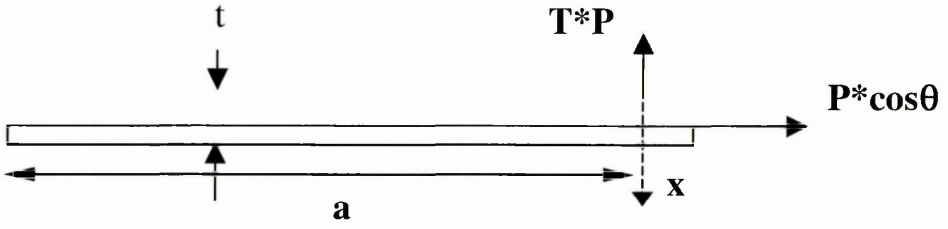

Figure 39 Schematic load distribution in a lap joint

The stress distribution in the sheet due to the shear load moment is found from

$\int \sigma(x) dx = P$ and $\int \sigma(x) \cdot x \cdot dx = 0$ to be

$\sigma = \frac{2P}{t}\left(2 - 3\frac{x}{t}\right)$, where x = distance from sheet interface.

[77] Nordberg, H. McCann, S. Overlap Joining of Stainless Steel Sheets, AvestaPolarit Research Foundation publication, 2004

resulting in a maximal stress at the inner surface of $\sigma = \frac{4P}{t}$,

a stress at the outer surface $\sigma = -\frac{2P}{t}$

and the neutral line at x=2t/3

The shear load create a moment $M = \frac{2t}{3} \cdot P$

Due to the symmetry, the calculated deflection by the moment and by the transverse load must take out each other, Thus

$\frac{2}{3} t \cdot P \cdot \frac{a^2}{2EI} = T \cdot P \frac{a^3}{3EI}$ resulting in a value for the factor $T = \frac{t}{a}$

Using line load (P = P/b, b = width) and beam theory the rotation due to the moment and the transverse force can be calculated as

$\theta_M = \frac{M \cdot a}{EI} = \frac{2 \cdot t \cdot P}{3} \cdot \frac{a}{EI}$ and $\theta_T = \frac{TP \cdot a^2}{2 \cdot EI} = \frac{P \cdot t}{a} \cdot \frac{a^2}{2 \cdot EI}$

Since $\theta_{Total} = \theta_M - \theta_{Peell} = \theta$ the total (net) rotation is

$$\theta = \frac{2 \cdot t \cdot P}{3} \cdot \frac{a}{EI} - \frac{P \cdot t}{2} \frac{a}{EI} = \frac{P \cdot t \cdot a}{EI} = \frac{2 \cdot a}{E \cdot t^2} \cdot P$$

Thus,

$$\theta = \frac{2 \cdot z \cdot a}{E \cdot t^2} \cdot P$$

Equation 4 Similar Thickness Rotation Angle Calculation

If there is a gap between the two sheets, the rotation angle θ, can be calculated using Equation 4 and using Equation 5 to calculate the variable "z" if no interfacial gapis present "z" is equal to one.

$$z = \frac{3 \cdot c}{2 \cdot t} + \frac{6 \cdot t + 9 \cdot c}{6 \cdot t + 4 \cdot c}$$

Equation 5 Interfacial Gap Variable

P = line load (N/mm)

a = "free" half-length of the specimen or sheets (mm)

t = sheet thickness (mm)

2c = distance between sheets or bondline thickness (mm)

θ = rotation in Radians

E = Elastic Modulus (190MPa) (MPa)

The model showed that for normal combinations of loads and sheet thickness (t), the rotation rarely exceeded three degrees.

The limiting nominal stress for which this elastic model holds is local plasticity. In a lap joint this occurs first at the inner fibre (the surface where the sheets join).

The fibre stress is

$$\sigma_{max} = 4 \cdot \frac{P}{t}$$

For a typical stainless steel with $R_{p0.2}$ = 300 MPa this means that the inner fibre of a 1.0, 1.5 and 2.0 mm thick sheet yields for a line load of 75, 112 and 150 N/mm. Beyond these values the elastic theory starts to break down and the calculated values are increasingly inaccurate[77].

2.16.6 Fracture Mechanics

The fatigue life of a component is made up of initiation and propagation stages. The size of the crack at the transition from initiation to propagation is usually unknown and often depends on the view of the analyst and the size of the component being analysed. Nevertheless the distinction between the initiation life and propagation life is important. At low strain amplitudes up to 90% of the life may be taken up with initiation, while at high amplitudes the majority of the fatigue life may be spent propagating a crack. Fracture mechanics approaches are used to estimate the propagation life and require that an initial crack size be known or assumed[78].

Linear elastic fracture mechanics (LEFM) principles are used to relate the stress magnitude and distribution near the crack tip to:

1. Remote stresses applied to the cracked component
2. The crack size and shape
3. The material properties of the cracked component

The general form of the LEFM equations can be seen in Equation 6 below.

$$\sigma_{ij} = \frac{K}{\sqrt{2\pi r}} \cdot f(\theta)$$

Equation 6 General form to determine local stresses near the crack tip

Where:

K = the stress intensity factor

r and θ are cylindrical coordinates of a point with respect to the crack tip.

The stress intensity factor, K defines the magnitude of the local stresses around the crack tip.

[78] Bannantine, J. A. Comer, J. J. Handrock, J. L. Fundamentals of Metal Fatigue Analysis, 1990, Prentice Hall, Inc, pp88-89

This factor depends on loading, crack, crack shape, and geometric boundaries, with the general form given by:

$$K = f(g)\sigma\sqrt{\pi a}$$

Equation 7 Stress intensity factor

Where:

σ = Remote stress applied (not to be confuse with local stress σ_{ij} in Equation 6.

a = crack length

f (g) = correction factor that depends on specimen and crack geometry

Research conducted by Zhang et al, extended a structural-stress concept developed for spot welds to laser welds following a degree of modification[79].

The stresses in the direct vicinity of the weld were characterised by stress intensity factors, with the objective being to make a connection between the nominal structural stress and the stress-intensity factors.

In order to develop the approach, the gap between the sheets was regarded as a crack in the terms of fracture mechanics[79].

Zhang concluded that the weld was always subjected to non-homogeneous stresses over its length and that the length did not make a linearly proportional contribution to the increase in the load bearing capacity. For this reason Zhang et al concluded that the dimensioning must be based on local stress ability, (e.g. structural stress, parameter p_a or notch stress) which was around one third lower for laser welds than for spot welds.

The structural stress or parameter p_a was calculated from the following equation:

$$p_a = K_{a,mix} / A \approx \sigma_{a(ns)}(1 + 0.5B_1(b_w / t_1 + b_w / t_2 - 1.2) + C_1(t_1 / t_2 - 1))\sqrt{b_w}$$

Equation 8 Structural stress calculation[79]

[79] Zhang, G. Sinhg, S. Hahn, O. Kurzok, P. Methods of predicting the fatigue lives of laser-beam welded lap welds subjected to shear stresses, Welding and Cutting, February 2002, pp 96 – 103

2.16.7 Similar & Dissimilar Metal Spot Welded Fatigue Failures

Marples investigated the resistance spot welding of 1.2mm V1437 – 1mm 304 dissimilar metal joints. The line load range fatigue properties of this joint can be seen in Graph 9, compared with both 1mm 304 and 1.2mm V1437 similar metal spot welded fatigue properties.

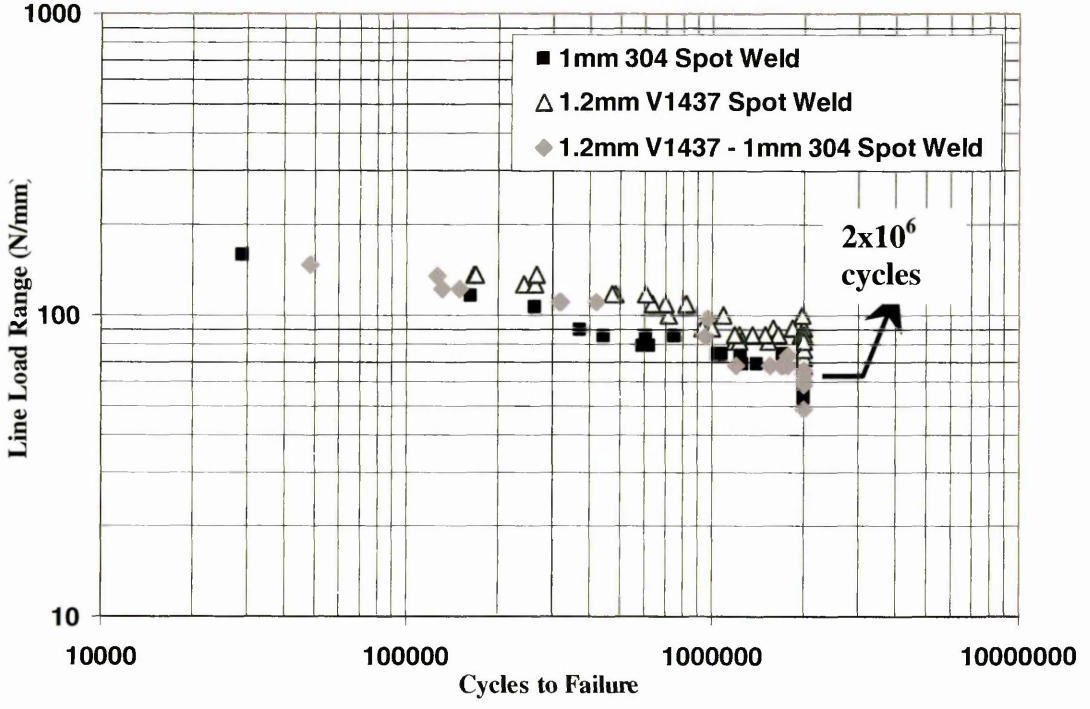

Graph 9 Similar and dissimilar metal resistance spot welded fatigue comparison

Graph 9 displays very similar fatigue results however, the 1mm 304 possessed the lowest fatigue properties. The dissimilar metal joint with an increase in sheet thickness with the 1.2mm V1437 possessed slightly higher fatigue properties and the 1.2mm V1437 similar metal joint with a further increase in sheet thickness possessed the highest fatigue properties.

Research conducted by Wray investigated the fatigue properties of similar metal resistance spot welded duplex stainless steel grades. The four grades tested during the investigation range in alloy content from the relatively lean 2101 duplex stainless steel to the relatively high alloyed 2507 duplex stainless steel.

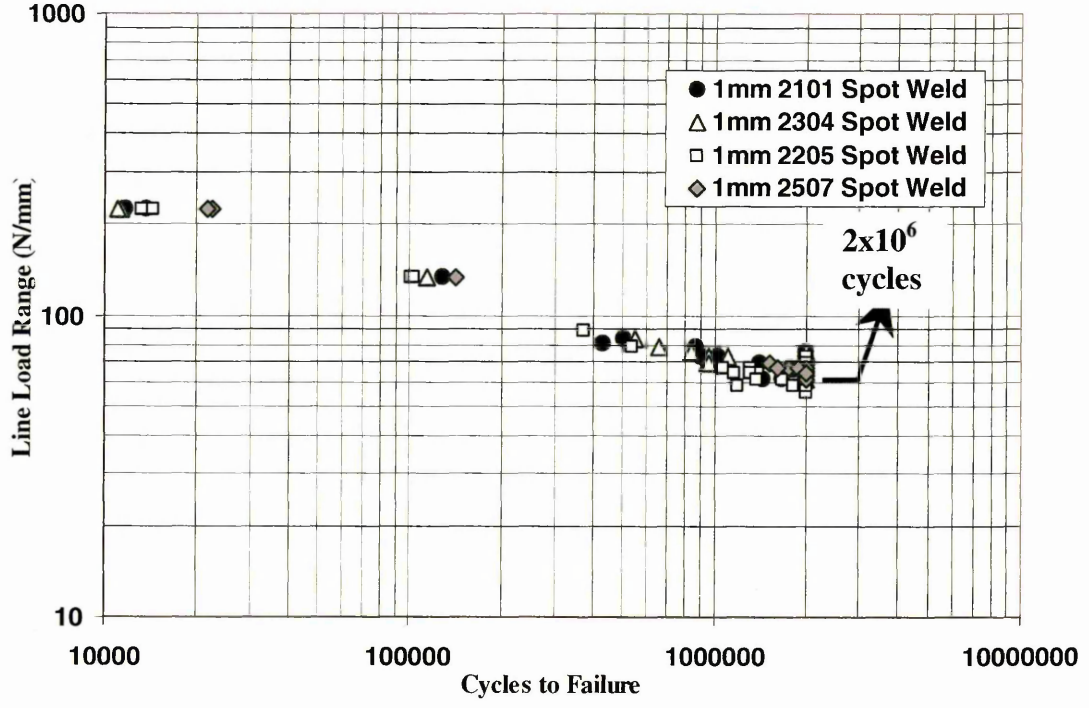

Graph 10 Similar metal resistance spot welded duplex stainless steel fatigue comparison

It can be seen the four grades possessed similar fatigue properties. It should be noted that the same electrode diameter was used to produce the spot welds, resulting in similar nugget diameters.

Wray also compared the fatigue properties of dissimilar thickness grades, the results of which can be seen in the following graph.

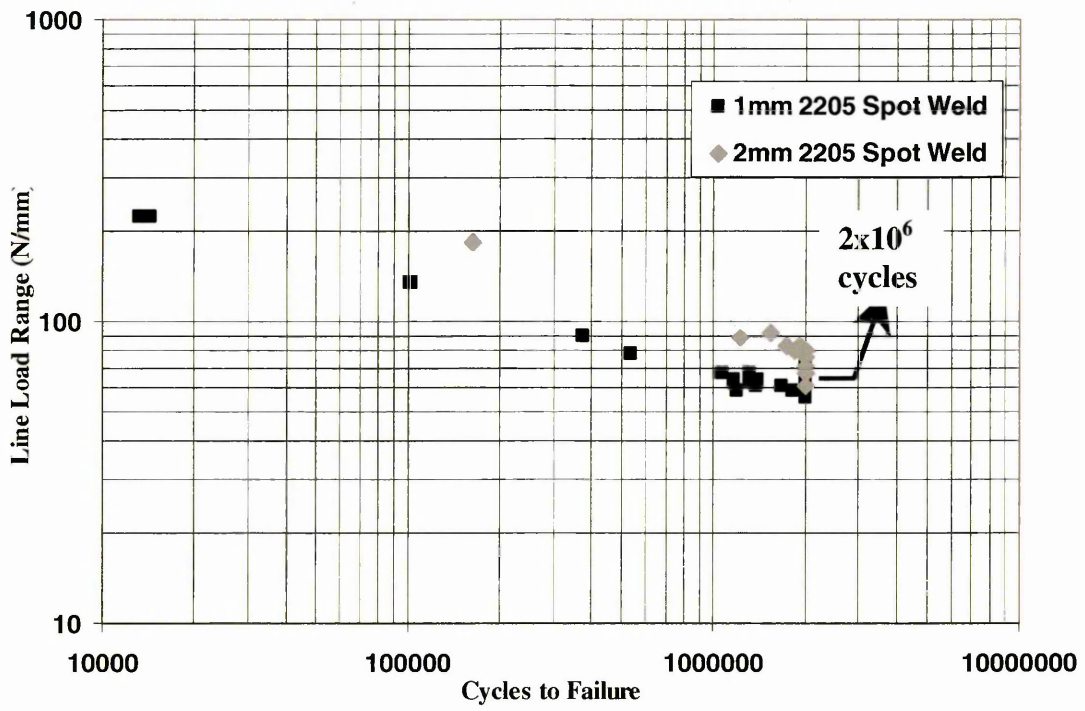

Graph 11 Effect of sheet thickness on the resistance spot welded duplex stainless steel fatigue

Wray found that increasing the sheet thickness improved the fatigue properties of the lap joint. It should be noted that the electrode diameter was the same for the two joints. A similar trend was found by Linder et al for similar metal laser welded lap joint fatigue results.

2.16.8 Adhesive Bonded Lap Joint Fatigue Properties

The effects of bondline thickness on the fatigue properties of 1.5mm (sheet thickness) 304 lap joints was analysed by Boyes[80]. It can be seen from Graph 12, that lower fatigue properties were achieved with the thicker bondline.

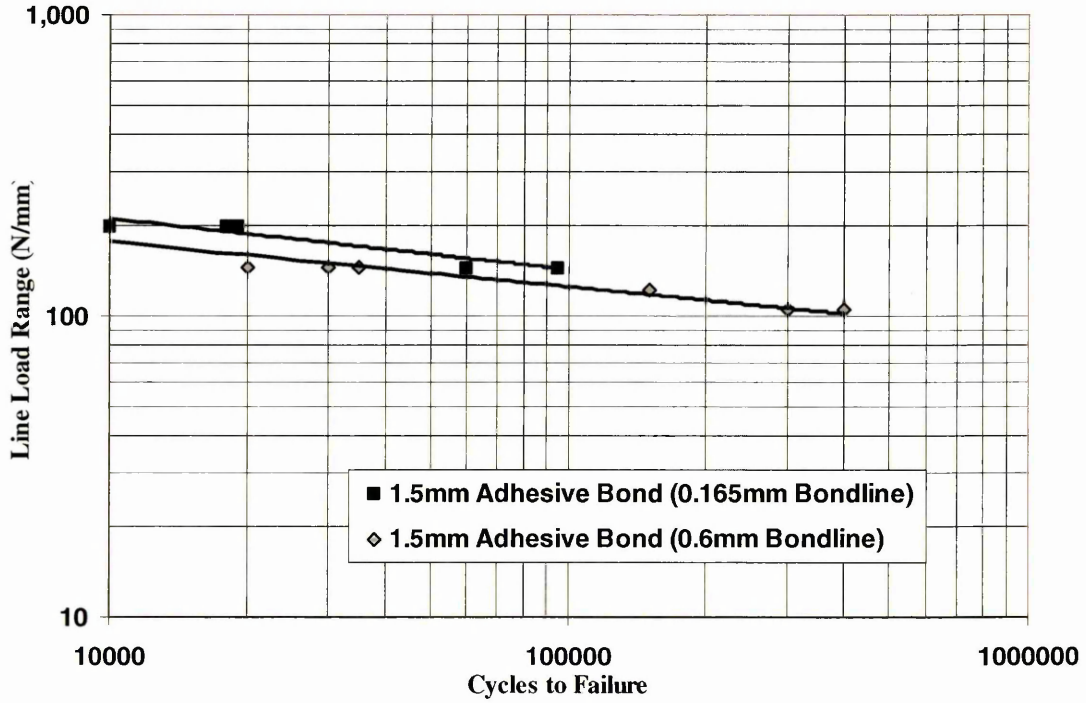

Graph 12 1.5mm 304 similar metal adhesive bonded lap joint fatigue properties with different bondline thickness[80]

The bondline thickness has a similar effect on adhesive bonded lap joint fatigue properties as the introduction of an interfacial gap in a laser welded lap joint. The increased bondline thickness increases the eccentricity of the applied fatigue load producing an increase in the applied bending moment to the joint, reducing fatigue properties. The bonded area was the same for the two adhesively bonded joints.

However, it should be noted that adhesively bonded lap joint fatigue failure occurs either in the adhesive itself or at the interface between the adhesive and the adherent.

[80] Boyes, B. Adhesive bonding of stainless steel, PhD thesis, Sheffield Hallam University, 1998

In summary, the experimental program aimed to provide answers to the following questions.

1. What are the tensile and fatigue controlling factors of dissimilar metal laser welded lap joints?; including the effects of:
    a. Sheet thickness
    b. Weld width
    c. Interfacial gap
    d. Zinc-coating (liquid metal embrittlement)
    e. Material tensile properties
    f. Weld bead composition
    g. Solidification mode (austenitic stainless steel)
2. How do the tensile and fatigue results of laser welded lap joints compare with those of current automotive joining methods (resistance spot welding)?
3. What are the "problems" associated with laser welding zinc-coated mild steel to stainless steel and can these "problems" be overcome?

3 *Experimental Technique*

3.1 Introduction

Two industrial CO_2 laser welders were used to produce welded samples The initial trials, which included welding similar and dissimilar metal laser welded lap and butt joints, were carried out using a Trumpf 5kW CO_2 laser welder. The specifics of the Trumpf 5kW CO_2 laser welder and the welding trials conducted can be seen in section 3.1.1.

Further trials were carried out using a Rofin 2kW CO_2 industrial laser welder. Inevitably, the welding speed was reduced to produce a similar power density at the source to allow full penetration welds. However, this welder provided greater laser-optics flexibility and beam control. This welder was used to produce similar and dissimilar metal laser welded lap and butt joints. The specifics of the Rofin 2kW CO_2 laser welder and welding trials conducted can be seen in section 3.1.1.1.3.

3.1.1 Trumpf 5kW CO_2 Laser Welder

Similar and dissimilar metal laser welds were produced using a Trumpf 5kW CO_2 industrial laser welder. This laser is a 'class 4' laser product with mirror optic beam delivery. As with all laser-welding processes there is some loss of power from the source to the work piece, thus, a laser power of 5 kW at the source resulted in a measured 3.8 kW at the work piece.

The laser beam energy distribution was of the gausssian type with a spot size of 0.3mm. This equated to a power density of 54kW/mm^2 at the work piece. The diameter of the beam containing 86% of the total power was 0.26mm.

Owing to the nature of the beam delivery; when welding zinc coated mild steel, the focal length (distance from the centre of the focusing mirror to the work piece) is kept relatively high to reduce the possibility of damage to the focusing mirror from zinc spatter. Hence, the focal length during the laser welding trials was 250mm.

A number of welding trials were conducted using this laser welder. These can be split into three separate sets of trials, each with different aims, which can be seen below.

1. Process optimisation and joint configuration
2. Material optimisation
3. Fatigue specimen production

Each of these trials will now be explained in further detail.

3.1.1.1 Process Optimisation and Joint Configuration

The initial welding trials were used to hone the laser welding process parameters with regard to the production of similar and dissimilar metal lap and butt joints. The steels used in the initial welding trials were:

- 1mm 304 austenitic stainless steel
- 1mm 2205 duplex stainless
- 1.2mm V1437 zinc-coated mild steel

The laser welding process parameters controlled during these laser welding trials were:

- Welding speed
- Focal position
- Shielding gas flow rate

The length of the overlap in the lap joint configuration was also controlled.

Initially, the welding power was set at the 5kW maximum (continuous beam mode); however, due to degradation of the optics the measured power at the work piece was 3.8kW. The focal length, which is the distance from the focusing mirror to the work piece surface, remained a constant length of 250mm. This was to reduce damage to the focusing mirror from zinc spatter. Helium was used as the shielding gas which was fed to the weld at a rate of 25L/min trailing the welding beam. The focal point was initially focussed on the surface of the top-sheet (0mm focal position).

3.1.1.1.1 Welding Speed

Laser welding trials were conducted to determine the highest attainable lap joint welding speed whilst achieving full penetration. 1.2mm V1437, 1mm 304 and 1mm 2205 similar metal welds, and 1.2mm V1437-1mm 304 and 1.2mm V1437-1mm 2205 dissimilar metal welds were produced and assessed with the welding speed set at 2.3m/min. Trials were then conducted with increased welding speeds of 3.0m/min, 2.9m/min, 2.8m/min and 2.6m/min respectively. The weld penetration of each laser welded lap joint was visually assessed after each weld run.

3.1.1.1.2 Focal Position Optimisation

The effects of the focal position, with regard to sheet penetration was assessed by producing three different laser welds at a welding speed sufficient to give minimal penetration using a focal position of 0mm (top-sheet surface). Thus, a further two laser welds were produced with a focal position 1mm above and -1mm below the top-sheet surface, see Figure 40 below. The penetration of these three welds was then compared visually to determine the optimum focal position for this particular system (welding parameters and sheet composition/properties).

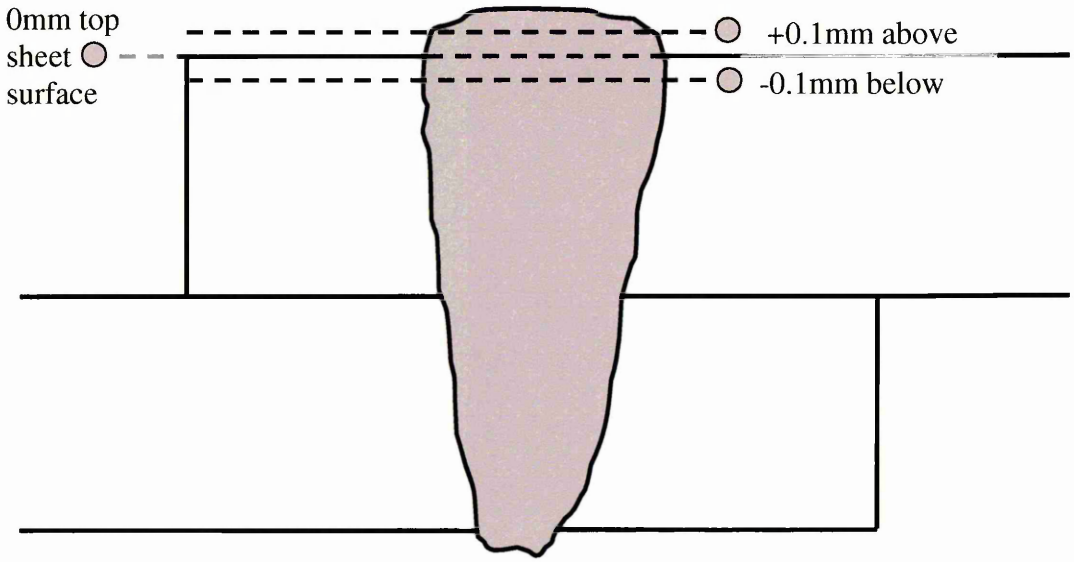

Figure 40 Schematic diagram showing the different focal positions used during the 'Process Optimisation' laser welding trials

3.1.1.1.3 Shielding Gas Flow Rate

The shielding gas flow rate was originally set at 25L/min. However, comparisons of plasma suppression were made by producing welds with a shielding gas flow rate of 30L/min and 20L/min respectively. A visual examination of the welds was carried out to assess the penetration and weld bead quality.

3.1.1.1.4 Overlap Length

The overlap length was set at 30mm for the similar and dissimilar metal lap joints. However, to aid in the evacuation of zinc vapour from the internal lap face, dissimilar metal laser welded lap joints were produced using an overlap of 10mm. The laser welds produced were examined visually to assess penetration and weld bead quality.

3.1.1.2 Material Optimisation

The second set of welding trials using the Trumpf 5kW CO_2 laser welder followed the tensile, and more specifically, the lap shear results produced from the "Process Optimisation and Joint Configuration" trials.

Thinner gauges of both austenitic and duplex stainless steels were laser welded to 1.2mm V1437 zinc-coated mild steel in the lap joint configuration. These thinner gauge stainless steels were:

- 0.6mm 301 austenitic stainless steel
- 0.7mm 301 austenitic stainless steel
- 0.78mm 2205 duplex stainless steel

The welding parameters used were, again, determined from the "Process Optimisation and Joint Configuration" welding trials. With the laser power set at the maximum 5kW (3.8kW at the work piece) and a focal length of 250mm; a welding speed of 2.6m/min was used. The focal position was 0.1mm above the surface and the shielding gas flow rate was 20L/min. The laser welds produced were assessed visually and consequently lap shear tested.

3.1.1.3 Fatigue Specimen Production

The third and final welding trials using the Trumpf 5kW CO_2 laser welder were to produce the laser welds which would be fatigue tested. Four dissimilar laser welds were produced with the following configurations:

- 1mm 304 (top) – 1.2mm V1437 Lap Joint
- 1.2mm V1437 (top) – 1mm 304 Lap Joint

- 0.78mm 2205 (top) – 1.2mm V1437 Lap Joint
- 1.2mm V1437 (top) – 0.78mm 2205 Lap Joint

It should be noted that "top" in the above laser welded lap joint configurations denotes the steel at the top of the lap joint, which is impinged by the incoming laser beam. The selection of these configurations was based on the lap shear results from the previous two welding trials. These four configurations all achieved greater than 100% weld efficiency; that is, the lap shear failure occurred in the parent material of the 1.2mm V1437 zinc-coated mild steel at 45° shear and not in the weld itself.

The welding parameters used to produce these four lap joints were determined from the previous two welding trials. The maximum laser power (3.8kW at the work piece) was used with a focal length of 250mm. The focal position was 0.1mm above the surface of the top sheet and helium shielding gas with a flow rate of 20 L/min was used. An overlap length of 25mm was selected to allow comparison with fatigue data from current literature.

3.1.1.4 Rofin 2kW CO2 Laser Welder

Similar and dissimilar metal laser welds were produced using a Rofin 2kW CO_2 industrial laser welder. This laser welder uses a mirror optic beam delivery in a similar way to the Trumpf 5kW CO_2 laser. The main difference however between the two lasers, aside from the welding power, is the reduced focal length of the Rofin 2kW CO_2 mirror optic system which was 65mm. Ordinarily, this reduced focal length would result in damage to the focusing mirror due to zinc spatter; however, this problem was overcome with the use of an air knife between the focusing mirror and the work piece.

Only one set of laser welding trials was undertaken using this industrial laser welder. The aim of this set of trials was to produce four joints that were to be fatigue tested. The process was optimised using a series of test welds, which were visually examined before the welds for fatigue testing were produced.

3.1.1.4.1 Fatigue Specimen Production

Due to the reduced power of Rofin laser welder in comparison to the Trumpf, a lower welding speed was required to achieve a similar power density. Hence, a number of welds were produced and visually examined before the fatigue specimens were produced. The focal position selected was -1mm below the surface; the helium trailing gas flow rate was 25L/min. The focal position was adjusted to effectively defocus the laser beam. This, in conjunction with a reduced welding speed, increases the heat input and produces a slower cooling and consequently solidification rate. This slower solidification rate, it was hoped, would allow more time for the zinc vapour from the internal lap face to escape the molten weld pool and reduce the chance of porosity. The overlap was 25mm, which was the same as the previous four fatigue tested lap joints to allow comparison with previous fatigue data.

Four laser welded joints were produced, these were:

- 1.2mm V1437 (top) – 1mm 2205 Lap Joint
- 1.2mm V1437 (top) – 1mm 2101 Lap Joint
- 1mm 2101 similar metal lap joint Lap Joint
- 1.2mm V1437 – 1mm 2101 Butt Joint

3.2 Material Tested

Four different grades of stainless steel were welded to the 1.2mm V1437 zinc-coated mild steel.

Stainless steel grades:

1. 1mm AvestaPolarit grade 18-8 (BS: 304s31, EN: 1.4301) with a 2B finish
2. 0.7mm AvestaPolarit grade 17-7 (BS: 301s21) with a bright annealed finish
3. 0.6mm AvestaPolarit grade 17-7 (BS: 301s21) with a bright annealed finish
4. 1mm AvestaPolarit grade 2205 (BS: 318s13, EN: 1.4301) with a brushed finish
5. 0.78mm AvestaPolarit grade 2205 (BS: 318s13, EN: 1.4301) with a brushed finish
6. 1mm AvestaPolarit grade 2101 with a brushed finish

3.2.1 Material Mechanical Properties

The actual base material mechanical properties were determined. The tensile test specimens were precision sheared from each sheet of material used.

The tensile tests were carried out using an Instron 4206 uniaxial tension-testing machine with a maximum load capacity of 150kN. Information output was via an IEEE port to a PC that contained Instron series XI software.

The velocity of each test was set at $10mm.min^{-1}$. These can be seen compared with the nominal base material mechanical data in the following tables.

1.2mm Volvo Truck Corporation (VTC) grade V1437

1.2mm V1439	$R_{p0.2}$ (MPa)	R_m (MPa)	A_5 (%)	Hv
Nominal	260	380	30	-
Actual	300	420	-	140

Table 3 1.2mm V1437 mechanical properties (nominal and actual)

Stainless steel grades:

1mm AvestaPolarit grade 18-8 (BS: 304s31, EN: 1.4301) with a 2B finish

1mm 304	$R_{p0.2}$ (MPa)	Rm (MPa)	A_5	Hv
Nominal	310	620	57	-
Actual	310	627	-	163

Table 4 1mm 304 mechanical properties (nominal and actual)

0.7mm AvestaPolarit grade 17-7 (BS: 301s21) with a bright annealed finish

0.7mm 302	$R_{p0.2}$ (MPa)	Rm (MPa)	A_5	Hv
Nominal	250	600	45	-
Actual	Not Tested	588	-	Not Tested

Table 5 0.7mm 301 mechanical properties (nominal and actual)

0.6mm AvestaPolarit grade 17-7 (BS: 301s21) with a bright annealed finish

0.6mm 302	$R_{p0.2}$ (MPa)	Rm (MPa)	A_5	Hv
Nominal	250	600	45	-
Actual	No Tested	572	Not Tested	Not Tested

Table 6 0.6mm 301 mechanical properties (nominal and actual)

1mm AvestaPolarit grade 2205 (BS: 318s13, EN: 1.4301) with a brushed finish

1mm 2205	$R_{p0.2}$ (MPa)	Rm (MPa)	A_5	Hv
Nominal	510	750	35	310
Actual	680	853	-	260

Table 7 1mm 2205 mechanical properties (nominal and actual)

0.78mm AvestaPolarit grade 2205 (BS: 318s13, EN: 1.4301) with a brushed finish

0.78mm 2205	$R_{p0.2}$ (MPa)	Rm (MPa)	A_5	Hv
Nominal	510	750	35	-
Actual	580	702	-	257

Table 8 0.78mm 2205 mechanical properties (nominal and actual)

1mm AvestaPolarit grade 2101 with a brushed finish

1mm 2101	$R_{p0.2}$ (MPa)	Rm (MPa)	A_5	Hv
Nominal	530	750	30	240
Actual	650	800	-	250

Table 9 1mm 2101 mechanical properties (nominal and actual)

3.2.2 Material Chemical Composition

1.2mm Volvo Truck Corporation (VTC) grade V1437

	C	Si	Mn	S	P	Ni	Cr	Cu	V	Al	N
Mass (%)	0.08	0.01	0.32	0.009	0.013	0.02	0.03	0.02	0.002	0.041	0.0037

Table 10 1.2mm V1437 chemical composition

Stainless steel grades:

1mm AvestaPolarit grade 18-8 (BS: 304s31, EN: 1.4301) with a 2B finish

	C	Si	Mn	P	S	Cr	Ni	N
Min (%)	-	-	-	-	-	18.0	8.0	-
Max (%)	0.03	0.75	2.0	0.045	0.015	19.0	10.0	0.1
Mass (%)	0.021	0.27	1.45	0.024	0.003	18.16	8.20	0.06

Table 11 1mm 304 chemical composition

0.7mm AvestaPolarit grade 17-7 (BS: 301s21) with a bright annealed finish

	C	Si	Mn	P	S	Cr	Ni	N
Min (%)	0.05	-	-	-	-	16.0	6.0	-
Max (%)	0.15	-	-	-	-	18.0	8.0	0.11
Mass (%)	Not Tested							

Table 12 0.7mm 301 chemical composition

0.6mm AvestaPolarit grade 17-7 (BS: 301s21) with a bright annealed finish

	C	Si	Mn	P	S	Cr	Ni	N
Min (%)	0.05	-	-	-	-	16.0	6.0	-
Max (%)	0.15	-	-	-	-	18.0	8.0	0.11
Mass (%)	Not Tested							

Table 13 0.6mm 301 chemical composition

1mm AvestaPolarit grade 2205 (BS: 318s13) with a brushed finish

	C	Si	Mn	P	S	Cr	Ni	N
Min (%)	-	-	-	-	-	21.0	4.5	2.5
Max (%)	0.03	-	-	-	-	23.0	6.5	3.5
Mass (%)	0.019	0.42	1.45	-	-	22.41	5.77	0.18

Table 14 1mm 2205 chemical composition

0.78mm AvestaPolarit grade 2205 (BS: 318s13, EN: 1.4301) with a brushed finish

	C	Si	Mn	P	S	Cr	Ni	N
Min (%)	-	-	-	-	-	21.0	4.5	2.5
Max (%)	0.03	-	-	-	-	23.0	6.5	3.5
Mass (%)	0.021	0.4	1.38	-	-	22.11	5.6	0.22

Table 15 0.78mm 2205 chemical composition

1mm AvestaPolarit grade 2101 with a brushed finish

	C	Si	Mn	P	S	Cr	Ni	Mo	N
Nominal (%)	0.03	-	5	-	-	21.5	1.5	0.3	0.22
Actual (%)	0.029	0.65	5.0	-	-	21.59	1.54	0.3	0.23

Table 16 1mm 2101 chemical composition

3.2.3 Zinc Coating

The Volvo Truck Corporation (VTC) grade V1437 had been hot dipped galvanised to the VTC – Z100 specification. The mass per unit area has been based on a density of 7.14g.cm^{-3}. The zinc coating properties can be seen in Table 17 below.

Mass		**Coating thickness per coated surface**	
Triple spot test (g.m^{-2})	Single spot test (g.m^{-2})	µm (nominal)	µm (min)
100 – 140	85 – 115	7	5

Table 17 1.2mm V1437 zinc mass and coating thickness

3.3 Joint Configuration

The flexibility of the laser system allowed both laser welded lap and butt joints to be produced. Both these welding configurations present their own problems with regard to laser weldability and are addressed in more detail in the following two sections.

3.3.1 Butt Joint

Laser welded butt joints were produced by butting two steel sheets together and running the laser beam along the centre of the two-sheet interface. This can be seen in Figure 41, where zinc coated mild steel has been welded to stainless steel. Both similar and dissimilar metal butt joints were produced.

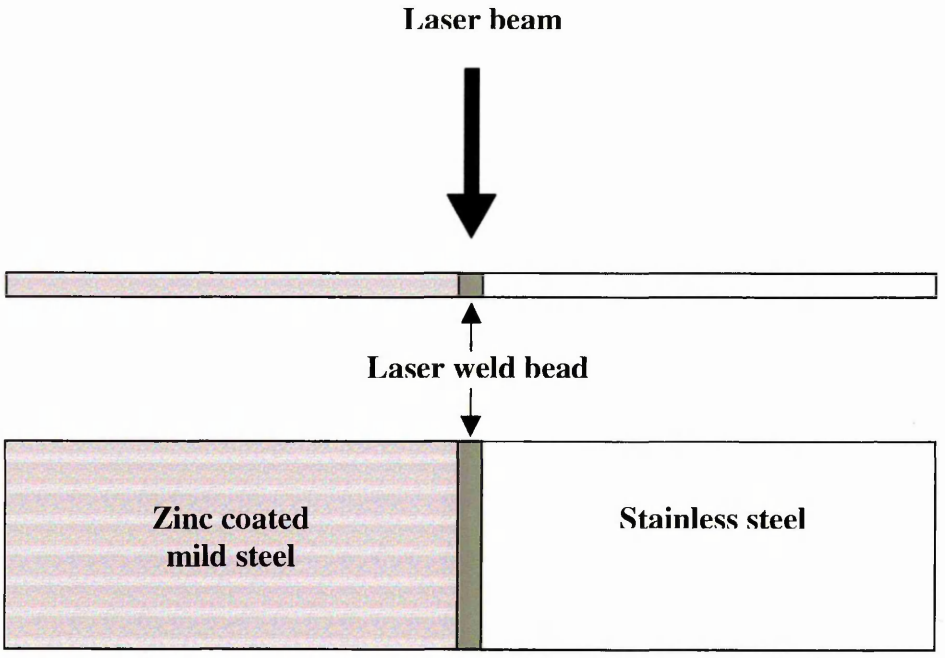

Figure 41 Schematic diagram showing the butt weld configuration

The critical aspects to be considered when producing laser-welded butt joints are the fit up between the two sheets to be joined and, provided good fit up is achieved, alignment of the laser beam along the centre of the two sheets.

Good fit up is critical in laser-welded butt joints in both the 'y' and 'z' axis. These can be seen in Figure 42 below with respect to the laser beam and welding direction.

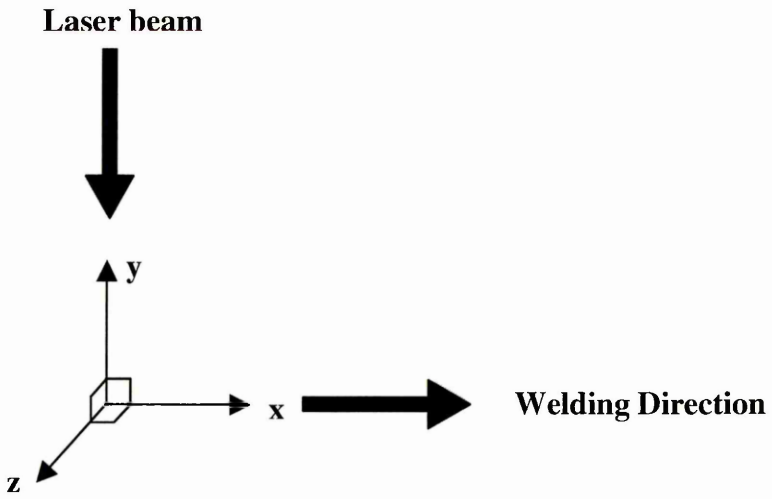

Figure 42 Butt joint critical fit up axis with respect to laser beam direction

Thus, to improve fit up in the 'z' axis, the samples were all 'precision-sheared' along the edge to be welded. This reduced any gap between the sheets to <10% of the sheet thickness, which is sufficient to remove under fill and concavity of the weld bead.

Hydraulic clamps were used to produce the butt joints with the Trumpf 5kW CO_2 industrial laser welder. This removed any deflection within the sheets inherent from manufacture and improved the fit up with respect to the 'y' axis.

In comparison, laser welded butt joints produced with the Rofin 2kW CO_2 industrial laser welder used a set of mechanical point clamps to remove any deflection within the sheets, and again improved the fit up in the 'y' axis.

When satisfactory fit up between the sheets was achieved, a low power-density laser spot, similar to a laser pointer, was placed on the joint surface. This laser spot traversed across the sheets using CNC positioning and allowed a laser-weld alignment test to be completed. During the laser-weld test, which could be done very slowly, observations would reveal if the spot moved away from the two-sheet interface into either parent material. Thus alignment of the laser beam along the length of the weld was achieved allowing for good reproduction and highly consistent welds.

3.3.2 Lap joint

Laser welded lap joints were produced by overlapping two sheets of steel. The laser beam then traversed down the centre of the overlap, impinging on the surface of the top material, and produced a weld between the two sheets. This can be seen in Figure 43. Both similar and dissimilar metal laser welded lap joints were produced.

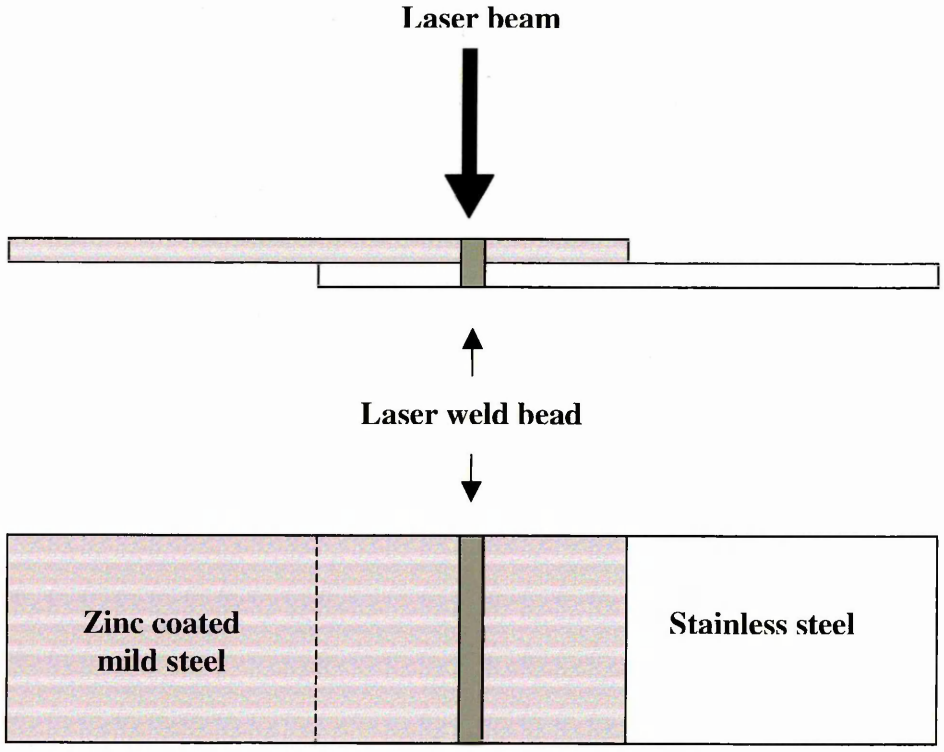

Figure 43 Schematic diagrams showing the lap joint configuration

It should be noted that the lap joint configuration allows two joints to be produced for a particular dissimilar set of steels. For example, Figure 43 illustrates a dissimilar metal laser welded lap joint between zinc coated mild steel and a stainless steel. It can be seen that the laser beam impinges on the surface of the zinc coated mild steel, which is at the top of the lap joint. Thus, the two steels can be reversed and a laser-welded lap joint can be produced with the laser impinging on the surface of the stainless steel. This can be seen in Figure 44.

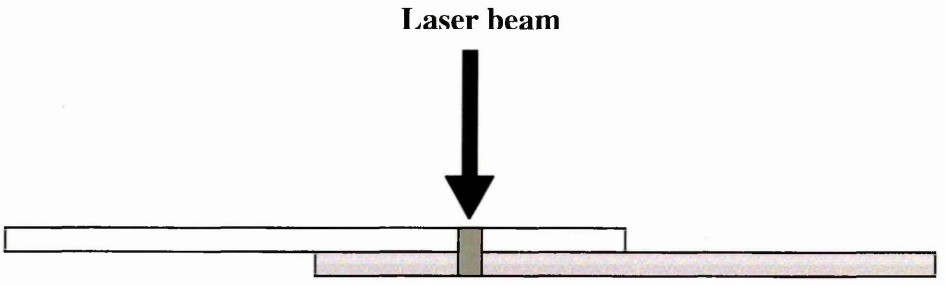

Figure 44 Schematic showing a reverse of the lap joint configuration in Figure 43

The advantage of the lap joint configuration is that it removes problems associated with edge preparation, inherent within the butt joint configuration. This makes the lap joint much more flexible and attractive to industry. However, similar precautions were taken to achieve alignment as in the production of the laser –welded butt joints.

Marking the bottom sheet at the edge of the overlap allowed the two sheets and the overlap (L) to be aligned. Marking the top sheet at half the length (L/2) of the overlap allowed the laser weld to be produced at the centre of the overlap.

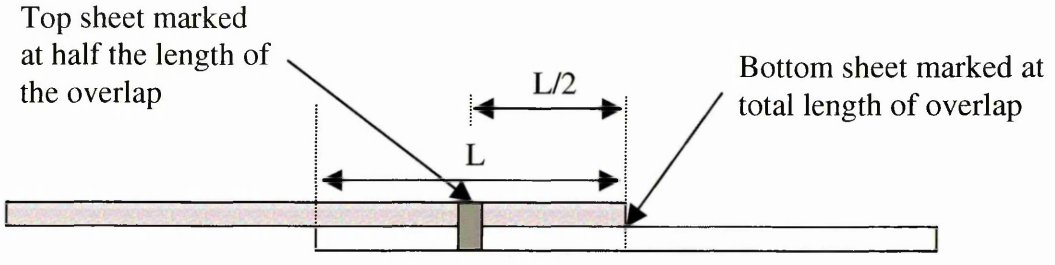

Figure 45 Diagram to show the markings required to ensure lap joint fit up

3.4 Mechanical Testing

A range of mechanical tests were employed to determine and compare the properties of similar and dissimilar metal laser welded butt and lap joints.

The first tests were tensile and lap shear tests. These tests were used to characterise the effects of the laser welding process variables on the quality and strength of the laser weld produced.

3.4.1 Tensile Testing

Tensile testing was completed on each of the base materials. The actual base material properties are compared to the nominal values in Table 3 to Table 9, in section 3.2.1.

Tensile tests were also completed on similar and dissimilar metal laser welded butt joints. The tensile test specimens were precision sheared from the welded sheets.

All tensile tests were carried out using an Instron 4206 uniaxial tension-testing machine with a maximum load capacity of 150kN. Information output was via an IEEE port to a PC that contained Instron series XI software.

The velocity of each test was set at $10mm.min^{-1}$.

The results recorded for each test were:

1. Max load (kN)
2. Energy break (J)
3. Energy yield (J)
4. Maximum displacement (mm)

The data from the PC was also used to generate the load extension curves.

3.4.1.1 Butt Joints

Three tests were completed for each base material and laser-weld, and the average results were taken. The Instron series XI software was able to calculate the standard deviation for each set of three test results. Four tests were completed when a special cause variation result was generated.

The geometry used for the base material and butt joint tensile tests can be seen in Figure 46 below.

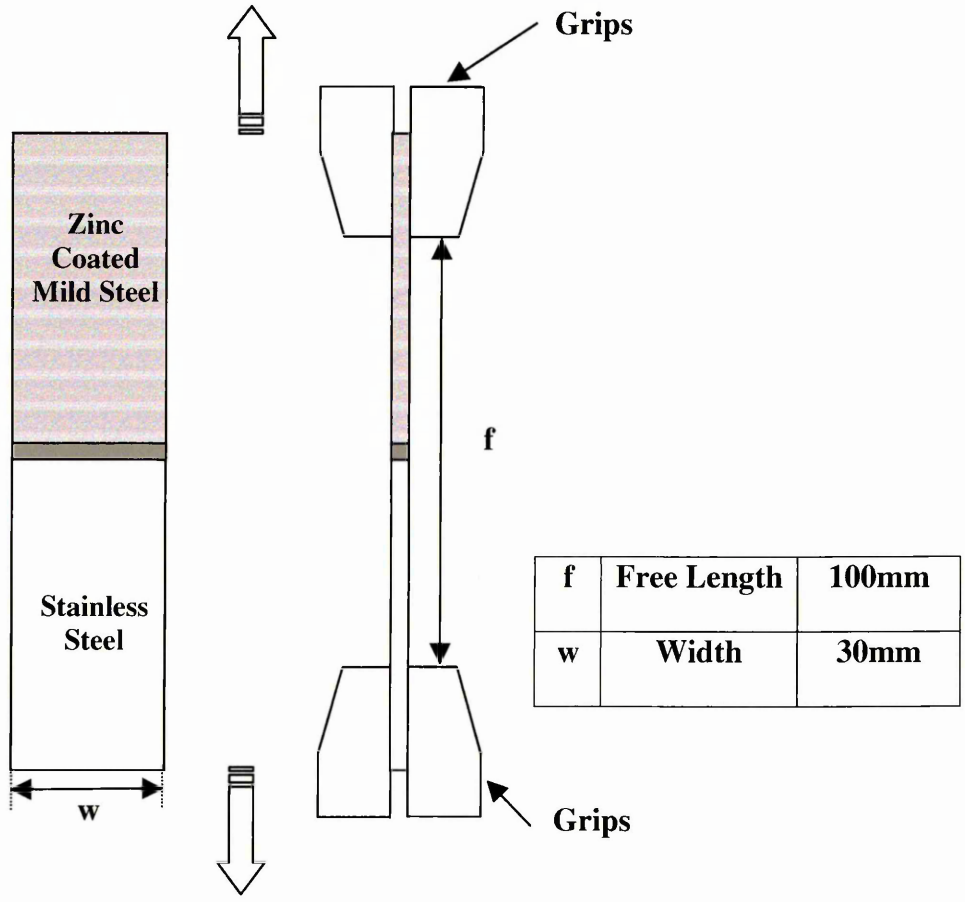

f	Free Length	100mm
w	Width	30mm

Figure 46 Butt joint tensile test schematic with sample dimension

3.4.2 Lap Shear Testing

Similarly, lap shear testing was completed on similar and dissimilar metal laser welded lap joints. The lap shear test specimens were precision sheared from the welded sheets. To simulate the loading applied to the joint, spacers were integrated into the lap shear testing. It should be noted that the thickness of each spacer was the same as the opposite sheet thickness. This removed any rotation or stress on the lap joint prior to lap shear test commencement.

Three tests were completed for each set of trials and the average and standard deviation of each set was calculated. In a similar manner to the butt joint tests, a fourth test would be conducted if a special cause variation was seen.

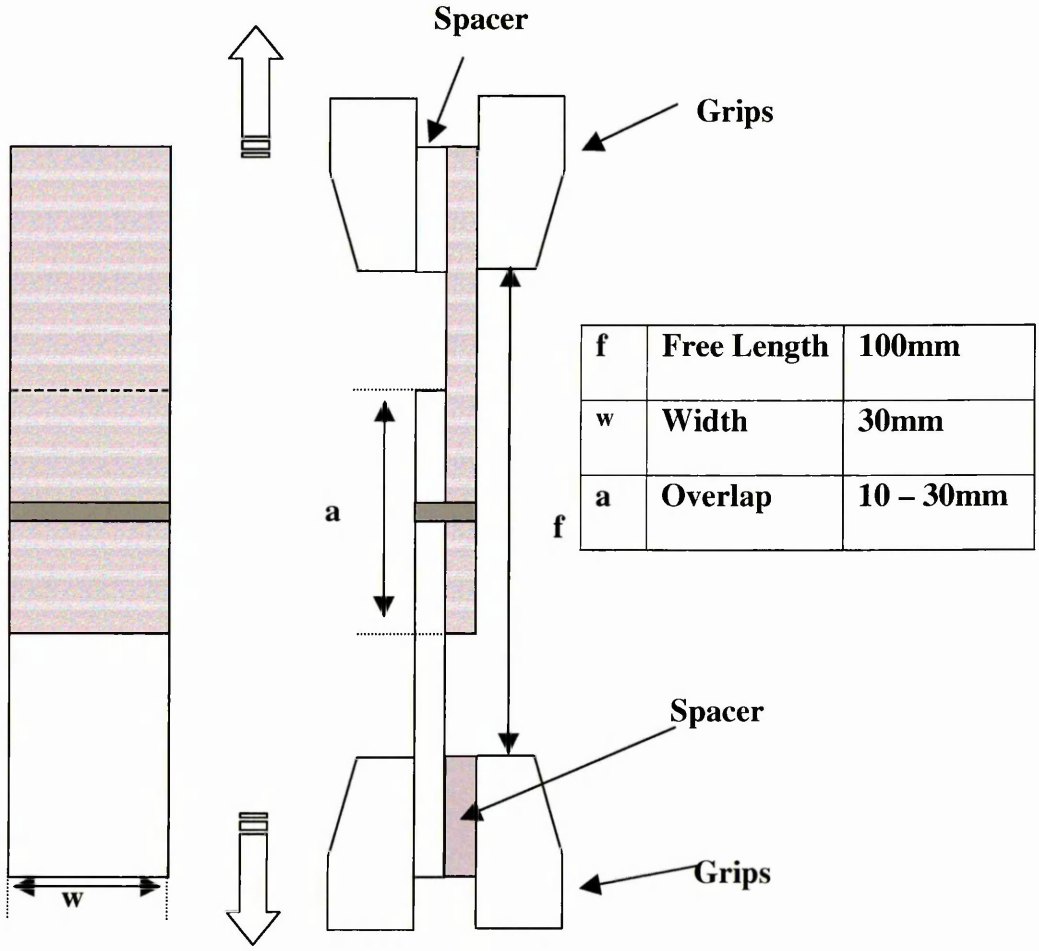

f	Free Length	100mm
w	Width	30mm
a	Overlap	10 – 30mm

Figure 47 Schematic showing lap joint shear test and sample dimensions

3.4.3 Fatigue Testing

Fatigue testing was completed in air on eight similar/dissimilar metal laser welded lap and butt joints. As explained in section 3.1, these joints were produced in two separate welding trials using the Trumpf 5kW and the Rofin 2kW CO_2 laser welders respectively.

The fatigue tests carried out were of the tension/tension type with a sinusoidal waveform. The load ratio (minimum load/maximum load) was 0.05 = R. The fatigue test frequency was selected on the basis of the highest attainable frequency whilst achieving applied load resolution. Thus, the fatigue test frequencies were 50Hz for the lap joints and 20Hz for the butt joints. A temperature sensor was placed on the surfaces of the lap joint to assess the temperature during the test. Even at the higher frequencies (50Hz), the sample did not show an increase in temperature. Joint survival at $2x10^6$ cycles was considered "run out" and the test was terminated. Failure was defined as total sheet separation, see section 2.16.1.1; which allowed the fatigue machine, waveform generator, and cycle counter to trip when >2mm actuator travel occurred.

Both lap and butt joint fatigue specimens were water jet cut from 1m long laser welds. A 10mm strip was cut from both ends of the laser weld and discarded, thus no start and stop point was included in a sample.

The water jet diameter was 1mm, with tolerances of ± 0.2mm. The kerf deviation was 0.1mm – 0.2mm.

3.4.3.1 Lap Joint Fatigue Specimen Geometry

The fatigue specimen geometry (width, overlap and free length) was selected to allow comparison between stainless steel similar metal and mild steel similar metal laser welded fatigue results[70].

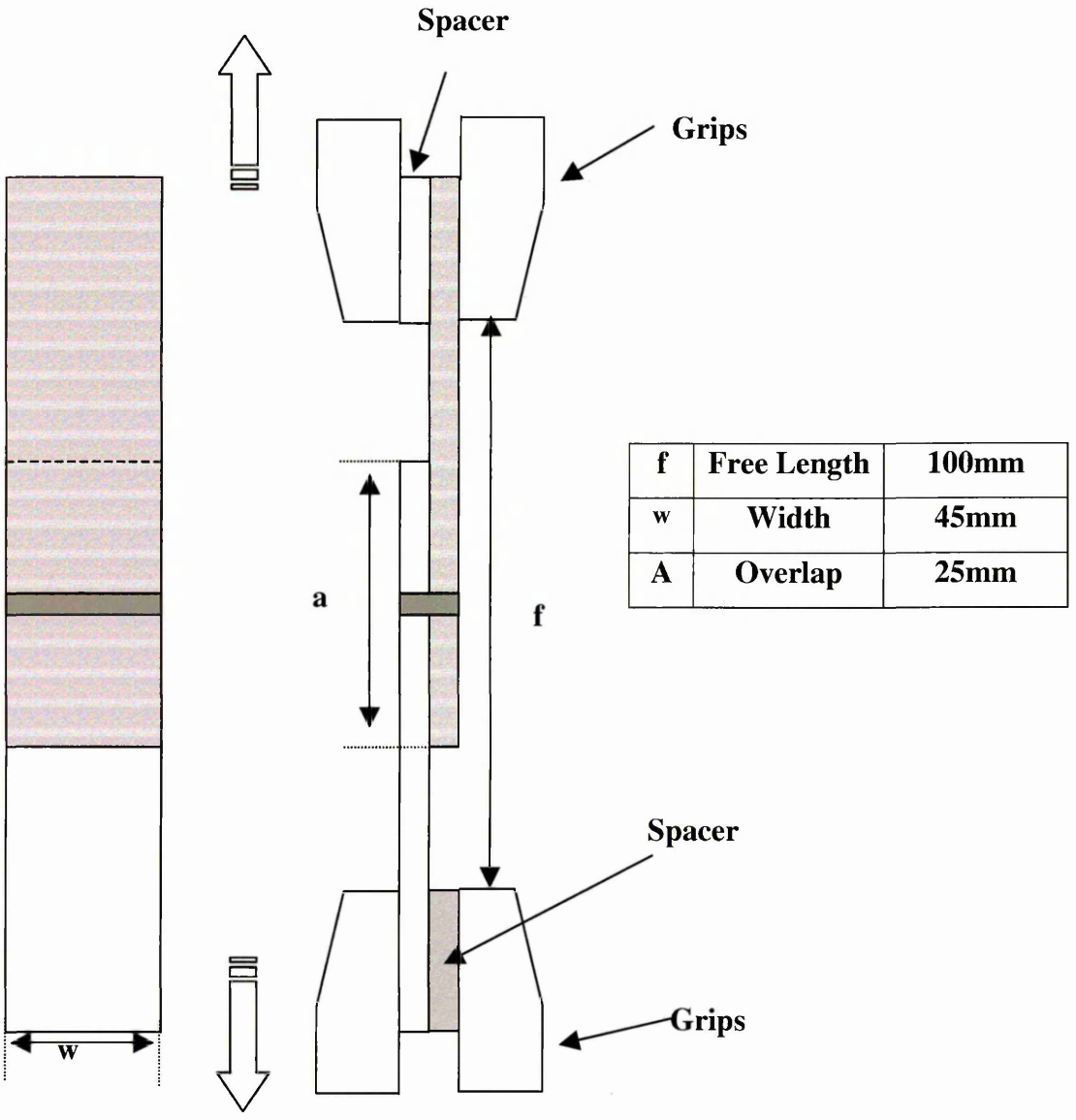

f	Free Length	100mm
w	Width	45mm
A	Overlap	25mm

Figure 48 Schematic diagram showing the la p joint fatigue test dimensions

3.4.3.2 Butt Joint Fatigue Specimen Geometry

The butt joint fatigue specimen dimensions, primarily the free length and width, were the same as the lap joint fatigue specimens. This was to allow comparison between the butt joint fatigue results with the lap joint fatigue results.

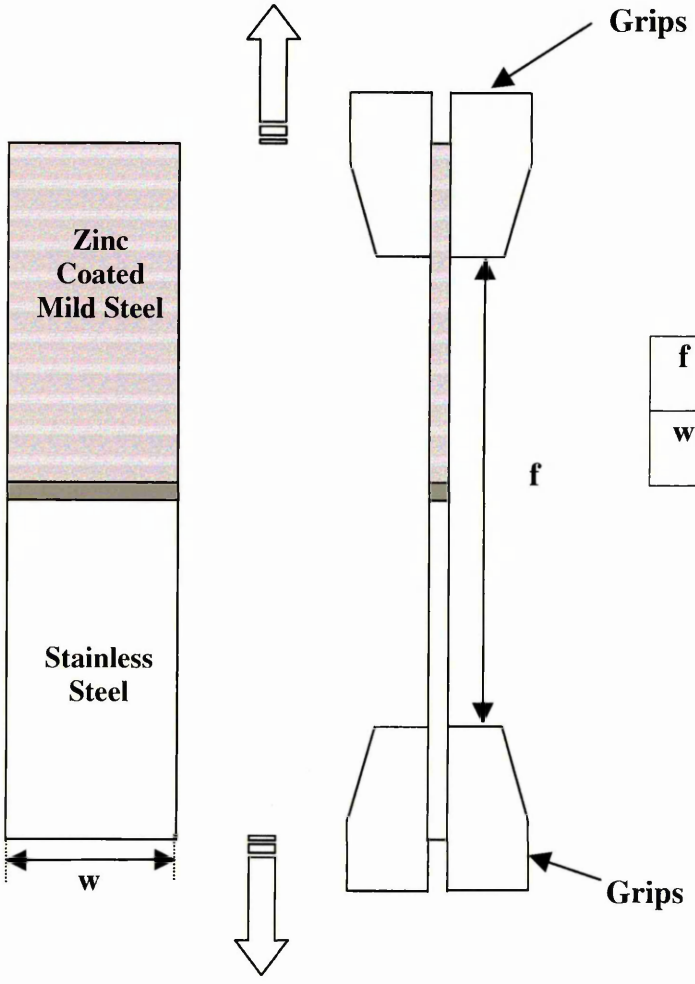

f	Free Length	100mm
w	Width	45mm

Figure 49 Schematic diagram showing the butt joint fatigue test dimensions

3.4.3.3 Fatigue Tests - Staircase Method

The staircase method was employed to determine the statistically valid mean fatigue strength at $2x10^6$ cycles, see section 2.16. Preliminary testing was conducted to give an indication of the first load level used in the staircase method. The load increment used was 0.1kN for the similar and dissimilar metal lap joints and 0.2kN for the dissimilar metal butt weld. A minimum number of twenty tests were conducted in each staircase to allow the mean fatigue strength to be statistically validated[81].

The staircase (or "up-and-down") method of testing is a variation of the "Probit" method. It requires fewer specimens than the latter but is useful only when the primary interest is in the mean fatigue strength corresponding to a pre-assigned cycle life, commonly $2x10^6$ cycles. The advantage gained in reducing the number of specimens tested can be offset by an increase in the time required to conduct the test.

In the staircase method the specimens are tested sequentially, one at a time. The first specimen is tested at a stress level equal to the estimated value of mean fatigue strength for the prescribed number of cycles. If the specimen fails before the pre-assigned cycle life ($2x10^6$ cycles), the next specimen is tested at a stress level that is one increment below the first stress level, and so forth[82].

Ideally, most of the tests should be made at three stress levels, chosen so that approximately 50 per cent of the test specimens survive at the middle stress level, about 70 per cent survive at the lower stress level, and about 30 per cent survive at the higher stress level[82].

---

[81] Nordberg, H. Discussion with Supervisor, Sheffield Hallam University, 2001

[82] A Guide for Fatigue Testing and the Statistical Analysis of Fatigue Data, Prepared by Committee E- on Fatigue, American Society for Testing and Materials, 1963, pp 13-15

Thus, the selection of the proper increment of stress level is very important. Too large an increment may produce a simple pass-fail threshold. Too small an increment and large numbers of tests may have to be carried out to produce three (or more) active levels. Increasing the number of active levels will also increase the standard deviation and reduce the accuracy of the mean fatigue strength.

Previous data for the same or similar materials is needed in order to choose the initial stress level effectively. If none is available, some preliminary testing may be required, however, if the correct initial stress level and increment are chosen, it is possible to determine the statistically valid mean fatigue strength at $2x10^6$ cycles with approximately twenty tests[81].

For each staircase method produced, the following calculations were used to determine the statistically valid mean fatigue line load range (N/mm) and standard deviation.

Statistical calculations

The mean fatigue line load range at $2x10^6$ cycles was calculated using the following equation:

$$X = P_0 + d(\frac{A}{F} - \frac{1}{2}) \qquad \textbf{(N/mm)}$$

Equation 9 Mean fatigue line load range

Statistical Validity

The statistical validity of the mean fatigue line load range was calculated using the following equation:

$$\frac{(F * B - A^2)}{F^2} = \textbf{>0.3 and <1.2}$$

Equation 10 Staircase statistical validity

If the value was between 0.3 and 1.2, the staircase was statistically valid.

Standard Deviation

The standard deviation of the mean fatigue line load range was calculated from the following equation:

$$s = 1.620 * d\left\{\left(\frac{F * B - A^2}{F^2}\right)\right\} + 0.029 \qquad \textbf{(N/mm)}$$

Equation 11 Standard deviation of the staircase

Where:

X = Mean fatigue line load (N/mm)

s = Standard deviation

P_0 = Total stress (N/mm) for step 0

F = Total number of failures

d = Stress interval (N/mm) or load interval (N)

$A = \Sigma(i * f_i)$

$B = \Sigma(i^2 * f_i)$

i = Step number

f_i = Number of failures in a step

3.4.3.4 Fatigue Tests - S-N Curve

For each laser-welded joint, an S-N curve was generated. Three load levels were selected above the apparent mean fatigue strength at $2x10^6$ cycles to produce the S-N curve. Three tests were conducted at each load level to verify the results. The frequency of these tests was reduced (20-30Hz) to allow accurate load resolution at the increased applied load ranges.

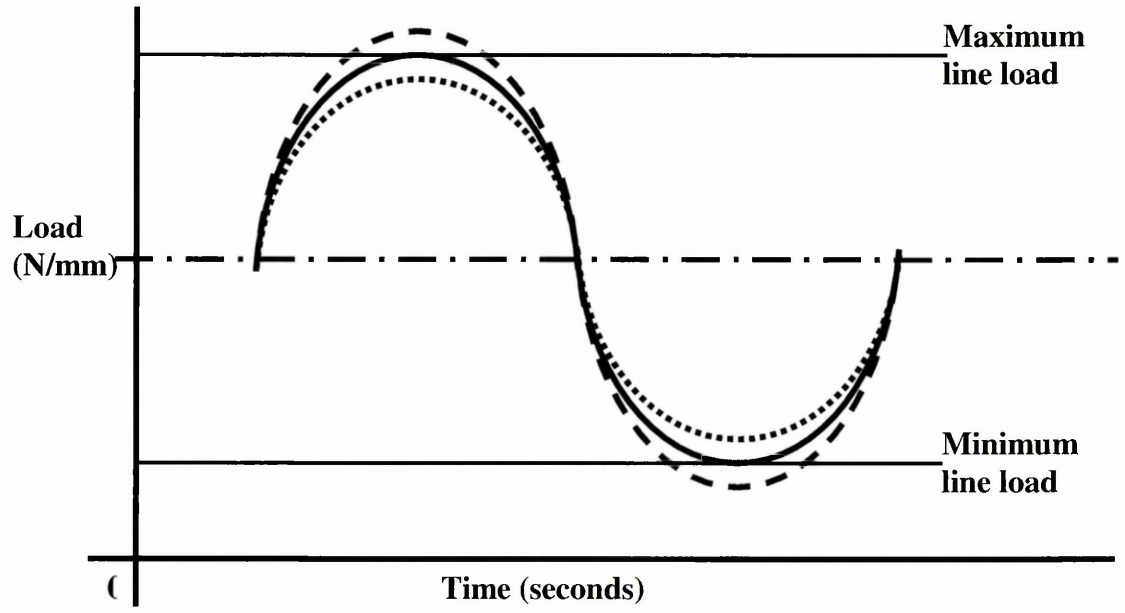

Figure 50 Schematic showing the poor load resolution produced by conducted fatigue tests at too high a frequency

If the frequency of these tests had not been reduced, the actual minimum and maximum applied load would have either under or over achieved the set load. This can be seen in Figure 50 by the two dotted sign waves. This would have significantly reduced the repetition of the fatigue tests and ultimately increased the scatter of the S-N curve fatigue results.

3.4.4 Lap Joint Rotation Tests

As explained in section 2.15.2.1, a lap joint subjected to a tensile load, whether from a lap shear or fatigue test, will rotate. Thus, a test designed by Nordberg and McCann[83] was used to analyse and quantify the degree of lap joint rotation for a given applied load.

A low intensity laser beam was reflected from a mirror (see Figure 51), which was adhesively bonded to the overlap surface of the lap joint. The reflected beam was directed to a flat white canvas that was positioned one metre from the lap joint. The initial (zero) position was marked on the canvas' surface prior to loading. The lap joint was then subjected to incremental loading until the sample began to plastically deform. The test was then terminated. There was some diffraction of the laser light during the reflection process and the reflected spot size on the canvas was approximately 5mm.

Further rotation tests were carried out with the laser spot being reflected on a sheet of white paper which reduced the spot diameter to ~ 4mm. The rotation was measured by placing a line at the centre of the laser spot. The error of the rotation test introduced by marking and measuring the laser displacement was thus estimated to a rotation angle error of $\pm 0.1°$.

To provide an accurate rotation angle for the lap joints during fatigue loading, the free length of the rotation tests was carried out at 100mm, this being the free length used during the fatigue tests.

[83] McCann, S. Adhesive Bonding of Stainless Steels, PhD Thesis, Materials Research Institute, Sheffield Hallam University, July, 2003

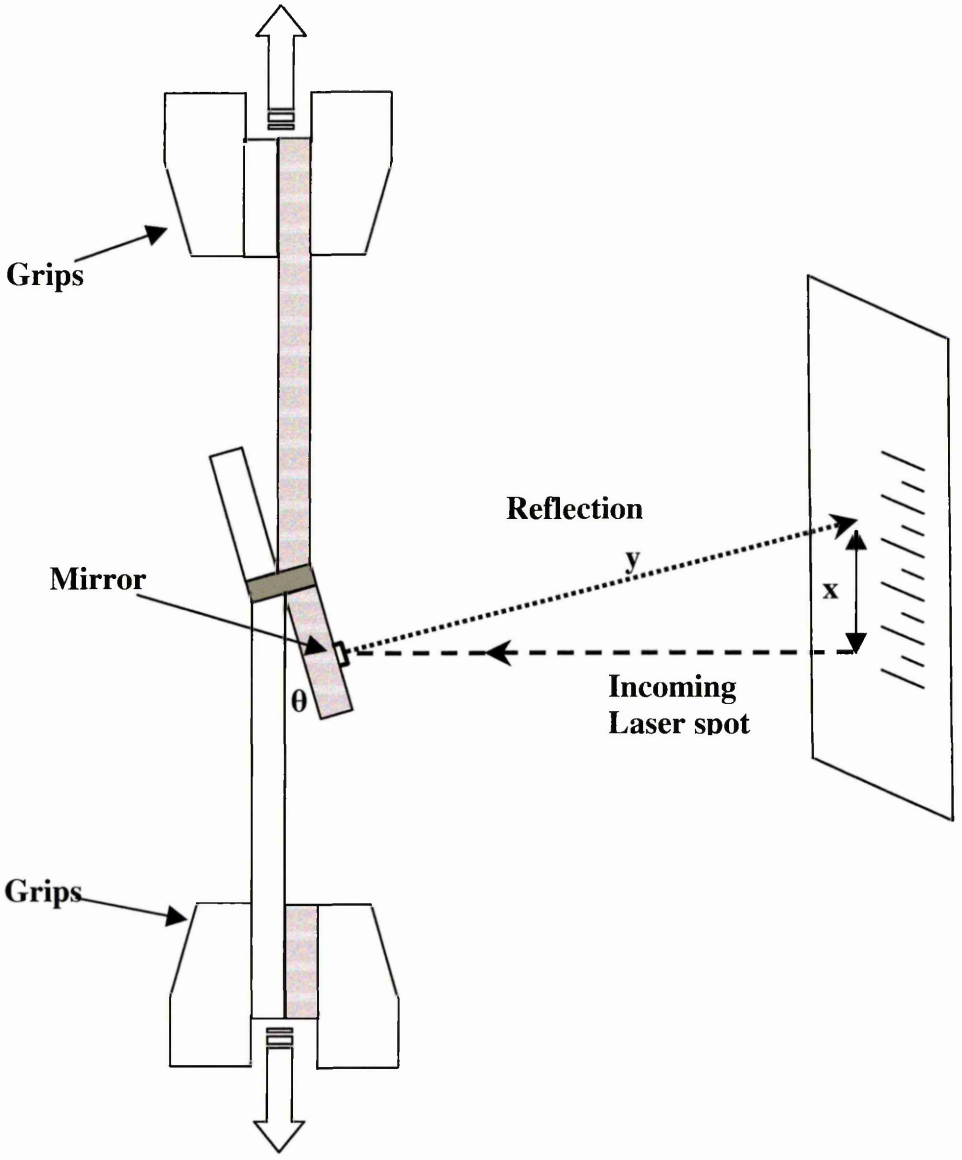

Figure 51 Schematic diagram showing the lap rotation test

The rotation angle was then calculated using simple trigonometry.

$$\theta^\circ = 57.3*ASIN\ (x/y)$$

Equation 12 Lap joint rotation calculation

3.5 Metallography

A number of metallographic techniques were used to provide information from similar and dissimilar metal laser-welded lap and butt joints.

For the majority of the metallographic techniques, the laser welds were hot mounted in conductive bakelite. The use of conductive bakelite allowed advanced SEM examination to be carried out; this included secondary and back-scattered electron imaging analysis. Weld bead measurements and compositional analysis was also conducted using optical and SEM analysis respectively.

3.5.1 Etchants

A number of etchants were used to provide microstructural data and to allow visual examination of the laser weld bead. Due to the existence of the passive layer on the stainless steel; the stainless steel etchants tend to be much more aggressive than those used for mild steel, for example, boiling nitric acid and electrolytic etching. These etchants are too severe for zinc coated mild steel grades and over-etch the mild steel structure very quickly. Thus, in most cases, a compromise had to be found, usually the laser welds would be etched for the zinc-coated mild steel and secondly for the stainless steel.

3.5.1.1 Stainless Steel

A number of etchants were used to provide different structural information.

Kallings reagent was used to show contrast between austenite, ferrite and martensite. This etchant was used primarily with the duplex dissimilar metal welds.

Schaftmeisters reagent, which is a grain boundary etchant, was used to provide images of the austenitic grain structure.

3.5.1.2 Zinc Coated Mild Steel (V1437)

Nitric acid in solution with alchohol produces a solution called Nital. Nital, with a typical nitric acid concentration of 2 & 6% is the most common etchant for mild steel. The increased concentration of 6% Nital provides a more powerful etchant that requires a shorter duration to suitably etch a mild steel sample. Nital is a grain boundary etchant which is useful for examining the grain structure of mild steel.

3.5.2 Microhardness Testing

A microhardness traverse was completed on dissimilar metal lap and butt joints. A microhardness machine with an integrated ocular micrometer was used to produce the microhardness grid with a 0.25mm increment. A load of 500g was used. Thus, a microhardness grid across the weld was produced, which allowed a comparison of laser weld microhardness for different welding parameters. An example of the grid can be seen in Figure 52.

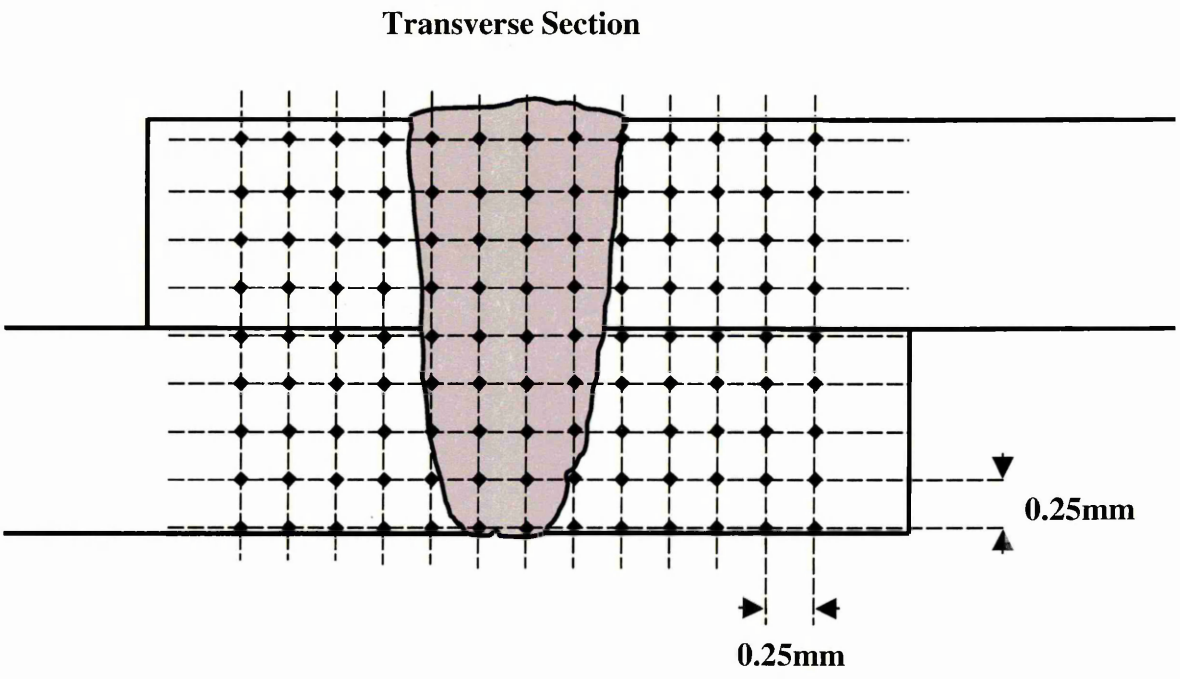

Figure 52 Microhardness grid (0.25mm) across a laser welded lap joint

3.5.3 Optical Analysis

Optical microscopy of dissimilar metal butt and lap joints was carried out. This was to allow investigation into the weld bead profiles and, when suitably etched, to visually characterise the degree of weld bead dilution and provide images which show contrast between the base materials, heat affected zone (HAZ) and the weld bead.

3.5.3.1 Weld Bead Widths

Similar and dissimilar metal laser welded lap joint profiles were examined using a Vanox optical microscope. The examination was used to determine the average weld width between the sheets. Transverse sections of the welds were mounted prior to grinding and were polished before being suitably etched, see section 3.5.1. Optical analysis was then carried out.

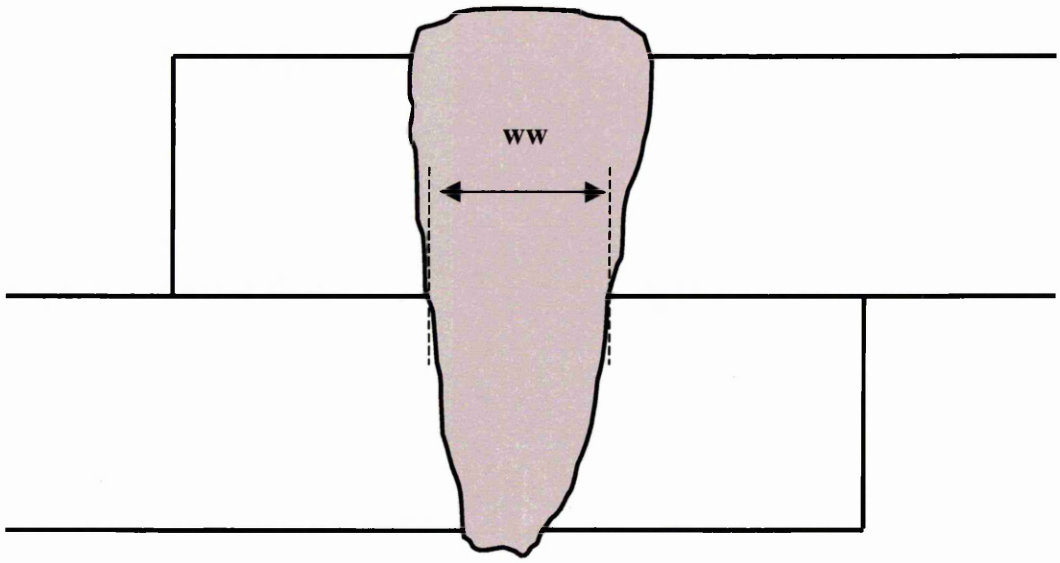

3.5.3.2 Fatigue Failure Analysis

Similar and dissimilar metal laser-welded lap and butt joints were optically analysed to provide information on the fatigue failure of the joints. Transverse sections were mounted in conductive bakelite and subsequently ground, polished and etched. The aim of the fatigue failure analysis was to characterise the fatigue initiation sites and angle of propagation etc, with respect to the laser welded joint. The equipment used was an optical microscope with an integral digital camera. A PC with image capture software was connected to the digital camera, which allowed the images to be manipulated to enhance analysis.

3.5.3.2.1 Butt Joints

Dissimilar metal laser-welded butt joints were analysed to determine and compare fatigue failure positions, for example, failure in the weld bead, failure between the weld and zinc-coated mild steel or failure between the weld bead and the stainless steel.

3.5.3.2.2 Lap Joints

Similar and dissimilar metal laser-welded lap joints were analysed to determine and compare fatigue failure in the mild steel and the stainless steel, with regard to initiation site, distance from the laser weld bead centre and propagation angle.

3.5.4 Scanning Electron Microscopy

A scanning electron microscope (SEM) was used in both secondary electron and back scattered electron mode to allow further examination of similar and dissimilar laser welded butt and lap joints. The SEM used was a Philips XL40, which is computer controlled with integrated software that allows qualitative and quantitative chemical analysis. The SEM allowed higher magnification images to be produced with excellent resolution and improved depth of field/focus in comparison to the optical microscope.

3.5.4.1 Fatigue Failure Analysis

Further fatigue failure analysis of the lap and butt joints was undertaken. This was to provide higher magnification images of the fatigue cracks and analysis of the initiation sites. As well as the standard secondary electron mode of SEM analysis, back-scattered electron mode was used to determine if the fatigue cracks propagated preferentially in or around a particular phase. Thus, the back scattered electron mode was used to produce images whose contrast was atomic-number dependent.

3.5.4.2 Weld Bead Compositions

The compositions of dissimilar metal laser-welded butt and lap joints were analysed to determine the weld bead chemical composition and the effects of the welding process parameters on the weld bead compositions. It was not possible to isolate the laser welds and have the weld beads chemically analysed as the size of the laser weld was too small. Consequently, the laser welds were mounted in conductive bakelite and chemically analysed using the Philips XL40 SEM.

The XL40 is equipped with Energy Dispersive X-ray analysis (EDX). It also has the ability to semi-quantitatively identify the elements present in a sample. This is done by returning the relative percentage of counts from each element selected. Hence, the stainless steel parent material was semi-quantifiably analysed for Fe, Cr and Ni, determining the relative percentage of each respective elements k_α counts. Since the actual parent material composition was known, it was possible to relate the relative percentages to the actual percentages. The microhardness grid was then used as a reference and analysis of the laser weld bead commenced. If, for example, the Cr and Ni relative percentages of the weld bead dropped by 50%, the corresponding calculated Cr and Ni chemical content would fall by 50%, thus a 50% dilution of the stainless steel would have occurred. Since the zinc-coated mild steel is very lean, the error introduced by ignoring the other elements in the zinc-coated mild steel and the stainless steel was relatively small (estimated <2%).

3.5.4.2.1 Butt Joints

Six dissimilar metal laser welded butt joints were analysed. Three of these dissimilar metal laser welded butt joints were 1mm 304 laser welded to zinc-coated mild steel; the other three were 0.78mm 2205 laser welded to zinc-coated mild steel. These were welded with the same welding parameters apart from the laser welding speed which was increased from 3.0m/min to 3.5m/min, and finally, to 4.0m/min respectively.

The weld bead compositions were analysed to determine the effects of welding speed on the dilution and stirring mechanism (Marangoni flow) and ultimately the composition of the weld bead.

3.5.4.2.2 Lap Joints

Four dissimilar metal laser-welded lap joints were analysed. Two were 1mm 304 laser welded to zinc-coated mild steel (both configurations, one with the stainless steel on the top of the lap and the second with the zinc-coated mild steel on the top of the lap) and two were 1mm 2205 laser welded to zinc-coated mild steel (again, both configurations).

4 *Results*

4.1 Introduction

The results chapter follows a similar direction dictated by the experimental techniques stated in chapter 3. Thus, the results can be split into the following sections:

- *Mechanical Testing*
  - Laser weld lap shear/tensile properties – **Trumpf 5kW CO_2 laser welder**
    - **Process optimisation and joint configuration** - lap shear (lap-joint) and tensile (butt-joint) properties
    - **Material optimisation** - Thinner gauge stainless steel lap joints
  - Laser weld lap shear/tensile properties – **Rofin 2kW CO_2 laser welder**
    - **Fatigue specimen production** – lap shear (lap-joint) and tensile (butt-joint) properties
  - Laser welded lap joint fatigue properties – **Trumpf 5kW CO_2 laser welder**
    - **1mm 304 (top) – 1.2mm V1437** dissimilar metal lap joint
    - **1mm 304 – 1.2mm V1437 (top)** dissimilar metal lap joint
    - **0.78mm 2205 (top) – 1.2mm V1437** dissimilar metal lap joint
    - **0.78mm 2205 – 1.2mm V1437 (top)** dissimilar metal lap joint
  - Laser welded lap/butt joint fatigue properties – **Rofin 2kW CO_2 laser welder**
    - **1mm 2205 – 1.2mm V1437 (top)** dissimilar metal lap joint
    - **1mm 2101 – 1.2mm V1437 (top)** dissimilar metal lap joint
    - **1mm 2101 – 1mm V1437** dissimilar metal butt joint
    - **1mm 2101 – 1mm 2101** similar metal lap joint

- ***Lap Joint Rotation Tests***
- ***Weld Bead Metallography***
  - Microhardness testing results
  - Weld bead composition results
  - Fatigue failure analysis

4.2 Laser-Welded Butt Joint Tensile Properties – Trumpf 5kW CO_2 Laser Welder (Process Optimisation/Joint Configuration Trials)

As stated in section **3.1.1**, similar and dissimilar metal laser-welded butt joints were produced with a range of parameters. Each weld was examined visually for signs of porosity and blow holes in the laser weld bead; tensile properties were also determined.

4.2.1 Similar Metal Laser Welded Butt Joint Results

The welding parameters used for the similar and dissimilar metal butt joint laser welding trials were:

- Welding power: 3.8kW (workpiece)
- Welding speed: **4.0m/min**
  3.5m/min
- Focal point: Sheet surface
- Focal length: 250mm
- Trailing gas flow rate: 20L/min

Thus, all of the welding parameters were fixed, except the welding speed. In the following graphs the welding speed can be seen on the 'x' axis under the respective data.

Graph 13 below shows the similar metal butt joint ultimate tensile strength (R_m) results. It should be noted that the 4m/min and 3.5m/min on the 'X' axis denote the laser welding speed used to produce the laser weld. This graph allows comparison of the ultimate tensile strength (R_m) with regard to welding speed.

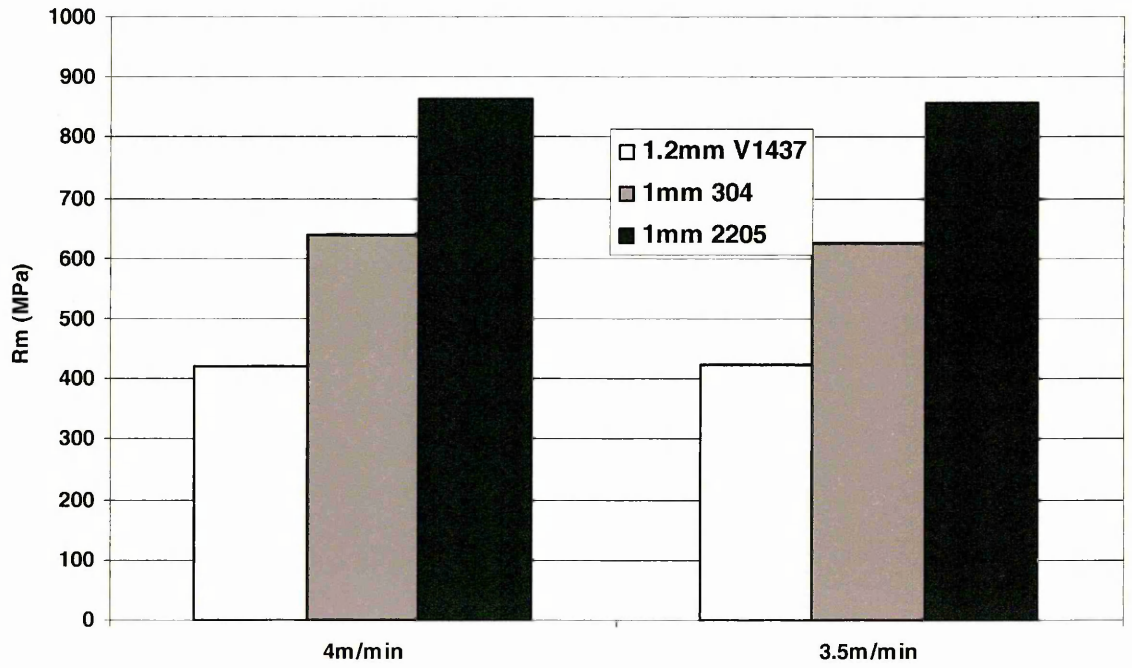

Graph 13 Graph to show the effects of laser welding speed on the R_m properties of three similar metal butt joints

- 1.2mm V1437 similar metal butt joint tensile failure occurred in the parent material of the V1437 zinc coated mild steel at 45° shear.
- 1mm 304 and 1mm 2205 similar metal laser welded butt joint tensile failure occurred at the edge of the weld in the HAZ.

Graph 14 shows the percentage elongations to failure for the similar metal laser welded butt joints. Again, the two welding speeds used for the production of the butt joints can be seen on the 'x' axis. This graph compares the percentage elongation to failure with respect to welding speed.

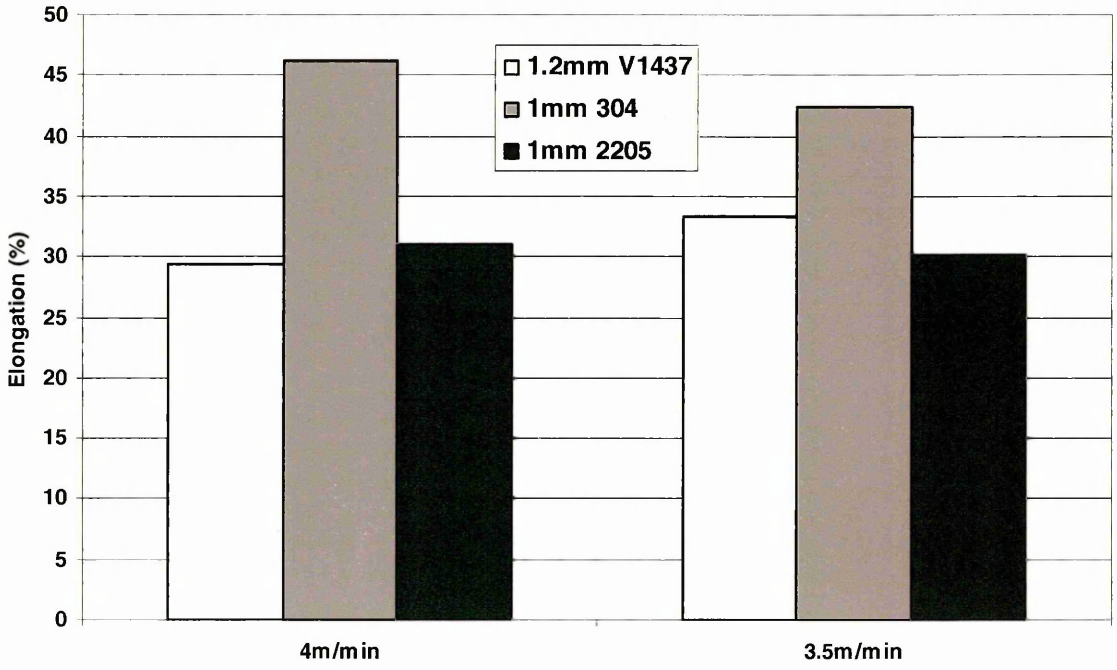

Graph 14 Graph to show the effects of laser welding speed on the % elongation properties of three similar metal butt joints

The following table compares the similar metal butt joint tensile properties with the actual parent material tensile properties.

	R_m (MPa)	% Elongation
1.2mm V1437 (parent)	420	30
1.2mm V1437 (similar metal butt joint)	420	31.4
1mm 304 (parent)	627	57
1mm 304 (similar metal butt joint)	632.6	44.2
1mm 2205 (parent)	853	35
1mm 2205 (similar metal butt joint)	860	30.6

Table 18 comparison between the parent material tensile properties and the similar metal laser welded butt joint tensile properties

4.2.2 Dissimilar Metal Laser Welded Butt Joint Results

The welding parameters used for the similar and dissimilar metal butt joint laser welding trials were:

- Welding power: 3.8kW (work piece)
- Welding speed: **4.0m/min**

  3.5m/min

  3.0m/min
- Focal point: Sheet surface
- Focal length: 250mm
- Trailing gas flow rate: 20L/min

Thus, the welding parameters were fixed with the exception of the welding speed which was sequentially increased. In the following graphs, the welding speed can be seen on the 'x' axis under the respective data.

Graph 15 below shows the dissimilar metal butt joint ultimate tensile strength (R_m) results. It should be noted that the welding speed can be seen on the 'x' axis under the respective data. This graph allows comparison of the ultimate tensile strength (R_m) with regard to welding speed.

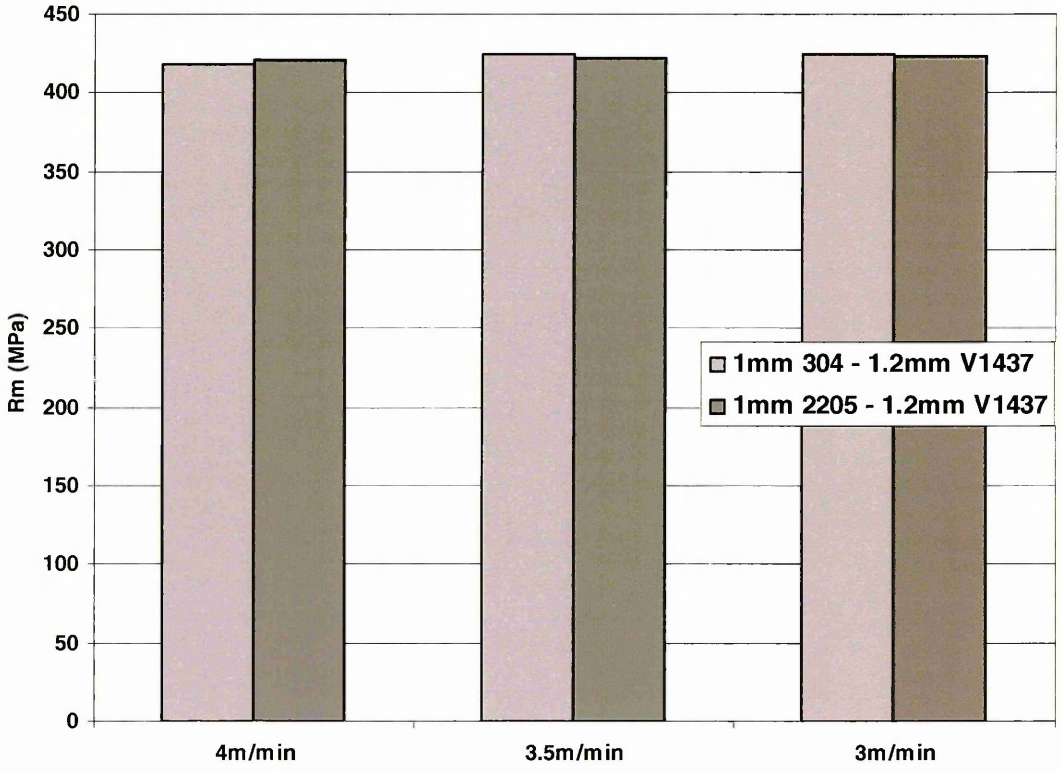

Graph 15 Graph to show the effects of laser welding speed on the R_m properties of two dissimilar metal butt joints

- The three dissimilar metal laser welded butt joints between 304 and V1437 all failed in the parent material of the V1437 zinc-coated mild steel at 45° shear away from the weld.
- The three dissimilar metal laser welded butt joints between 2205 and V1437 all failed in the parent material of the V1437 zinc-coated mild steel at 45° shear away from the weld.

Graph 16 shows the percentage elongations to failure for the dissimilar metal laser welded butt joints. Again, the welding speed can be seen on the 'x' axis under the respective data. This graph allows comparison of the elongations to failure with respect to welding speed.

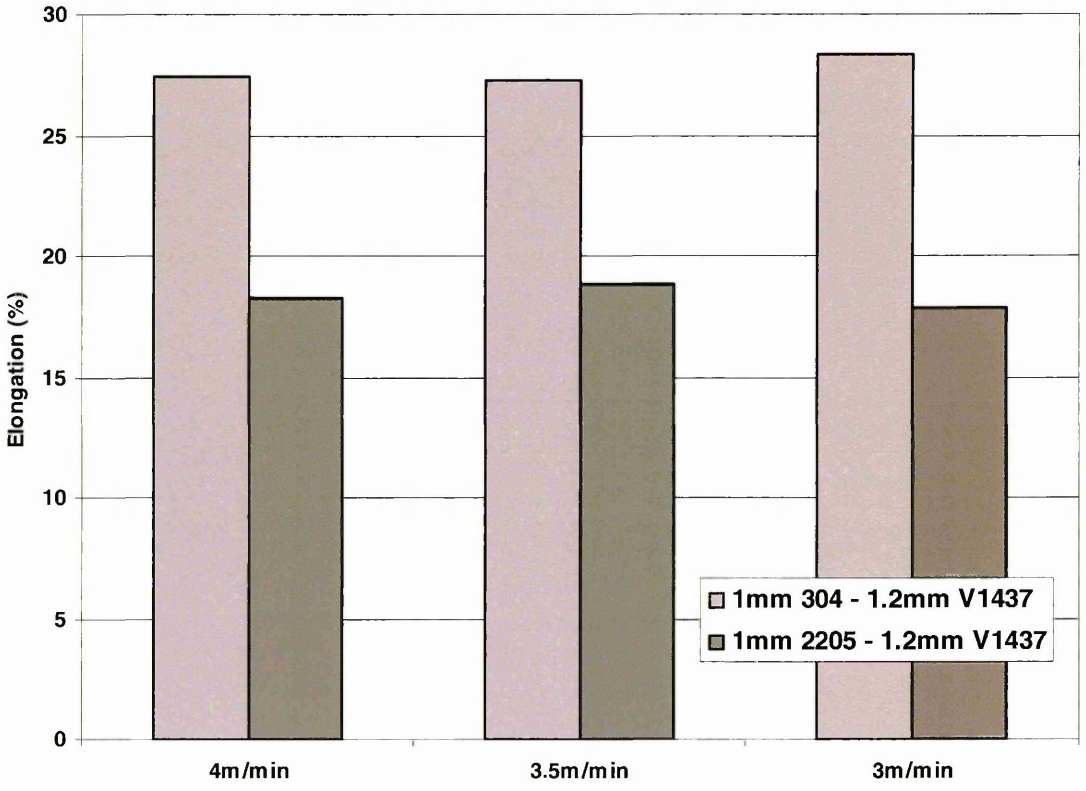

Graph 16 Graph to show the effects of laser welding speed on the % elongation properties of two dissimilar metal butt joints

4.3 Laser-Welded Lap Shear Properties – Trumpf 5kW CO_2 Laser Welder (Process Optimisation/Joint Configuration Trials)

As stated in **chapter 3, section 3.1.1**, similar and dissimilar metal laser-welded lap joints were produced with a range of parameters. Each weld was visually examined for signs of porosity and blow holes in the laser weld bead and also to assess the consistency of penetration. The lap shear properties of each weld were then determined. Thus, the optimum welding parameters for each configuration was determined, this being defined as the highest welding speed whilst achieving full consistent penetration.

4.3.1 Similar Metal Laser Welded Lap Shear Results

The laser welding parameters which provided the highest lap shear properties for 1.2mm V1437 zinc-coated mild steel similar metal lap joints were:

- Welding power: 3.8kW (work piece)
- Welding speed: 2.3m/min
- Focal point: 0.1mm above top sheet surface
- Focal length: 250mm
- Trailing gas flow rate: 25L/min
- Overlap: 10mm
- Interfacial gap: None

However, very poor V1437 similar metal lap joints were produced in terms of weld quality. Each weld bead showed signs of blow holes, and porosity with inconsistent, if any, penetration being achieved. Hence the laser welding process was not optimised for this similar metal lap joint configuration.

The optimised parameters for both 1mm 304 and 2205 stainless steel similar metal laser welded lap joints were:

- Welding power: 3.8kW (work piece)
- Welding speed: 2.6m/min
- Focal point: 0.1mm above top sheet surface
- Focal length: 250mm
- Trailing gas flow rate: 25L/min
- Overlap: 30mm
- Interfacial gap: None

Graph 17 below, shows the similar metal laser welded lap shear properties produced using the optimum welding parameters.

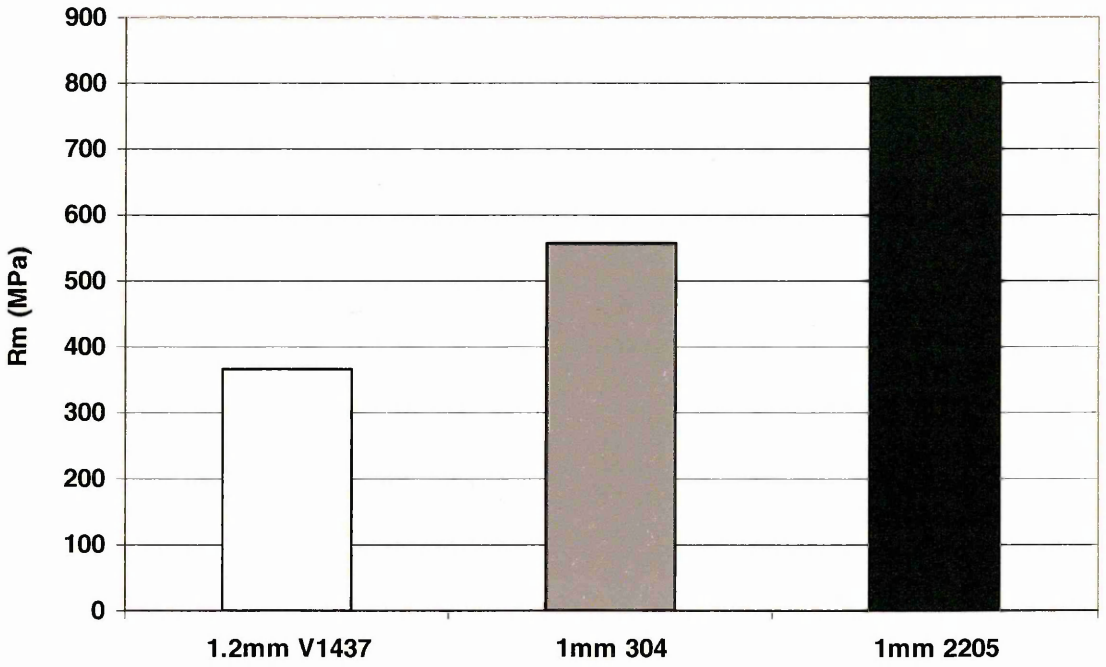

Graph 17 shows the similar metal lap shear properties produced with the optimum welding parameters

The 1.2mm V1437 and stainless steel (1mm 304 and 1mm 2205) similar metal lap shear failures occurred in the HAZ at the edge of the weld bead.

The failures occurred across the region used for the cross sectional area in the calculation of the Rm stress (MPa).

The following table compares the similar metal weld lap shear properties with the actual parent material tensile properties.

	R_m (MPa)	% Elongation
1.2mm V1437 (parent)	420	30
1.2mm V1437 (similar metal lap joint)	366	19
% Parent	**87%**	**63%**
1mm 304 (parent)	627	57
1mm 304 (similar metal lap joint)	557	23
% Parent	**89%**	**40%**
1mm 2205 (parent)	853	35
1mm 2205 (similar metal lap joint)	810	12
% Parent	**95%**	**34%**

Table 19 Comparison between the parent material tensile properties and the similar metal laser welded lap shear properties

Graph 18 shows the percentage elongations to failure for the similar metal laser welded lap joints. This graph allows comparison of the elongations to failure for the three similar metal lap joints.

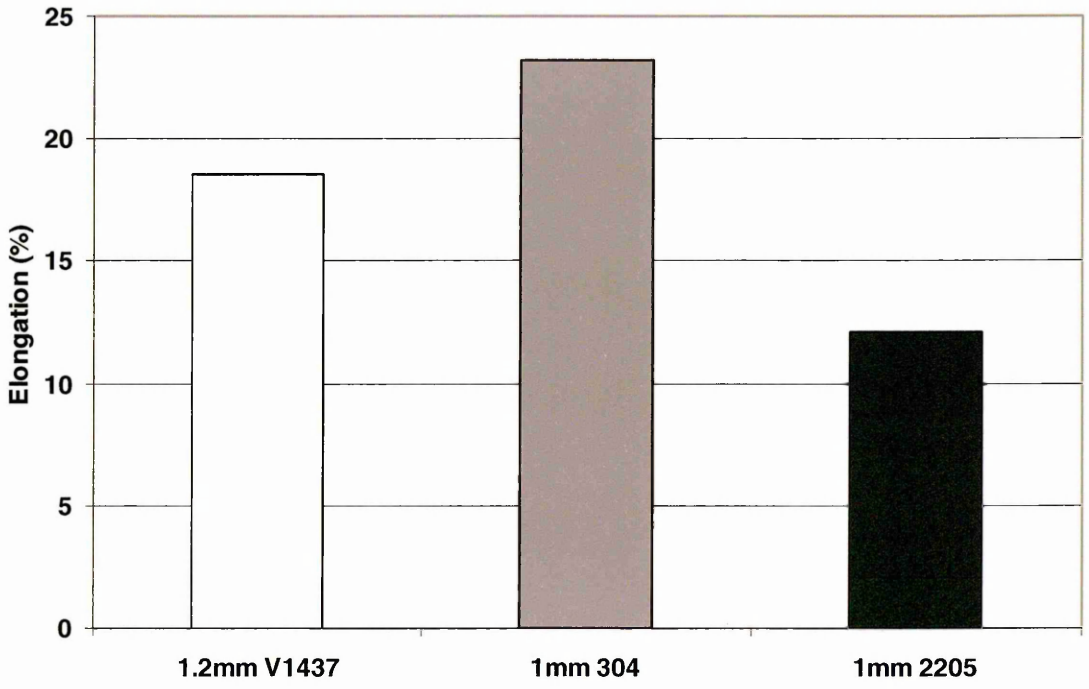

Graph 18 Comparison of similar metal lap joint % elongations

4.3.2 Dissimilar Metal Laser Welded Lap Shear Results

The optimum laser welding parameters for the four dissimilar metal lap joint configurations were:

- Welding power: 3.8kW (work piece)
- Welding speed: 2.3m/min
- Focal point: 0.1mm above top sheet surface
- Focal length: 250mm
- Trailing gas flow rate: 20L/min
- Overlap: 10mm
- Interfacial gap: None

Graph 19 below, shows the dissimilar metal laser welded lap shear properties produced using the optimum welding parameters. For comparison, the similar metal lap shear results are also presented.

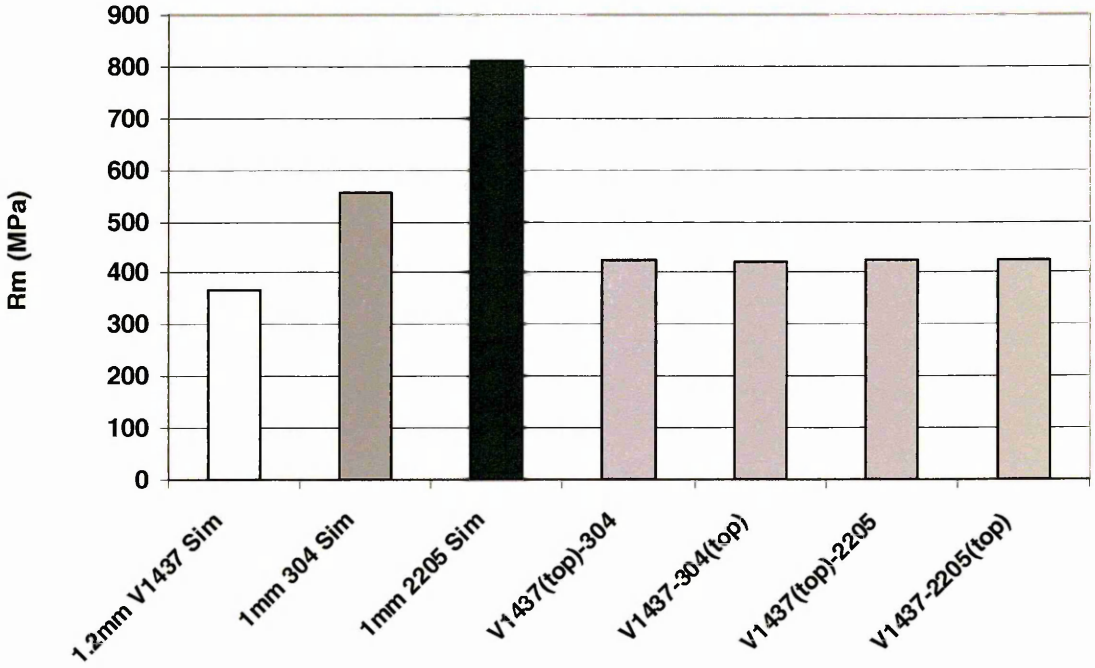

Graph 19 shows the dissimilar metal lap shear properties produced with the optimum welding parameters

All four dissimilar metal lap joints failed in the parent material of the mild steel at 45° shear away from the laser weld.

Graph 20 shows the percentage elongations to failure for the dissimilar metal laser welded lap joints. This graph allows comparison of the elongations to failure for the three similar metal lap joints.

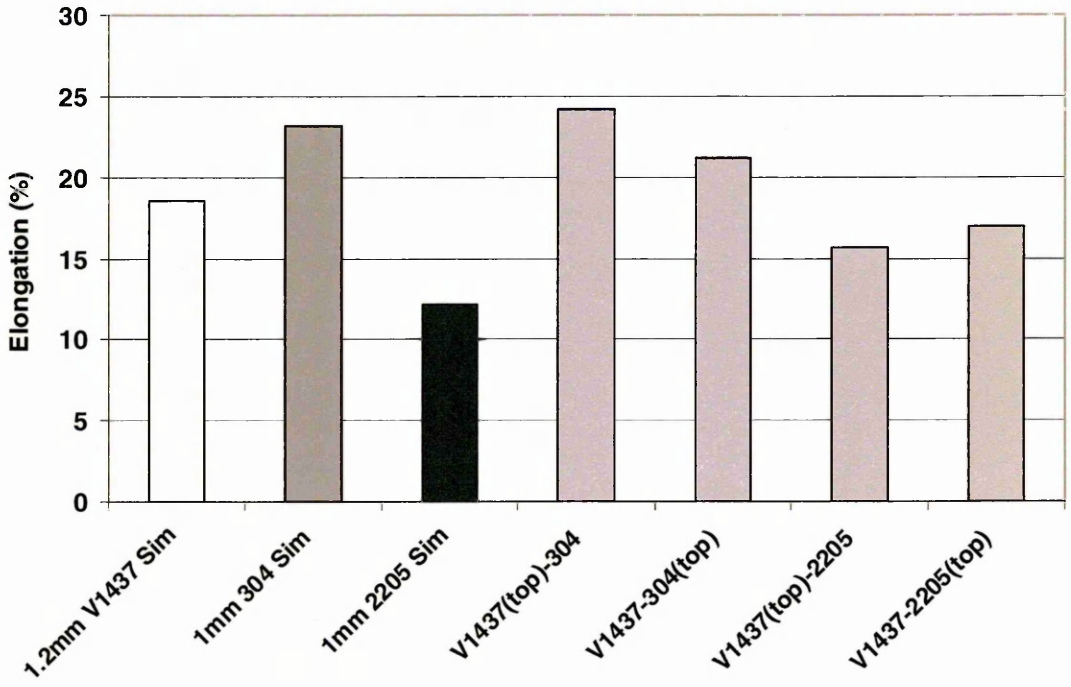

Graph 20 compares the lap shear percentage elongations to failure for dissimilar metal lap joints

4.4 Laser-Welded Lap Shear Properties – Trumpf 5kW CO_2 Laser Welder (Material Optimisation Trials)

As stated in 3.1.1.2, thinner gauges of stainless steel were laser welded to 1.2mm V1437 in the lap joint configuration.

The welding parameters used were determined from the original welding trials:

- Welding power: 3.8kW (work piece)
- Welding speed: 2.6m/min
- Focal point: 0.1mm above top sheet surface
- Focal length: 250mm
- Trailing gas flow rate: 20L/min
- Overlap: 10mm
- Interfacial gap: None

Graph 21 below shows the lap shear properties of dissimilar metal laser welds produced with thinner gauge stainless steel.

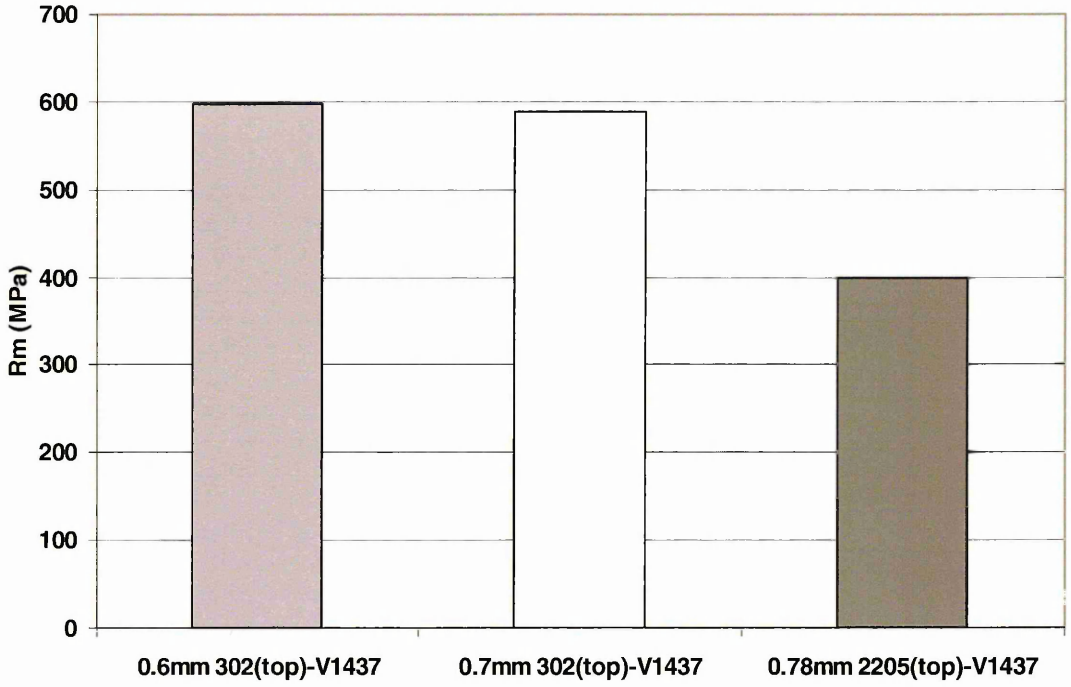

Graph 21 shows the lap shear properties of dissimilar metal laser welds with thinner gauge stainless steel

- Lap shear failure occurred in the parent material of both the 0.6 and 0.7mm 302 stainless steel when welded to 1.2mm V1437.
- However, the lap shear failure occurred in the parent material of the 1.2mm V1437 for the dissimilar metal lap joint when welded to 0.78mm 2205.

Note: the Rm has been calculated for the thickness of the failed sheet

Graph 22 below shows the lap shear percentage elongation properties of dissimilar metal laser welds produced with thinner gauge stainless steel.

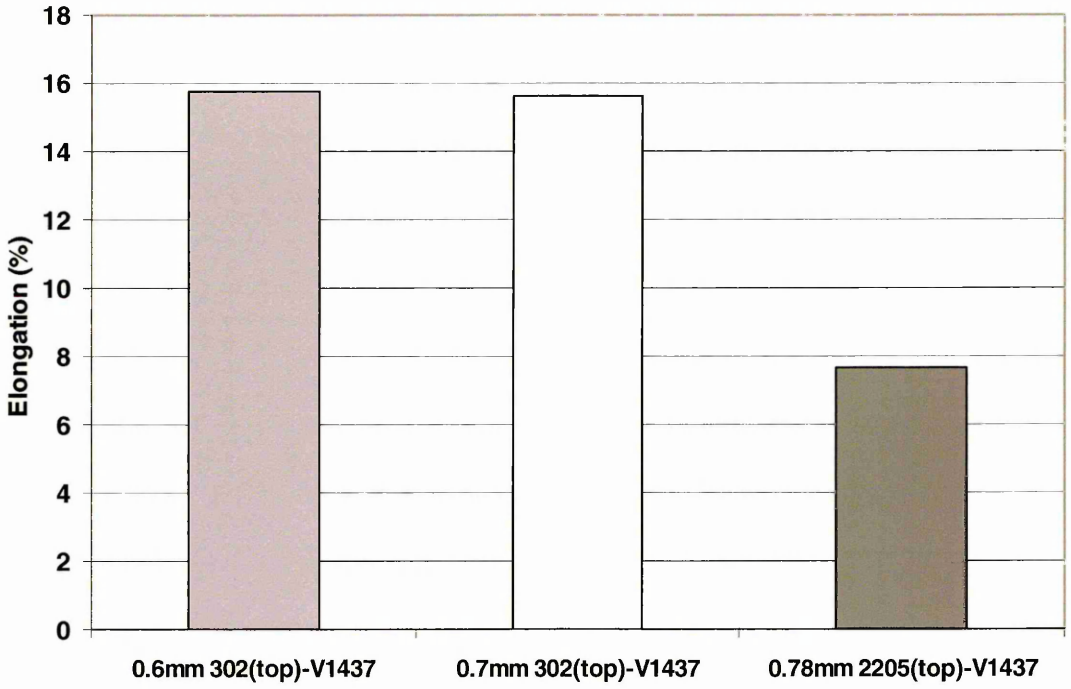

Graph 22 shows the lap shear elongation properties of dissimilar metal laser welds with thinner gauge stainless steel

4.5 Laser-Welded Tensile/Lap Shear Properties – Rofin 2kW CO_2 Laser Welder (Fatigue Specimen Production)

The Rofin 2kW CO_2 laser welding parameters used to produce the similar and dissimilar metal lap joints were:

- Welding power: 2kW (work piece)
- Welding speed: 1m/min
- Focal point: 4mm above top sheet surface
- Focal length: 67.5mm
- Trailing gas flow rate: 20L/min
- Overlap: 25mm
- Interfacial gap: None

The welding parameters used to produce the dissimilar metal butt joint were:

- Welding power: 2kW (work piece)
- Welding speed: 1.5m/min
- Focal point: 0mm (sheet surface)
- Focal length: 67.5mm
- Trailing gas flow rate: 20L/min
- Overlap: N/A
- Interfacial gap: N/A

The laser welds produced were:

- 1.2mm V1437 (top) – 1mm 2205 dissimilar metal lap joint
- 1.2mm V1437 (top) – 1mm 2101 dissimilar metal lap joint
- 1mm 2101 – 1mm 2101 similar metal lap joint
- 1.2mm V1437 – 1mm 2205 dissimilar metal butt joint

Graph 23 below shows the tensile and lap shear properties of the similar and dissimilar metal laser welded butt and lap joints produced with the Rofin 2kW CO_2 laser welder.

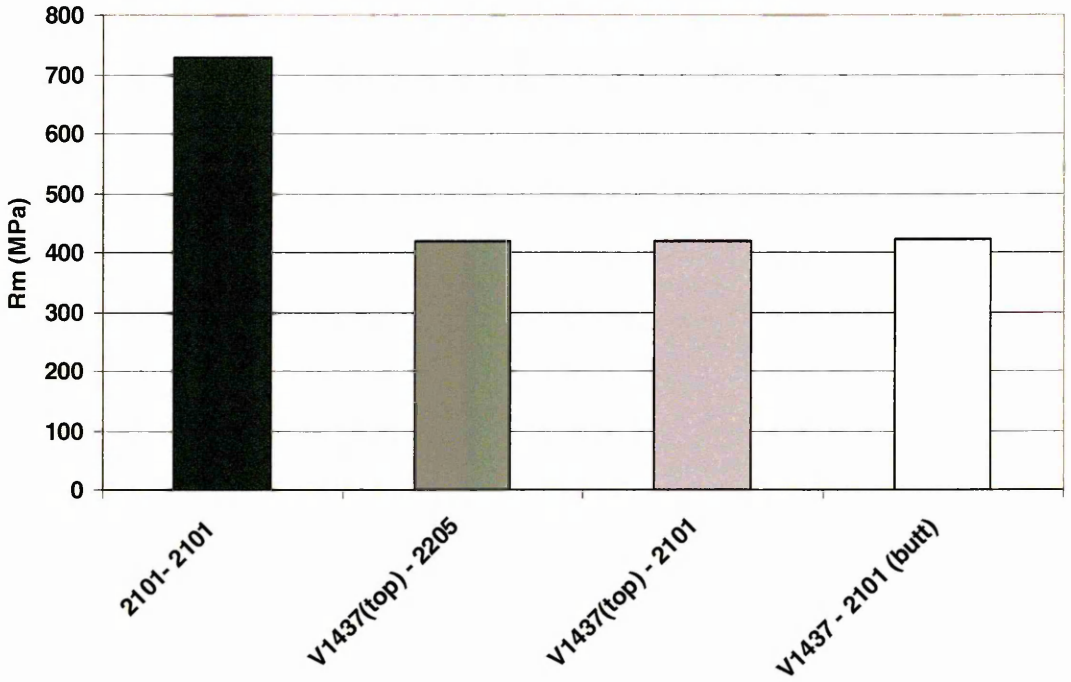

Graph 23 Graph to show the tensile and lap shear properties of similar and dissimilar metal laser welded lap and butt joints

- Similar metal 1mm 2101 lap shear failure occurred at the edge of the weld in the HAZ.
- Dissimilar metal lap shear failure occurred in the parent material of the 1.2mm V1437 at 45° shear away from the weld for both configurations.
- Dissimilar metal butt joint failure occurred in the parent material of the 1.2mm V1437 at 45° shear away from the weld.

Graph 24 below shows the tensile and lap shear percentage elongation properties of the similar and dissimilar metal laser welded butt and lap joints produced with Rofin 2kW CO_2 laser welder.

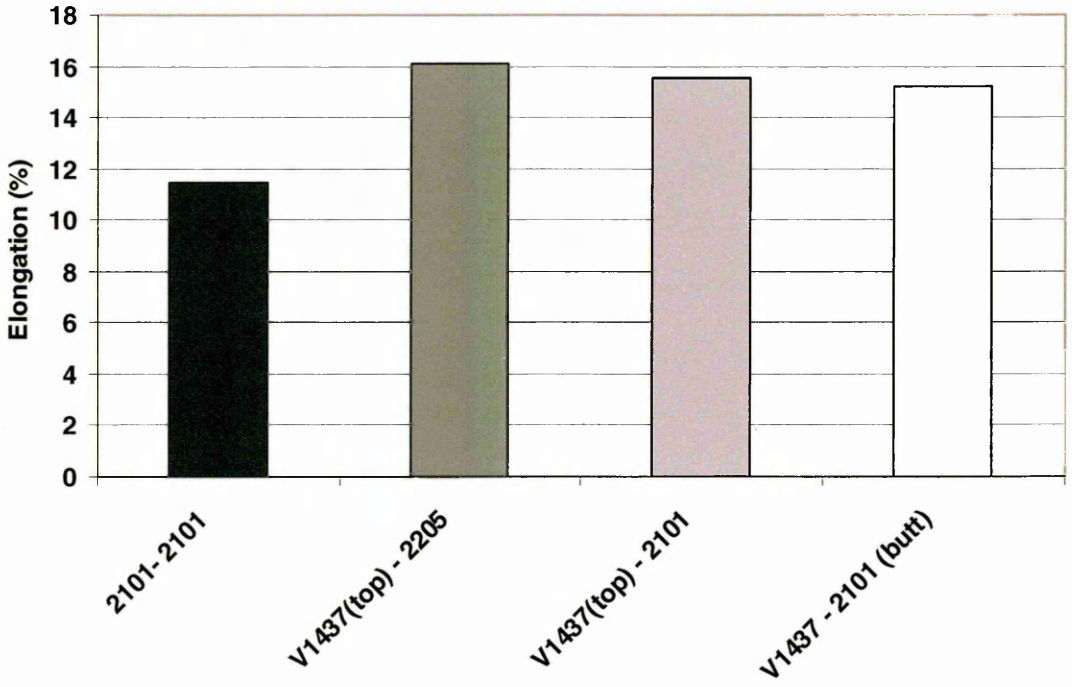

Graph 24 Graph to show the percentage elongation properties of similar and dissimilar metal laser weld butt and lap joints

4.6 Lap Joint Fatigue Properties – Trumpf 5kW CO_2 Laser Welder

Four dissimilar metal laser welded lap joints were fatigue tested in air to produce an S-N curve and to determine the statistically valid mean fatigue line load range at $2x10^6$ cycles. These joints all possessed >100% weld efficiency, that is, lap shear failure occurred in the parent material of the 1.2mm V1437 zinc-coated mild steel.

The fatigue properties of each joint are presented using the line load range units. This is simply the applied load range per unit length. This unit allows the comparison of dissimilar thickness lap joint fatigue properties as no cross section is used to calculate a relevant stress. It should be noted that the fatigue failures occurred randomly in either the 1.2mm V1437 or the stainless steel for each configuration. Hence, during the staircase method, it was common to have failure occurring in both materials for the same applied load level. This posed problems when calculating the respective stresses and is illustrated in Graph 25. It is apparent that there are three potential stresses which can be calculated for a dissimilar metal joint. This can cause discrepancies when comparing the fatigue properties of dissimilar thickness, dissimilar metal joints. The line load range unit (N/mm) is the force (N) per unit length (mm) and is not based on an area; hence, it allows the fatigue properties of dissimilar thickness joints to be compared more easily also allowing comparison of discontinuous welding processes such as resistance spot welding. The staircase and S-N curve of the lap joints produced using the Trumpf laser welder can be found in Appendix 8.1.

Graph 25 illustrates the displacement of results that can occur if one of the three thicknesses is used to calculate a stress. This can lead to misinterpretations when the fatigue results between dissimilar thickness joints are compared.

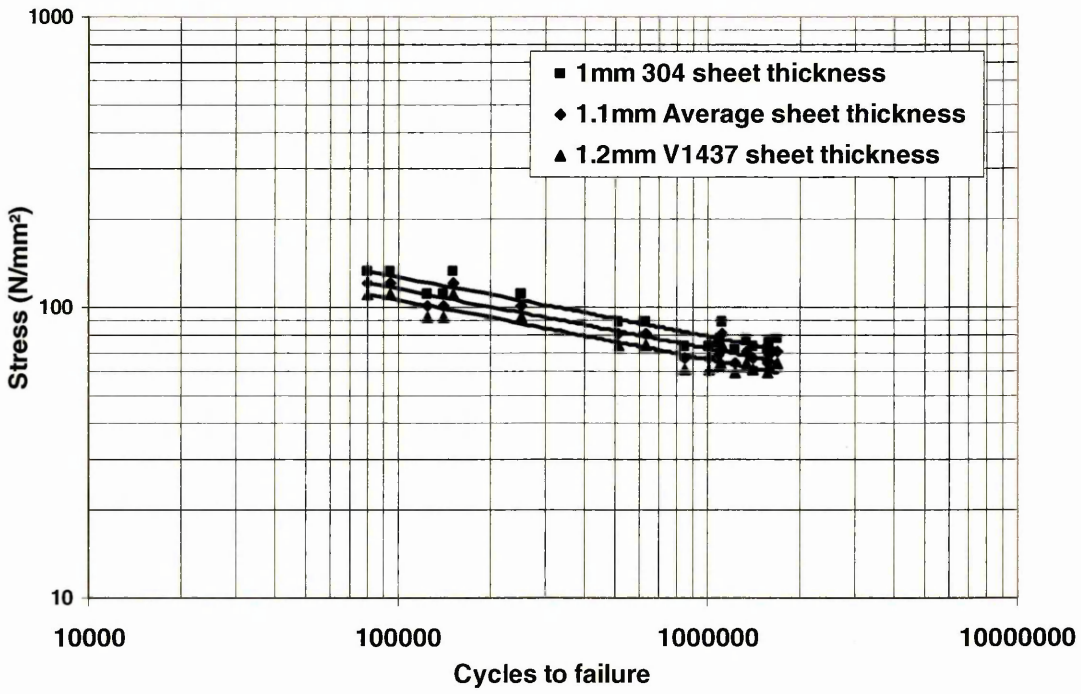

Graph 25 Graph to show the displacement of fatigue results when stress is calculated using different thickness

The applied bending moment unit first used by Linder et al[70] was assessed with regard to lap joint fatigue property comparisons. It can be seen in Graph 26, on the following page, that the applied bending moment and line load units allow similar comparisons to be made.

Graph 26 compares the lap joint fatigue results from this investigation using both the applied bending moment and the line load units.

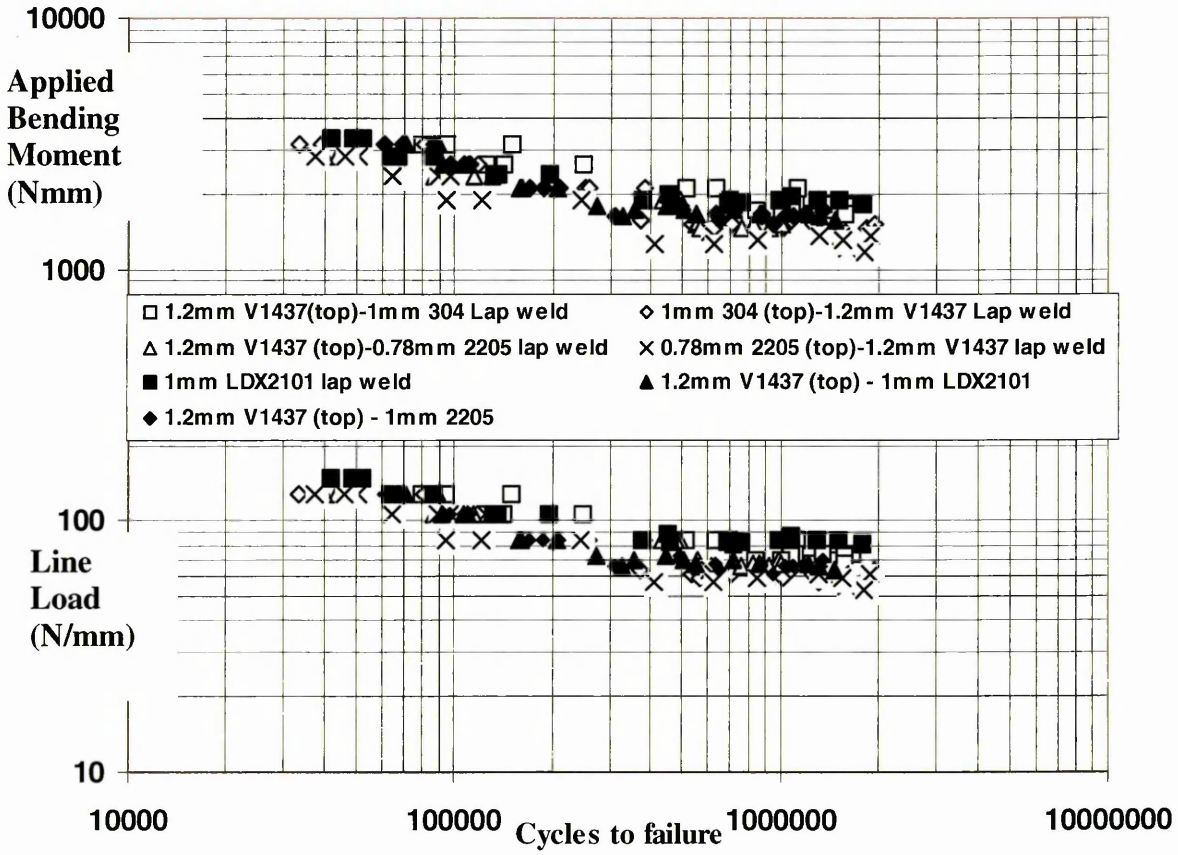

Graph 26 Fatigue scatter comparison between the applied bending moment and line load units

Apart from the obvious displacement of results, no significant alternative trends to the fatigue properties could be made with the applied bending moment comparisons.

For this reason the line load range unit was considered to be the most appropriate and was used throughout this investigation.

1mm 304 (top) – 1.2mm V1437 Fatigue Results

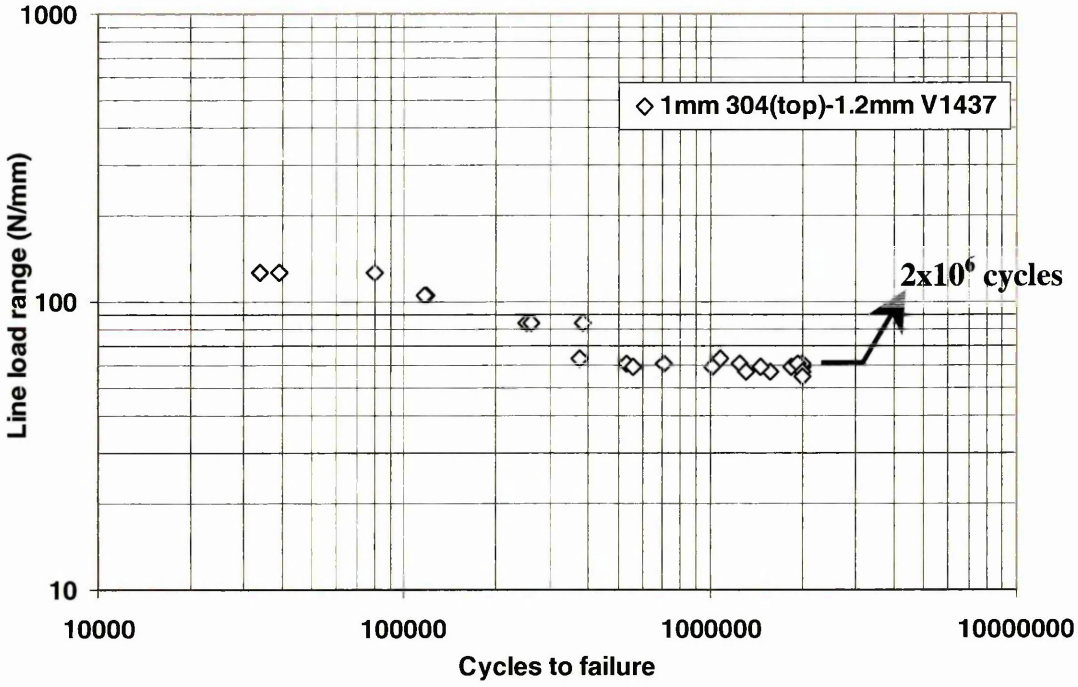

Graph 27 Graph to show the line load range fatigue properties for the 1mm 304 (top) – 1.2mm V1437 lap joint

Mean Fatigue Line Load Range at $2x10^6$ cycles

$P_0 + d (A / F - 0.5) = \mathbf{X}$ **(N/mm)**

$54.89 + 2.22 (30 / 12 - 0.5) = \mathbf{59.3}$ **(N/mm)**

Statistical Validity

$(F * B - A^2) / F^2 = \mathbf{>0.3 \text{ and } <1.2}$

$(12 * 86 - 30^2) / 12^2 = \mathbf{0.9}$

Standard Deviation

$1.620 * d \{(F * B - A^2) / F^2 + 0.029\} = \mathbf{S}$ **(N/mm)**

$1.620 * 2.22 \{(12 * 86 - 30^2) / 12^2 + 0.029\} = \mathbf{3.4}$ **(N/mm)**

Thus, the mean fatigue line load range at $2x10^6$ cycles for the lap joint configuration 1mm 304 (top) – 1.2mm V1437 is **59.3 N/mm** with a standard deviation of **3.4 N/mm** or **6%** and is statistically valid.

1.2mm V1437 (top) – 1mm 304 Fatigue Results

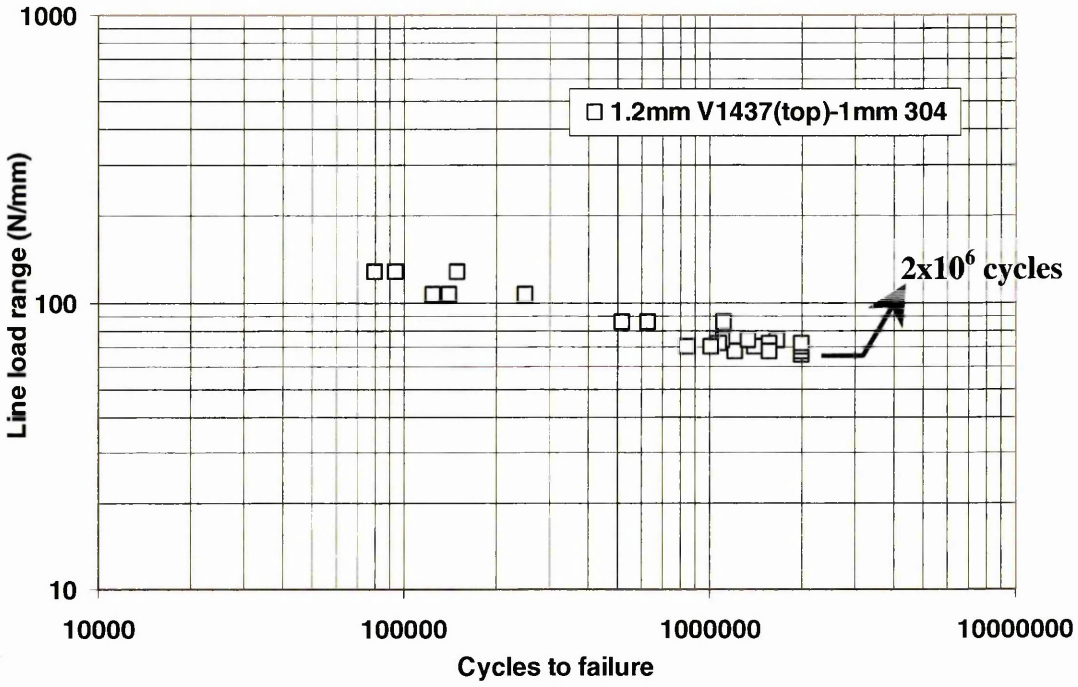

Graph 28 Graph to show the line load range fatigue properties for the 1.2mm V1437 (top) – 1mm 304 lap joint

Mean Fatigue Line Load Range at $2x10^6$ cycles

$P_0 + d (A / F - 0.5) = \mathbf{X}$ **(N/mm)**

$65.44 + 2.22 (26 / 10 - 0.5) = \mathbf{70.1}$ **(N/mm)**

Statistical Validity

$(F * B - A^2) / F^2 = \mathbf{>0.3 \text{ and } <1.2}$

$(10 * 80 - 26^2) / 10^2 = \mathbf{1.2}$

Standard Deviation

$1.620 * d \{(F * B - A^2) / F^2 + 0.029\} = \mathbf{S}$ **(N/mm)**

$1.620 * 2.22 \{(10 * 80 - 26^2) / 10^2 + 0.029\} = \mathbf{4.6}$ **(N/mm)**

Thus, the mean fatigue line load range at $2x10^6$ cycles for the lap joint configuration 1.2mm V1437 (top) – 1mm 304 is **70.1 N/mm** with a standard deviation of **4.6 N/mm** or **6%** and is statistically valid.

0.78mm 2205 (top) – 1.2mm V1437 Fatigue Results

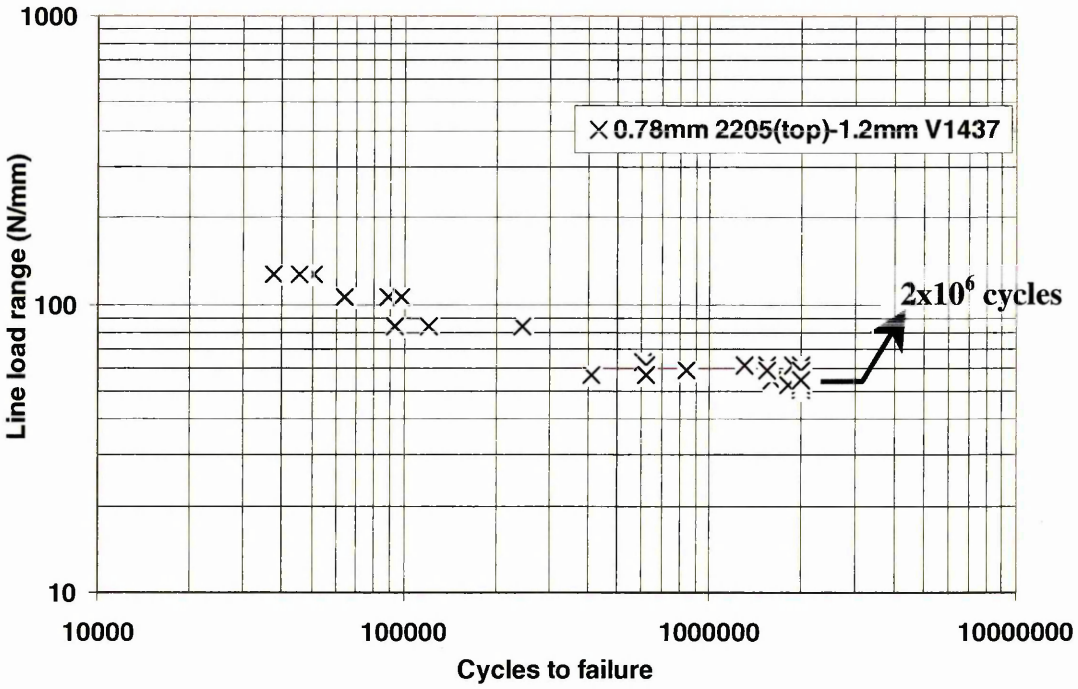

Graph 29 Graph to show the line load range fatigue properties for the 0.78mm 2205 (top) – 1.2mm V1437 lap joint

Mean Fatigue Line Load Range at $2x10^6$ cycles

$P_0 + d (A / F - 0.5) = \mathbf{X}$ **(N/mm)**

$50.67 + 2.22 (27 / 8 - 0.5) = \mathbf{57.1}$ **(N/mm)**

Statistical Validity

$(F * B - A^2) / F^2 = \mathbf{>0.3 \text{ and } <1.2}$

$(8 * 105 - 27^2) / 8^2 = \mathbf{1.7}$

Standard Deviation

$1.620 * d \{(F * B - A^2) / F^2 + 0.029\} = \mathbf{S}$ **(N/mm)**

$1.620 * 2.22 \{(8 * 105 - 27^2) / 8^2 + 0.029\} = \mathbf{6.3}$ **(N/mm)**

Thus, the mean fatigue line load range at $2x10^6$ cycles for the lap joint configuration 0.78mm 2205 (top) – 1.2mm V1437 is **57.1 N/mm** with a standard deviation of **6.3 N/mm** or **11%**, this is not statistically valid.

1.2mm V1437 (top) – 0.78mm 2205 Fatigue Results

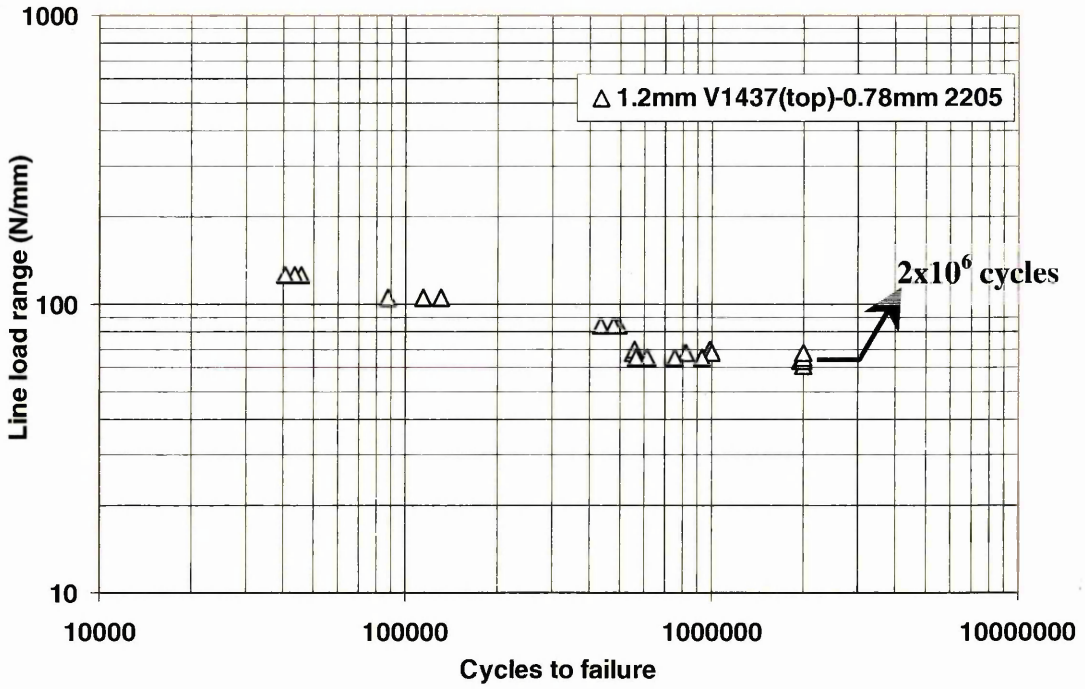

Graph 30 Graph to show the line load range fatigue properties for the 1.2mm V1437 (top) – 0.78mm 2205 lap joint

Mean Fatigue Line Load Range at $2x10^6$ cycles

$P_0 + d (A / F - 0.5) = \mathbf{X}$ **(N/mm)**

$61.22 + 2.22 (26 / 10 - 0.5) = \mathbf{65.9}$ **(N/mm)**

Statistical Validity

$(F * B - A^2) / F^2 = \mathbf{>0.3 \text{ and } <1.2}$

$(10 * 76 - 26^2) / 10^2 = \mathbf{0.8}$

Standard Deviation

$1.620 * d \{(F * B - A^2) / F^2 + 0.029\} = \mathbf{S}$ **(N/mm)**

$1.620 * 2.22 \{(10 * 76 - 26^2) / 10^2 + 0.029\} = \mathbf{3.1}$ **(N/mm)**

Thus, the mean fatigue line load range at $2x10^6$ cycles for the lap joint configuration 1.2mm V1437 (top) – 0.78mm 2205 is **65.9 N/mm** with a standard deviation of **3.1 N/mm** or **5%** and is statistically valid.

4.7 Lap and Butt Joint Fatigue Properties – Rofin 2kW CO_2 Laser Welder

Four similar and dissimilar metal laser welded butt and lap joints were fatigue tested in air to produce an S-N curve and to determine the statistically valid mean fatigue line load range at $2x10^6$ cycles. These joints possessed >100% weld efficiency (apart from the 1mm 2101 similar metal lap joint), that is, tensile and lap shear failure occurred in the parent material of the 1.2mm V1437 zinc-coated mild steel.

The welds were produced with the following welding parameters:

1.2mm V1437 (top) – 1mm 2205 & 1mm 2101 – 1mm 2101

1.2mm V1437 (top) – 1mm 2101

- Welding power: 2kW (work piece)
- Speed: 1m/min
- Focal point: 4mm above top sheet surface
- Focal length: 67.5mm
- Trailing gas flow rate: 20L/min
- Overlap: 25mm
- Interfacial gap: None

The staircase and S-N curve of the butt and lap joints produced using the Rofin laser welder can be found in Appendix 8.2.

1.2mm V1437 – 1mm 2101 butt joint

- Welding power: 2kW (work piece)
- Speed: 1.5m/min
- Focal point: 0mm sheet surface
- Focal length: 67.5mm
- Trailing gas flow rate: 20L/min
- Overlap: N/A
- Interfacial gap: N/A

The fatigue properties of each joint are again presented using the line load range units.

1.2mm V1437 (top) – 1mm 2205 Fatigue Results

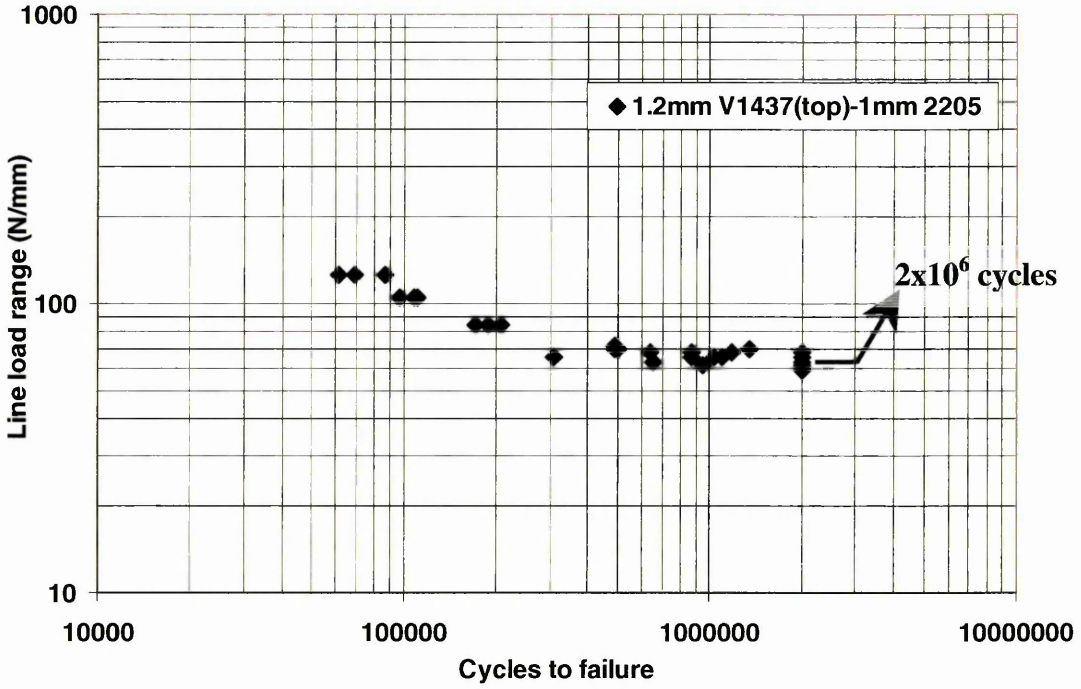

Graph 31 Graph to show the line load range fatigue properties for the 1.2mm V1437 (top) – 1mm 2205 lap joint

Mean Fatigue Line Load Range at $2x10^6$ cycles

$P_0 + d (A / F - 0.5) = \mathbf{X}$ **(N/mm)**

$59.11 + 2.22 (32 / 10 - 0.5) = \mathbf{65.1}$ **(N/mm)**

Statistical Validity

$(F * B - A^2) / F^2 = \mathbf{>0.3 \text{ and } <1.2}$

$(10 * 114 - 32^2) / 10^2 = \mathbf{1.16}$

Standard Deviation

$1.620 * d \{(F * B - A^2) / F^2 + 0.029\} = \mathbf{S}$ **(N/mm)**

$1.620 * 2.22 \{(10 * 114 - 32^2) / 10^2 + 0.029\} = \mathbf{4.3}$ **(N/mm)**

Thus, the mean fatigue line load range at $2x10^6$ cycles for the lap joint configuration 1.2mm V1437 (top) – 1mm 2205 is **65.1 N/mm** with a standard deviation of **4.3 N/mm** or **7%** and is statistically valid.

1.2mm V1437 (top) – 1mm 2101 Fatigue Results

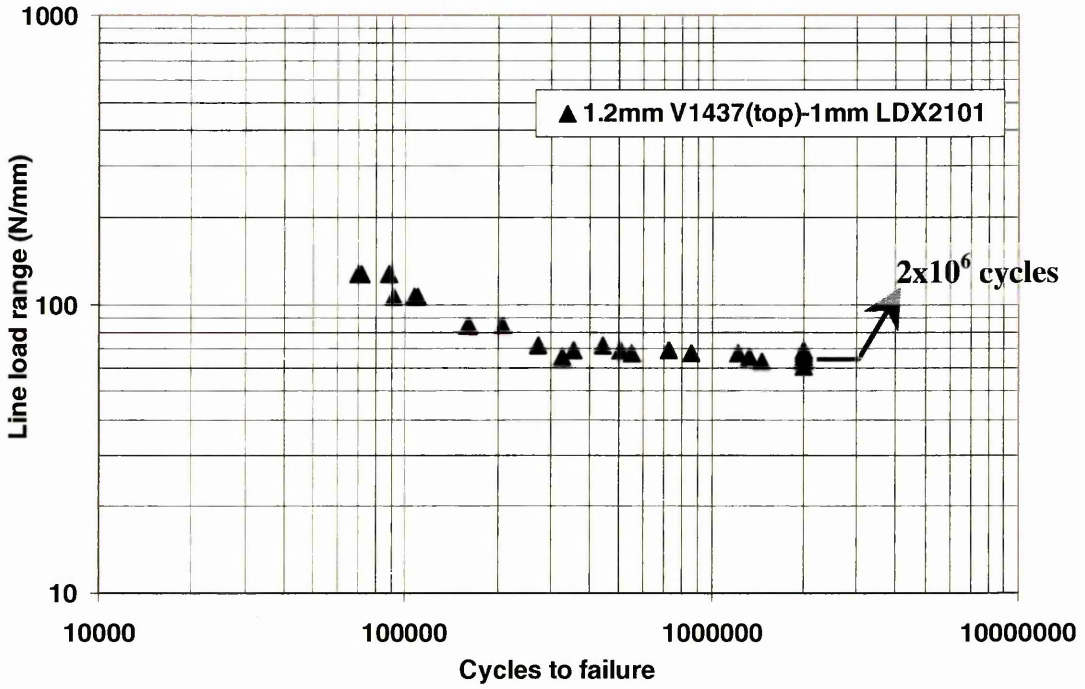

Graph 32 Graph to show the line load range fatigue properties for the 1.2mm V1437 (top) – 1mm 2101 lap joint

Mean Fatigue Line Load Range at $2x10^6$ cycles

$P_0 + d (A / F - 0.5) = \mathbf{X}$ **(N/mm)**

$61.22 + 2.22 (26 / 9 - 0.5) = \mathbf{66.5}$ **(N/mm)**

Statistical Validity

$(F * B - A^2) / F^2 = \mathbf{>0.3 \text{ and } <1.2}$

$(9 * 84 - 26^2) / 9^2 = \mathbf{0.99}$

Standard Deviation

$1.620 * d \{(F * B - A^2) / F^2 + 0.029\} = \mathbf{S}$ **(N/mm)**

$1.620 * 2.22 \{(9 * 84 - 26^2) / 9^2 + 0.029\} = \mathbf{3.7}$ **(N/mm)**

Thus, the mean fatigue line load range at $2x10^6$ cycles for the lap joint configuration 1.2mm V1437 (top) – 1mm 2101 is **66.5 N/mm** with a standard deviation of **3.7 N/mm** or **5%** and is statistically valid.

1mm 2101 – 1mm 2101 Similar Lap Joint Fatigue Results

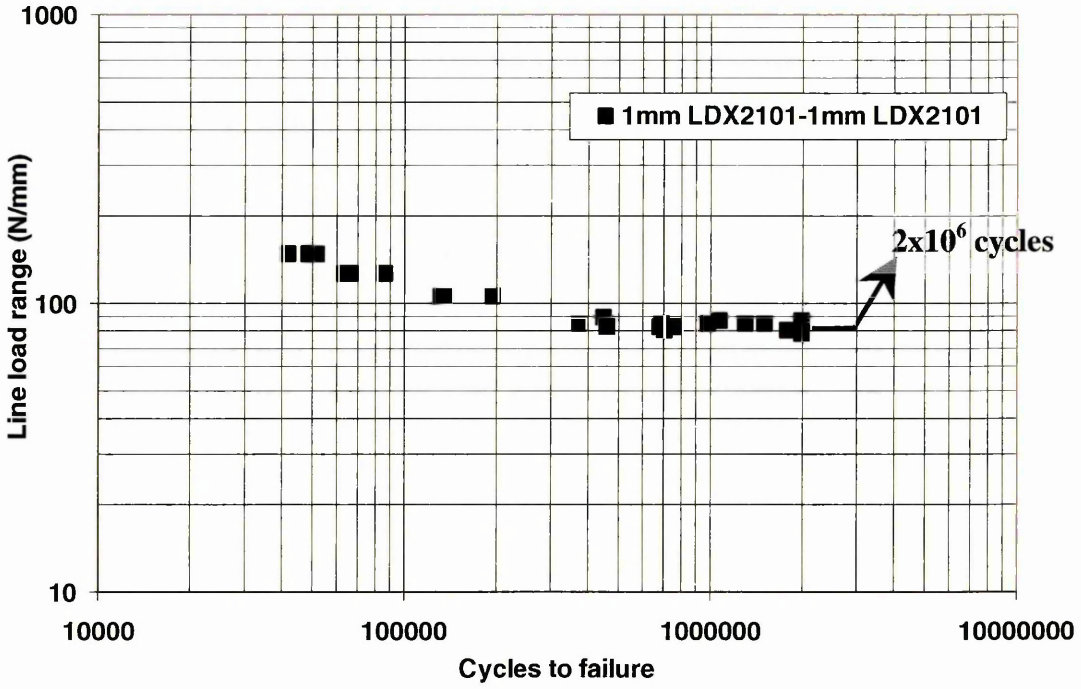

Graph 33 Graph to show the line load range fatigue properties for the 1mm 2101 – 1mm 2101 lap joint

Mean Fatigue Line Load Range at $2x10^6$ cycles

$P_0 + d (A / F - 0.5) = \mathbf{X}$ **(N/mm)**

$78.11 + 2.22 (31 / 11 - 0.5) = \mathbf{83.3}$ **(N/mm)**

Statistical Validity

$(F * B - A^2) / F^2 = \mathbf{>0.3 \text{ and } <1.2}$

$(11 * 99 - 31^2) / 11^2 = \mathbf{1.06}$

Standard Deviation

$1.620 * d \{(F * B - A^2) / F^2 + 0.029\} = \mathbf{S}$ **(N/mm)**

$1.620 * 2.22 \{(11 * 99 - 31^2) / 11^2 + 0.029\} = \mathbf{3.9}$ **(N/mm)**

Thus, the mean fatigue line load range at $2x10^6$ cycles for the lap joint configuration 1mm 2101 – 1mm 2101 is **83.3 N/mm** with a standard deviation of **3.9 N/mm** or **5%** and is statistically valid.

1.2mm V1437 (top) – 1mm 2101 Dissimilar Butt Joint Fatigue Results

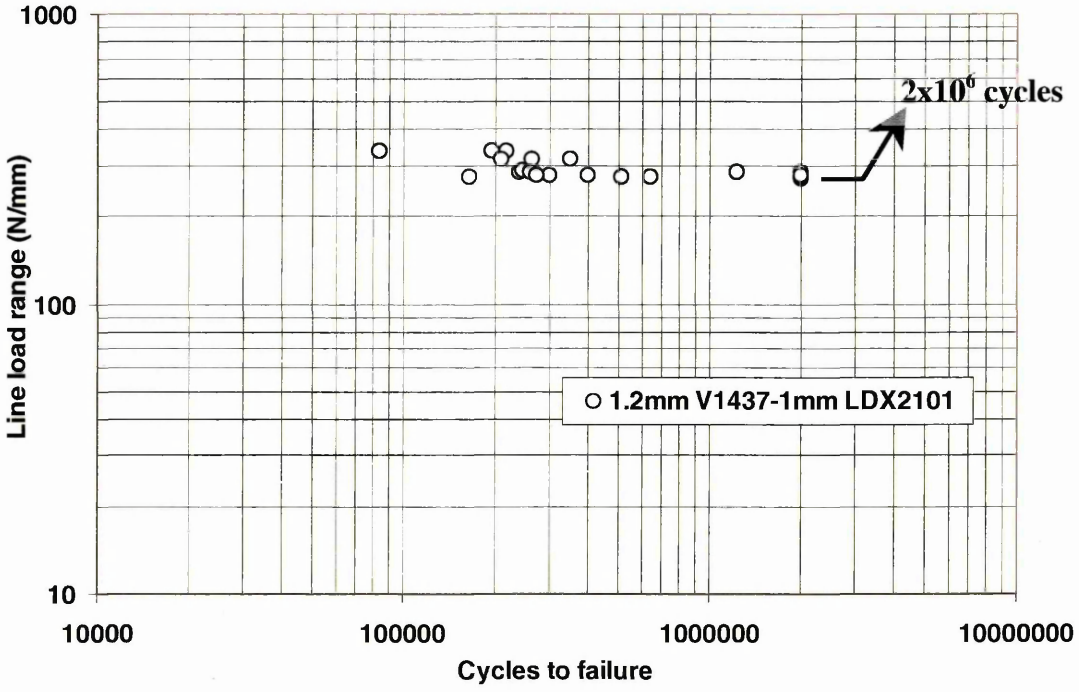

Graph 34 Graph to show the line load range fatigue properties for the 1.2mm V1437 – 1mm 2205 butt joint

Mean Fatigue Line Load Range at $2x10^6$ cycles

$P_0 + d (A / F - 0.5) = \mathbf{X}$ **(N/mm)**

$270.22 + 4.44 (22 / 10 - 0.5) = \mathbf{277.8}$ **(N/mm)**

Statistical Validity

$(F * B - A^2) / F^2 = \mathbf{>0.3 \text{ and } <1.2}$

$(10 * 58 - 22^2) / 10^2 = \mathbf{0.96}$

Standard Deviation

$1.620 * d \{(F * B - A^2) / F^2 + 0.029\} = \mathbf{S}$ **(N/mm)**

$1.620 * 4.44 \{(10 * 58 - 22^2) / 10^2 + 0.029\} = \mathbf{7.1}$ **(N/mm)**

Thus, the mean fatigue line load range at $2x10^6$ cycles for the lap joint configuration 1.2mm V1437 – 1mm 2101 is **277.8 N/mm** with a standard deviation of **7.1 N/mm** or **3%** and is statistically valid.

4.8 Lap Joint Rotation Results

The rotation angles against the corresponding line loads were determined for the following similar and dissimilar metal lap joints.

1mm 2101 – 1mm 2101	similar metal lap joint
1mm 304 – 1.2mm V1437 (top)	dissimilar metal lap joint
0.78mm 2205 – 1.2mm V1437 (top)	dissimilar metal lap joint

As stated in section 3.4.4, the joint rotation was determined for a 100mm free length (this was the free length used during the fatigue tests).

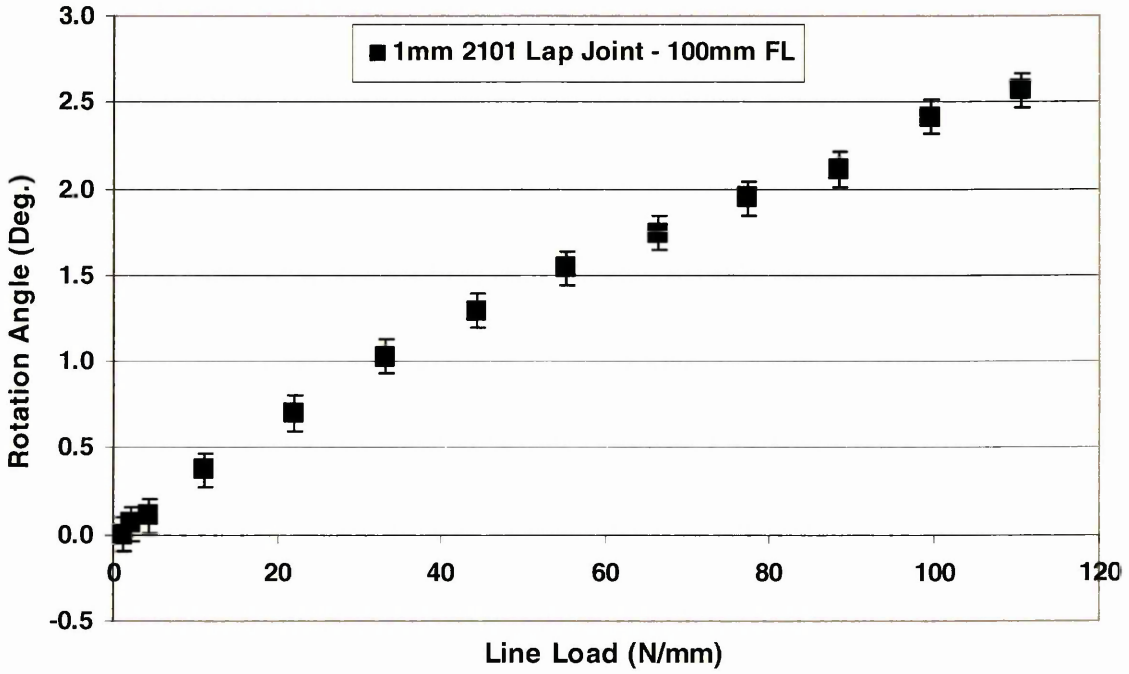

Graph 35 1mm 2101 lap joint maximum rotation angle as a function of line load range

The estimated error of these experimental tests was due to the diffraction of the reflected laser beam. The reflected spot size was ~5mm, with the displacement being consistently marked by the centre of the diffracted spot. Hence, an error of +/- 0.1^{o} was estimated for the rotation tests. The lap joint rotation graphs for 1mm 304 – 1.2mm V1437 (top) and 0.78mm 2205 – 1.2mm V1437 can be found in Appendix 8.3.

4.9 Metallographic Results

4.9.1 Base Material Metallography

The following images show the base material structures for 304, 2205, 2101 and V1437. Image 5 below shows the 1.2mm V1437 base material (ferrite and small islands of pearlite) grain structure. This image was etched with 2% nital.

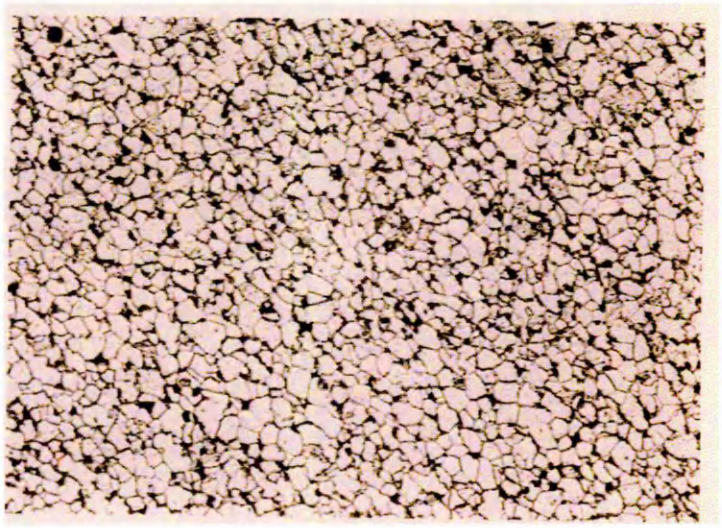

Image 5 Shows the 'as received' 1.2mm V1437 microstructure at x200 magnification

Image 6 below shows the 1mm 304 base material (austenitic) grain structure. This image was electrolytic etched with 60% nitric acid.

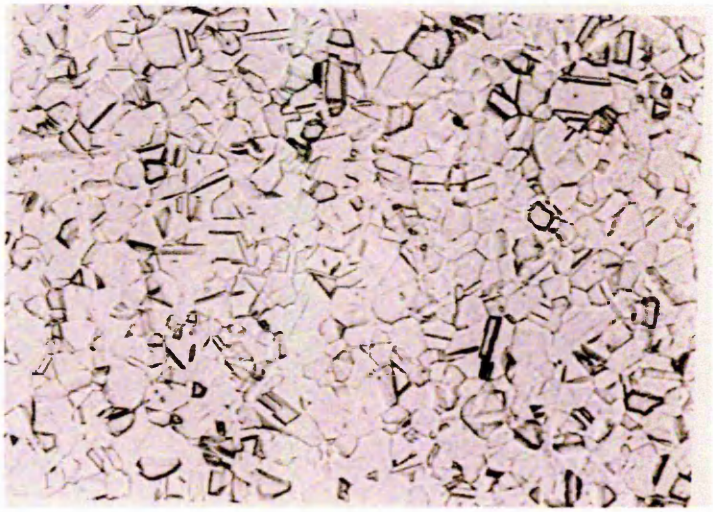

Image 6 Shows the 'as received' 1mm 304 microstructure at x200 magnification

Image 7 below shows the 1mm 2205 base material grain structure. This image was potentiostatic etched with 10% w/v Oxalic acid (NaOH). The darker areas are ferrite and the lighter areas are austenite, approximately 50% of each.

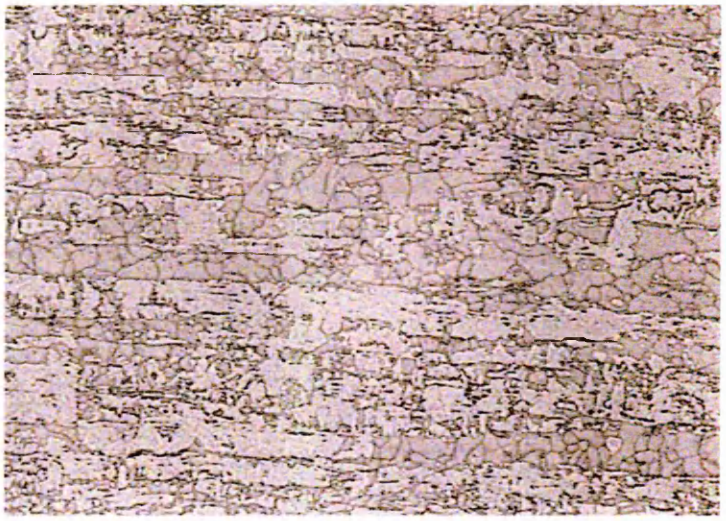

Image 7 Shows the 'as received' 1mm 2205 microstructure at x200 magnification

Image 8 below shows the 1mm 2101 base material grain structure. This was potentiostatic etched using 10% w/v Oxalic acid (NaOH). The darker areas are ferrite and the lighter areas are austenite, approximately 50% of each.

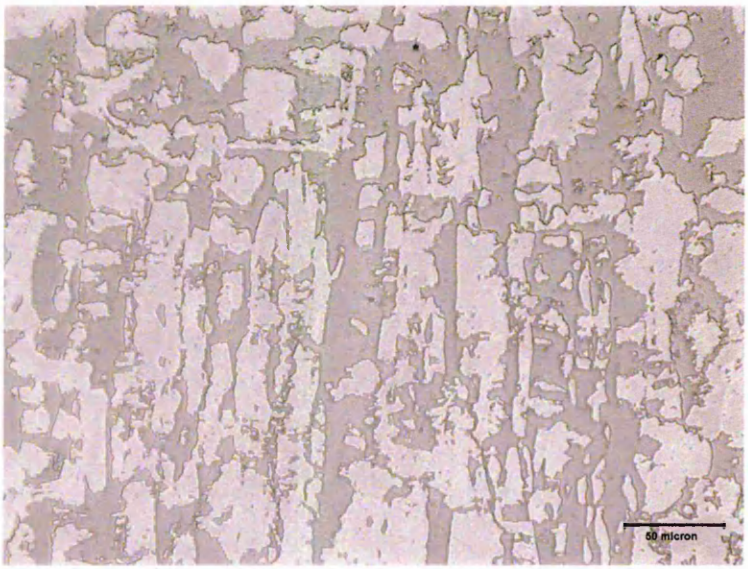

Image 8 Shows the 'as received' 1mm 2101 microstructure – scale bar

4.9.2 Weld Bead Metallography

4.9.2.1 Lap Joint Weld Widths

The weld width of each laser welded lap joint was determined to investigate the effects of the laser welding parameters on the weld width and the effects of weld width on the fatigue properties of the joints.

Table 20 shows the average weld width (+/-0.05mm estimated error) between the sheets from each laser welded lap joint.

Laser Welder	Lap Joint Configuration	Weld Width (mm)
Trumpf 5kW CO_2		
	1mm 304 (top) – 1.2mm V1437	1.3
	1.2mm V1437 (top) – 1mm 304	1.4
	0.78mm 2205 (top) – 1.2mm V1437	0.9
	1.2mm V1437 (top) – 0.78mm 2205	1.2
Rofin 2kW CO_2		
	1.2mm V1437 (top) – 1mm 2205	1.4
	1.2mm V1437 (top) – 1mm 2101	1.4
	1mm 2101 – 1mm 2101	1.4

Table 20 Lap joint weld widths between the sheets

4.10 Weld Bead Microhardness Results

The following microhardness grids were produced using the procedure stated in section 3.5.2.

4.10.1 Butt Joint Microhardness Results

Butt weld microhardness grids were produced to compare the effects of the welding parameters on the microhardness and shape of the laser weld beads.

The welding parameters used to produce the dissimilar metal butt joints were:

- Welding power: 3.8kW (work piece)
- Speed: **P1 = 4.0m/min**

  P2 = 3.5m/min

  P3 = 3.0m/min
- Focal point: Sheet surface
- Focal length: 250mm
- Trailing gas flow rate: 20L/min

Thus, the majority of the welding parameters were fixed, with the welding speed being altered. In the following graphs, P1, P2 and P3 denote the parameter sets with the corresponding welding speeds.

The following graphs show the distribution of microhardness across the laser butt weld for the 1mm 304 – 1.2mm V1437 configuration. **LHS = 304, RHS = V1437.**

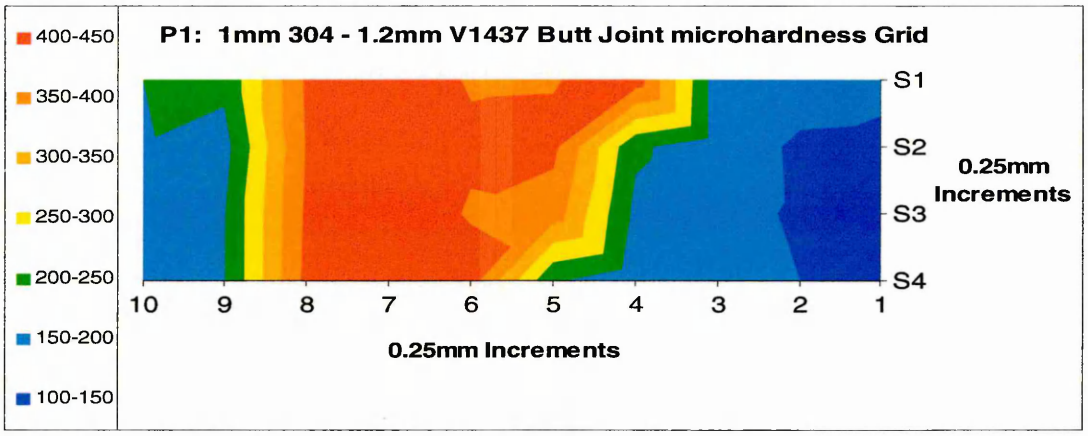

Graph 36 Microhardness grid for P1: 1mm 304 – 1.2mm V1437 dissimilar metal butt joint

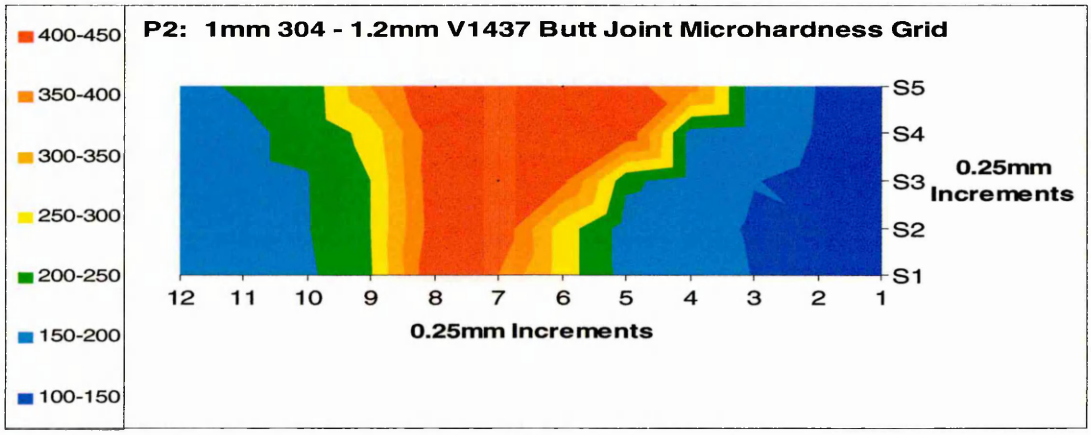

Graph 37 Microhardness grid for P2: 1mm 304 – 1.2mm V1437 dissimilar metal butt joint

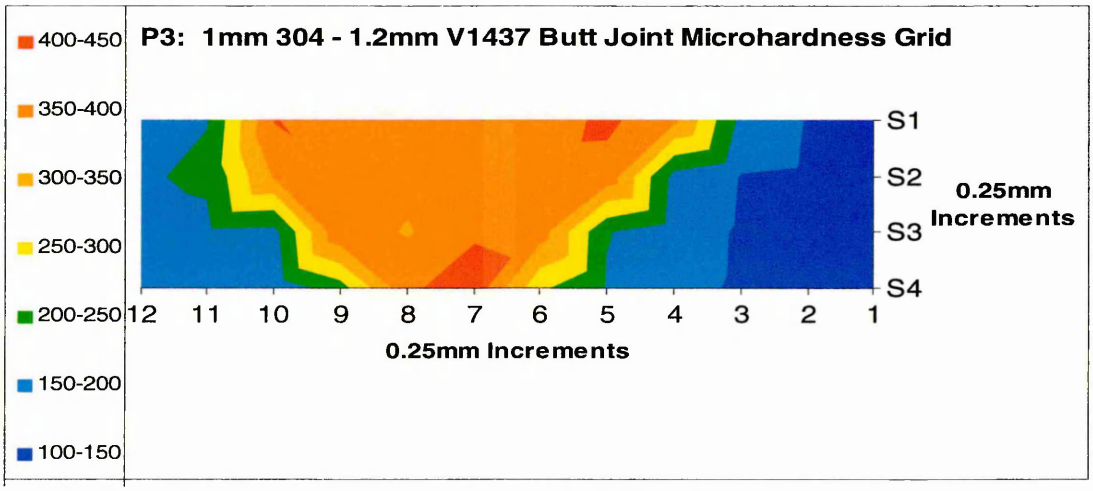

Graph 38 Microhardness grid for P3: 1mm 304 – 1.2mm V1437 dissimilar metal butt joint

*Please note: Originally printed in colour.

The following graphs show the distribution of microhardness across the laser butt weld for the 1mm 2205 – 1.2mm V1437 configuration. **LHS = 2205, RHS = V1437.**

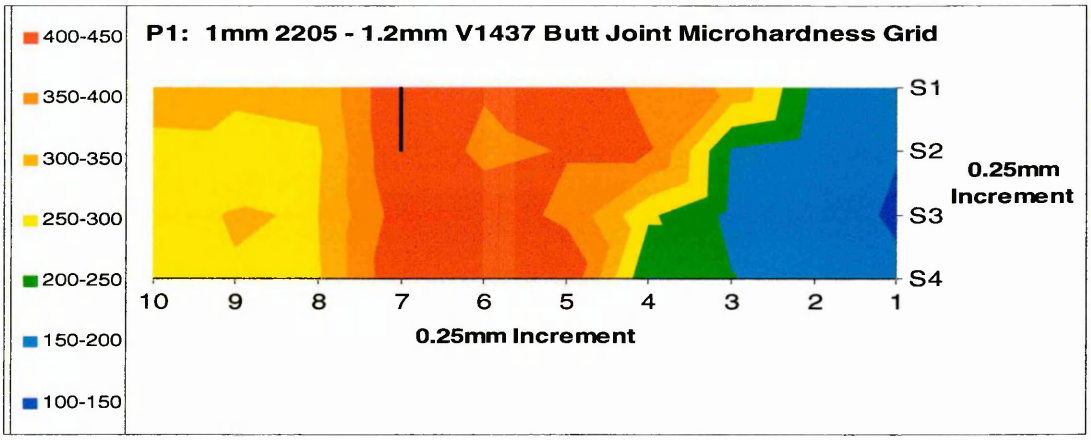

Graph 39 Microhardness grid for P1: 1mm 2205 – 1.2mm V1437 dissimilar metal butt joint

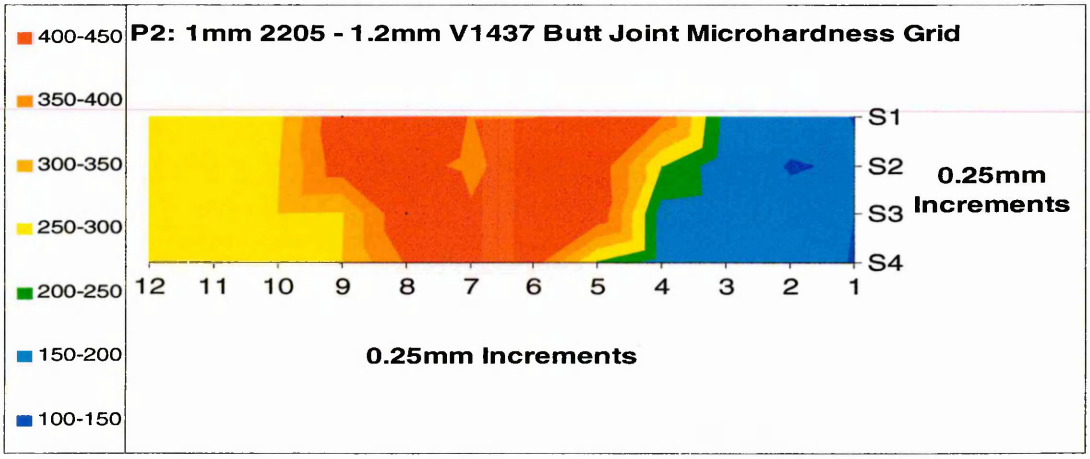

Graph 40 Microhardness grid for P2: 1mm 2205 – 1.2mm V1437 dissimilar metal butt joint

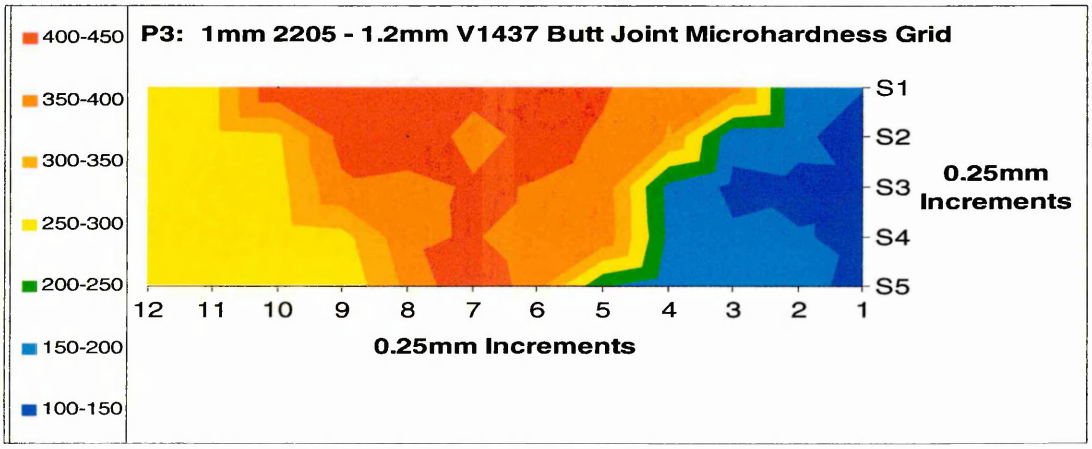

Graph 41 Microhardness grid for P3: 1mm 2205 – 1.2mm V1437 dissimilar metal butt joint

*Please note: Originally printed in colour.

4.10.2 Lap Joint Microhardness Results

Lap joint weld microhardness grids were produced to compare the effects of the welding configuration on the microhardness and shape of the laser weld beads.

The welding parameters used to produce the dissimilar metal lap joints were:

- Welding power: 3.8kW (work piece)
- Speed: 2.3m/min – 304 dissimilar metal welds
  2.6m/min – 2205 dissimilar metal welds
- Focal point: 0.1mm above top sheet surface
- Focal length: 250mm
- Trailing gas flow rate: 20L/min

Thus, the welding parameters were fixed, with the welding configuration being controlled.

The following two graphs show the distribution of microhardness across two dissimilar metal lap joints. The configurations were:

- 1mm 304 (top) – 1.2mm V1437

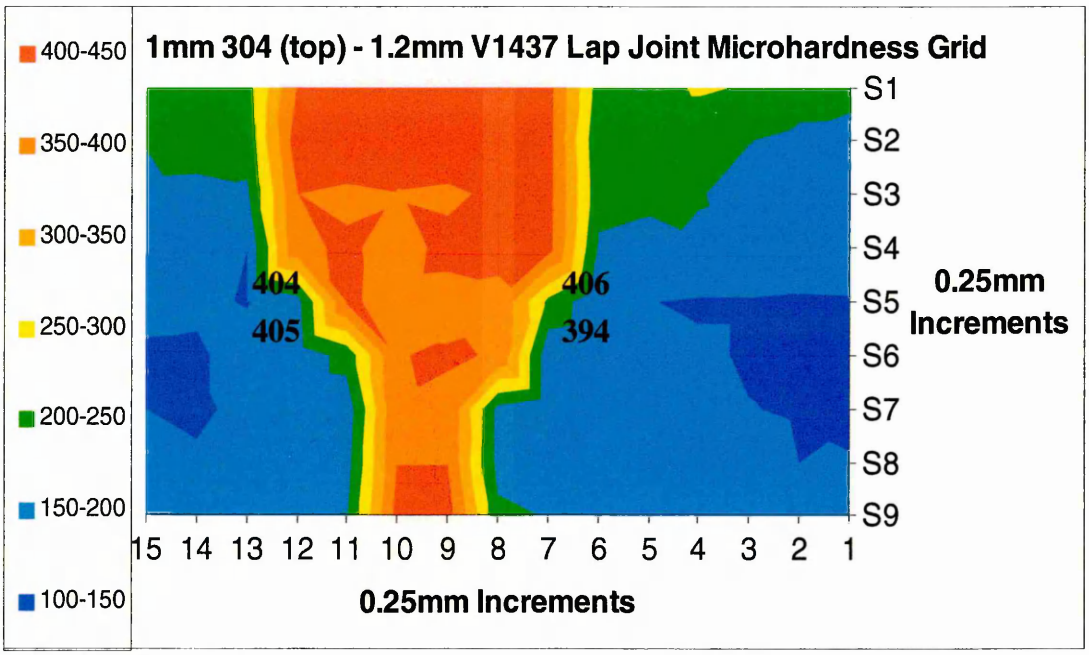

Graph 42 Microhardness grid: 1mm 304 (top) – 1.2mm V1437 dissimilar metal lap joint

- 1.2mm V1437 (top) – 1mm 304

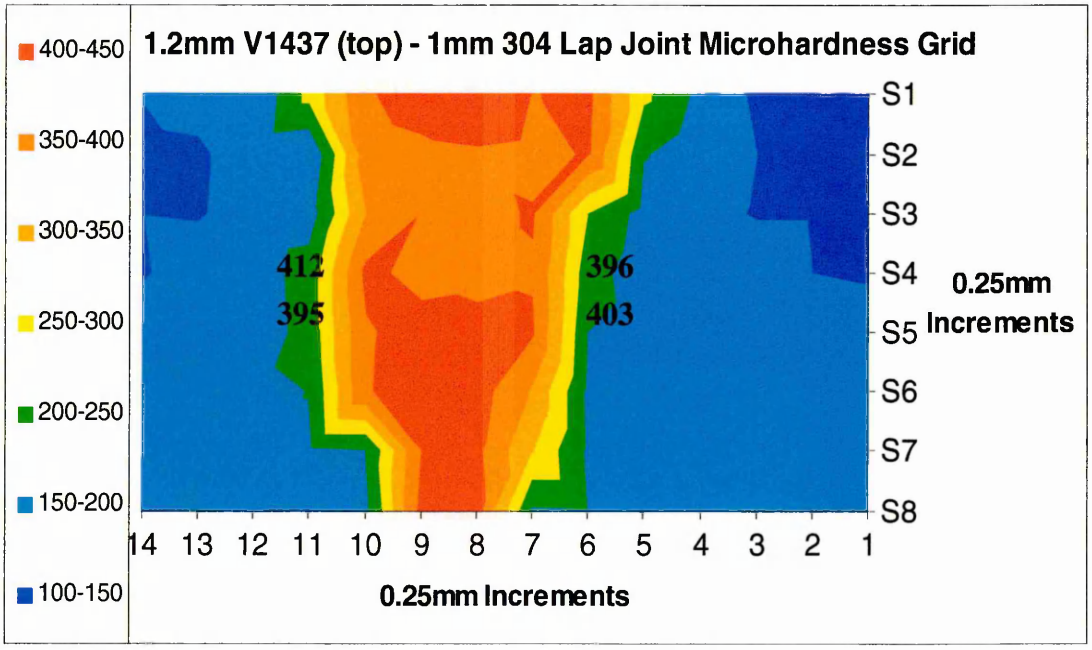

Graph 43 Microhardness grid: 1.2mm V1437 (top) – 1mm 304 dissimilar metal lap joint

The following two graphs show the distribution of microhardness across two dissimilar metal lap joints. The configurations were:

- 0.78mm 2205 (top) – 1.2mm V1437

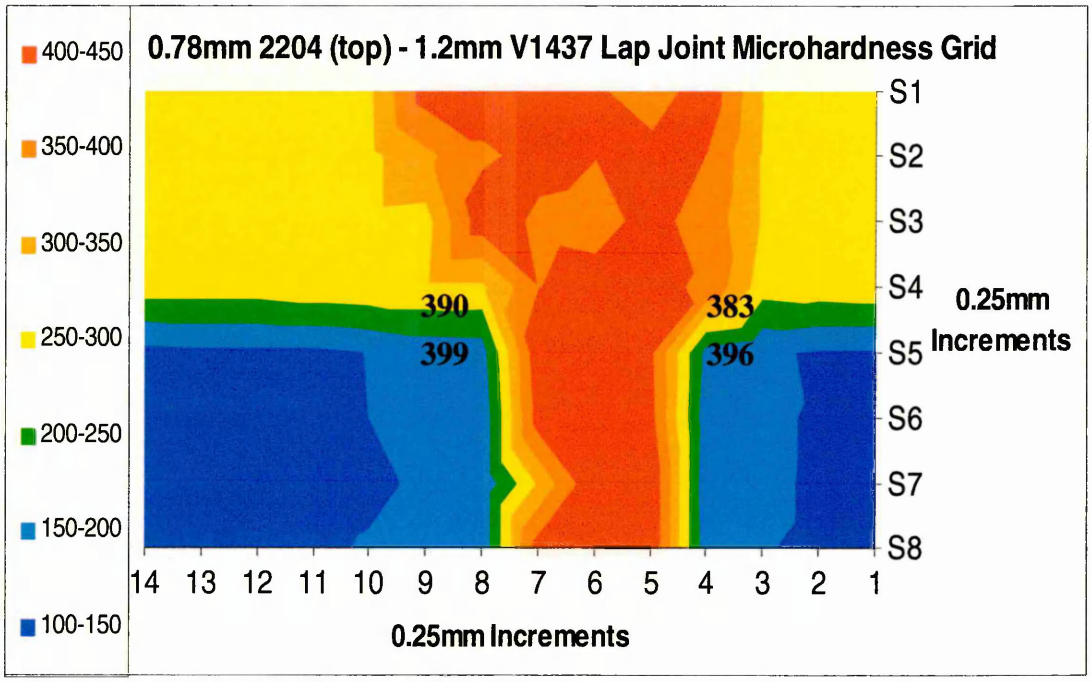

Graph 44 Microhardness grid: 0.78mm 2205 (top) – 1.2mm V1437 dissimilar metal lap joint

- 1.2mm V1437 (top) – 0.78mm 2205

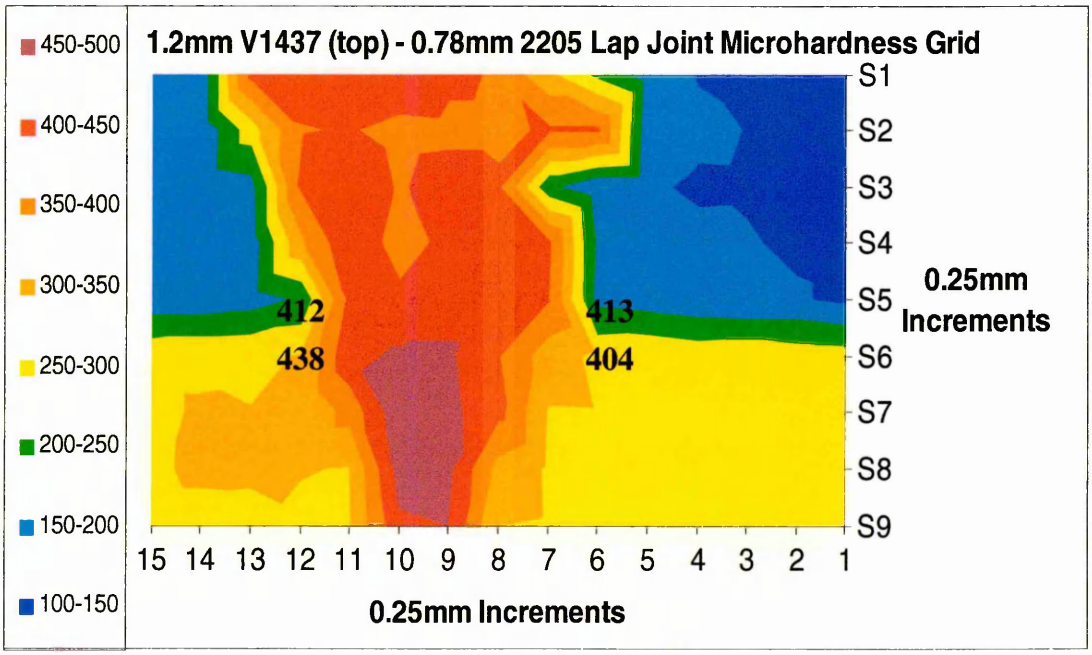

Graph 45 Microhardness grid: 1.2mm V1437 (top) – 0.78mm 2205 dissimilar metal lap joint

4.11 Weld Bead Composition Results

The composition of the butt and lap joint weld beads was determined using the method described in section 3.5.4.2. The following images, graphs and corresponding Schaeffler diagrams show the butt joint dilutions calculated for different welding speeds and the lap joint dilutions which occurred with the same laser welding parameters for the different configurations (both the V1437 and the 304 or 2205 at the top of the lap joint.

The welding parameters used to produce the dissimilar metal butt joints were:

- Welding power: 3.8kW (work piece)
- Speed: **P1 = 4.0m/min**

  P2 = 3.5m/min

  P3 = 3.0m/min
- Focal point: Sheet surface
- Focal length: 250mm
- Trailing gas flow rate: 20L/min

Thus, the majority of the welding parameters were fixed, with the welding speed being altered. In the following graphs, P1, P2 and P3 denote the parameter sets with the corresponding welding speeds.

The welding parameters used to produce the dissimilar metal lap joints were:

- Welding power: 3.8kW (work piece)
- Speed: 2.3m/min – 304 dissimilar metal welds

  2.6m/min – 2205 dissimilar metal welds
- Focal point: 0.1mm above top sheet surface
- Focal length: 250mm
- Trailing gas flow rate: 20L/min

Thus, the welding parameters were fixed, with the welding configuration being altered.

4.11.1 Butt Joint Weld Bead Compositions

Parameter set 1 **(P1)**: 1mm 304 – 1.2mm V1437

The following speed maps were produced using a Philips XL40 SEM.

1mm 304

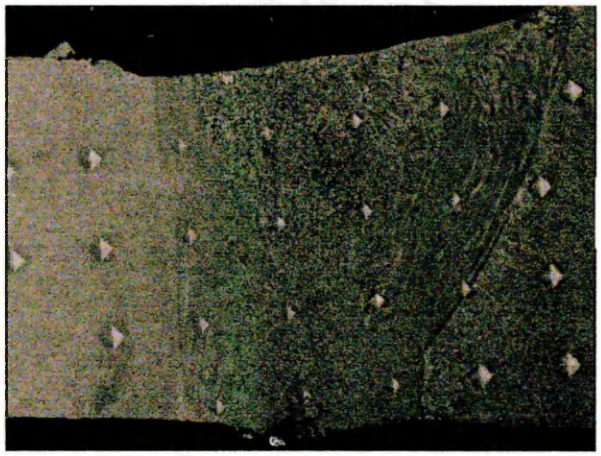

1.2mm V1437

Image 9 Secondary electron image from parameter set 1: 1mm 304 – 1.2mm V1437 butt joint

1mm 304

1.2mm V1437

Image 10 Speed map for Cr from parameter set 1: 1mm 304 – 1.2mm V1437 butt joint

1mm 304

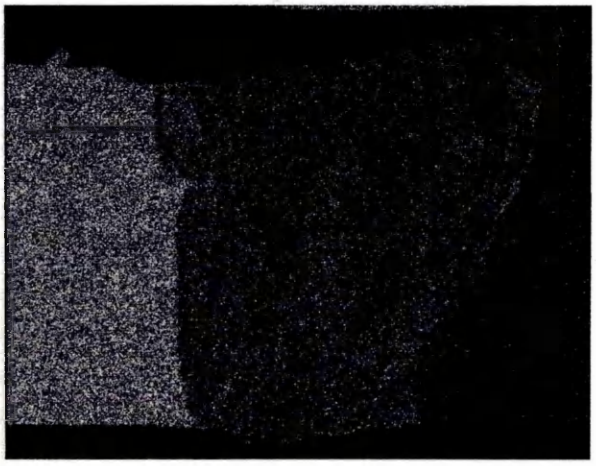

1.2mm V1437

Image 11 Speed map for Ni from parameter set 1: 1mm 304 – 1.2mm V1437 butt joint

The two graphs below show the actual percentages of Chromium and Nickel within the weld bead. **P1 = 4.0m/min**

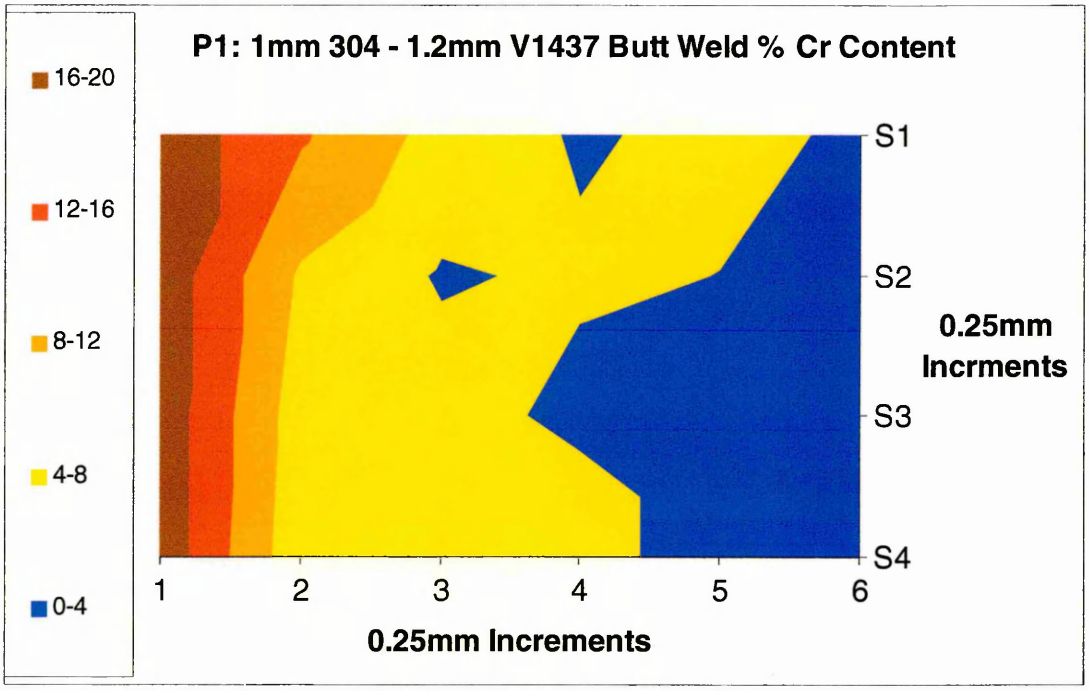

Graph 46 Weld bead % Chromium content from parameter set 2: 1mm 304 – 1.2mm V1437 butt joint

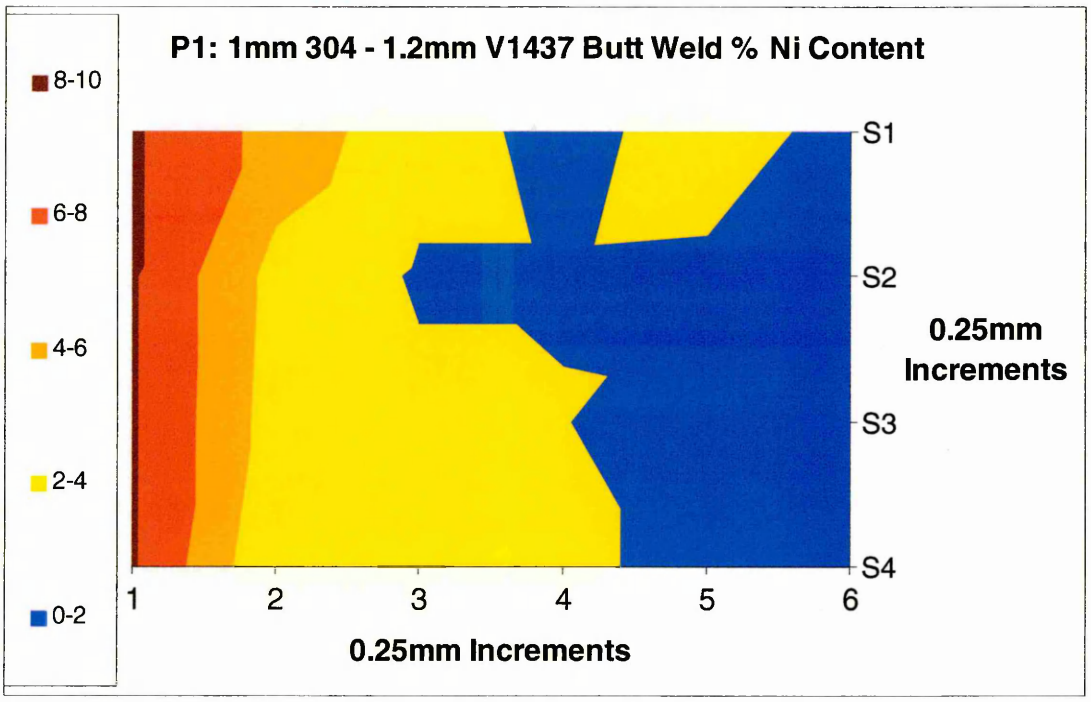

Graph 47 Weld bead % Nickel content from parameter set 2: 1mm 304 – 1.2mm V1437 butt joint

The data used to produce the weld bead composition graphs was then used to predict the dilution and phases present in the laser weld bead. The range of composition found in the weld bead can be seen on the modified Schaeffler diagram below.

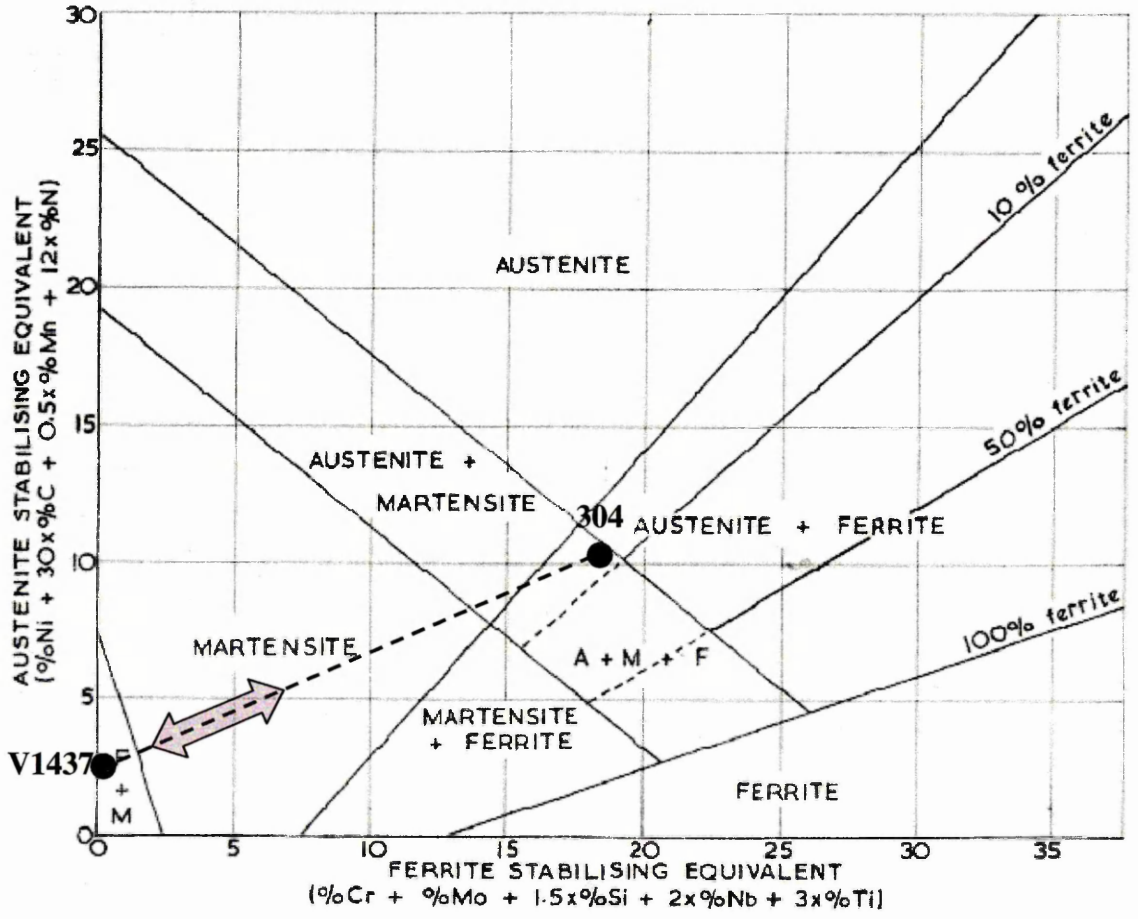

Figure 53 Shows the predicted weld bead composition for the 4m/min 1.2mm V1437 – 1mm 304 butt weld

Hence, the predicted weld bead micro structure would be martensite.

The composition analysis of the laser welded butt joints for P2 and P3 can be seen in Appendix 8.4.

4.11.2 Lap Joint Weld Bead Compositions

The composition of the laser welded lap joints were determined to compare the effects of welding configuration on the dilution and weld bead compositions produced.

1mm 304 (top) – 1.2mm V1437 & 1mm 304 – 1.2mm V1437 (top)

- Welding power: 3.8kW (work piece)
- Speed: **2.3m/min**
- Focal point: 0.1mm above top sheet surface
- Focal length: 250mm
- Trailing gas flow rate: 20L/min
- Overlap: 10mm
- Interfacial gap: None

0.78mm 2205 (top) – 1.2mm V1437 & 0.78mm 2205 – 1.2mm V1437 (top)

- Welding power: 3.8kW (work piece)
- Speed: **2.6m/min**
- Focal point: 0.1mm above top sheet surface
- Focal length: 250mm
- Trailing gas flow rate: 20L/min
- Overlap: 10mm
- Interfacial gap: None

1mm 304 (top) – 1.2mm V1437

The two graphs below show the actual percentages of Chromium and Nickel within the weld bead.

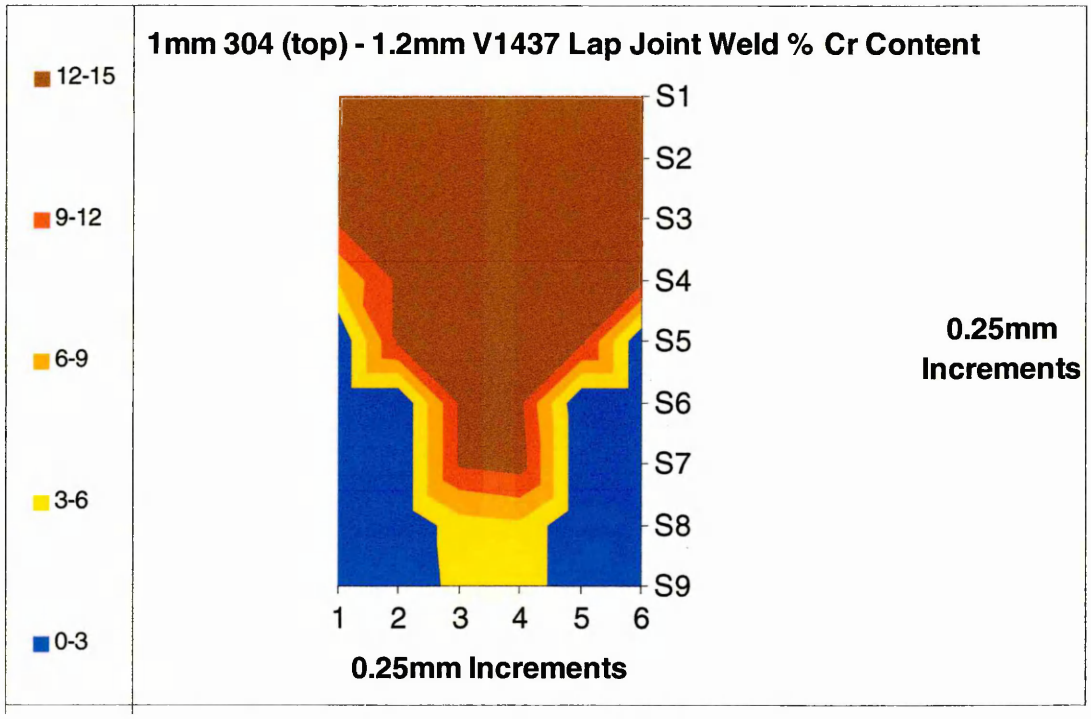

Graph 48 Weld bead % Chromium content: 1mm 304 (top) – 1.2mm V1437 lap joint

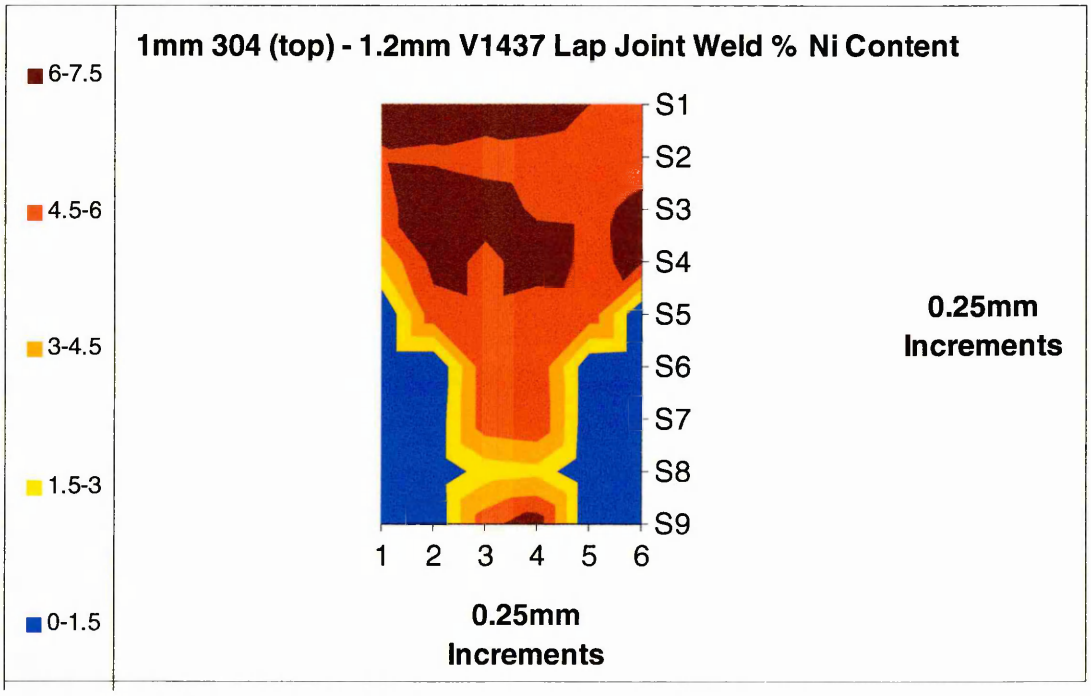

Graph 49 Weld bead % Nickel content: 1mm 304 (top) – 1.2mm V1437 lap joint

The data used to produce the weld bead composition graphs was then used to predict the dilution and phases present in the laser weld bead. The range of compositions found in the weld bead can be seen on the modified schaeffler diagram below.

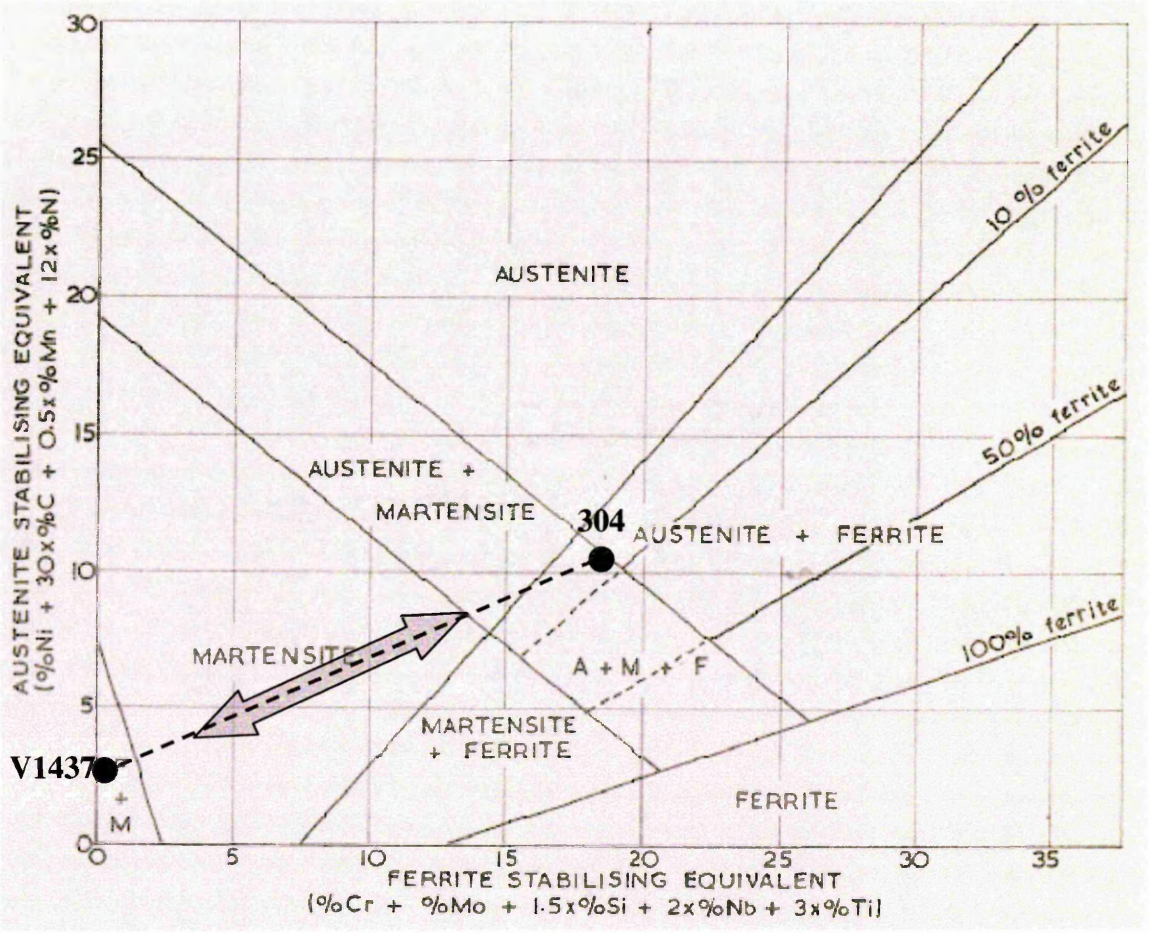

Figure 54 Shows the predicted weld bead composition for the 1mm 304 (top) - 1.2mm V1437 lap joint

Hence, the predicted weld bead micro structure would be martensite.

The composition analysis of the laser welded lap joints can be seen in Appendix 8.5.

4.12 Fatigue Failure Analysis

As explained in section 3.5.3.2, a range of procedures were used to characterise the fatigue failure of laser welded lap joints. Optical microscopy was used to characterise the fatigue failures of dissimilar metal lap joints. All the images were from fatigue failures produced during the staircase method.

4.12.1 Optical Fatigue Failure Analysis – Dissimilar Metal Lap Joints

The following optical images show lap joint fatigue failure from four dissimilar metal lap joints. These images show that lap joint fatigue failure occurred in both materials for each joint configuration within the staircase method.

1mm 304 (top) - 1.20mm V1439 fatigue failures

Image 12 Shows a fatigue specimen in which fatigue failure occurred in the 304

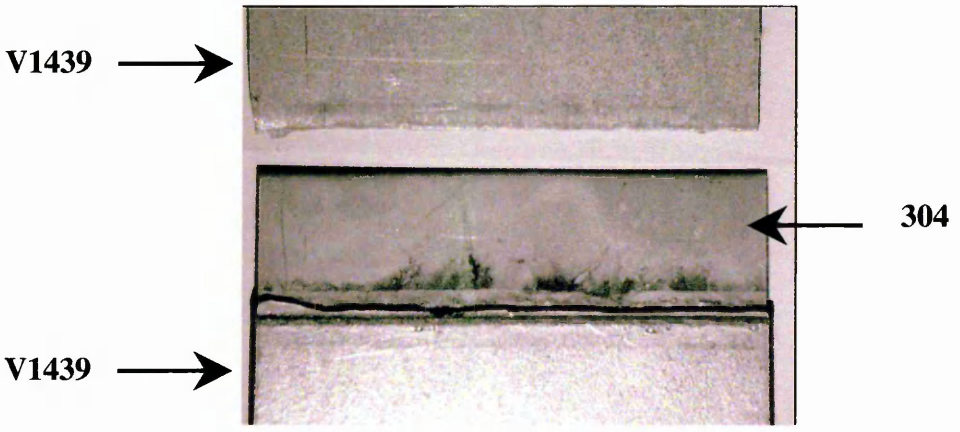

Image 13 Shows a fatigue specimen in which fatigue failure occurred in the V1439

1.20mm V1439 (top) - 1mm 304 fatigue failures

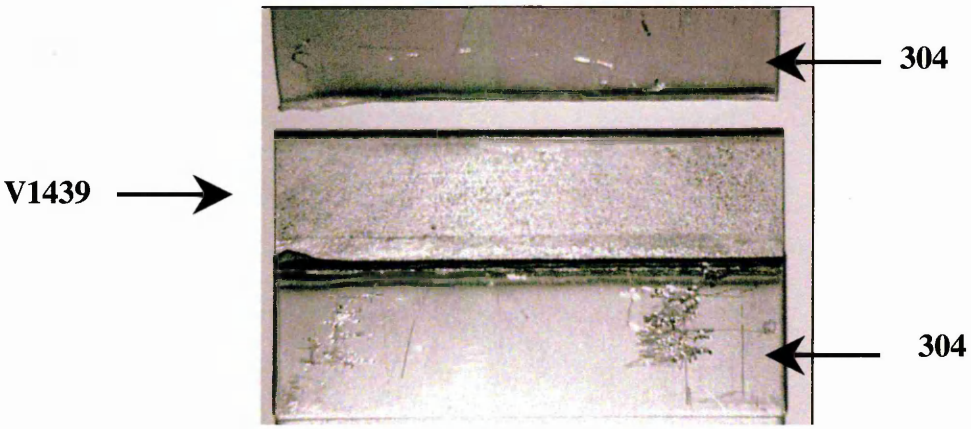

Image 14 Shows a fatigue specimen in which fatigue failure occurred in the 304

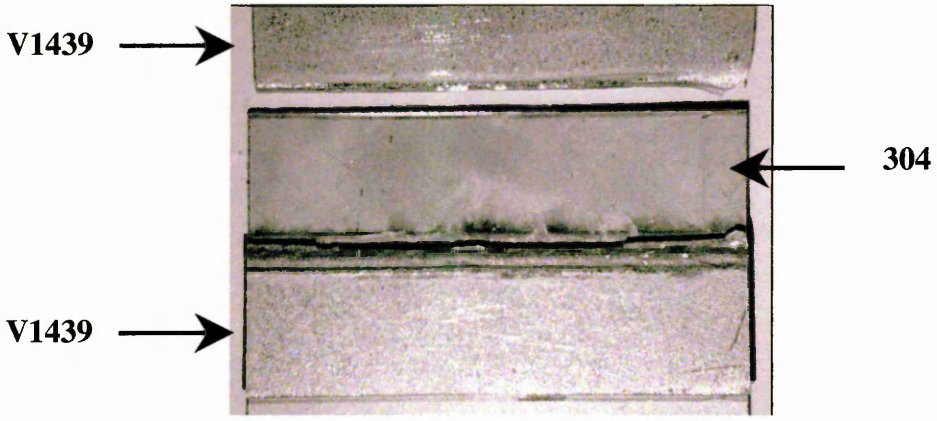

Image 15 Shows a fatigue specimen in which fatigue failure occurred in the V1439

1.20mm V1439 (top) - 0.78mm 2205 fatigue failures

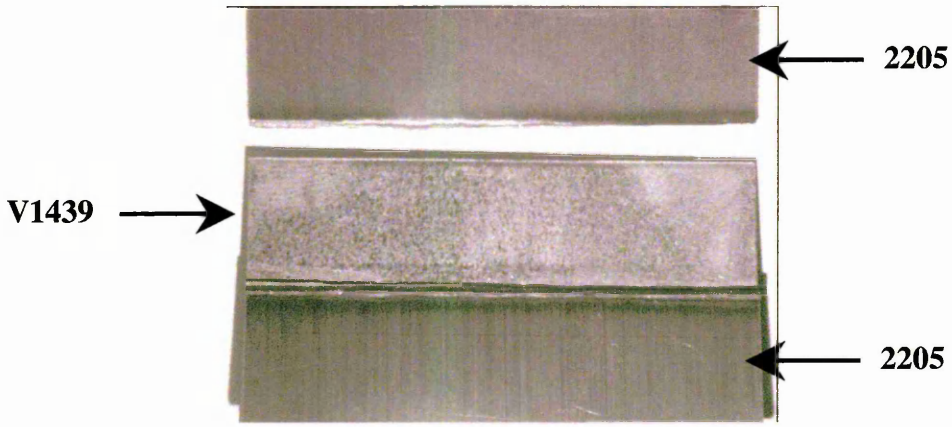

Image 16 Shows a fatigue specimen in which fatigue failure occurred in the 2205

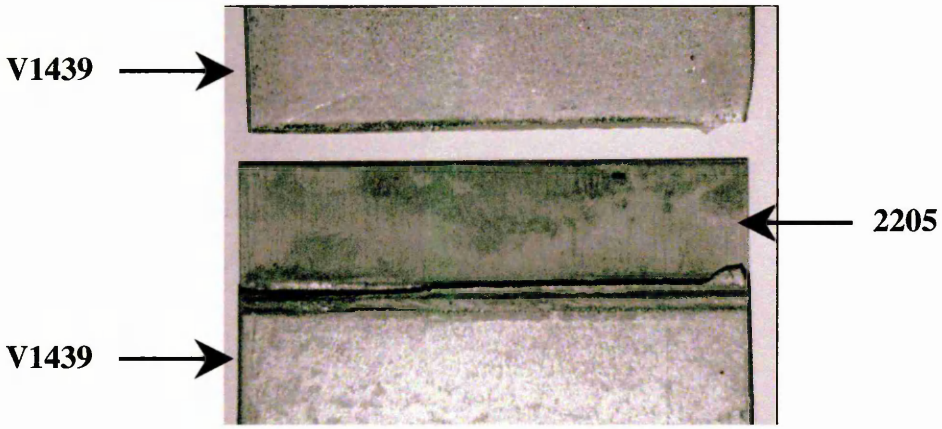

Image 17 Shows a fatigue specimen in which fatigue failure occurred in the V1439

0.78mm 2205 (top) - 1.20mm V1439 fatigue failures

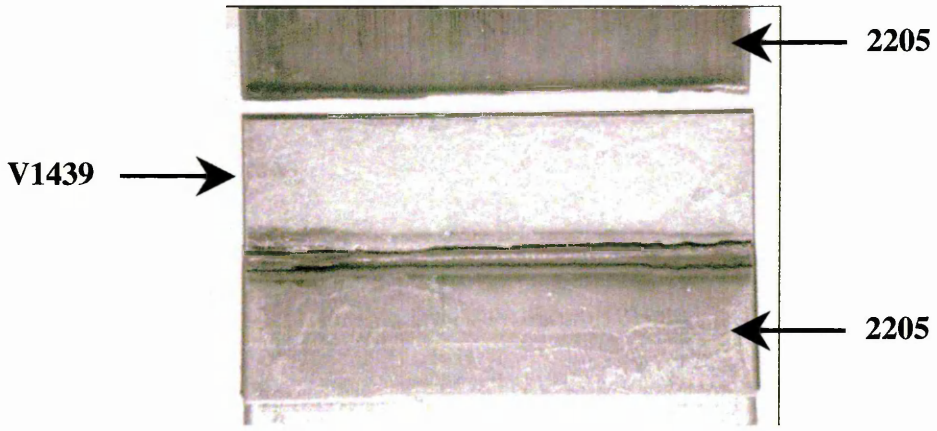

Image 18 Shows a fatigue specimen in which fatigue failure occurred in the 2205

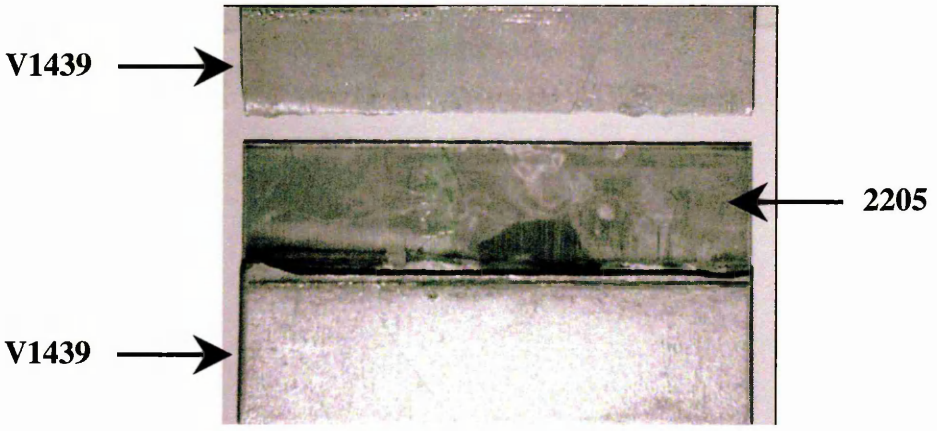

Image 19 Shows a fatigue specimen in which fatigue failure occurred in the V1439

4.12.2 Optical Fatigue Initiation Analysis – 2101 Similar Metal Lap Joint

The following optical images were taken from staircase fatigue failures (>1x10^6 cycles). A 1mm 2101 similar metal lap joint fatigue failure can be seen in Image 20 below, where fatigue failure has occurred in the sheet at the bottom of the lap joint. Fatigue crack initiation occurs at the internal lap face, the crack then propagates across the sheet. This sample was electrolytic etched in 60% Nital

Image 20 Fatigue sample cross-section showing fatigue failure in the bottom sheet for 1mm 2101 similar metal lap joint

As the following two images show, initiated fatigue cracks do not propagate with preference to the weld bead or heat affected zone etc.

Image 21 below shows fatigue crack initiation occurring from the internal lap face and propagation into the weld bead with no apparent plastic deformation or sheet tearing.

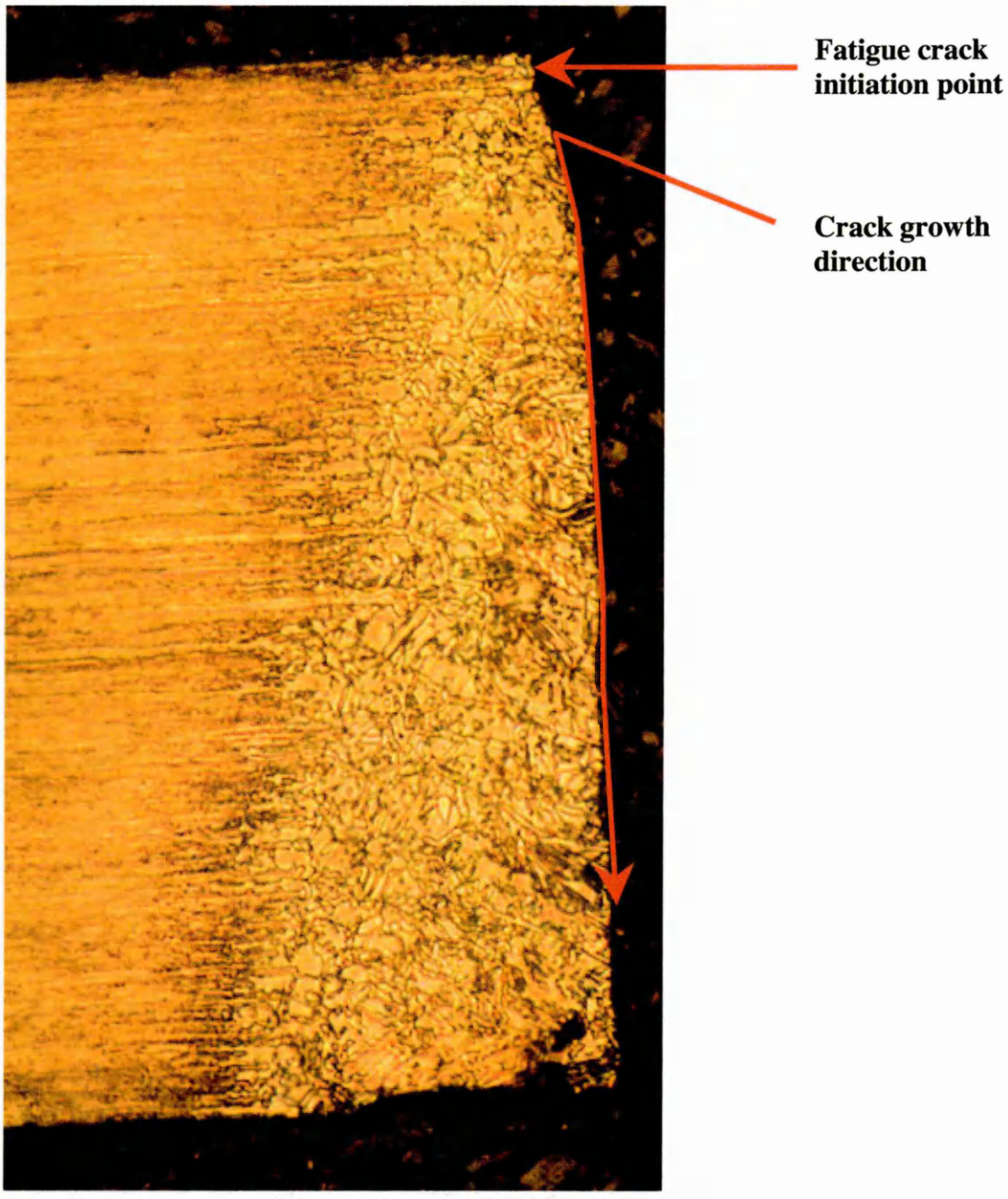

Image 21 Fatigue crack propagation from the HAZ at the internal lap face into the weld bead

Image 22 below shows a fatigue crack initiating at the internal lap face and propagating along the weld bead/heat affected zone interface. Approximately 60% along the sheet thickness the fatigue crack changes direction and propagates into the weld bead. The change in propagation direction appears to be accompanied by the onset of plastic deformation and consequently sheet tearing.

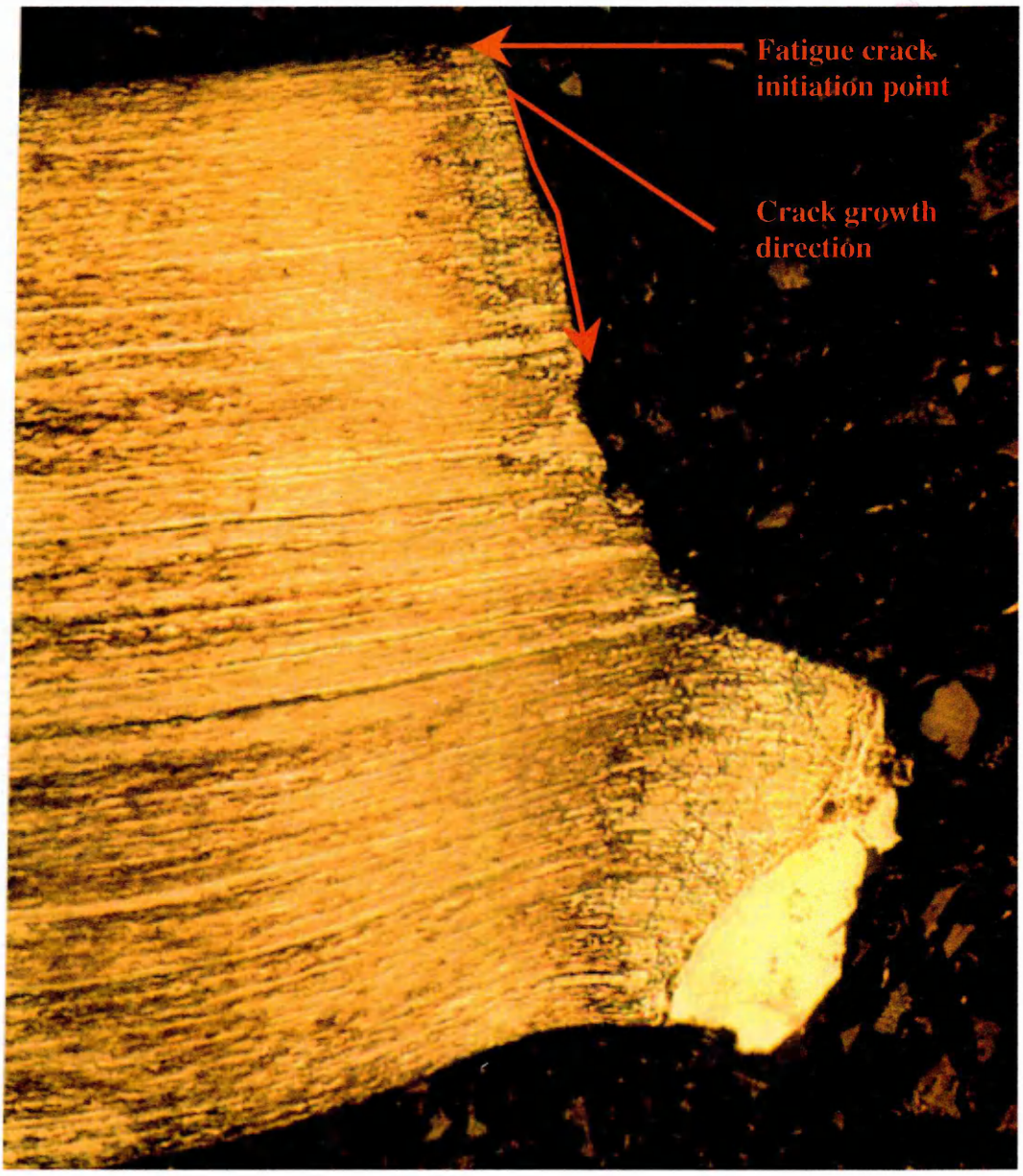

Image 22 Change in Fatigue crack propagation direction from the HAZ into the laser weld bead

Image 23 and Image 24 show a fatigue failure in the bottom sheet of a 1mm 2101 laser welded lap joint. Both images show that a fatigue crack is present in the top sheet (opposite side) of the lap joint.

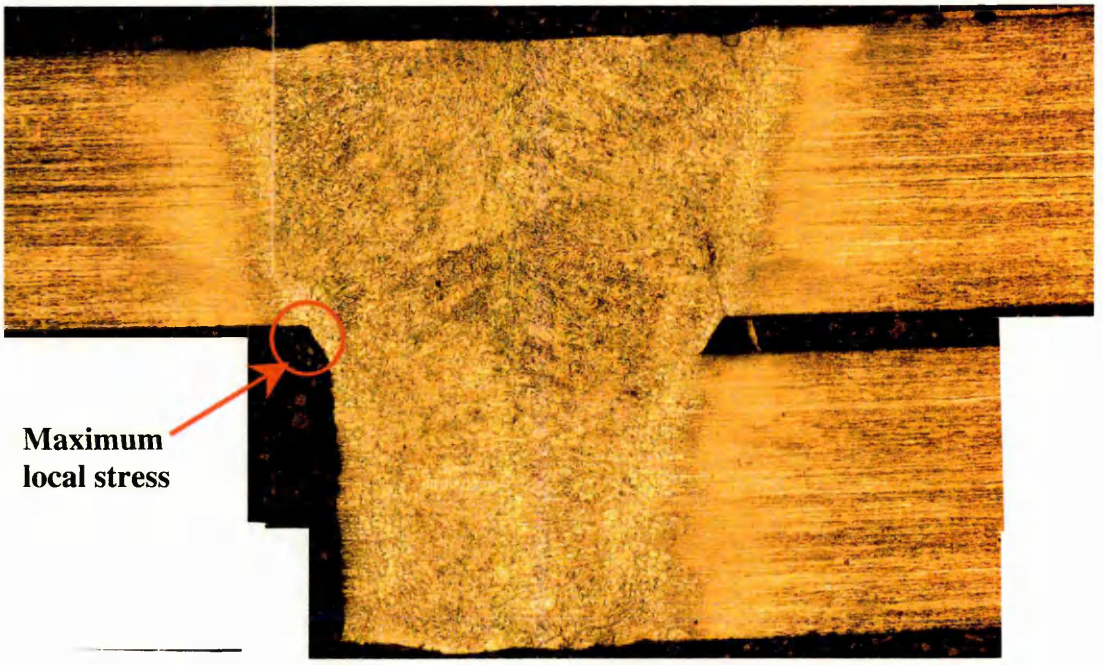

Image 23 1mm 2101 lap joint fatigue failure with a fatigue crack present at the opposite side of the lap joint

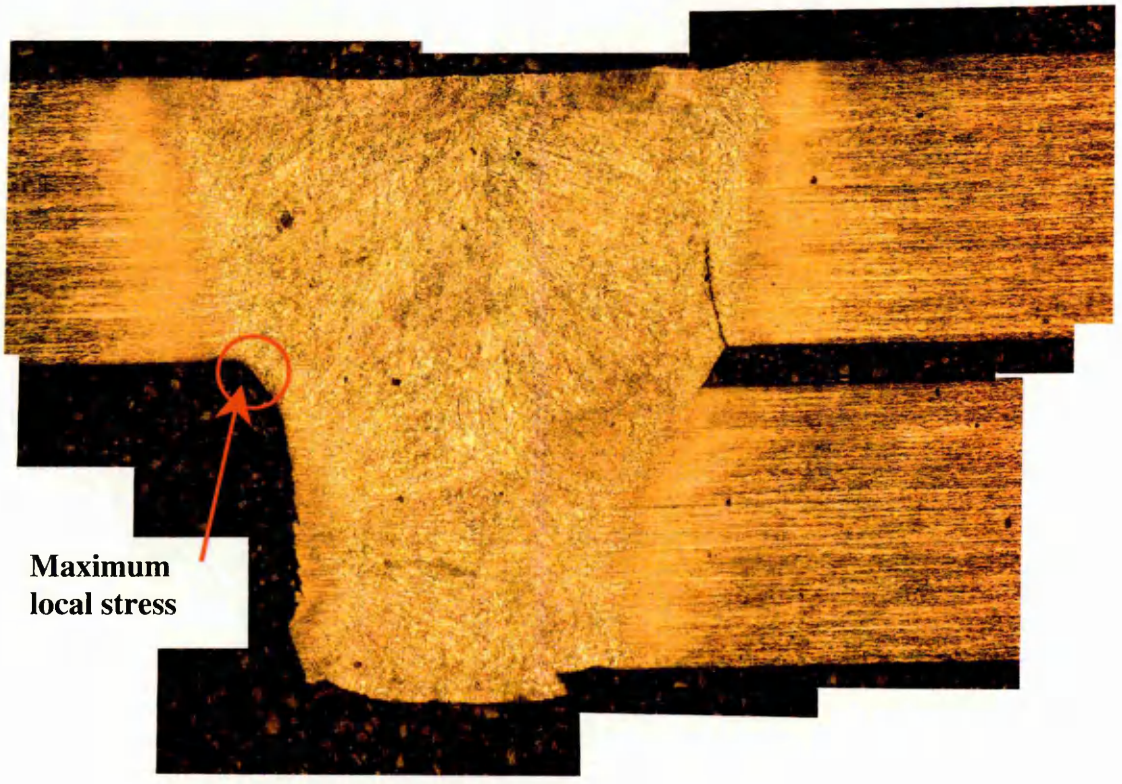

Image 24 1mm 2101 lap joint fatigue failure with a fatigue crack present at the opposite side of the lap joint

Image 25 and Image 26 show the respective close up images of the propagated fatigue cracks from Image 23 and Image 24. As both the images show, there is no evidence of plastic deformation in and around the crack area.

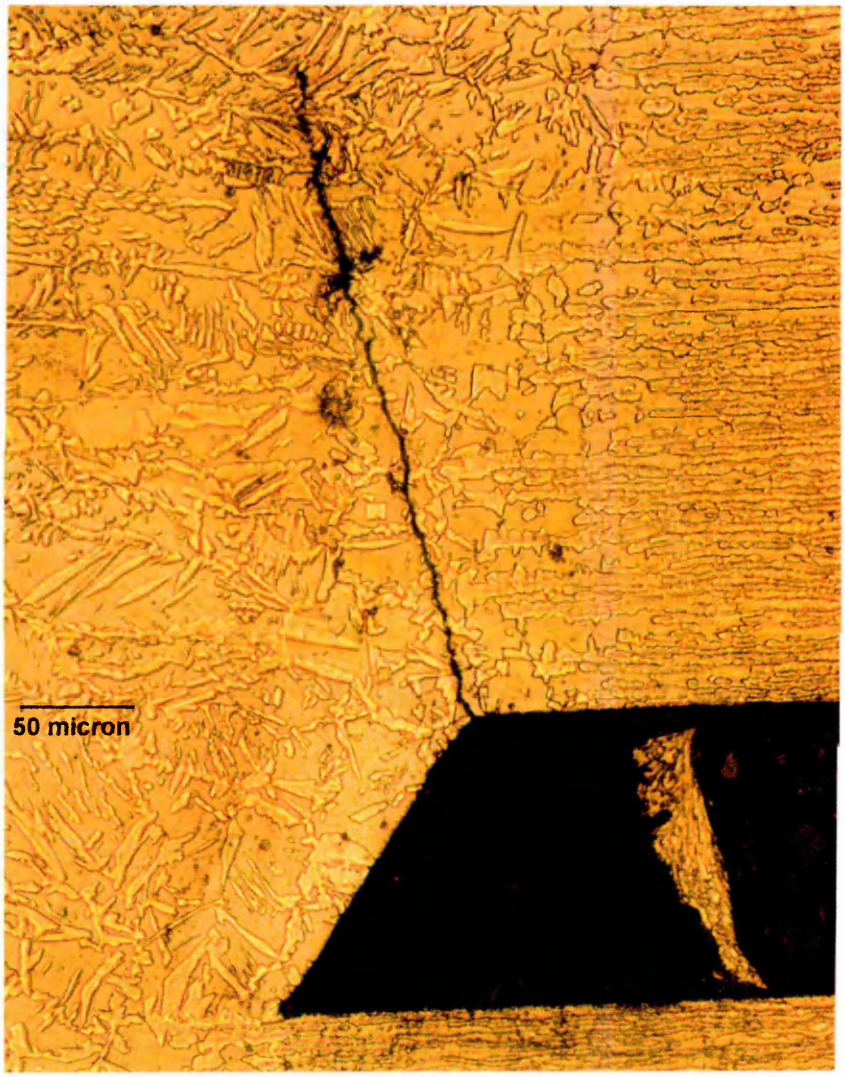

Image 25 Close up image of the propagated fatigue crack from Image 23 2101 similar metal lap joint

Image 26 Close up image of the propagated fatigue crack from Image 24 2101 similar metal lap joint

SEM Fatigue Initiation Analysis – 1mm 2101 Similar Metal Lap Joint

The following SEM images show a close up of 2101 similar metal lap joint fatigue crack initiation including a further higher magnification image of the crack tip.

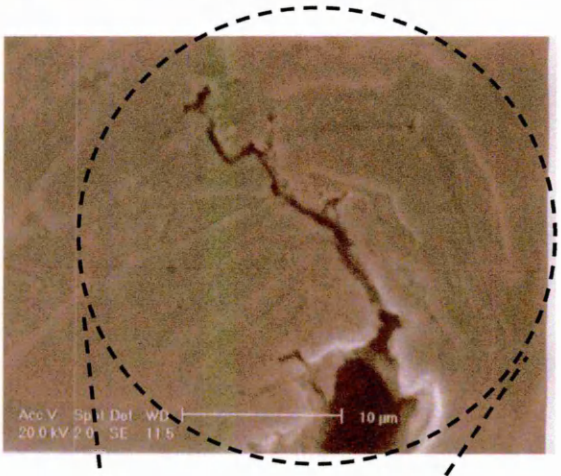

Image 27 SEM 2101 similar metal lap joint fatigue crack tip image

Image 28 SEM 2101 similar metal lap joint fatigue crack – same image as Image 26

4.12.3 Optical Fatigue Initiation Analysis – Dissimilar Metal Lap Joints

The following optical images were taken from dissimilar metal lap joints. The samples were fatigue tested; however, the tests were terminated prior to failure and total sheet separation. The samples were then mounted and analysed for the presence of fatigue cracks.

The following close up images are taken from the internal lap faces of the sheets. The illustration below shows the position of images presented.

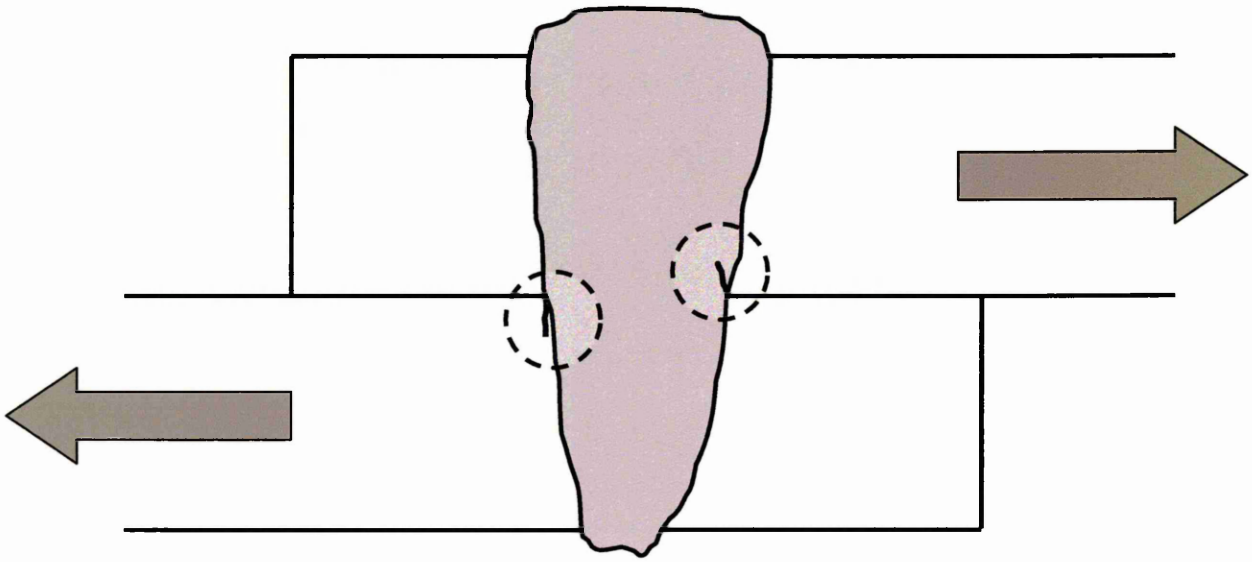

Figure 55 Schematic diagram showing the positions of the "close-up" dissimilar metal fatigue initiation sites

1.2mm V1437 (top) – 1mm 2101 dissimilar metal lap joint

Composite lap joint image showing the presence of fatigue cracks in both materials

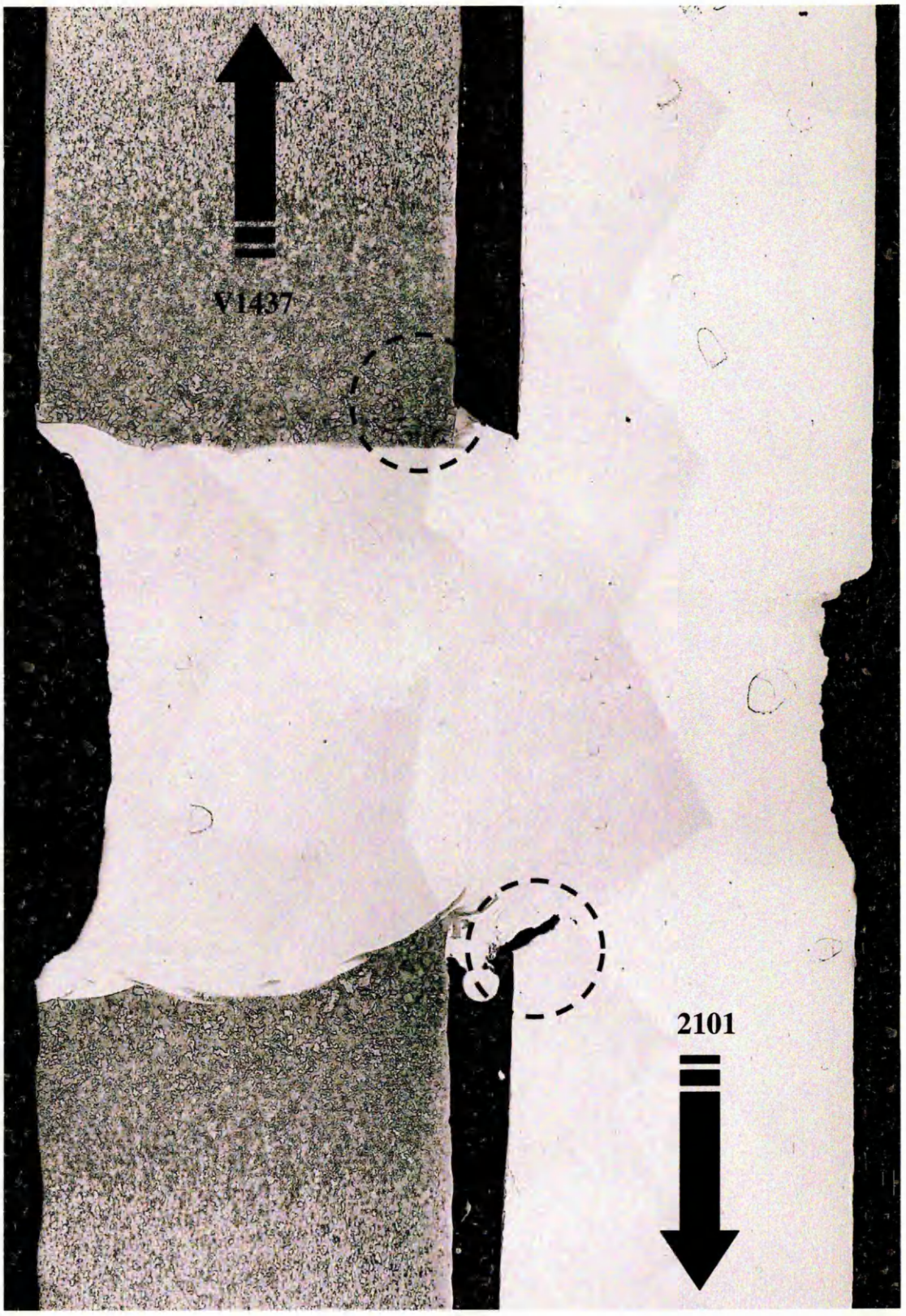

Image 29 1.2mm V1437(top) – 1mm 2101 dissimilar metal lap joint showing fatigue cracks in both materials

1.2mm V1437 (top) – 1mm 2101 dissimilar metal lap joint

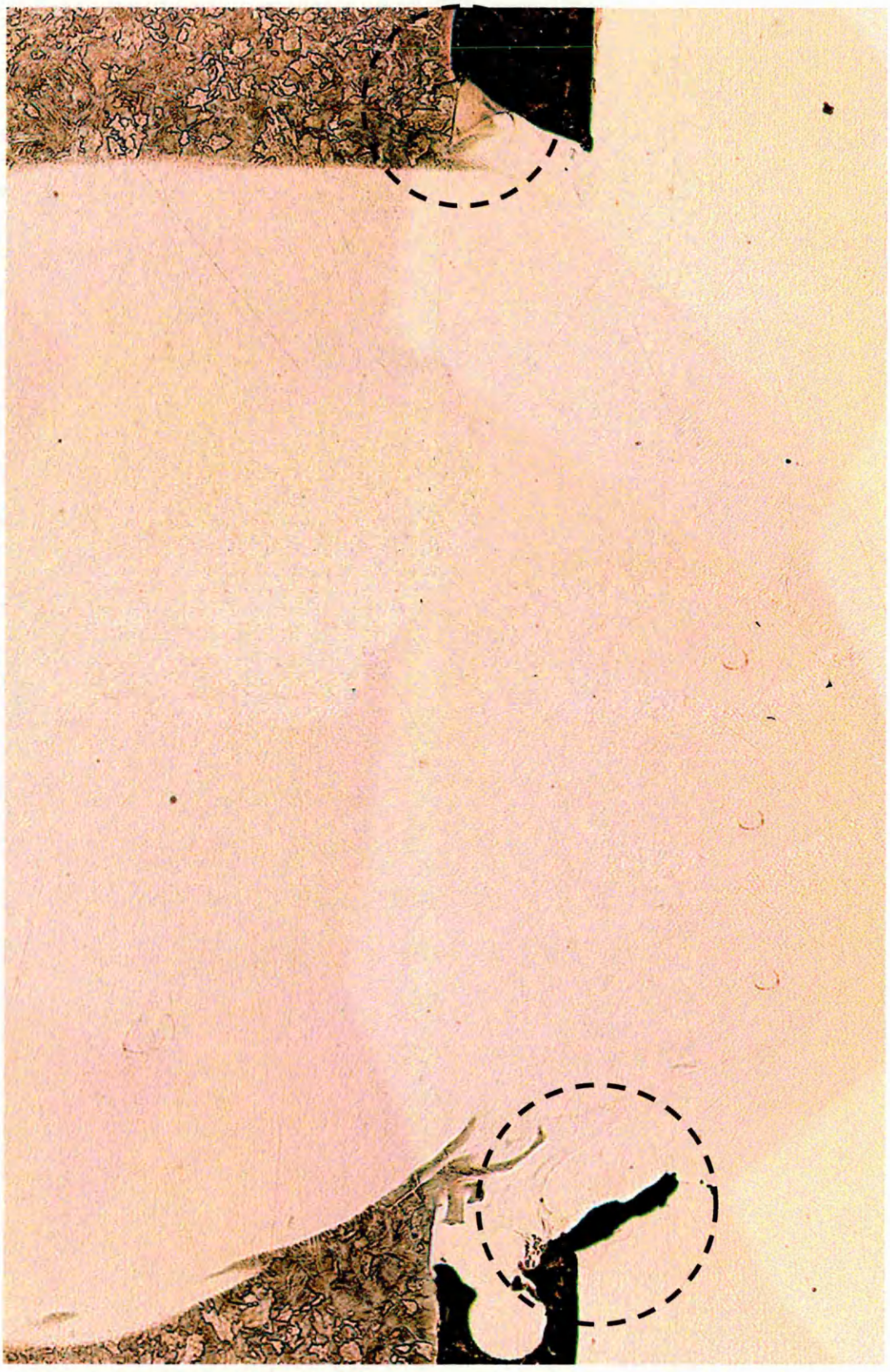

Image 30 1.2mm V1437(top) – 1mm 2101 dissimilar metal lap joint showing fatigue cracks in both materials

1.2mm V1437 (top) – 1mm 2205 dissimilar metal lap joint

The following optical images show a 1.2mm V1437 fatigue crack at high magnification.

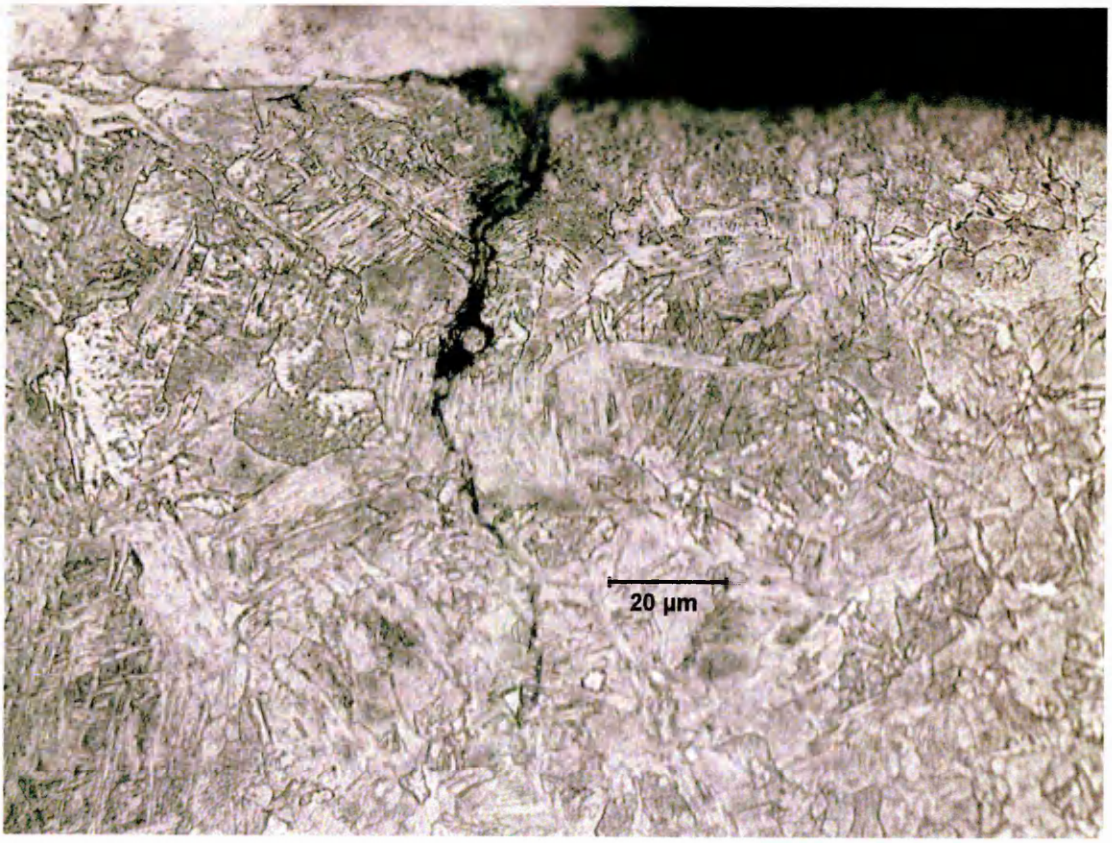

Image 31 1.2mm V1437(top) – 1mm 2205 lap joint fatigue crack in the 1.2mm V1437

The following optical images show a 1mm 2205 fatigue crack at high magnifications.

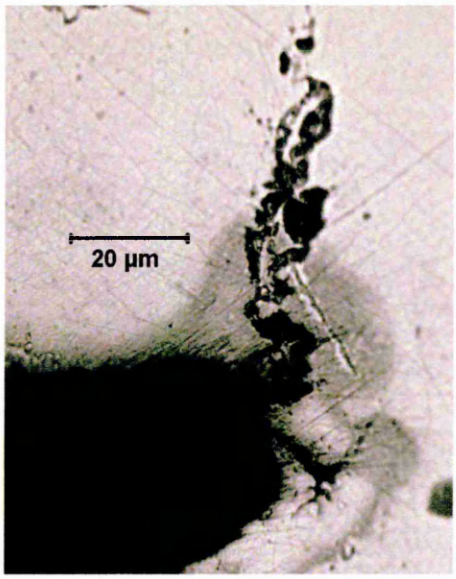

Image 32 1.2mm V1437(top) – 1mm 2205 lap joint fatigue crack in the 1mm 2205

4.12.4 SEM Fatigue Initiation Analysis – Dissimilar Metal Lap Joints

The following SEM images were taken from dissimilar metal lap joints. The samples were fatigue tested; however, the fatigue tests were terminated prior to failure and total sheet separation. The samples were then mounted and analysed for the presence of fatigue cracks.

The following close up images are taken from the internal lap faces of the sheets. The illustration below shows the position of images presented.

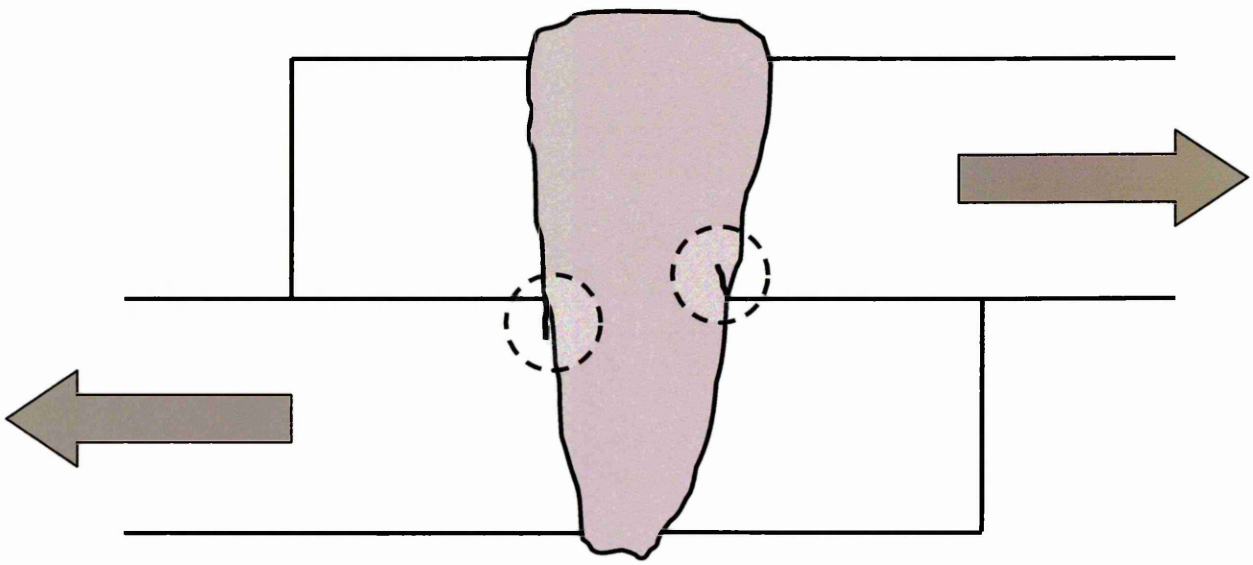

Figure 56 Schematic diagram showing the positions of the "close-up" dissimilar metal fatigue initiation sites

1.2mm V1437 (top) – 1mm 2101 dissimilar metal lap joint

Image 33 and Image 34 are secondary electron and back scattered electron images of a fatigue crack present in the 1mm 2101 at the bottom of the lap joint.

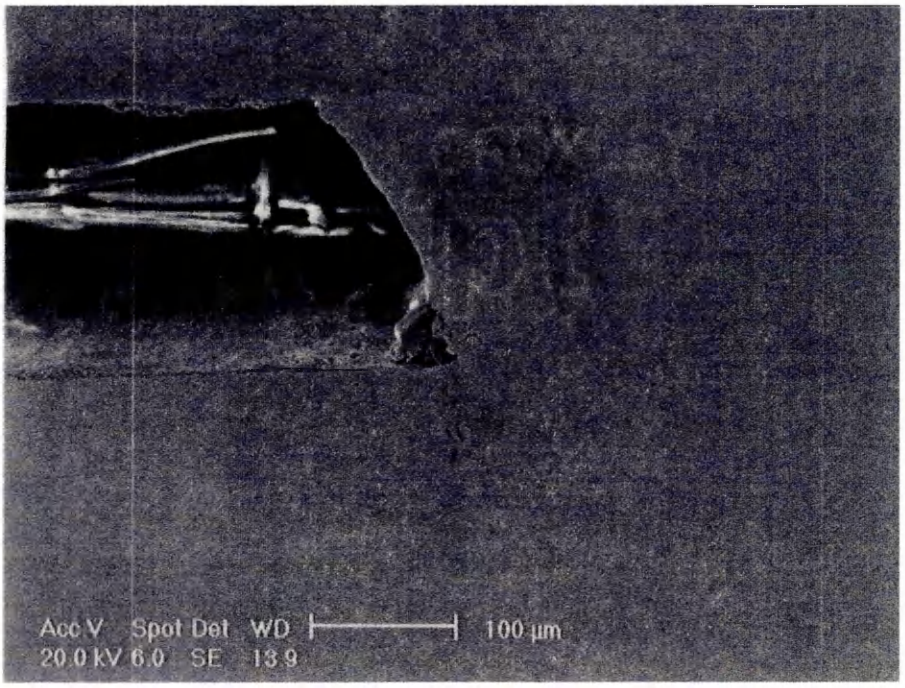

Image 33 Secondary electron image showing fatigue crack initiation in the 1mm 2101 from 1.2mm V1437 (top) – 1mm 2101 dissimilar metal lap joint

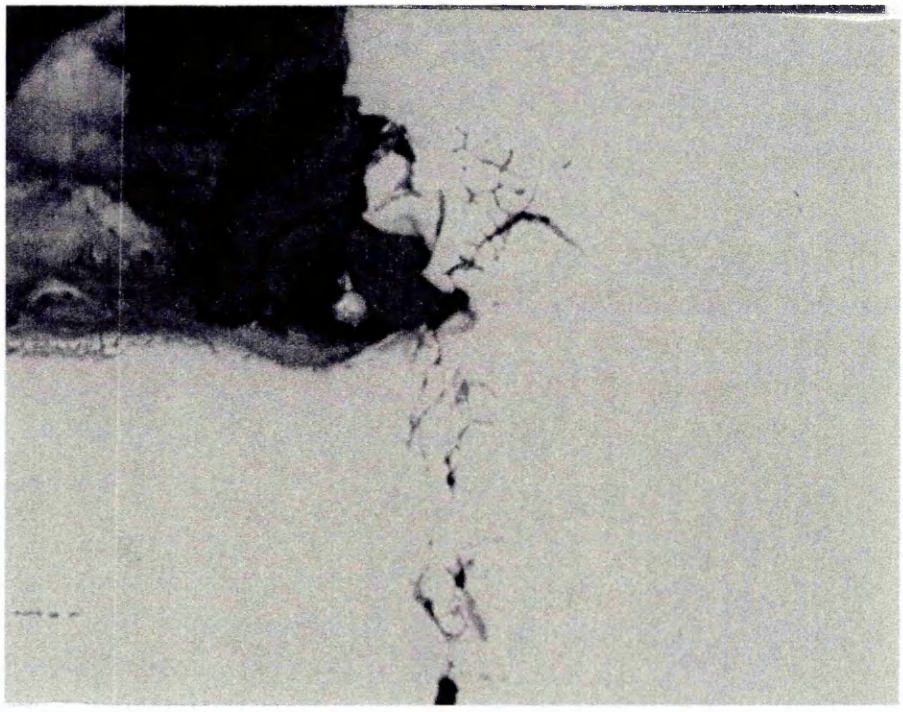

Image 34 Back scattered electron image showing fatigue crack initiation in the 1mm 2101 from 1.2mm V1437 (top) – 1mm 2101 dissimilar metal lap joint

Image 35 and Image 36 are secondary electron and back scattered electron images of a fatigue crack present in the 1.2mm V1437 zinc coated mild steel at the top of the lap joint.

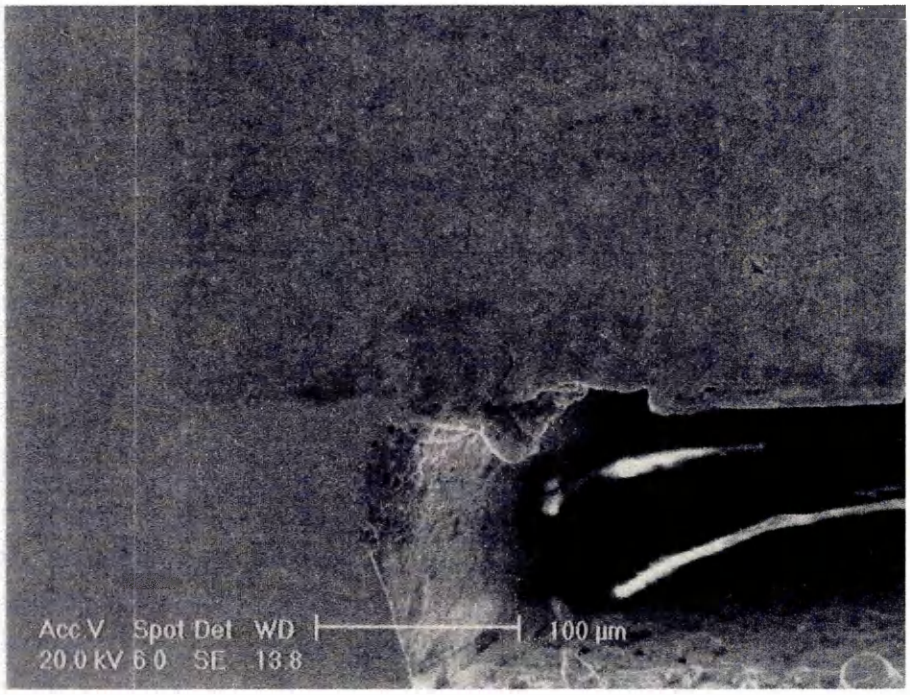

Image 35 Secondary electron image showing fatigue crack initiation in the 1.2mm V1437 from 1.2mm V1437 (top) – 1mm 2101 dissimilar metal lap joint

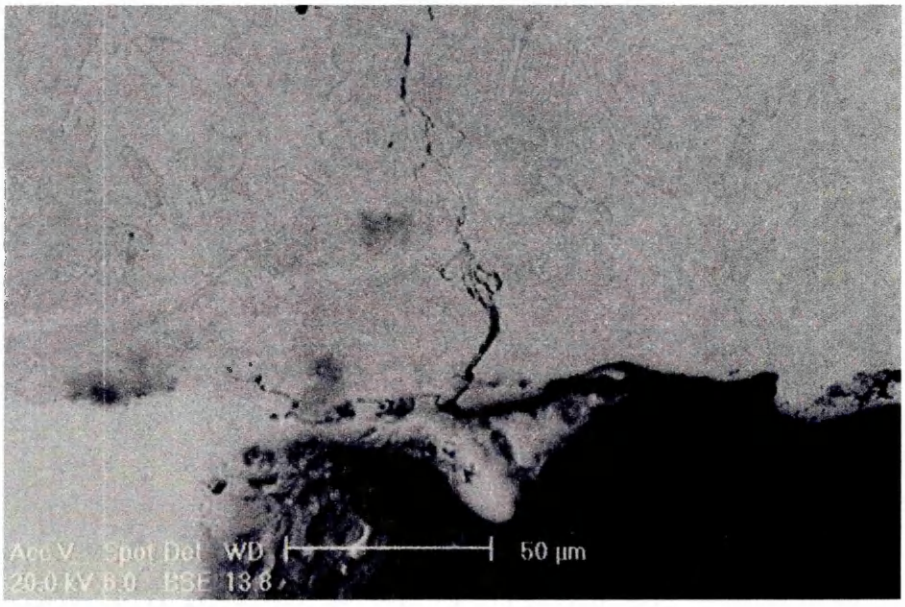

Image 36 Back scattered electron image showing fatigue crack initiation in the 1.2mm V1437 from 1.2mm V1437 (top) – 1mm 2101 dissimilar metal lap joint

1.2mm V1437 (top) – 1mm 2205 dissimilar metal lap joint

Image 37 is a secondary electron image of a fatigue crack present in the 1mm 2205 stainless steel at the bottom of the lap joint.

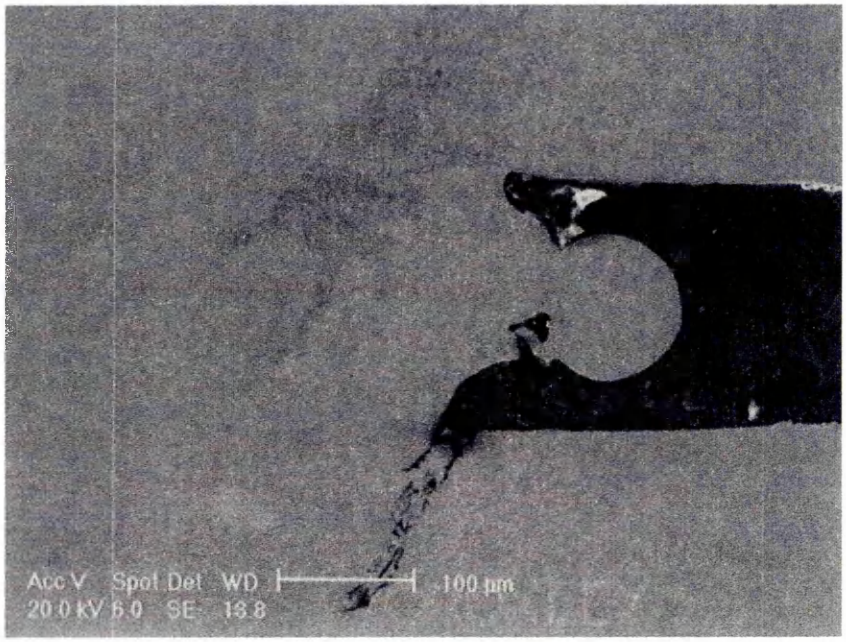

Image 37 Secondary electron image showing fatigue crack initiation in the 1mm 2205 from 1.2mm V1437 (top) – 1mm 2205 dissimilar metal lap joint

Image 38 is a secondary electron image of a fatigue crack present in the 1.2mm V1437 zinc coated mild steel at the top of the lap joint.

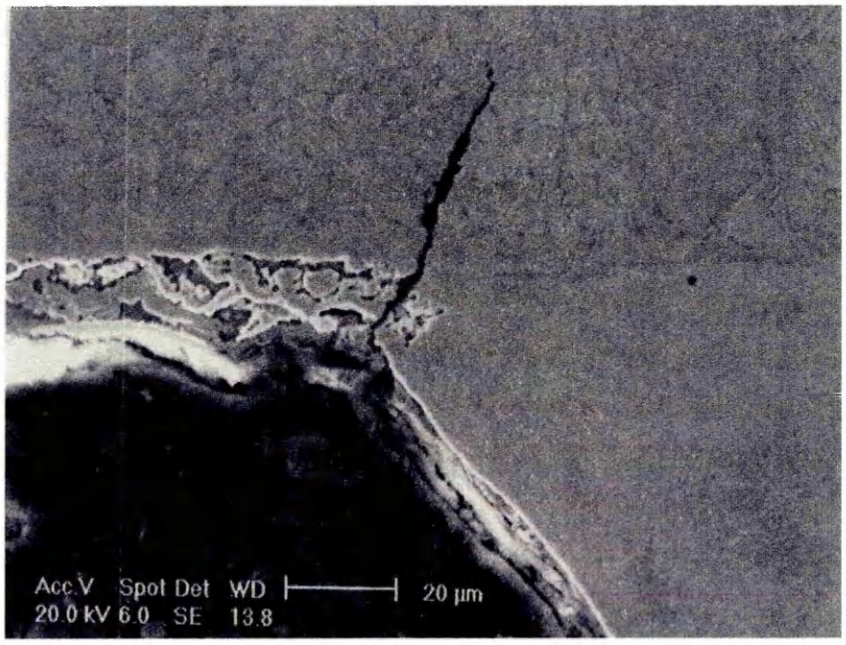

Image 38 Secondary electron image showing fatigue crack initiation in the 1.2mm V1437 from 1.2mm V1437 (top) – 1mm 2205 dissimilar metal lap joint

4.12.5 Optical Fatigue Failure Analysis – Butt Joints

The following images show the three types of dissimilar metal butt joint fatigue failures. Image 39 shows a 1.2mm V1437 – 1mm 2101 dissimilar metal butt joint fatigue failure in the centre of the weld metal.

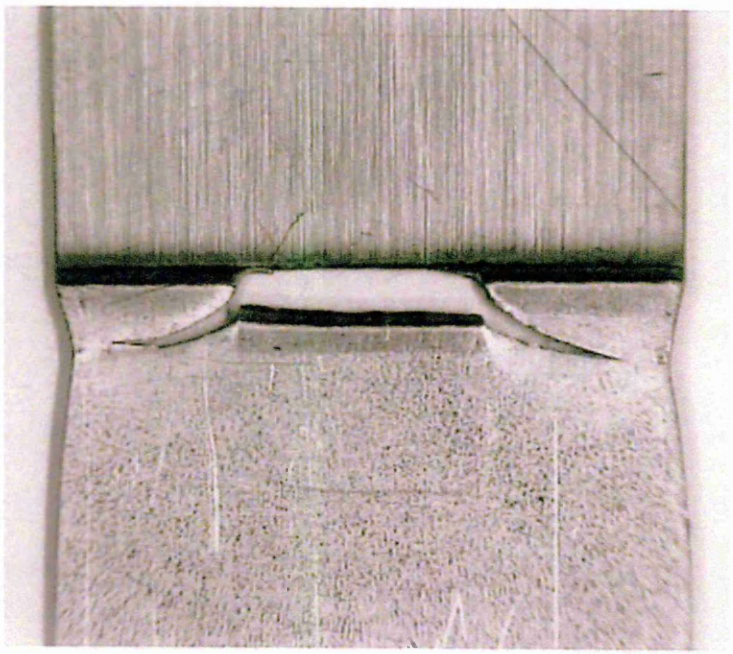

Image 39 1.2mm V1437 – 1mm 2101 dissimilar metal butt joint fatigue failure – centre weld failure

Image 40 shows a 1.2mm V1437 – 1mm 2101 dissimilar metal butt joint fatigue failure in the HAZ of the 1mm 2101 base material.

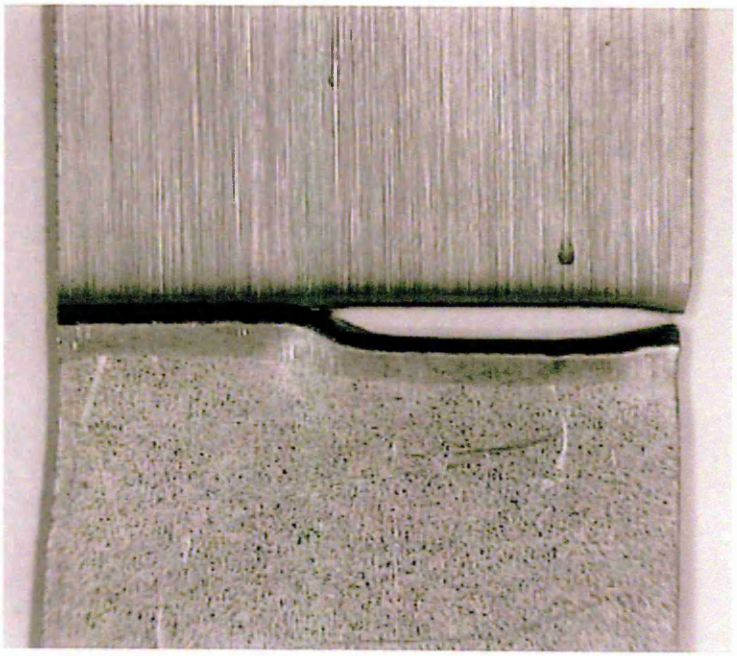

Image 40 1.2mm V1437 – 1mm 2101 dissimilar metal butt joint fatigue failure – 2101 HAZ failure

Image 41 shows a 1.2mm V1437 – 1mm 2101 dissimilar metal butt joint fatigue failure in the HAZ of the 1.2mm V1437 base material.

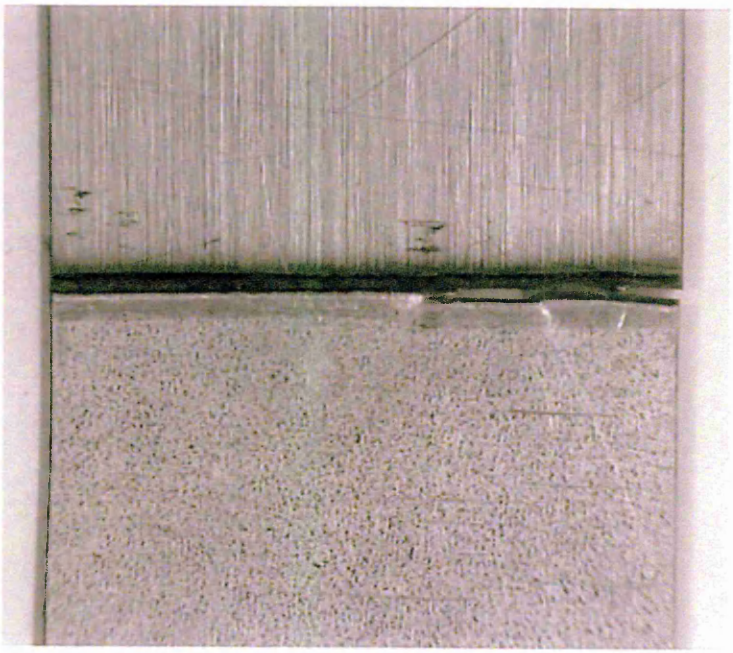

Image 41 1.2mm V1437 – 1mm 2101 dissimilar metal butt joint fatigue failure – V1437 HAZ failure

5 *Discussion*

5.1 Introduction

The discussions section has been split into the following sections:

- ***Laser Weld Quality***
  - Laser weld lap shear/tensile properties – **Trumpf 5kW CO_2 laser welder**
    - **Process optimisation and joint configuration** - lap shear (lap-joint) and tensile (butt-joint) properties
    - **Material optimisation** - lap shear (lap-joint) properties
  - Laser weld lap shear/tensile properties – **Rofin 2kW CO_2 laser welder**
    - **Fatigue specimen production** – lap shear (lap-joint) and tensile (butt-joint) properties
  - Laser welded lap joint fatigue properties – **Trumpf 5kW CO_2 laser welder**
    - **1mm 304 (top) – 1.2mm V1437** dissimilar metal lap joint
    - **1mm 304 – 1.2mm V1437 (top)** dissimilar metal lap joint
    - **0.78mm 2205 (top) – 1.2mm V1437** dissimilar metal lap joint
    - **0.78mm 2205 – 1.2mm V1437 (top)** dissimilar metal lap joint
  - Factors affecting dissimilar metal lap joint fatigue results
    - Weld bead microhardness
    - Weld bead composition
    - Stages of laser welded lap joint fatigue life
    - Geometric affects/Joint rotation
  - Laser welded lap/butt joint fatigue properties – **Rofin 2kW CO_2 laser welder**
    - **1mm 2205 – 1.2mm V1437 (top)** dissimilar metal lap joint
    - **1mm 2101 – 1.2mm V1437 (top)** dissimilar metal lap joint

- **1mm 2101 – 1mm V1437** dissimilar metal butt joint
- **1mm 2101 – 1mm 2101** similar metal lap joint

- Fatigue failure analysis
- Lap joint rotation
  - **Experimental Rotation**
- **Factors controlling lap joint rotation**
  - **Similar geometry & rotation angle**
  - **Effect of sheet thickness**
  - **Effect of interfacial gap**
  - **Effect of weld width**
  - **Effect of young's modulus**
  - **Partial penetration and double laser welds**
  - **Removal of joint rotation**
- **Spot weld fatigue comparison**

5.2 Laser Weld Quality

The initial laser welds were produced using the Trumpf 5kW CO_2 laser welder. The aim of the initial welding trials was to determine the highest welding speed whilst achieving full penetration for the similar and dissimilar metal lap joints. The presence of zinc at the internal lap face caused some problems with porosity and penetration.

Thus, investigations were carried out and measures were taken to prevent these problems during the fatigue specimen production using the lower power Rofin 2kW CO_2 laser welder.

The problems and preventative measures will now be discussed.

5.2.1 Trumpf 5kW CO_2 Laser Weld Quality

As stated in section 2.9.2, slower welding speeds are usually used when laser welding zinc-coated steel to allow adequate plasma suppression, however, this assumes a similar metal laser welded zinc-coated steel joint, which has twice the thickness of zinc as the dissimilar metal joints produced in this investigation. Similarly the use of shims to allow adequate zinc degasification from the internal lap face is suggested when the zinc coating thickness is >5μm (hot dipped galvanised coating). Again, this is assuming a similar metal lap joint configuration, with the dissimilar metal joint possessing half the zinc-coating thickness.

Thus, during the initial laser welding trials, no shims were used between the lap joints to allow for zinc degasification and the aim of the welding trials was to determine the highest welding speed whilst achieving full penetration for the lap joints.

Visual examination of the laser welded lap joint weld beads, however, revealed occasional signs of surface porosity in the laser weld bead and an occasional breakdown of penetration, see the following images.

It was noted that more frequent surface porosity occurred when the respective stainless steel was at the top of the lap joint.

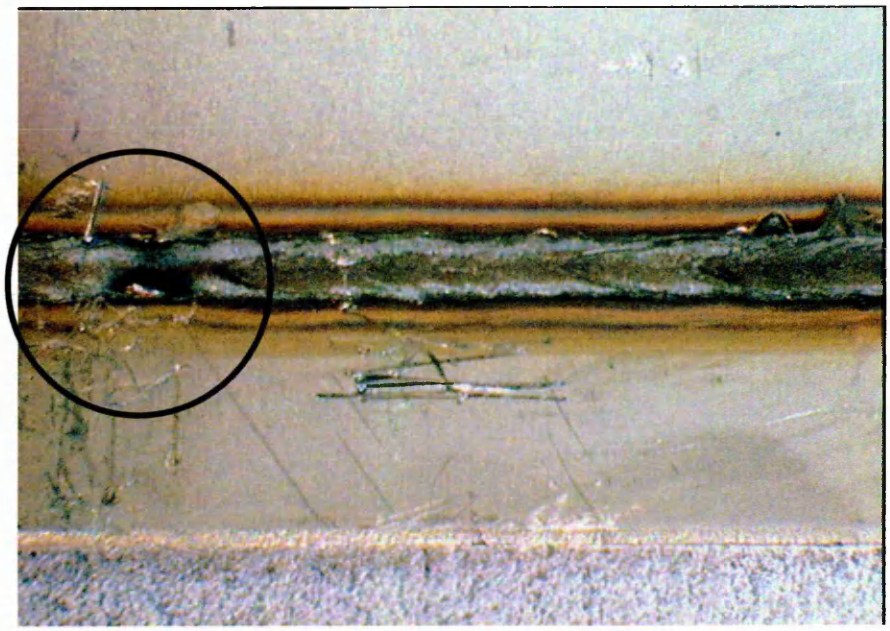

Image 42 Weld bead surface porosity in a 1mm 304 (top) – 1.2mm V1437 laser welded lap joint

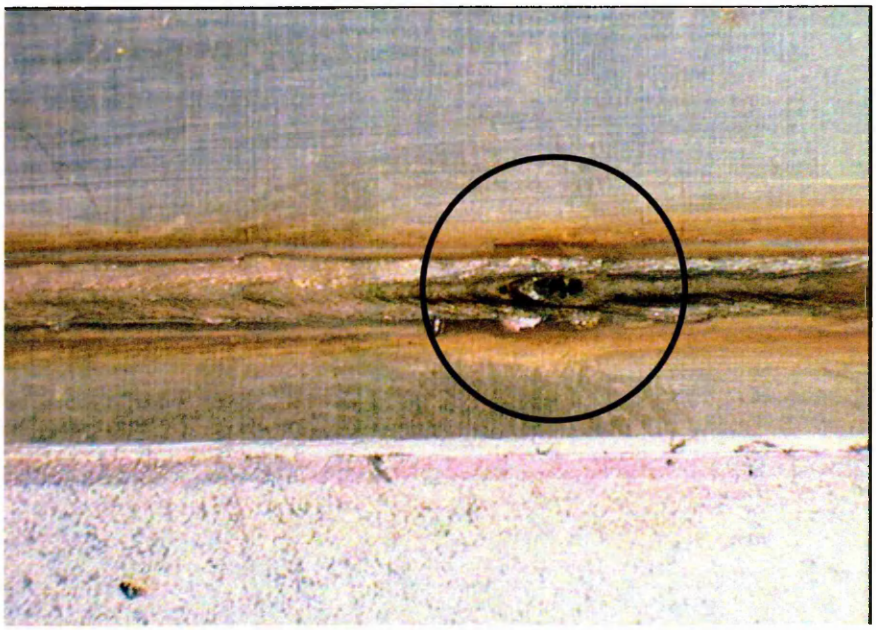

Image 43 Weld bead surface porosity in a 1mm 2205 (top) – 1.2mm V1437 laser welded lap joint

However, surface porosity was also observed when the 1.2mm V1437 was at the top of the lap joint.

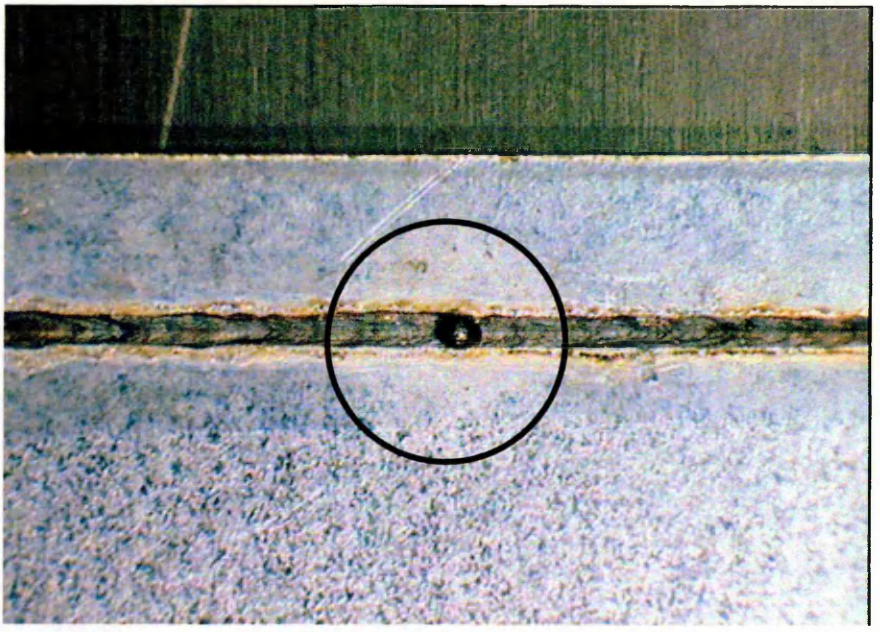

Image 44 Weld bead surface porosity in a 1.2mm V1437 (top) – 1mm 2205 laser welded lap joint

In contrast, the penetration was observed to break down more frequently when the 1.2mm V1437 was at the top of the lap joint.

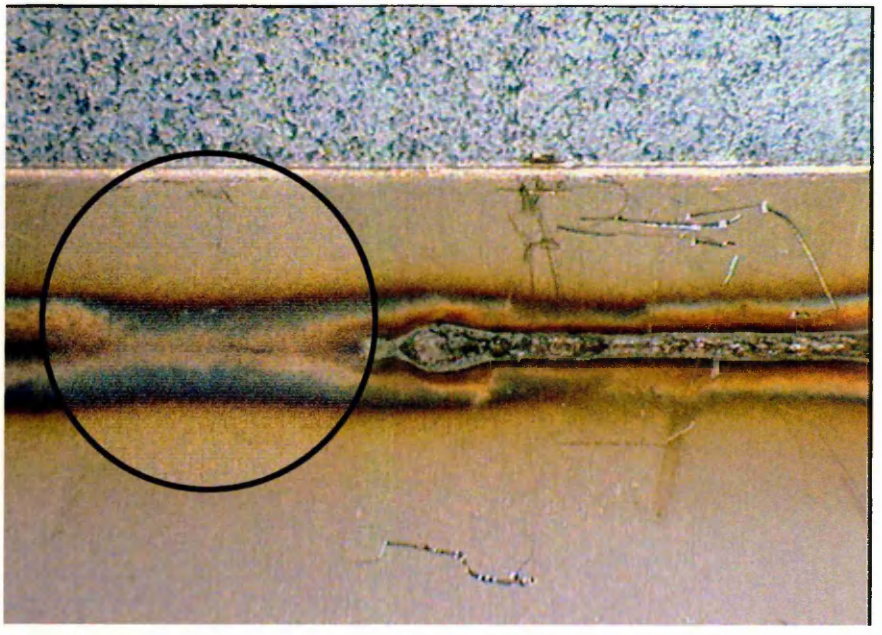

Image 45 Weld bead penetration breakdown in a 1.2mm V1437 (top) – 1mm 304 laser welded lap joint

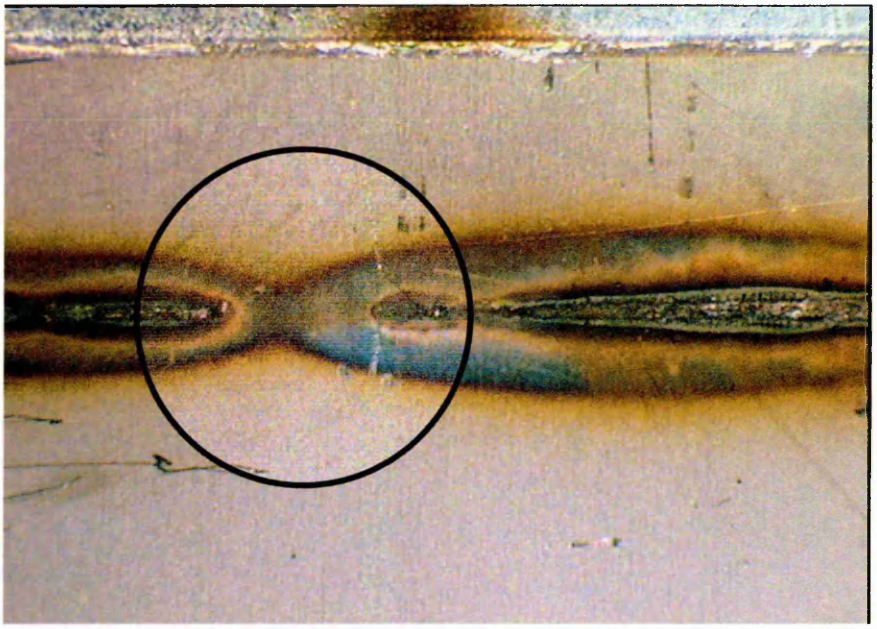

Image 46 Weld bead penetration breakdown in a 1.2mm V1437 (top) – 1mm 304 laser welded lap joint

Thus, the increased surface porosity which was seen when the respective stainless steel is at the top of the lap joint was due to the presence of zinc at the internal lap face. As no measures were taken to allow for zinc degasification from the internal lap face, high welding and consequent high cooling rate, the zinc vapour escaped through the molten weld bead producing porosity and blow holes in the weld bead surface.

The more frequent penetration break down which occurred when the 1.2mm V1437 was at the top of the lap joint was attributed to the higher welding speed which did not provide adequate suppression of the high density plasma formed. The high density plasma reduced the power density being absorbed by the joint, which reduced the penetration depth. Thus, when the respective stainless steel was at the top of the lap joint there was no zinc present at the top of the joint to vaporise, produce plasma and consequently reduce the power density being absorbed by the work piece.

It should be noted that these problems were observed with the 1.2mm V1437 similar metal lap joints as no interfacial gap or reduced welding speed was used.

Research has been conducted into the mechanism of plasma control during gas-assisted CO_2 laser welding. This research has shown that there is an optimum gas assist pressure, which is slightly higher than the metal vapour pressure produced[8485].

It can be seen from Figure 57, that the optimum gas assist pressure provides a plasma stream along the rear wall of the cavity. Too high gas assist pressure produces a central bead with surface porosity as there is no route for the plasma to escape due to the high gas assist pressure; hence, the vapour is incorporated into the weld bead causing surface porosity. Too little gas assist pressure does not adequately suppress the plasma formation, which reduces the energy being absorbed by the work piece.

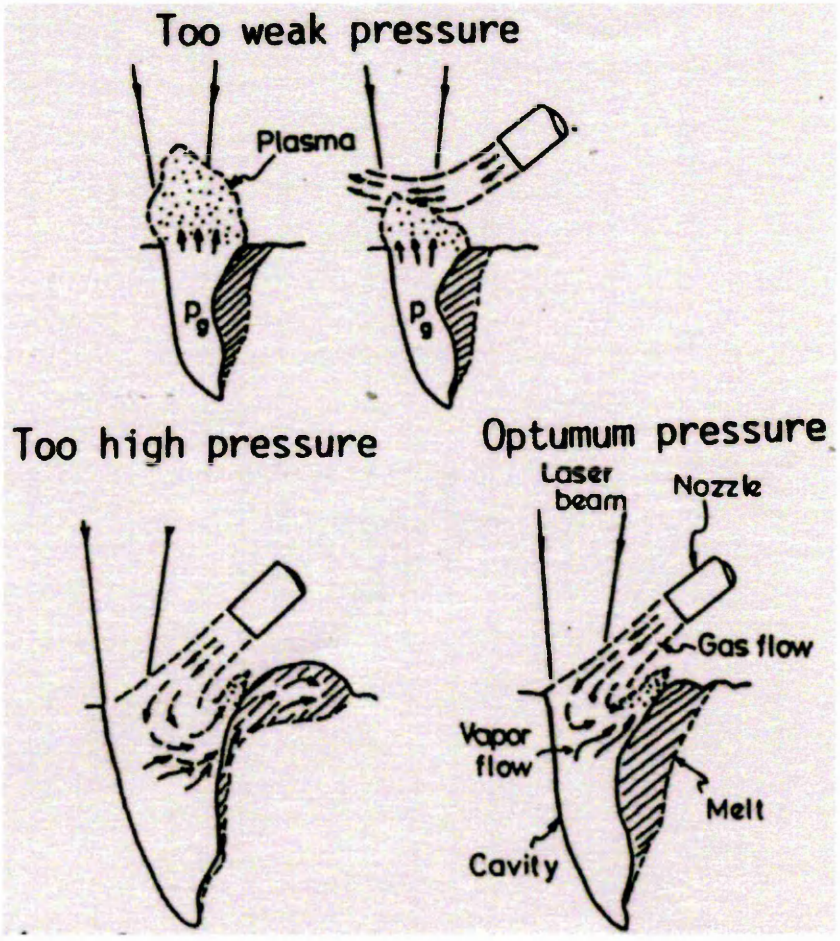

Figure 57 Effect of gas-assist pressure on plasma suppression in CO_2 laser welding[85]

[84] Arata, Y. Electron and Laser Beam Welding in Japan, Japan Institute of Welding, Commission IV, c/o Japan Welding Society, Kandasakumacho 1-11, Chiyodaku, Tokyo, Japan, pp293-304

[85] Miyamoto, I. Marou, H. Arata, Y. The Role of CO_2 Laser Welding, Proceedings of ICALEO'84, 44, 1984, pp1-7

Thus, the gas-assist flow rate (helium) which was found to produce the highest quality welds, in terms of surface porosity, using the Trumpft 5kW CO_2 laser welder was 25L/min. Lower quality laser welds were observed using both 20 and 30L/min gas-assist flow rate (helium).

It should be noted, however, that porosity was still observed even with the optimum gas assist pressure.

Research conducted by Linder et al, revealed that porosity in the laser weld bead did not affect the fatigue properties of similar metal stainless steel lap joints, if the porosity was contained in the centre of the laser bead and was not present at the edge of the weld at the internal lap face[70].

Research conducted by Kaitanov, revealed that incomplete or controlled penetration in the laser welded lap joint configuration did not affect the fatigue properties of the joint if a similar weld width between the sheets was achieved[71].

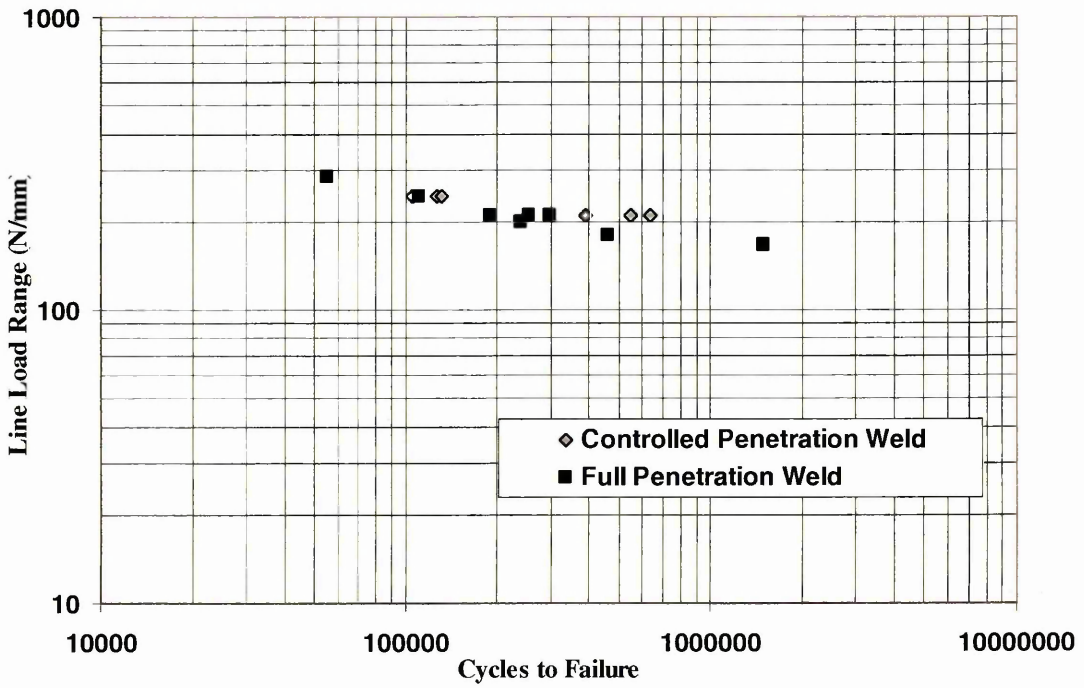

Graph 50 Comparison of 4mm 304 similar metal laser welded lap joint fatigue properties with full and partial penetration[87]

Thus, as the observed blow holes, surface porosity and break down of the penetration only occurred very occasionally throughout a laser welded length, fatigue testing was still carried out as it was assumed that these would not significantly affect the fatigue results.

5.2.2 Rofin 2kW CO_2 Laser Weld Quality

As stated in section 3.1.1.4, the Rofin 2kW CO_2 laser welder was used to produce four similar and dissimilar metal laser-welded butt and lap joints for fatigue testing. Two of which were dissimilar metal laser welded lap joints between stainless steel and 1.2mm V1437 zinc-coated mild steel.

The weld quality, that is, the consistency of penetration and reduction in the frequency of blows holes and porosity in the weld was improved by optimising:

- Welding power (kW)
- Welding Speed (m/min)
- Focal position (mm)

The power of the Rofin laser welder (2kW) was lower than that of the Trumpf (5kW) so a slower welding speed was used. As it can be seen from Figure 14 and Figure 15, the welding envelope for thinner materials covers a large range of welding power and speeds, thus allowing the production of welds in the lap joint configuration with full penetration over a range of welding speeds.

The focal length (distance from the focusing mirror to the work piece), see section 2.9.3, was shorter for the Rofin laser welding system (65mm – smaller f number) in comparison to the focal length of the Trumpf laser welding system (250mm). This produced a greater beam convergence, (seen in Figure 19), however measures had to be introduced to prevent damage to the focusing mirror owing to zinc spatter. This was overcome with the use of an air knife, see section 2.9.3.1, which allowed the laser welds to be produced with a 65mm focal length without damage to the focusing mirror.

Defocusing the laser beam reduces the laser power density, and consequently the weld penetration depth, unless extra power is available to compensate. Also, when using focusing systems with small f numbers (which produce large beam convergence angles), setting the focus height to achieve the required spot diameter is difficult because of the large beam convergence angle producing significant increases in spot diameter for small vertical movements of the optical system[86].

The greater beam divergence of the Rofin laser welding system allowed the effect of the focal position to be utilised to a greater extent. Hence, a focal position of 4mm above the surface of the top sheet was selected, which had the effect of defocusing the beam. The aim was to increase the specific heat input of the process, as the welding speed would have to be reduced to achieve adequate penetration; ultimately reducing the solidification rate, thus, allowing more time for the zinc vapour from the internal lap face to escape through the molten weld bead.

A similar technique has been investigated using twin spot lasers; see section 2.9.2, which produced an elongated weld bead to allow the zinc vapour to escape through the molten weld bead.

A lower welding speed was also used to increase the heat input of the Rofin laser welding system. The welding speed and power of the Rofin produced a heat input of 120 J/mm compared to the heat input of the Trumpf which was 88 J/mm for the dissimilar metal laser welded lap joints.

The increased specific heat input and defocused beam of the Rofin 2kW CO_2 laser welder produced a slower solidification rate to provide more time for the zinc vapour to escape through the molten weld bead. The slower welding speed used also provided adequate suppression of plasma to aid penetration.

---

[86] Dawes, C. J. Johnson, K. I. Watson, M. N. Developments in Laser Welding of Sheet and Plate, The Welding Institute, Abington Hall, Abington, Cambridge CB1 6AI, UK, pp213-223

The result was a series of laser welded lap joints with no porosity or blow holes observed in the weld beads and consistent penetration along the entire length of the weld. It should be noted that the use of the twin spot laser was to produce porosity free welds in similar metal zinc-coated steel laser welds, thus possessing twice the zinc coating thickness at the internal lap face. Hence, with only half the quantity of zinc present in the dissimilar metal lap joints, control of the specific heat input and focusing system was sufficient to remove the problems associated with the zinc coating.

The use of shims to produce a gap at the internal lap face was not introduced, as it was considered that this may reduce fatigue properties. This effect will be discussed in detail in section, 5.9.3.

5.2.3 Liquid Metal Embrittlement

No signs of LME were evident in any of the dissimilar metal lap joints produced with 1mm 304 austenitic stainless steel. No premature failures or especially low properties were observed during tensile, lap shear and lap joint fatigue testing throughout the trials, which could have been attributed to the effects of LME.

Energy dispersive x-ray analysis of the internal lap face of a dissimilar metal laser welded lap joint revealed the diffusion of zinc into the surface of the 1mm 304 austenitic stainless steel adjacent to the laser weld bead, however, no signs of cracking were evident. A similar investigation was carried out by Marples, who also observed diffusion of zinc into the surface of 1mm 304 at the internal lap face of a dissimilar metal spot welded joint between 1.2mm V1437 – 1mm 304. No reduction in spot welded lap shear or lap joint fatigue properties were noted[4].

5.3 Laser Welded Butt Joint Properties – Trumpf 5kW

5.3.1 Similar Metal Laser Welded Butt Joint Properties

As shown in Graph 13 and Graph 14, laser welding speed had no effect on the tensile strength and elongation properties of the three similar metal butt joints produced. The mode and positions of failure showed no change with welding speed, with failure occurring in the parent material of the 1.2mm V1437 and at the edge of the weld for the respective stainless steel joints. This was expected as the welding envelopes produced for thin sheets accommodate a wide range of welding speeds and power to produce high quality welds, see Figure 14.

When compared to the base material tensile properties the elongation to failure for the 1.2mm V1437 weld was similar to the base material, with failure occurring approximately half way between the grip and the weld at 45° shear after appreciable plastic deformation.

The elongation to failure for the 1mm 304 and 1mm 2205 similar metal butt joints was lower than the base material properties for the two respective stainless steel grades. The stainless steel grades showed no appreciable signs of necking and although the butt joints achieved the same tensile strength as the parent material stainless steel, failure occurred prior to achieving the elongation of the parent material, see Table 18 .

5.3.2 Dissimilar Metal Laser Welded Butt Joint Properties

Graph 15 shows that the laser welding speed had no effect on the tensile properties of dissimilar metal butt joints between 1.2mm V1437 - 1mm 304 and 1.2mm V1437 – 1mm 2205. This is due to the lower tensile properties, more specifically the lower Rp0.2, of the V1437 in comparison to the 1mm 304 and 1mm 2205 stainless steel. Thus tensile failure occurred in the parent material of the 1.2mm V1437 at 45° shear.

Laser welding speed had no effect on the dissimilar metal butt joint elongation to failure, see Graph 16. The elongation to failure, however, does reveal some interesting points. It can be seen from Graph 16 that the elongations to failure for the 1.2mm V1437 – 1mm 2205 dissimilar metal butt joints are approximately 60% of the V1437 base material elongation, see Table 18. This is because the yield strength of the 1mm 2205 is higher than the ultimate tensile strength of the 1.2mm V1437 (see Table 7 and Table 3 respectively) and thus, does not plastically deform during the tensile test.

The elongations to failure for the 1.2mm V1437 – 1mm 304 dissimilar metal butt joints show that both materials had plastically deformed during the tensile tests. The actual yield strengths for 1.2mm V1437 and 1mm 304 can be seen in Table 3 and Table 4 respectively and shows only a 10MPa difference between the two steels. However, at the load which equates to the 1.2mm V1437 yield stress, the equivalent stress in the 1mm 304 would be 50MPa above the 304 yield strength; hence, the 1mm 304 would begin to plastically deform first. Due to the higher work hardening rate of the 1mm 304 in comparison to the 1.2mm V1437, necking would occur preferentially in the 1.2mm V1437. The reduction in cross sectional area and increase in stress resulted in failure in the 1.2mm V1437. This explanation was further substantiated through the observation of the load – extension graph which showed no definitive yield point as seen in the

1.2mm V1437 base material tensile graph and the 1.2mm V1437 – 1mm 2205 dissimilar metal butt joint graph.

5.4 Laser Welded Lap Shear Properties – Trumpf 5kW Process Optimisation

5.4.1 Similar Metal Laser Welded Lap Shear Properties

As mentioned in section 4.3.1, poor quality 1.2mm V1437 similar metal lap joints were produced. The clamping arrangement of the Trumpf 5kW CO2 laser welder was a hydraulic press, which served to clamp the sheets with an even force over the entire length of the laser weld. No methods for allowing zinc-degasification of the internal lap face were introduced, for example shims or slower welding speeds. Thus, the combination of the high pressure, intimate sheet contact with no interfacial gap and the presence of two 5 - 7μm zinc coatings led to a breakdown of the laser welding process. This produced intermittent penetration, frequent blow holes and surface porosity in the weld bead. When these welds were tested however, most achieved >100% weld efficiency. Research has shown that the presence of porosity in the laser weld bead may not always reduce the tensile properties of the joints; if the porosity is contained within the weld bead and does no break the edge of the weld between the lap face then high tensile properties may still be achieved. Similarly, research has also shown that partial penetration laser welds can possess similar tensile and fatigue properties to full penetration laser welds[87].

The effect of the porosity and partial penetration on the tensile properties of the similar metal 1.2mm V1437 is reduced by its low tensile properties. The high laser weld hardness (~400 Hv) results in the weld not being suitably stressed for the porosity or partial penetration to have an effect as the weakest part of the joint is the parent 1.2mm V1437, which strains and necks increasing the local stress prior to failure at 45° shear.

Table 18 shows the 1.2mm V1437 similar metal lap joint failure occurred in the HAZ. Both the 1mm 304 and 1mm 2205 similar metal lap shear failures also occurred in the HAZ at 89% and 95% of the parent material tensile properties respectively. This is due to the joint configuration. The lap joint configuration, unlike the butt joint configuration, introduces an applied bending moment to the joint due to eccentricity of the applied load. This "misalignment" increases the local stress at the internal lap face adjacent to the weld that results in failure. See section 2.15.2.1 for an explanation of lap joint rotation. It should be noted that the eccentricity of the applied load and its effects will be covered in detail in the fatigue discussion section.

Graph 18 shows the elongations to failure for the similar metal lap joints. All three similar metal lap joint elongations to failure are lower than those achieved by the respective parent material (see Table 19) and similar metal butt joint elongations (see Table 18). Again, this was attributed to the rotation, and increase in local stress at the internal lap face.

5.4.2 Dissimilar Metal Laser Welded Lap Shear Properties

Although the similar metal stainless steel lap shear results are affected by rotation and the local stress at the internal lap face, the dissimilar metal lap joint failures for 1.2mm V1437 – 1mm 304 and 1mm 2205 occurred in the parent material of the 1.2mm V1437at 45° shear, (seen in Graph 19). The joint configuration, that is which material was at the top of the lap joint, had no effect on the lap shear failure.

The % elongation to failure for the 1.2mm V1437 – 1mm 2205 lap joint (both configurations) was lower than the 1.2mm V1437 – 1mm 304 lap joint (both configurations), see Graph 20. This was due to the 1mm 2205 not plastically deforming, so only half the 1.2mm V1438 was accommodating the strain.

This was substantiated by the load – extension graph which showed a definite yield point for the two configurations.

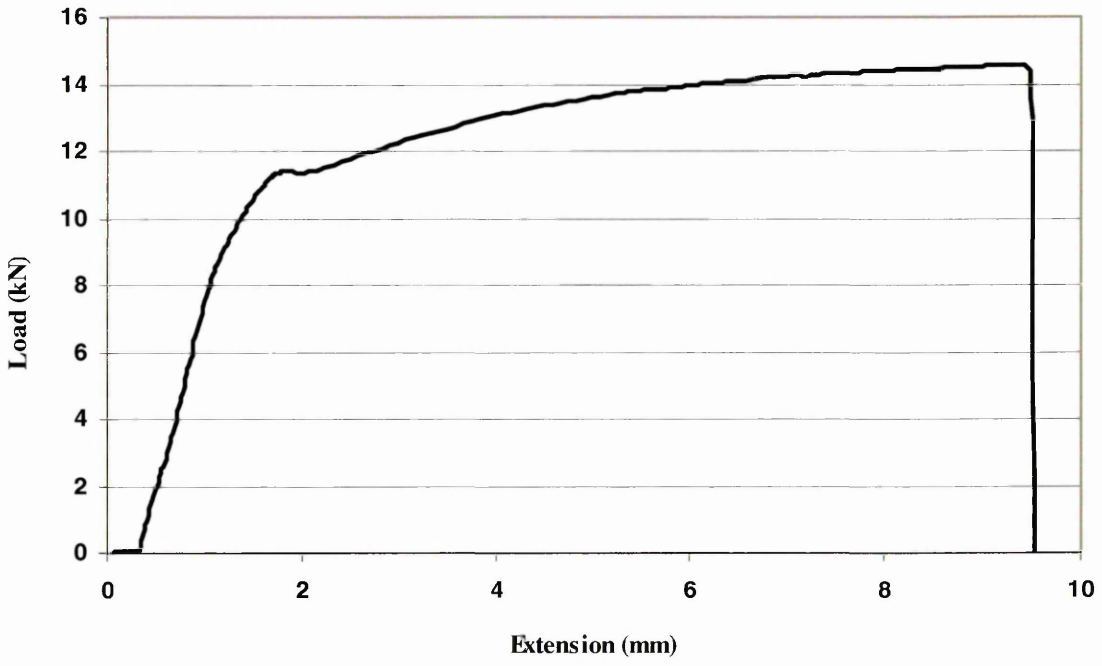

Graph 51 1mm 2205 – 1.2mm V1437 load extension graph showing a definite yield point

In comparison, the 1.2mm V1437 – 1mm 304 (both configurations) load – extension graph showed no definite yield point.

Graph 20 also allows comparison of the dissimilar metal lap joint % elongations with the similar metal lap joint elongations to failure. This shows that the 1.2mm V1437 – 1mm 2205 dissimilar metal lap joint elongation is lower than the 1.2mm V1437 similar metal lap joint elongation; again, because only half the 1.2mm V1437 is accommodating the strain during the lap shear tests. More interestingly, however, is comparison of the 1.2mm V1437 – 1mm 304 (both configurations) to the 1.2mm V1437 and 1mm 304 similar metal lap joint elongations to failure. The dissimilar joint values are higher than the 1.2mm V1437 similar metal values, which shows that the strain is accommodated equally in both materials for the 1.2mm V1437 – 1mm 304 and it is the increased work hardening rate of the 1mm 304 that produces failure in the 1.2mm V1437.

5.5 Laser Welded Lap Shear Properties – Trumpf 5kW Material Optimisation

5.5.1 Dissimilar Metal Laser Welded Lap Shear Properties

Thinner gauges of stainless steel were laser welded to 1.2mm V1437 in order to balance the tensile properties of the lap joints. It was thought that the very high tensile property difference between the 1.2mm V1437 and the 1mm stainless steel grades, specifically the 1mm 2205 (see Table 3 and Table 7 respectively) would cause fatigue failure to occur preferentially in the parent material of the 1.2mm V1437 and not the laser welded joint. Thus, thinner gauges of 302 austenitic stainless steel and 2205 duplex stainless steel were welded to 1.2mm V1437.

It can be seen from Graph 21 that lap shear failure occurred in the parent material of the 0.6 and 0.7mm 302 stainless steel (top) when welded to 1.2mm V1437 in the lap joint configuration. In comparison, the lap shear failure for the 0.78mm 2205 (top) – 1.2mm V1437 occurred in the parent material of the 1.2mm V1437 at 45° shear.

It should be noted that although the tensile properties of the 0.6mm and 0.7mm 302 are higher than the parent material 1.2mm V1437 failure, the reduced cross – sectional area of the 302 stainless steel correlated to a lower load to failure than the 1.2mm V1437 and hence, 302 parent material failures occurred. The tensile properties of the 0.6, 0.7mm 302 and 0.78mm 2205 can be seen in Table 6, Table 5 and Table 8 respectively.

In comparison, the 0.78mm 2205 yield strength was higher than the ultimate tensile strength of the 1.2mm V1437 and again did not plastically deform during the lap shear test.

Graph 22 shows the 0.78mm 2205 (top) – 1.2mm V1437 elongation to failure was lower than the 1.2mm V1437 similar metal elongation to failure due to only half the 1.2mm V1437 accommodating any strain throughout the lap shear tests.

Similarly, less than half the parent material elongation was achieved with the 0.6 and 0.7mm 302 – 1.2mm V1437 dissimilar metal lap joints. This was due to the 1.2mm V1437 not accommodating any strain and plastically deforming during the lap shear test. Consequently, the following joint configurations with "balanced" tensile properties were selected for fatigue testing.

- **1.2mm V1437 (top) – 1mm 304 dissimilar metal lap joint**
- **1mm 304 (top) – 1.2mm V1437 dissimilar metal lap joint**
- **1.2mm V1437 (top) – 0.78mm 2205 dissimilar metal lap joint**
- **0.78mm 2205 (top) – 1.2mm V1437 dissimilar metal lap joint**

These joints all possessed >100% weld efficiency, that is, lap shear failure occurred in the parent material of the 1.2mm V1437 away from the weld. The reduced thickness of the 2205 duplex stainless steel from 1mm to 0.78mm was to "balance" the tensile properties within the dissimilar metal lap joint, due to concerns that the softer parent material (1.2mm V1437) may fatigue with preference to the laser weld.

5.6 Laser Welded Tensile/Lap Shear Properties – Rofin 2kW CO_2 Laser Welder (Fatigue Specimen Production)

Graph 23 shows the tensile and lap shear properties of the similar and dissimilar metal laser welded butt and lap joints produced using the lower powered Rofin 2kW laser welder. Tensile and lap shear failure occurred in the parent material of the 1.2mm V1437 for the two dissimilar metal lap joints and dissimilar metal butt joint produced. This was expected since the yield strength of the 1mm 2205 and 2101 was higher than the ultimate tensile strength of the 1.2mm V1437.

The graph also shows the lap shear properties of the 1mm 2101 similar metal lap joint. It can be seen that the 1mm 2101 similar metal lap shear value was 91% of the 1mm 2101 parent tensile value, see Table 9 for 1mm 2101 parent properties. This is attributed to the rotation of the lap joint during the lap shear test, with lap shear failure occurring at the edge of the weld (highest local stress), the same position as the 1mm 2205 similar metal lap shear failures.

As shown in Graph 24, the two dissimilar metal lap joints and dissimilar metal butt joint possessed comparable elongations to failure. This was due to the respective stainless steels, 1mm 2205 and 1mm 2101 not plastically deforming.

The relationship between the elongation to failure for the 1mm 2101 similar metal lap joint and the parent material was comparable to the 1mm 2205 similar metal lap joints, achieving 38% of the parent material elongation to failure.

Thus, the four joints lap shear tested were selected for fatigue testing.

5.7 Laser Welded Lap Shear Property Comparison

The similar and dissimilar metal laser welded lap shear properties were compared with resistance spot welded lap shear properties of Marples and Wray for the same materials[4,72]. Resistance spot welding is currently the highest volume and most widely used automotive welding process and thus serves as the benchmark for comparison.

The following graphs are presented in lap shear line load, which is the applied load divided by the sample width. This unit allows comparison of laser welded lap shear properties with the discontinuous resistance spot welding lap shear properties. Unless otherwise stated the scatter of lap shear results was less than +/-1%.

The equations used to calculate the resistance spot weld line load and spot weld electrode diameter can be seen below.

Equation 13 shows the calculation used to determine the pitch spacing and consequently the width over which the applied load is divided to produce the line load lap shear value for the spot welded joints.

(14 x t) + 3 = spot weld pitch, centre to centre (mm)

where: t = sheet thickness

Equation 13 **Resistance spot welded pitch spacing equation based on sheet thickness[4]**

Equation 14 is used to calculate the electrode diameter used to produce the comparative spot welded lap shear properties

5 x ($\sqrt{}$ t) = electrode diameter

where: t = sheet thickness

Equation 14 **Resistance spot welded electrode diameter equation based on sheet thickness[4]**

5.7.1 Similar Metal Laser Welded Lap Shear Property Comparisons

The following graph shows the similar metal lap shear property comparisons between laser-welded lap joints and Marples' resistance spot welded lap joints[4].

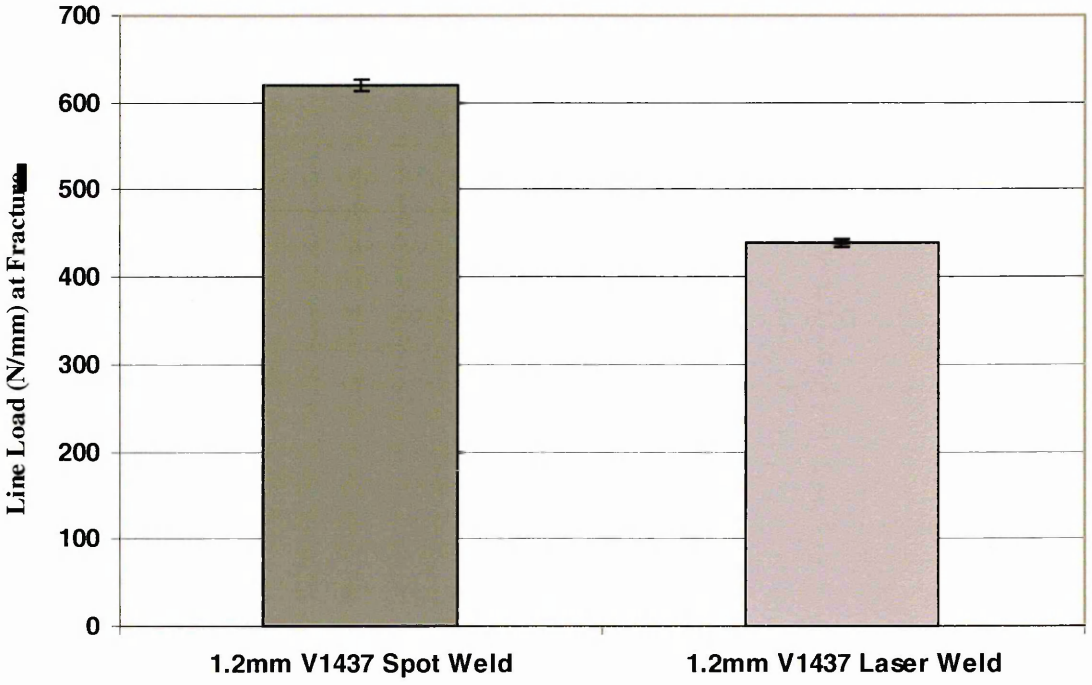

Graph 52 Lap shear line load (at fracture) comparison between 1.2mm V1437 spot and laser welded lap joint

The calculated pitch distance between the spot welds was 19.8mm with a nugget diameter of 6mm.

Thus, the graph shows that the 1.2mm V1437 spot welded joint is capable of withstanding a higher applied load per unit length than the 1.2mm V1437 laser welded lap joint. The mode of failure for the spot welded joint was by nugget pull out, which is the preferred mode of failure and denotes a high quality spot weld.

The following graph shows the similar metal lap shear property comparisons between laser-welded lap joints and Wray's resistance spot welded lap joints[72].

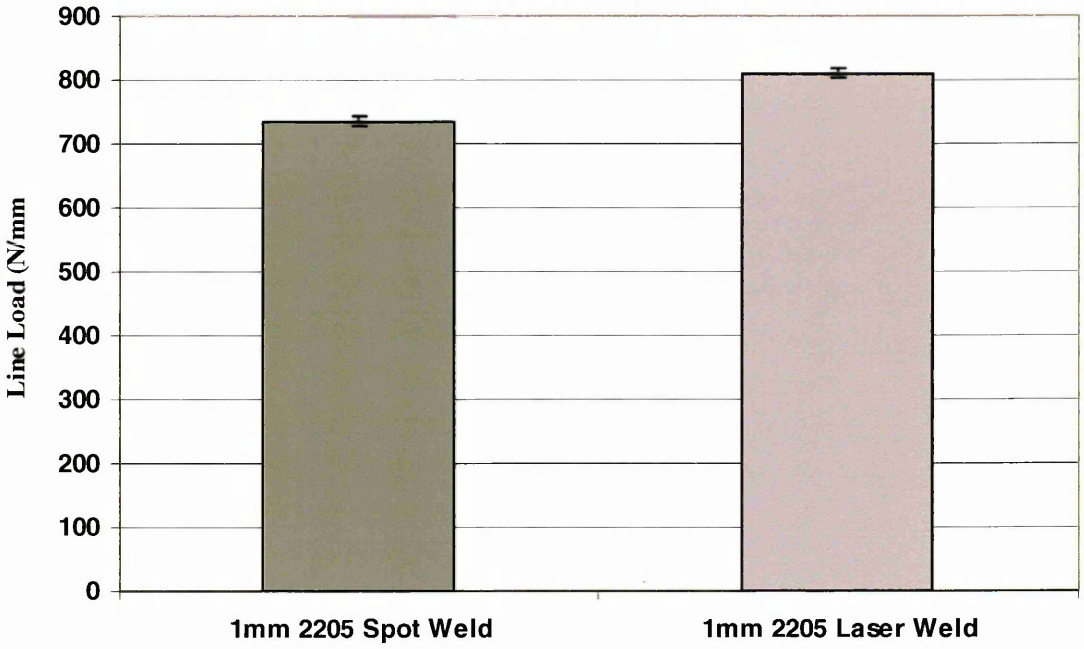

Graph 53 Lap shear line load (at fracture) comparison between 1mm 2205 spot and laser welded lap joint

The calculated pitch distance between the spot welds was 17mm with a nugget diameter of 5mm. Thus, the graph shows that the 1mm 2205 laser weld is capable of withstanding a higher applied load per unit length than the 1mm 2205 spot weld. Again, the mode of failure for the spot welded joint was by nugget pull out, which is the preferred mode of failure and denotes a high quality spot weld.

Graph 54, below, shows the 1mm 2101 laser welded lap shear properties compared with Wray's 1mm 2101 spot welded joint[72].

Graph 54 Lap shear line load comparison between 1mm 2101 spot and laser welded lap joint

The calculated pitch distance between the spot welds was 17mm with a nugget diameter of 5mm. Thus, the graph shows that the 1mm 2101 laser weld is capable of withstanding a similar load per unit length than the 1mm 2101 spot weld when the scatter is taken into account (+/-1%).

The mode of failure for the spot welded joint was by nugget pull out, which is the preferred mode of failure and denotes a high quality spot weld.

This further encouraged the use of the line load range to present the fatigue curves due to the problems of selecting a relevant cross-sectional area over which to calculate the stress.

As can be seen from Graph 27, the statistically valid mean fatigue line load range ($2x10^6$ cycles) for the 1mm 304 (top) – 1.2mm V1437 laser welded lap joint was 60.3 N/mm with a standard deviation of 3.4 N/mm.

The 1.2mm V1437 (top) – 1mm 304 laser welded lap joint and 1.2mm V1437 (top) – 0.78mm 2205 laser welded lap joint mean fatigue line load ranges ($2x10^6$ cycles) were 71.1 N/mm with a standard deviation of 4.6 N/mm and 66.9 N/mm with a standard deviation of 3.1 N/mm (shown in Graph 28 and Graph 30 respectively). Both these staircases were statistically valid.

One staircase, however, was not statistically valid, see Graph 29. The 0.78mm 2205 (top) – 1.2mm V1437 laser welded lap joint mean fatigue line load range ($2x10^6$ cycles) was 58.1 N/mm with a standard deviation of 6.3 N/mm. This was attributed to the introduction of an inconsistent gap between the sheets along the length of the weld. The Trumpf 5kW CO_2 laser welder used a hydraulic press to intimately clamp the sheets during the laser welding process. Observations of the joint configuration, for alignment, prior to laser welding showed the 0.78mm sheet on top of the lap joint deflecting slightly with the applied force of the press. This produced a slight inconsistent gap between the sheets which, in turn, reduced the weld width between the sheets which produced an increase in the scatter of the fatigue results and ultimately prevented the statistical validity of the staircase. A schematic diagram illustrating this effect can be seen in Figure 58.

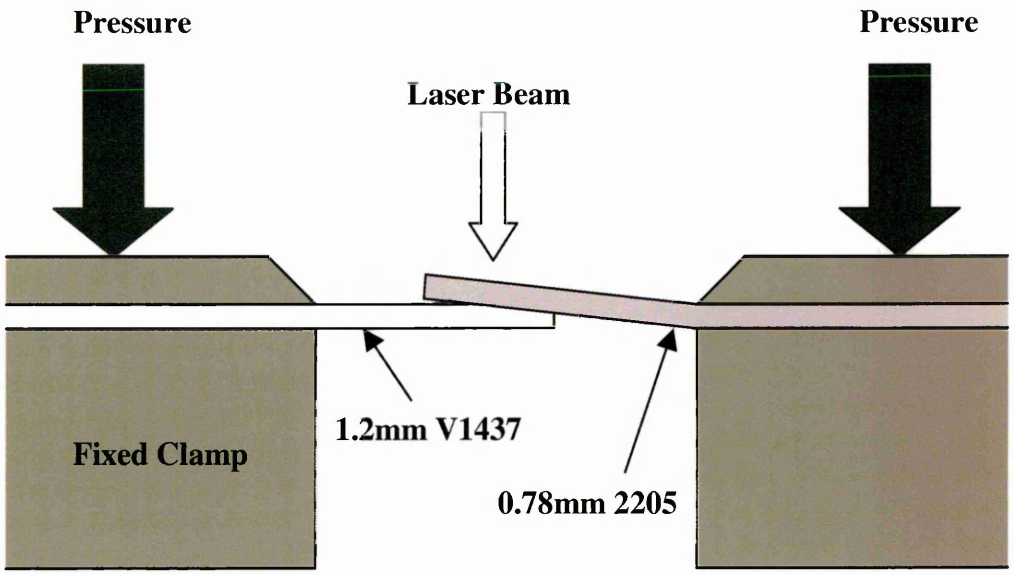

Figure 58 Schematic showing deflection and introduction of a gap in the 0.78mm 2205 (top) – 1.2mm V1437 lap joint

It can be seen that slight deflection of the 0.78mm 2205 occurred during the production of the laser welds. As well as affecting the statistical validity of the staircase, the reduced weld width and introduction of a gap between the sheets reduced the fatigue properties of the joint. Thus, it can be seen that this joint configuration achieved the lowest fatigue properties of the four dissimilar metal lap joints produced using the Trumpf 5kW CO_2 laser welder.

The following graphs compare the effects of joint configuration and weld width on the fatigue properties of the four dissimilar metal laser welded lap joints produced using the Trumpf 5kW CO_2 laser welder. It should be noted that only the failures were used in the generation of the following comparative graphs as this allowed a more accurate trend line to be inserted for ease of comparison.

The following graph shows the effect of joint configuration and weld width on the fatigue properties of the 1.2mm V1437 – 1mm 304 dissimilar metal lap joints.

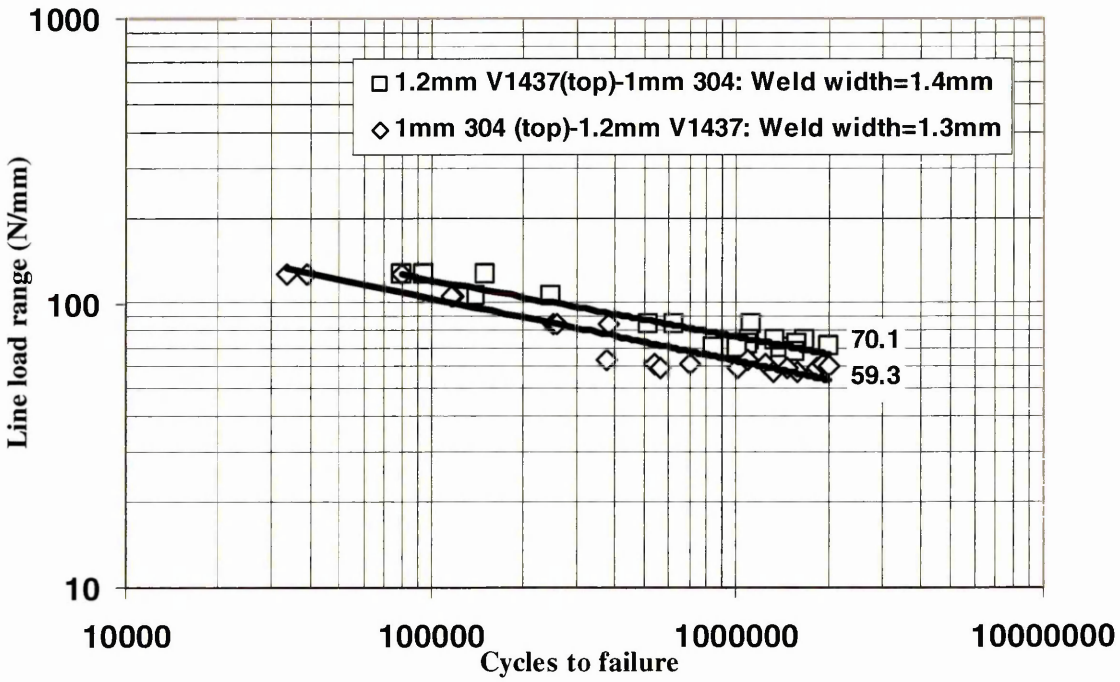

Graph 55 Joint configuration fatigue comparison for 1.2mm V1437 – 1mm 304 dissimilar metal lap joints

The mean fatigue line load ranges were 70.1 N/mm for the 1.2mm V1437 (top) – 1mm 304 and 59.3 N/mm for the 1mm 304 (top) – 1.2mm V1437. Thus, it can be seen that slightly higher fatigue properties were achieved when the 1.2mm V1437 was at the top of the lap joint. It is interesting to note the laser weld widths between the sheets for the corresponding lap joints, see Table 20. A weld width of 1.4mm was determined for the 1.2mm V1437 (top) – 1mm 304 and 1.3mm for the 1mm 304 (top) – 1.2mm V1437 lap joint. It would appear that increasing the weld width between the sheets increases the fatigue properties of the joint.

A similar trend can be seen in the following graph for the 1.2mm V1437 – 0.78mm 2205 lap joint fatigue comparison.

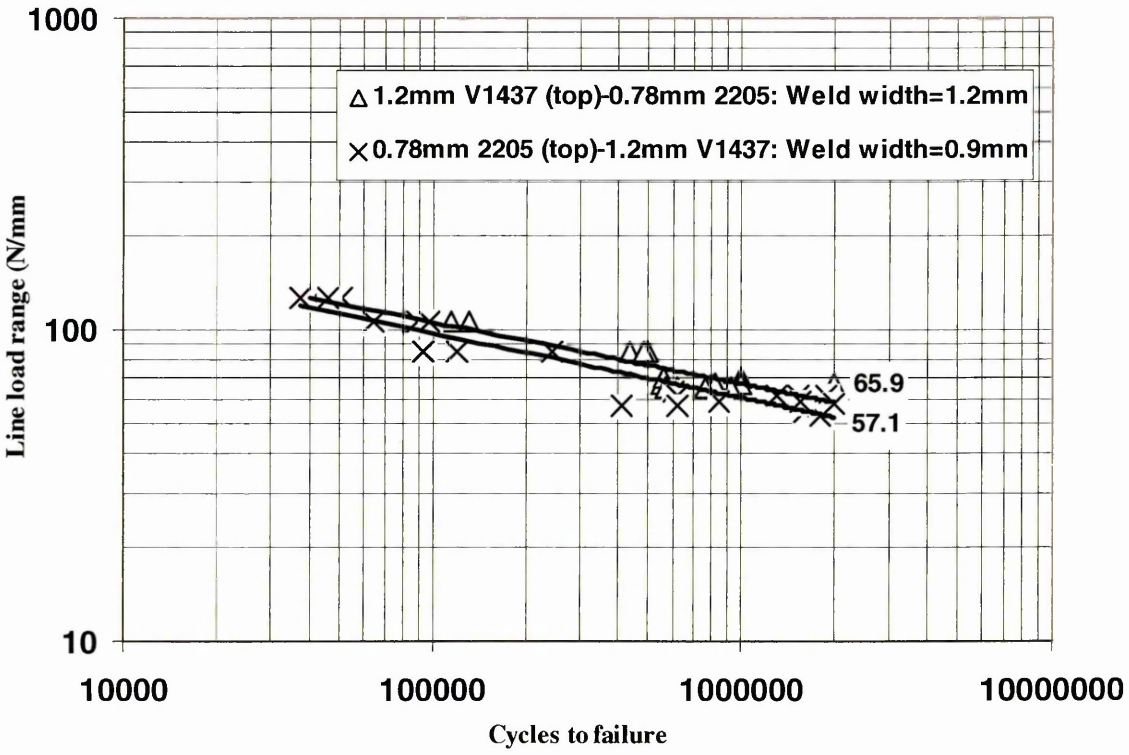

Graph 56 Joint configuration fatigue comparison for 1.2mm V1437 – 0.78mm 2205 dissimilar metal lap joints

The mean fatigue line load ranges were 65.9 N/mm for the 1.2mm V1437 (top) – 0.78mm 2205 and 57.1 N/mm for the 0.78mm 2205 (top) – 1.2mm V1437. Thus, it can be seen that higher fatigue properties were achieved when the 1.2mm V1437 was at the top of the lap joint. The laser weld widths between the sheets for the corresponding lap joints can be seen in Table 20. A weld width of 1.2mm was determined for the 1.2mm V1437 (top) – 0.78mm 2205 and 0.9mm for the 0.78mm 2205 (top) – 1.2mm V1437 lap joint.

This corroborates research carried out by Linder et al and results presented by Kaitanov for similar metal laser welded lap joints, who discovered that increasing the weld width increased the fatigue properties[70],[87].

It should be noted that a higher weld width was achieved when the 1.2mm V1437 was at the top of the lap joint. This was observed for both sets of dissimilar metal lap joints produced, however, the welding parameters (welding power and speed) were the same for each joint configuration.

Hence, analysis of the four dissimilar metal lap joints produced using the Trumpf 5kW CO_2 laser welder presented the following questions:

- Why were wider laser weld widths achieved when the 1.2mm V1437 was at the top of lap joint for both sets of dissimilar metal lap joints for the same welding parameters?
- Why did the lap joints with the wider weld width possess higher fatigue properties?

For these reasons, an investigation was conducted using the following tests and techniques to determine the factors affecting dissimilar metal lap joint fatigue strength.

- Laser weld microhardness
- Weld bead composition
- Lap joint rotation

The effects of each will now be discussed.

[87] Kaitanov, A. Comparable investigation of fatigue strength of laser welded overlap joints with full or controlled penetration, ASAB research foundation report, 97.1-5

5.9 Factors Affecting Laser Welded Lap Joint Fatigue Strength

As previously stated, the following areas were investigated to determine the effects of the laser welding parameters and joint configuration on the properties of laser welded butt and lap joints, the aim being to determine the factors affecting laser welded lap joint fatigue properties.

5.9.1 Weld Bead Microhardness

As explained in section 3.5.2, microhardness grids in 0.25mm increments were produced across a transverse section of the laser weld bead. The microhardness grids not only show the distribution of hardness across the weld bead, but indicate the weld bead shape and thus, can also be used to analyse the effects of the laser welding parameters, specifically welding speed, on the size and shape of the laser weld produced.

5.9.1.1 Dissimilar Metal Butt Joint Laser Weld Microhardness

Graph 36 to Graph 38 show the effects of three laser welding speeds, (4m/min, 3.5m/min and 3m/min) on the shape and microhardness of 1.2mm V1437 – 1mm 304 dissimilar metal laser welded butt joints.

Analysis of the three graphs showed that decreasing the welding speed from 4 m/min to 3m/min reduced the microhardness of the weld bead to <400Hv. This may improve the formability of the laser weld in, for example, the production of a composite blank where forming is carried out after welding, see Figure 2.

There is also a distinct change in the weld bead shape as the welding speed is reduced. This is attributed to the thermal properties of the dissimilar metals. As can be seen from Table 2, the thermal conductivity of mild steel is much greater than that of the three stainless steels. This allows the heat input from the laser welder to be more readily

dissipated in the mild steel than in the respective stainless steel grades, which tend to contain the heat input. This results in a laser weld bead whose geometry changes abrupt on the stainless steel side of the butt joint. As the welding speed is reduced, this effect is reduced and the weld bead shape becomes much more uniform. As well as comparing the microhardness plots this effect can also be seen in the three secondary electron images of the laser welds produced with the respective welding speeds. This serves to validate the method of weld bead shape analysis through the use of a microhardness grid.

Parameter set 1 (4m/min): 1mm 304 – 1.2mm V1437

1mm 304

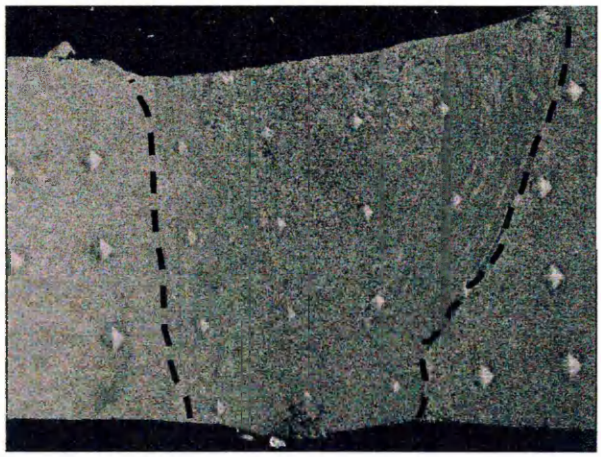

1.2mm V1437

Image 5 Secondary electron image from parameter set 1: 1mm 304 – 1.2mm V1437 butt joint

Parameter set 2 (3.5m/min): 1mm 304 – 1.2mm V1437

1mm 304

1.2mm V1437

Image 8 Secondary electron image from parameter set 2: 1mm 304 – 1.2mm V1437 butt joint

Parameter set 3 (3m/min): 1mm 304 – 1.2mm V1437

1mm 304

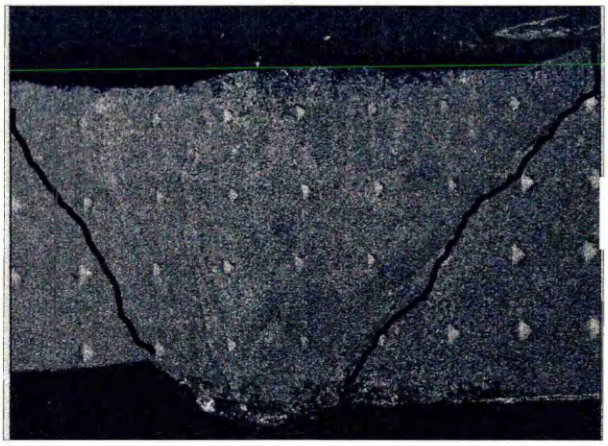

1.2mm V1437

Image 11 Secondary electron image from parameter set 3: 1mm 304 – 1.2mm V1437 butt joint

A similar trend can be seen for the 1mm 2205 – 1.2mm V1437 dissimilar metal butt joints in Graph 39 to Graph 41. The same three welding speeds were used (4m/min, 3.5m/min and 3m/min) and similar effects on the microhardness of the weld bead can be seen. With a welding speed of 3m/min, the laser weld bead possessed more areas with lower hardness than the welds produced at the increased laser welding speeds.

The shapes of the laser welds also follow the findings from the 1.2mm V1437 – 1mm 304 dissimilar metal butt joints, a welding speed of 4m/min producing a non-uniform weld bead due to the differences in the thermal conductivity of the mild steel and duplex stainless steel.

Thus, welding parameters can be used to control the hardness of laser weld beads and overcome the effects caused by the differing thermal properties of dissimilar metal laser welded butt joints to produce welds with a uniform appearance.

It should be noted that no change in tensile properties was seen for the laser welds produced at the three welding speeds with failure occurring in the parent material of the mild steel.

5.9.1.2 Dissimilar Metal Lap Joint Laser Weld Microhardness

Graph 42 and Graph 43 show the distribution of microhardness in the 1mm 304 – 1.2mm V1437 (both configurations) lap joints. It can be seen that both laser weld beads contain areas with microhardness >400 Hv and softer areas in the range of 350 – 400Hv.

A similar effect can be seen in the distribution of microhardness in the 0.78mm 2205 – 1.2mm V1437 lap joints (both configurations) shown in Graph 44 and Graph 45. There is, however, an area in the 1.2mm V1437 (top) – 0.78mm 2205 weld which achieved in excess of 450Hv. It would seem likely that this is due to the higher cooling rates associated at the bottom of the lap joint during the laser welding process.

The most important comparison that can be made between the graphs is of the microhardness of the material at the internal lap face. Because these values are similar, one could propose that tensile properties would also be comparable and thus have similar fatigue crack initiation susceptibility. This will be discussed in more detail in section 5.9.4.

Another comparison that can be made between the two sets of graphs is in the shape of the laser weld bead. It can be seen that the laser weld bead produced with the 1mm 304 on the top of the lap joint is non-uniform with a narrow penetration into the 1.2mm V1437 being achieved. The laser weld bead produced with the 1.2mm V1437 on the top, in comparison, is more uniform with a greater penetration width into the 1mm 304 being achieved.

The weld bead shapes produced using the 0.78mm 2205 show the same trend. A more uniform weld bead is achieved when the 1.2mm V1437 is at the top of the lap joint, with a greater penetration width into the lower sheet being achieved. In comparison, a non-uniform weld bead is produced when the 0.78mm 2205 is at the top of the lap joint, resulting in narrow penetration into the 1.2mm 1437.

This, as explained in section 5.9.1.1, is due to the thermal properties of the mild steel and respective stainless steel.

When the stainless steel grade is at the top of the lap joint, the lower thermal conductivity, which is approximately half that of the mild steel, results in heat being contained in the stainless steel. As heat is conducted through the stainless steel to the V1437 at the lap joint interface this heat is transferred more readily into the V1437 away from the lap joint interface producing a thin penetration into the V1437. This heat transfer situation can be seen in the following schematic diagram.

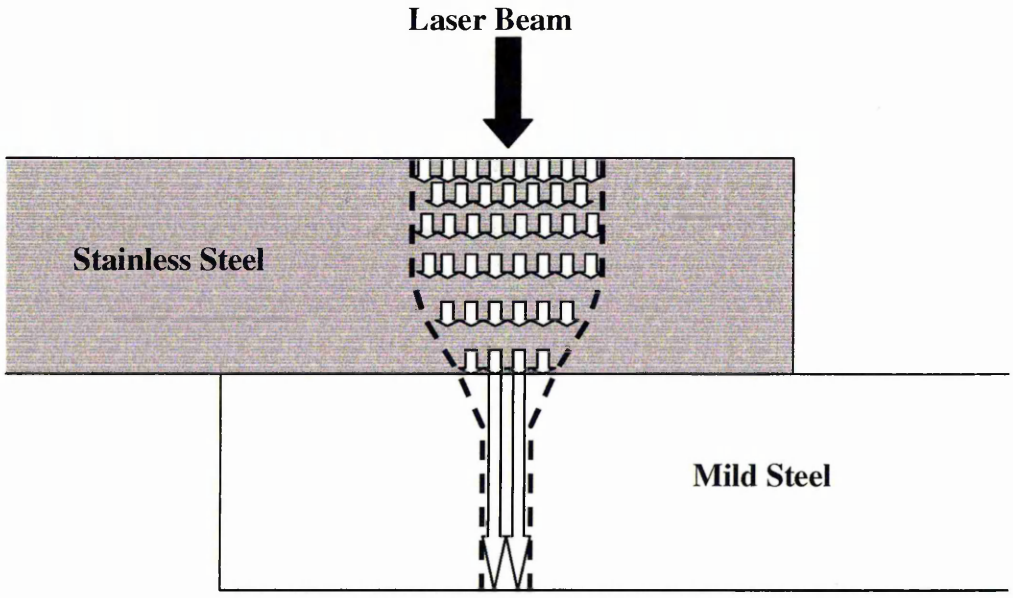

Figure 59 Schematic diagram showing weld bead formed due to base material thermal property differences – stainless steel on the top of the lap joint

Image 47 below shows the weld bead shape for 1mm 304 (top) - 1.2mm V1437.

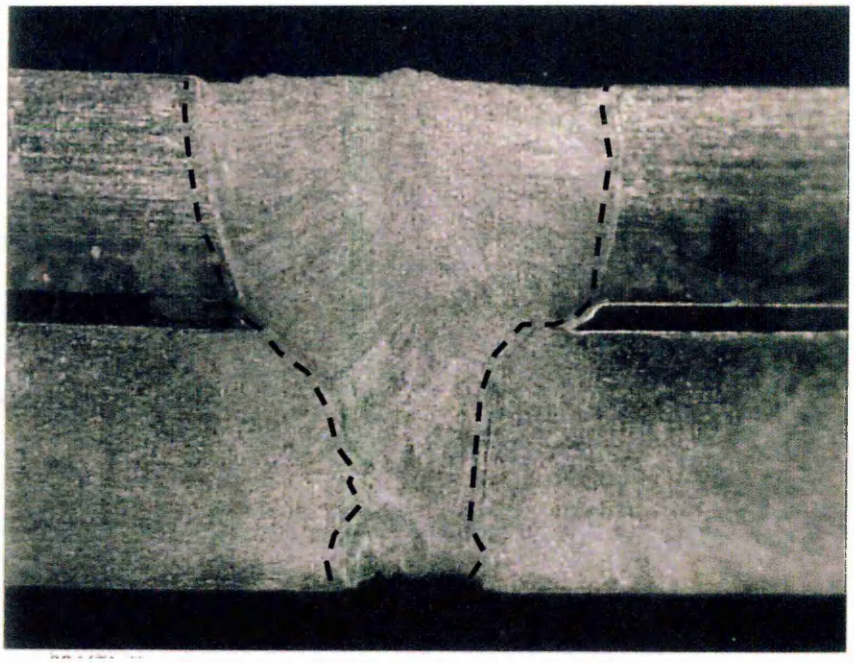

Image 47 Weld bead shape obtained when the 1mm 304 stainless steel is at the top of the lap joint

In comparison, when the 1.2mm V1437 is at the top of the lap joint, the heat is transferred readily through the material to the internal lap face. The heat is then transferred through the stainless steel at a lower rate, thus producing a wider weld penetration into the stainless steel. This is illustrated in the simple heat transfer schematic diagram seen below.

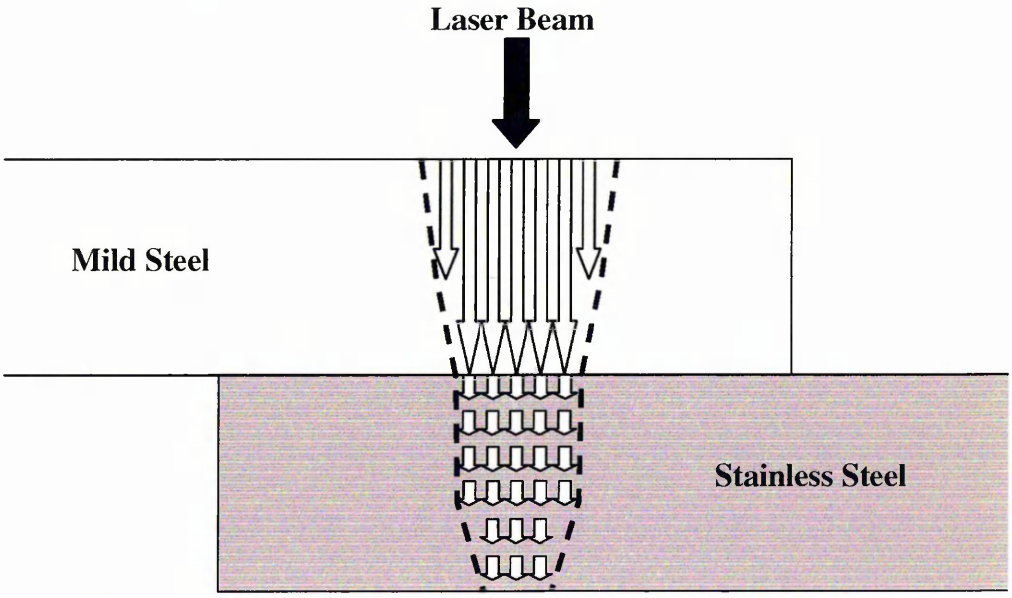

Figure 60 Schematic diagram showing weld bead formed due to base material thermal property differences – mild steel on the top of the lap joint

Image 48 shows the weld bead shape for 1.2mm V1437 (top) - 0.78mm 2205

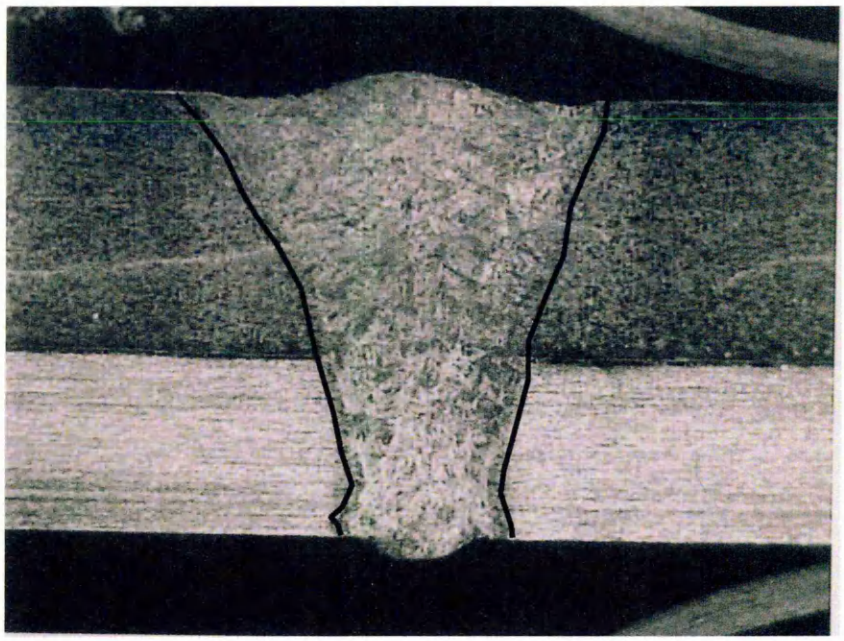

Image 48 Weld bead shape obtained when the 1.2mm V1437 is at the top of the lap joint

This explains why wider weld widths were seen when the 1.2mm V1437 was at the top of the lap joint for the same welding parameters compared to when the respective stainless steel was at the top of the lap joint.

5.9.2 Weld Bead Compositions

5.9.2.1 Butt Joint Weld Bead Compositions

Due to the low general heat input (high specific heat input) of the laser welding process, very high cooling rates are achieved. These high cooling rates do not provide sufficient time for the weld bead to become homogenous. Research conducted by Lampa et al[19], showed that 'stirring' of the laser weld occurs due to the effects of thermo-capillary flow (Marangoni convection) with surface velocities in the order of 1m/s. The driving forces for thermo-capillary flow in laser weld pools being described by two phenomena[88].

1. Surface tension flow
2. Buoyancy force

---

[88] Wang, Y.H. Kou, S Driving Forces for Convection in Weld Pools. Proceedings of the international Conference on Trends in Welding Research. May 18-22, 1986, Galinburg, TE, USA, pp. 65-69..

This stirring mechanism is produced by the temporal heat distribution within the laser weld bead, which produces surface tension driven flow and buoyancy flow. The material at the edges of the weld bead posses the lowest temperature as they are cooled by the surrounding parent material, while the highest temperature is at the centre of the weld bead.

This can be seen in Figure 61, which shows the temperature distribution on a 304 stainless steel surface heated with a laser beam with a Gaussian beam distribution[24].

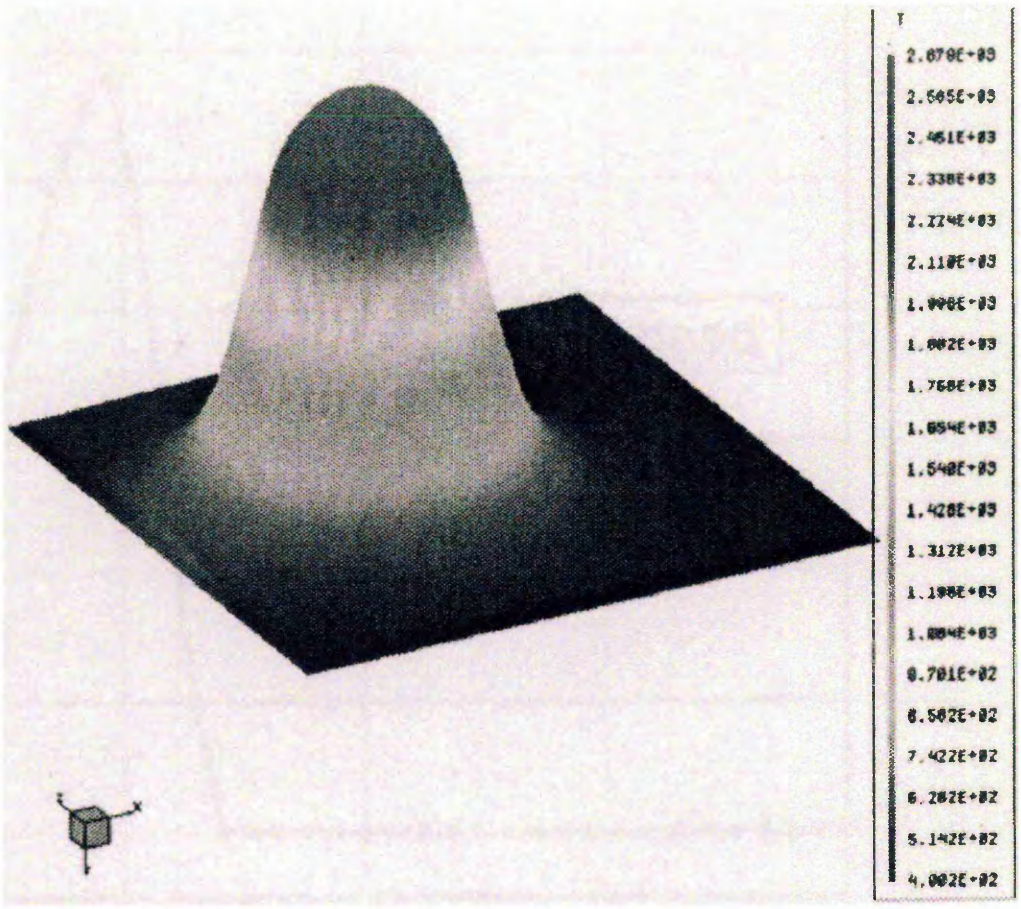

Figure 61 Temperature distribution on the surface of 304 stainless steel produced by a laser beam with a gausssian distribution[24]

In the same way, the heat distribution across the transverse section of a similar metal laser welded butt joint can be seen in Figure 62. Due to the lack of surface active agents such as sulphur and oxygen, which can reverse flow direction, the surface tension driven flow is from the centre to the edges of the laser weld bead.

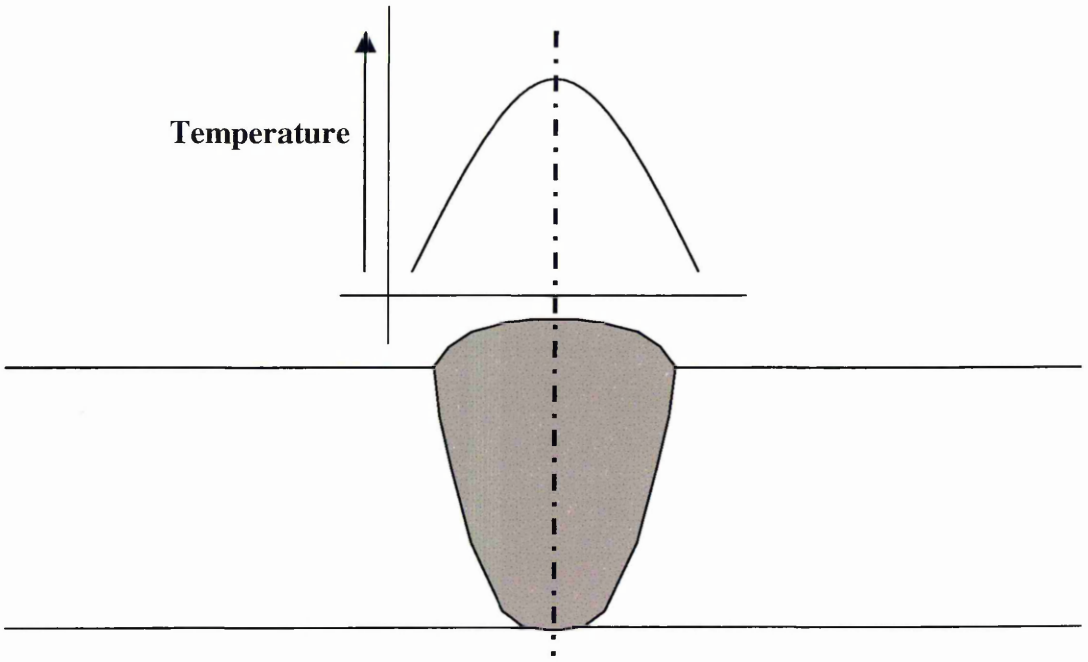

Figure 62 Heat distribution across the transverse section of a laser welded butt joint

The combined effect of the surface tension and buoyancy forces cause the cooler, more dense, molten weld metal at the edges of the weld bead to flow downward, whilst the hotter, less dense, molten weld metal in the centre of the weld bead flows upwards producing a stirring mechanism. This, in conjunction with the high cooling rate, owing to the high specific heat input of the laser welding process, results in a weld bead with a very inhomogeneous composition.

This effect can be seen clearly in the composition maps for chromium and nickel for the dissimilar metal butt joints and appears to become more pronounced at the lower welding speeds. This is due to the greater quantity of stainless steel being melted, as seen from the more uniform weld bead shape produced at the lower welding speeds, although the cooling rate is still sufficiently high to prevent homogeneity.

Comparison of the range of predicted weld microstructure reveals the extent that welding speed has on the relative amounts of both parent materials melted which forms

the weld bead. The following figures show the effects of welding speed on the predicted compositions of the dissimilar metal laser welded butt joint weld beads

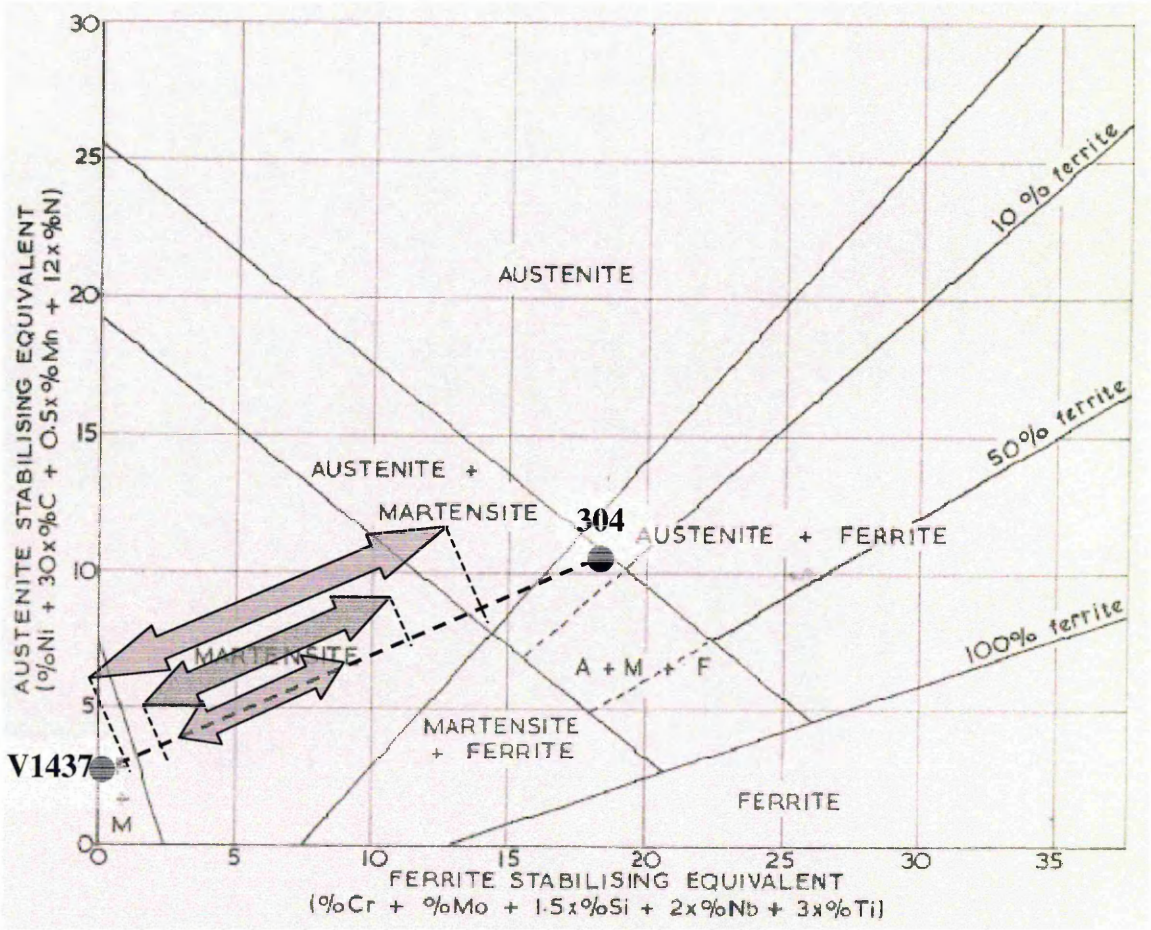

Figure 63 Effect of welding speed on the dilution and predicted weld bead compositions-1mm 304 – 1.2mm V1437 butt joint

The three arrows on Figure 63 denote the range of composition found in each 1mm 304 – 1.2mm V1437 butt joint weld bead. The smallest arrow denotes the 4m/min butt weld speed, with 3.5m/min and 3m/min represented by the middle and largest arrows respectively.

This shows that decreasing the laser welding speed increases the range of compositions present in the laser weld bead, demonstrated by the increase in arrow size on the graph. The weld beads remain inhomogeneous at the lower welding speeds due to the high solidification rate of the laser welding process (low general heat input). It can be seen that at the lowest welding speed of 3m/min, the largest amount of stainless steel is

melted, producing areas within the weld bead which contain up to 13 % chromium and 6% nickel.

Similarly, reducing the welding speed produced areas within the weld bead with a composition near the base material of the 1.2mm V1437. This corroborates the observation made in section 5.9.1.1, which shows that the shape of the weld bead becomes more uniform at lower welding speeds, with an increased weld bead penetration into the stainless steel. Thus, decreasing the welding speed increases the chromium and nickel contents found in the laser weld beads. This is also illustrated in the chromium and nickel butt weld content graphs which show net percentage increases in both chromium and nickel as the welding speed decreases.

Graph 78 and Graph 79 show the percentage of chromium and nickel in the weld bead for the 1mm 304 – 1.2mm V1437 butt joint produced at 3m/min. These graphs when compared to their respective speed maps for chromium and nickel (Image 57 and Image 58 respectively) show the effects of the stirring mechanism. A high chromium and nickel content flow can be seen moving down at the weld bead-304 stainless steel interface (more dense) and flowing upwards at the centre of the weld bead (less dense).

The interesting point noted from this investigation is that reducing the welding speed does not increase the homogeneity of the laser weld bead. In contrast, reducing the welding speed produces a more pronounced range of compositions in the dissimilar metal butt weld bead, with small predicted areas of martensite + austenite in the weld bead for the 3m/min butt joint; however none was observed. The higher welding speeds (3.5m/min and 4m/min) producing a fully martensitic weld.

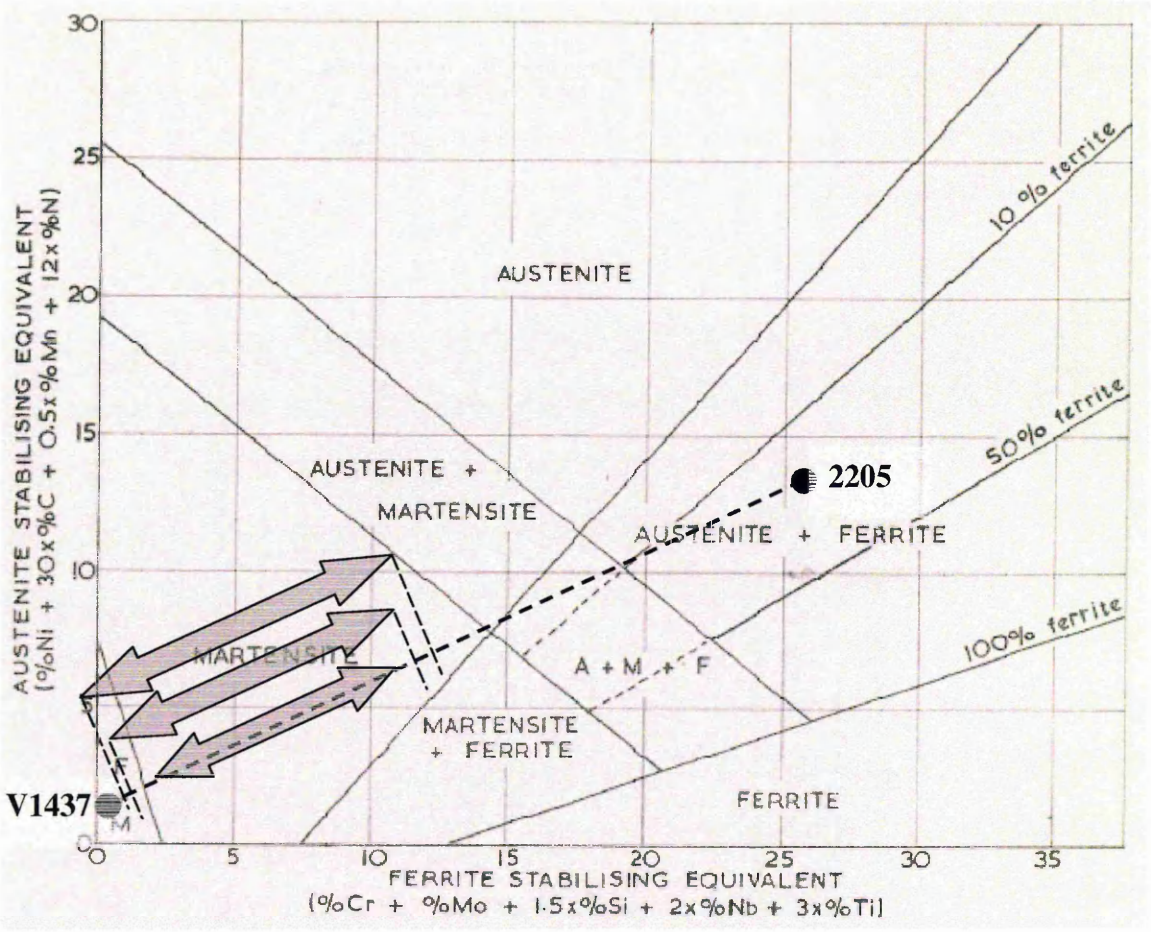

Figure 64 Effect of welding speed on the dilution and predicted weld bead compositions-0.78mm 2205 – 1.2mm V1437 butt joint

A similar trend can be seen with the 0.78mm 2205 – 1.2mm V1437 butt welds produced at the three laser-welding speeds. Again, the larger arrows correspond to the slower welding speeds which result in an increase in the range of compositions found in the weld bead. There is however, little effect on the predicted phase of the laser weld bead which is martensite, corroborated by the high weld bead microhardness >400Hv.

It should be noted that the increase in the range of butt weld bead composition had no affect on the tensile properties of the dissimilar metal butt joints, as failure occurred in the parent material of the 1.2mm V1437.

5.9.2.2 Lap Joint Weld Bead Compositions

The stirring mechanism that occurs in the laser welded lap joint weld bead is the same as the butt weld bead stirring mechanism. This stirring mechanism is produced by the thermo-capillary flow (Marangoni convection) within the laser weld bead. The material at the edges of the weld bead posses the lowest temperature as they are cooled by the surrounding parent material, whilst the highest temperature is at the centre of the weld bead. The heat distribution across the transverse section of a similar metal laser welded lap joint can be seen in Figure 65 below.

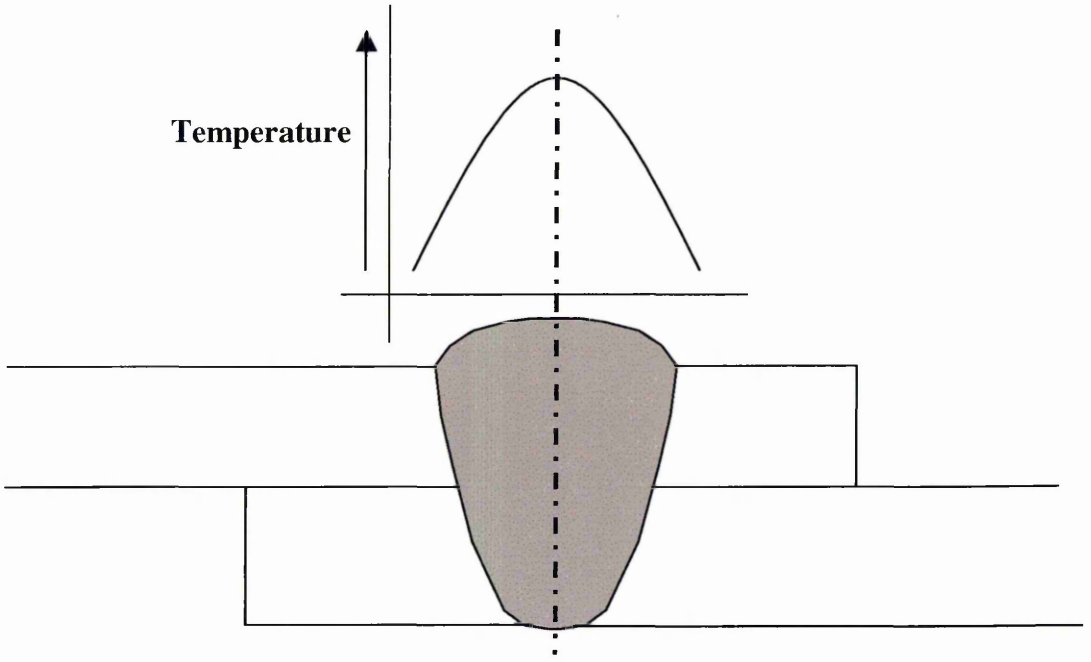

Figure 65 Heat distribution across the transverse section of a laser welded butt joint

The joint configuration does not affect the stirring mechanism, although it does control the quantity of the stainless steel and mild steel melted.

This is due to the thermal properties of the mild steel and respective stainless steel and the position within the lap joint configuration (top of the lap joint). As mentioned in section 5.9.1.2, a more uniform weld bead is achieved when the 1.2mm V1437 is at the top of the lap joint. Hence, a greater proportion of the material at the top of the lap joint is melted in comparison to the material at the bottom of the lap joint.

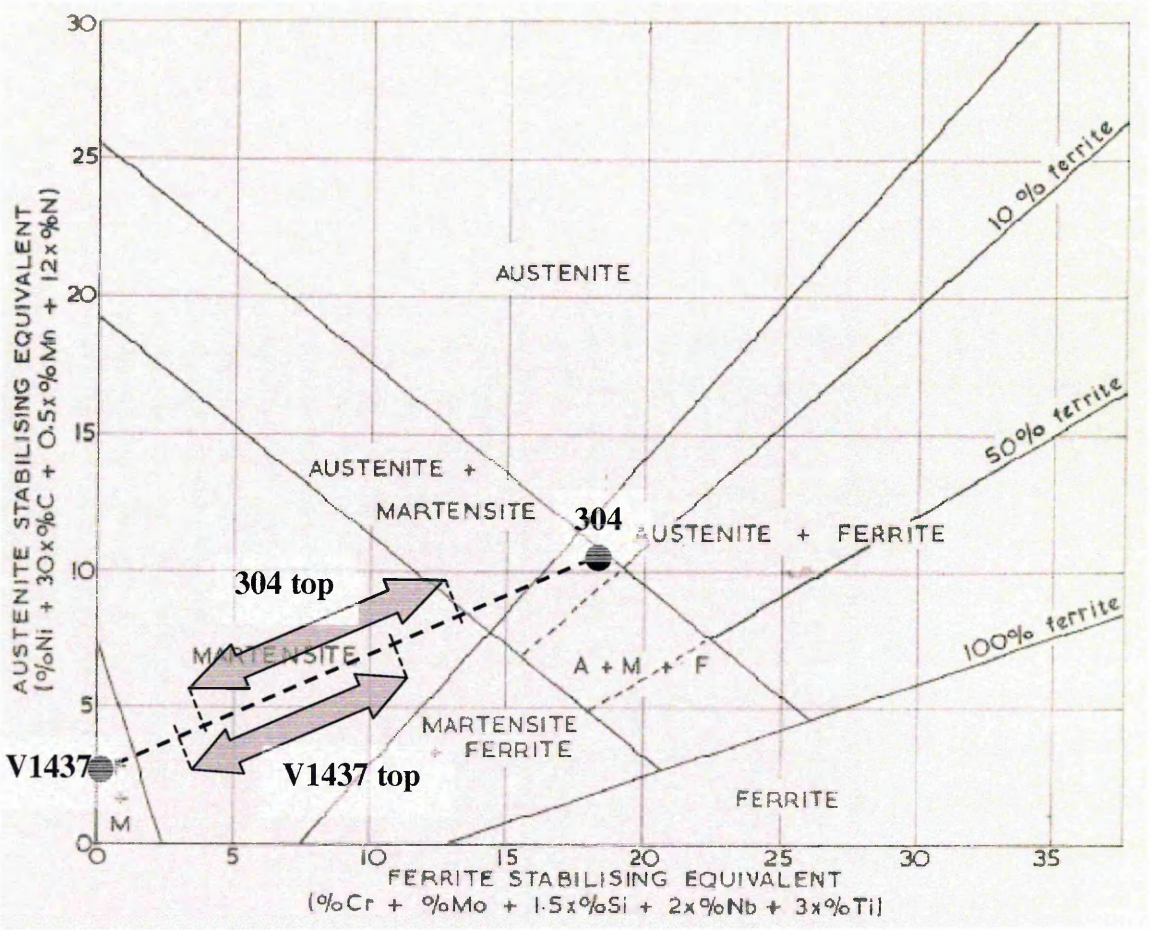

Figure 66 Effect of joint configuration on the dilution and predicted weld bead compositions-1mm 304 – 1.2mm V1437 lap joint

It can be seen from Figure 66 that the range of composition within the weld bead increases when the 1mm 304 is at the top of the lap joint. The range is also displaced towards the 304 base material composition. It can be seen that when 1.2mm V1437 is at the top of the lap joint, the range of composition within the weld bead is displaced towards the 1.2mm V1437 base material composition. This effect can also be seen from Graph 48, Graph 49 and Graph 86, Graph 87; which show that lower chromium and nickel contents were found in the weld bead when the 1.2mm V1437 was at the top of the lap joint. Although a range of chromium and nickel has been found in the weld bead (see Graph 48, Graph 49 and Graph 86, Graph 87); the predicted weld bead phase is martensite. This would explain the high microhardness of the laser weld beads, all of which were in excess of 400Hv, see section 4.10.

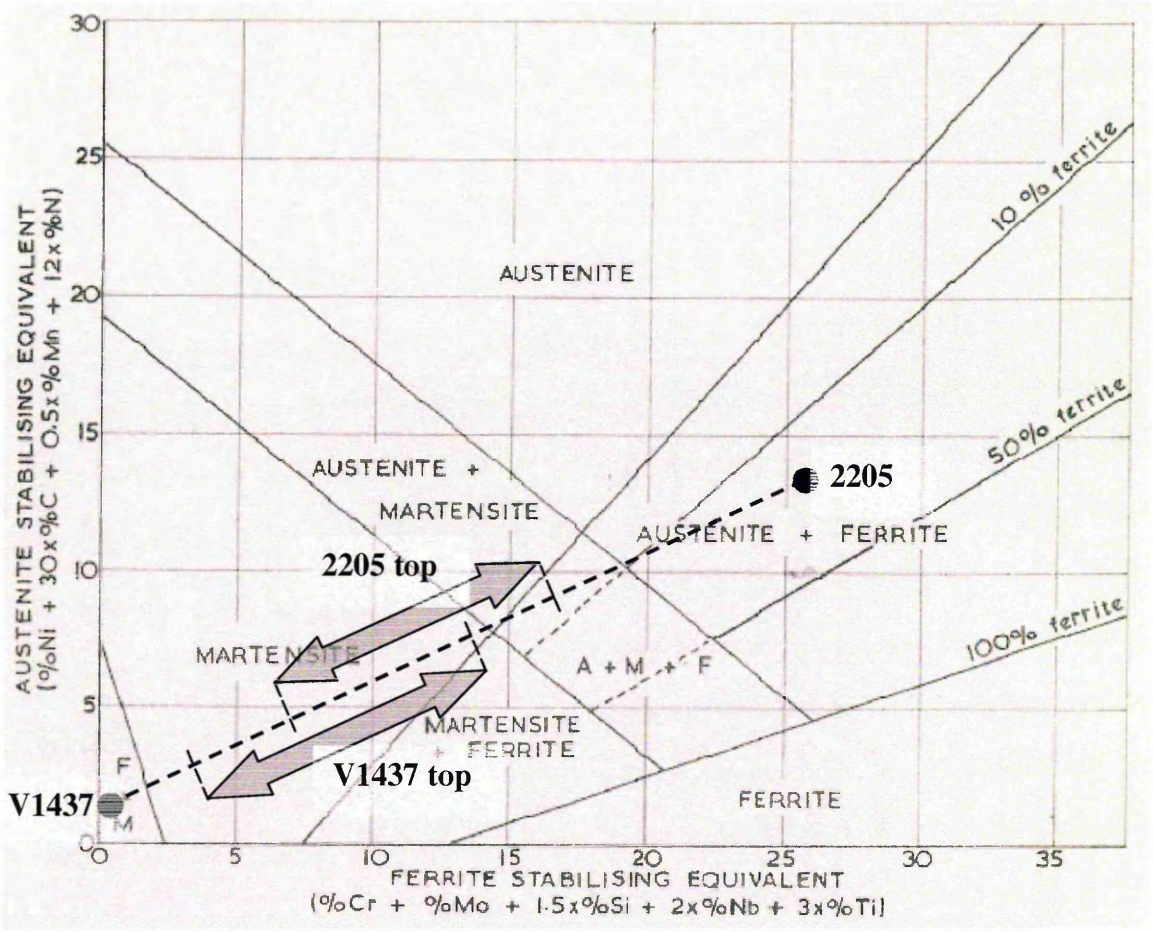

Figure 67 Effect of joint configuration on the dilution and predicted weld bead compositions-0.78mm 2205 – 1.2mm V1437 lap joint

Figure 67 shows that the range of weld composition is displaced towards the 2205 base material point when the 2205 is at the top of the lap joint. It can be seen that when 1.2mm V1437 is at the top of the lap joint, the range of composition within the weld bead is displaced towards the 1.2mm V1437 base material. This effect can also be seen from Graph 88 to Graph 91, which show that lower chromium and nickel contents were found in the weld bead when the 1.2mm V1437 was at the top of the lap joint.

Although a range of chromium and nickel is found in the weld bead (see Graph 88 to Graph 91), the predicted weld bead phase is martensite. This would explain the high microhardness of the laser weld beads, all of which were in excess of 400Hv; see section 4.10.

From the extensive investigation into the composition, dilution and consequently the predicted phases present in the laser welded butt and lap joint weld beads, no evidence was found that these factors had a controlling effect on the tensile, lap shear and ultimately the fatigue properties of the respective joints.

The only fatigue-controlling factor was the microhardness of the material at the internal lap faces of the joints. All were similar within a particular joint, suggesting that the tensile properties and also the fatigue crack initiation and early crack growth rates would be comparable. The bulk microhardness was not found to be a lap shear or fatigue controlling factor.

Tests were conducted to determine the primary solidification mode of the dissimilar metal joints containing 1mm 304 austenitic stainless steel. Although, the Cr_{eq}/Ni_{eq} ratios were in the range of 1.4 – 1.6, a pronounced increase in the Fe content due to the dilution of the two compositions strengthened the ferrite primary solidification phase. This was the preferred primary phase as this mode of solidification has a superior resistance to solidification cracking than primary austenite, which is attributed to reduced wetting of boundaries by liquid films and the complicated crack paths these boundaries form[49], see section 2.12.1.

The investigation, hence, proceeded into the geometric factors introduced by the lap joint welding configuration to determine if this had an effect on dissimilar metal lap joint fatigue properties.

5.9.3 Stages of Laser Welded Lap Joint Fatigue Life

Discussion of the "effect of geometry" on the fatigue life of a laser welded lap joint is complicated by the lack of uniform definitions of fatigue crack initiation, the stages of fatigue crack propagation, and fatigue failure. Research carried out by Wang et al divided the fatigue life of a tensile-shear spot welded lap joint into three stages[89].

Stage *I* – Crack initiation and early crack growth

At the end of Stage *I*, a detectable crack or a crack of some agreed (small) size is present at the periphery of the weld nugget[89].

Stage *II* – Crack propagation from the periphery of the nugget through the thickness of the sheet to its external surface

Early growth proceeds initially at an angle of 66Deg, but ultimately the growth during this period is nearly perpendicular to the sheet so that the sheet thickness is roughly equal to the crack length at the end of Stage *II*[89].

Stage *III* – Crack propagation laterally across the specimen width until failure occurs through plastic instability (tearing or rupture)[89].

With this in mind, the proposed stages of fatigue life for a laser welded lap joint are:

Stage *I* – Initiation and early crack growth (multiple crack)

Stage *II* – Crack propagation (multiple crack)

Stage *III* – Failure due to plastic instability and separation through tearing and rupture of the remaining material.

The proposed stages of laser welded lap joint fatigue life can be linked with the test conducted by Linder et al from section 2.16.1.1, which assessed the stiffness of a similar metal laser welded lap joint during its fatigue life. Figure 33 shows that the lap

[89] Wang, P.C., Corten, H.T., and Lawerence, F.V. A Fatigue Life Prediction Method for Tensile-Shear Spot Welds, "SAE Technical Paper 850370, Society of Automotive Engineers, Warrendale, PA 1985

joint stiffness remained constant throughout the majority of its fatigue life (Stages *I*), falling dramatically prior to failure (Stage *II*).

Stage *I* is concerned with fatigue crack initiation and early crack. Multiple fatigue cracks initiate and early stage crack growth occurs. Multiple initiation sites were first proposed by Linder et al for similar metal laser welded lap joints, see section 5.11. This was observed during the analysis of dissimilar metal lap joint fatigue failures from this investigation (also section 5.11). At the end of Stage *I* fatigue crack growth will have occurred at multiple initiation sites along the length of the weld, however no reduction to the stiffness of the joint will have occurred.

Stage *II* is concerned with crack propagation. At the transition to Stage *II* the multiple fatigue cracks have propagated to the extent where the stiffness of the joint is reduced. The reduction in joint stiffness causes the joint to rotate increasingly under the applied load. This increases the local stresses and consequently the crack growth rate.

Stage *III* is concerned with sheet separation and failure. The transition to Stage *III* occurs when the net cross section can no longer withstand the applied load, plastic instability occurs and the remaining material tears and ruptures until the sheets separate.

This would suggest that the majority of laser welded lap joint fatigue life is concerned with early crack growth (multiple), where no reduction in lap joint stiffness occurs (Stage *I*). Once the multiple fatigue cracks have propagated to the extent where the stiffness is reduced (transition to Stage *II*), failure occurs rapidly through plastic tearing of the remaining material (Stage *III*).

The effect of geometry on the fatigue properties or, more specifically, the early stage crack growth rate (Stage I) can now be discussed.

5.9.4 Effect of Lap Joint Geometry

As stated in section 2.15.2, when lap joints are subjected to a tensile load in either lap shear or fatigue, the misalignment (eccentricity) of the applied load introduced by the lap joint configuration results in rotation of the lap joint, see section 3.4.4.

Linder et al proposed that load misalignment produced an applied bending moment to the joint, which could be explained by analysing the reaction forces and moments that occur in the laser welded lap joint specimen, see section 2.15.2[70,71]. It can be seen from Equation 2 that increasing the sheet thickness, (or average sheet thickness for dissimilar thickness lap joints), will increase the applied bending moment to the joint. The introduction of an interfacial gap between the sheets will also increase the applied bending moment to the joint.

Thus, the result of the misalignment, applied bending moment and consequent joint rotation, is an increase in the local stress at the internal lap surface, which can be seen in Figure 34, and corresponds to the position of similar metal stainless steel laser welded fatigue initiation sites[70].

It is reasonable to state that increasing the rotation angle will increase the local stress at the internal lap face, which will increase the early stage crack growth rate. More specifically, one could postulate that the fatigue life of a similar metal laser welded lap joint would be controlled by:

1. The applied load and, consequently, the severity of the local stress at the internal lap surface (directly related to the extent of rotation)
2. The early stage crack growth rate of the material at the internal lap face

This theory may also be applied to, and thus explain, the fatigue properties of dissimilar thickness and dissimilar metal lap joints.

The local stress generated at the internal lap surface of a dissimilar thickness joint would be the same since the rotation angle at both internal lap surfaces is equal (geometry dependent).

In relation to the four original dissimilar metal laser welded lap joints produced using the Trumpf 5kW laser welder, random fatigue failures were noted; however, this was originally thought to be due to the 'balanced tensile properties' of the lap joints by using thinner gauge stainless steel (1mm 304 and 0.78mm 2205). Analysis of the material at the internal lap faces revealed that the microhardness values were comparable, supporting the fact that the tensile properties and also the fatigue crack initiation and crack growth rates would be similar.

It is known that there is a major influence of metallurgical variables on the fatigue crack propagation at both high and low ΔK levels. In the case of dissimilar metal lap joints, if the material at the internal lap faces was microstructurally similar, that is free from pores, inclusions, precipitates and the presence of large secondary phase areas; one could postulate that the early stage fatigue crack growth rate would be comparable in both materials for both high and low ΔK levels.

In the case of intermediate ΔK levels fatigue crack propagation is relatively structure insensitive hence the propagation rate would also be similar promoting random fatigue failure in either of the dissimilar metals[90].

It can be seen in section 4.10.2 that the microhardness of the material at the internal lap faces was similar, suggesting that the material properties were also similar.

[90] Hertzberg, R. W. Deformation and fracture mechanics of engineering materials, 4th edition, John Wiley & Sons, Inc, ISBN 0-471-01214-9, pp 648-649

In light of these findings, research was directed towards the investigation of dissimilar metal laser welded lap joint fatigue properties between materials with large tensile property differences. If the theory that lap joint fatigue properties were controlled by applied load and the local stress at the internal lap face (joint rotation) and the early crack growth rate of the material at the internal lap face, then fatigue failure should still occur randomly in either the high strength stainless steel (1mm 2101 and 2205) or the relatively low strength 1.2mm V1437 if the material properties at the internal lap faces were similar.

5.10 Laser Welded Lap and Butt Joint Fatigue Properties – Rofin 2kW

As previously stated, the joint configurations chosen for further fatigue testing incorporated thicker gauges of stainless steel. Section 5.5 states it was originally thought that the tensile properties of the dissimilar metal lap joints need to be balanced to prevent preferential fatigue failure of the relatively low strength 1.2mm V1437 over the laser welded lap joint, hence the reduced thickness 2205 (0.78mm) duplex stainless steel grade. This was further substantiated by the random nature of the fatigue failures throughout the four dissimilar metal lap joints produced using the Trumpf 5kW laser welder due to tensile property balance being achieved. However, after analysing the factors that effect lap joint fatigue properties, the aim was to determine whether dissimilar metal lap joint fatigue properties were geometry dependent and consequently that fatigue failure occurred randomly in either the zinc-coated mild steel or the respective higher strength stainless steel. Hence, the following joints were chosen for fatigue testing, these joints also allow a range of comparisons to be made with the previous four dissimilar metal laser welded lap joints.

1.2mm V1437 (top) – 1mm 2205	dissimilar metal lap joint
1.2mm V1437 (top) – 1mm 2101	dissimilar metal lap joint
1mm 2101 – 1mm 2101	similar metal lap joint
1.2mm V1437 – 1mm 2101	dissimilar metal butt joint

It can be seen from Table 3, Table 7 and Table 9 respectively that the tensile strength of the 1.2mm V1437 is below the yield strength of both the 1mm 2205 and 1mm 2101.

Both the 1.2mm V1437 (top) – 1mm 2205 and 1.2mm V1437 (top) – 1mm 2101 staircase methods were statistically valid, which can be seen in Graph 31 and Graph 32 respectively. In comparison with the previous four laser-welded lap joints (Graph 27 - Graph 30), fatigue failure also occurred randomly in either the 1.2mm V1437 or the respective 1mm stainless steel throughout the fatigue testing program. In some cases failure occurred in both materials for the same applied load level during the staircase method.

This would suggest that the local stress at the internal lap faces are comparable and, more importantly, that the early fatigue crack growth rate of both the materials at the internal lap face is the same.

This further substantiated the hypothesis that dissimilar metal laser welded lap joint fatigue properties were independent of base material properties, even when the two base material tensile properties were significantly different, and were controlled by the applied load and the local stress at the internal lap face produced by joint rotation, which is, in turn, controlled by sheet thickness, interfacial gap and weld width.

Thus, with random fatigue failure being noted for these dissimilar metal lap joints the investigation proceeded into characterisation of the initiation site and propagation angles of the fatigue cracks; the emphasis being on the comparability of these fatigue failures from both materials of a respective lap joint.

5.11 Fatigue Failure Analysis

It can be seen from Image 12 to Image 19 that fatigue failure occurred in both the 1.2mm V1437 and the respective 1mm 304 and 0.78mm 2205 for each laser welded lap joint produced using the Trumpf 5kW CO_2 laser welder. The fatigue failure occurred at the edge of the weld at the internal lap face for all the failures.

More importantly, however, was the characterisation of the fatigue initiation point and propagation angles for the dissimilar metal laser welded lap joints produced with large tensile properties differences. The fatigue failures of these joints, produced using the Rofin 2kW laser welder, are investigated within this section.

As previously stated; dissimilar metal lap joint fatigue failures occurred randomly in both materials; this would suggest that the local stress and early fatigue crack growth rate of the material at the internal lap surface of both sheets must be similar. If this was the case, one would expect to find evidence of propagating fatigue cracks at the internal lap surface of the opposite material to which fatigue failure and separation occur. There were, however, a number of problems to be overcome before this could be determined.

Research conducted by Linder et al, revealed that the laser weld bead oscillated in width over its length[70]. This effect can be seen in Figure 68, and was observed during the determination of the weld widths in this investigation, the weld width being determined by measuring, regrinding and measuring to provide 5 weld width measurements for each sample before taking the average.

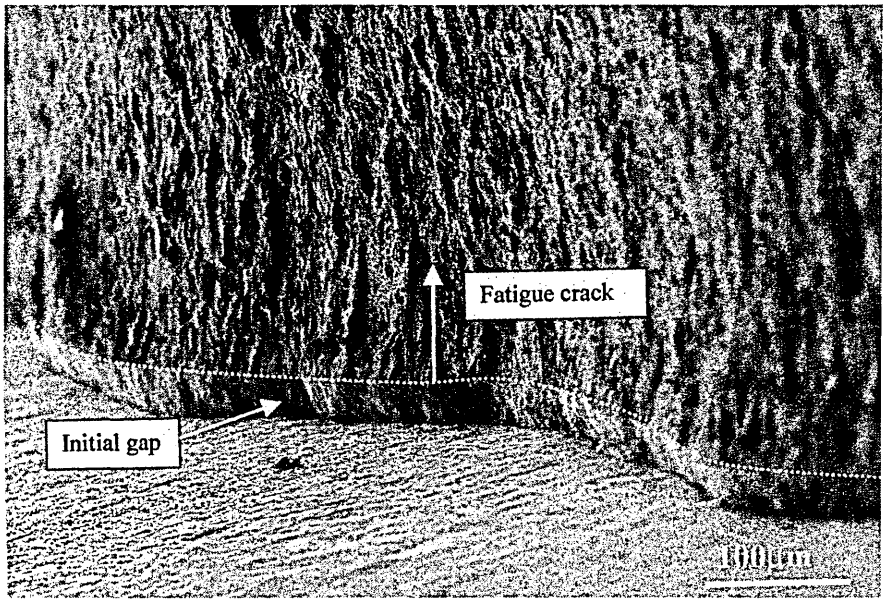

Figure 68 SEM image showing the oscillating weld width – the dotted line indicates the boundary between the initial gap and where fatigue cracking takes place[70]

This led Linder et al to predict that fatigue crack initiation would occur at certain points along the length of the laser weld, see Figure 69 below.

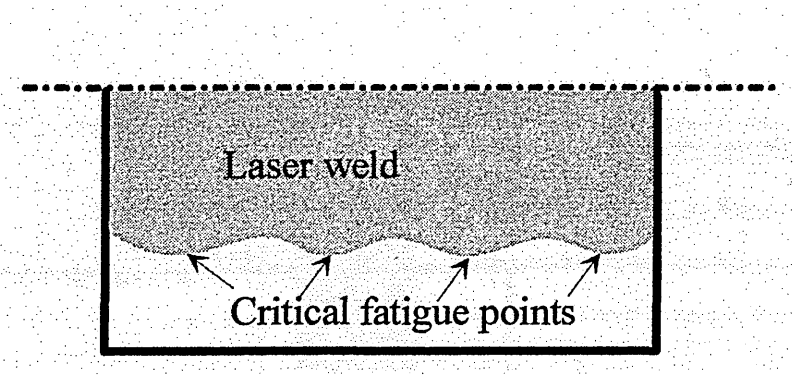

Figure 69 A schematic drawing of a laser-weld from above, showing oscillating weld width, and the location fatigue crack will probably initiate[70]

Thus, fatigue cracks would not be present along the entire length of the sample and would occur intermittently at the points where the weld bead was the widest due to oscillation of the weld bead width (similar to a spot weld periphery).

Image 20 shows fatigue failure in a 1mm 2101 similar metal lap joint, which displays no evidence of fatigue crack propagation from the internal lap face in the opposite sheet. Further grinding of three 2101 similar metal lap joint fatigue failures revealed evidence of a crack in the opposite sheet to fatigue failure, see Image 23 and Image 24. Further examination of the cracks was conducted to determine whether the cracks were produced by tearing during fatigue failure of the opposite sheet or whether they were in fact propagating fatigue cracks. It can be seen from higher magnification optical analysis (Image 25 and Image 26) that there is no evidence of plastic deformation around the cracks suggesting that they are in fact propagated fatigue cracks. This was substantiated by SEM analysis of the crack from Image 25 that showed the crack tip (see Image 27). The crack tip can be seen to be relatively 'sharp' in comparison to the majority of the crack, which has opened due to the cyclic loading from the tension/tension fatigue tests.

Although these images show signs of fatigue cracks present on the opposite side to fatigue failure, the lap joints are still of the similar metal type. The aim of this investigation was to determine if fatigue cracks were present in both materials for a dissimilar metal lap joint prior to fatigue failure.

Thus, observations of the fatigue tests were undertaken to determine if it was possible to predict the fatigue failure of a lap joint sample. It was noted that the sound of the machine increased prior to failure, probably due to contact between the propagating crack surfaces from Stage *II*. A test was consequently stopped and restarted to test the theory and failure occurred after 20 - 30 seconds (~1000 – 1500 cycles).

This would suggest that the crack growth rate during Stage *II* is much higher than the early crack growth rate during Stage *I*. This can be explained by considering that once the lap joint stiffness decreases due to the multiple propagating cracks (Stage *II*), the joint will rotate more under the applied load. The increased joint rotation will increase the local stress at the crack tips (more mode I loading), hence the crack growth rate will increase until the net section is no longer able to withstand the applied load and failure occurs through tearing and plastic instability.

Hence, a number of tests were terminated when the noise of the test increased. This was done for 1.2mm V1437 (top) – 1mm 2205 and 1.2mm V1437 (top) – 1mm 2101 lap joint samples (the lap joints with large base material property differences).

After examination, regrinding and examination etc of the lap joints, evidence of fatigue cracks in both materials (in the same transverse section) prior to failure was discovered. For the 1.2mm V1437 (top) – 1mm 2101 lap joint configuration, evidence of a fatigue crack in the 1mm 2101 (bottom of the lap joint) can be seen in Image 33 and Image 34; it can be seen the back scattered electron mode provided better contrast of the crack than the secondary electron mode. From the same transverse section, evidence of a fatigue crack can be seen in the 1.2mm V1437 (top of the lap joint) in Image 35 and Image 36, again the back scattered electron images providing better contrast.

The same effect can be seen in Image 37 and Image 38, which show fatigue cracks propagating from the internal lap face in the 1mm 2205 (bottom of the lap joint) and 1.2mm V1437 (top of the lap joint) from the same transverse section of a 1.2mm V1437 (top) – 1mm 2205 dissimilar metal lap joint.

Similar and dissimilar metal laser welded fatigue crack angles were determined and compared to the angles found by Linder et al and predicted by Helin.

The 1mm 2101 similar metal lap joint fatigue crack angle was determined and can be seen in Image 25.

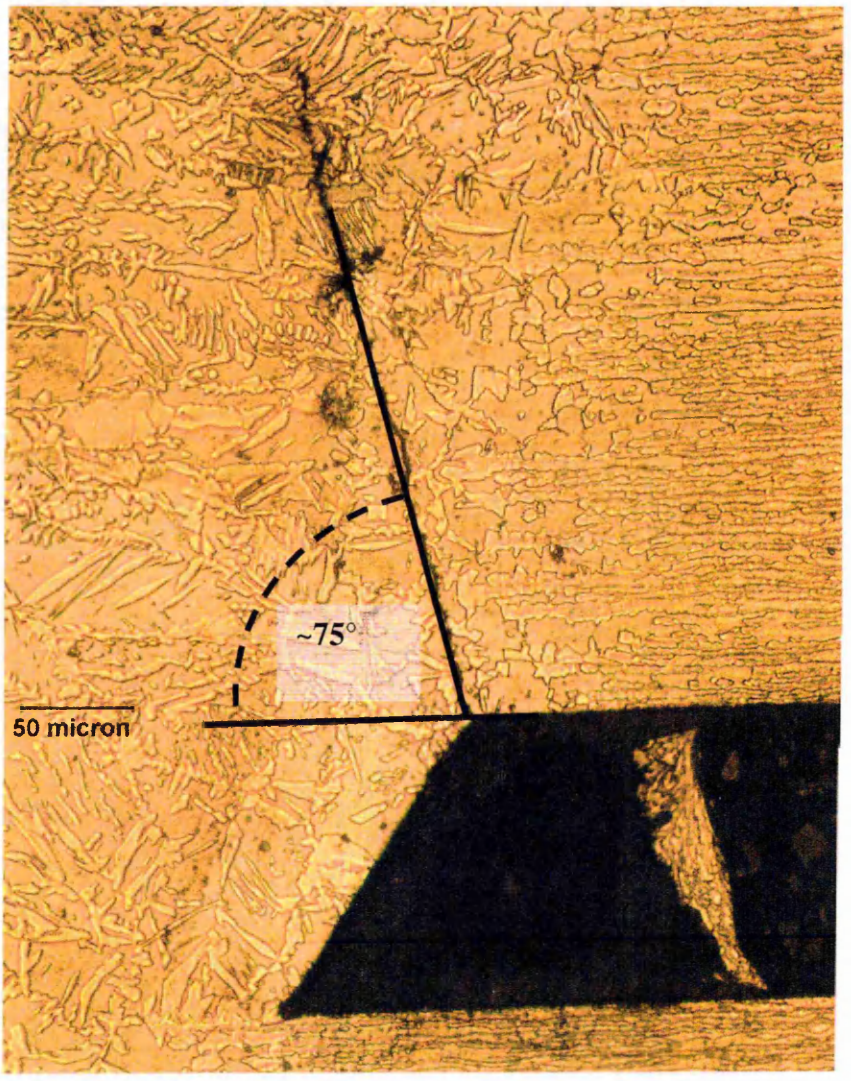

Image 49 Close up image of the propagated fatigue crack from Image 23 2101 similar metal lap joint

Hence, it can be seen that the 1mm 2101 similar metal lap joint fatigue crack angle is approximately 75°, a similar angle to those reported by Linder et al for similar metal stainless steel lap joints.

1.2mm V1437 (top) – 1mm 2101 dissimilar metal lap joint

Composite lap joint image showing the presence of fatigue cracks in both materials

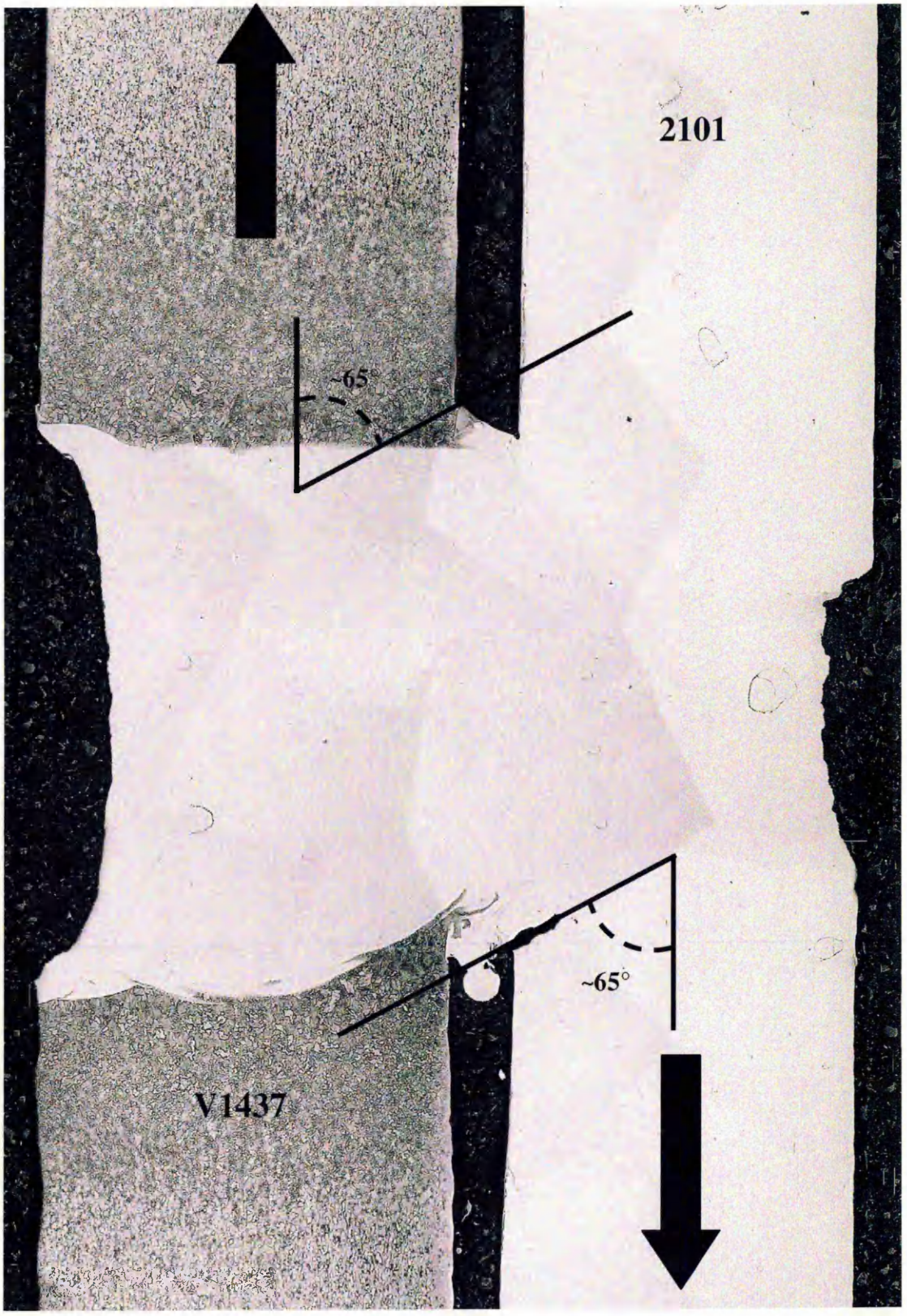

Image 50 1.2mm V1437(top) – 1mm 2101 dissimilar metal lap joint showing fatigue cracks in both materials

1.2mm V1437 (top) – 1mm 2205 dissimilar metal lap joint

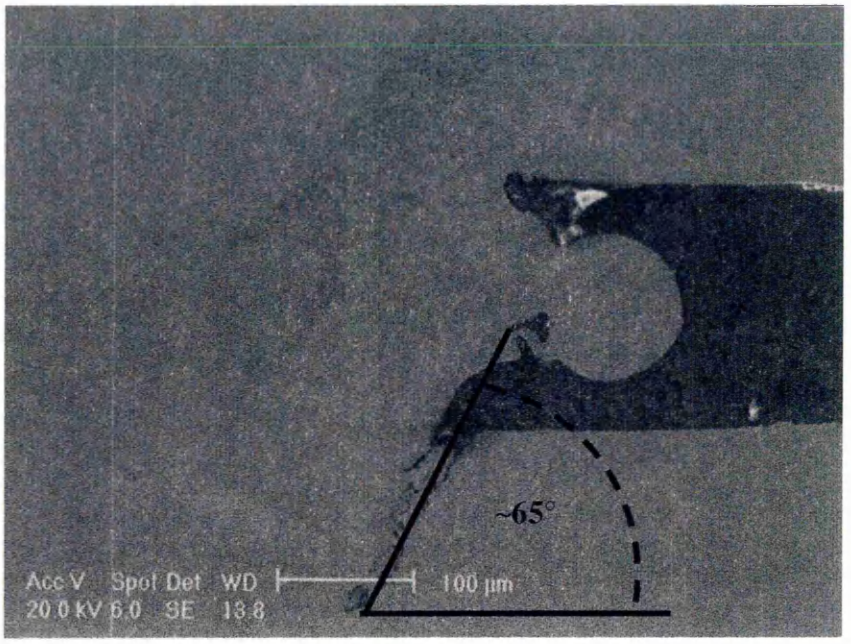

Image 51 Secondary electron image showing fatigue crack initiation in the 1mm 2205 from 1.2mm V1437 (top) – 1mm 2205 dissimilar metal lap joint

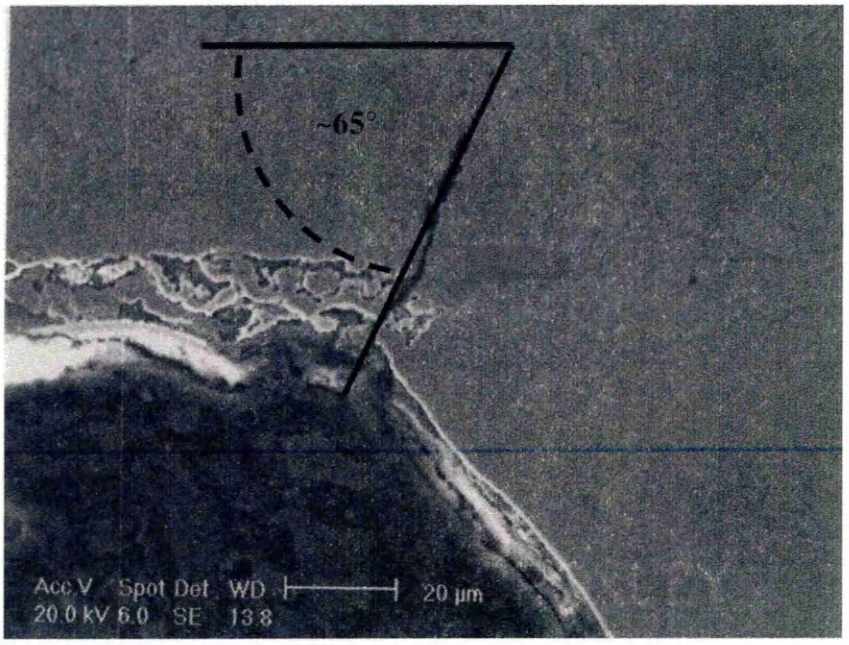

Image 52 Secondary electron image showing fatigue crack initiation in the 1.2mm V1437 from 1.2mm V1437 (top) – 1mm 2205 dissimilar metal lap joint

It can be seen that the angle of fatigue crack propagation is approximately 65° for the dissimilar metal lap joints. This is lower than the fatigue crack angles found by Linder et al. More importantly, however, is that the fatigue crack propagation angle is the same in both materials in a dissimilar metal lap joint (1mm 2205 and 2101 to 1.2mm V1437).

In summary, the increased noise from the fatigue samples prior to failure (~<2000 cycles) corresponded to the change from Stage *I (early crack growth)* to Stage *II,* suggesting that the majority of lap joint fatigue life is concerned with the early crack growth; once the transition to Stage *II* has occurred, the crack growth rate increases due to the reduction of stiffness, the increase in rotation and the local stress until the net section can no longer withstand the applied load and failure occurs through plastic tearing and rupture.

In light of this investigation, the following statements may be made:

- Fatigue cracks occur intermittently along the length of the weld bead
- The early stage crack growth rate (Stage *I*) of both materials is comparable
- The transition to Stage *II* occurs at a similar cycle life
- The Stage *II* crack growth rate is much higher than the early crack growth rate
- Reducing the lap joint stiffness increases joint rotation, which increases the local stress at the crack tips and consequently the crack growth rate

These can be used to explain the observed random nature of the fatigue failures.

The investigation was directed towards determining the factors that effect joint rotation, the severity of the local stress, early crack growth rate and consequently the fatigue life.

5.12 Lap Joint Rotation

The model proposed by Nordberg and McCann in section 2.16.5 was used to predict the rotation of laser-welded lap joints[77]. The equation used to predict the rotation angle of laser-welded lap joints can be seen in Equation 4. If there is a gap between the two sheets, Equation 5 is used to calculate the variable "z" (note: "z" is also included for joints with no interfacial gap and is equal to 1).

It should be noted that the model assumes symmetry, thus, it can only be used for similar thickness lap joints. Also, it does not take into account the effects of weld width.

In light of this; for a similar thickness, similar metal lap joint, the model predicts:

- Increasing the sheet thickness reduces the rotation angle per line load.
- The introduction of an interfacial gap between the sheets increases the rotation angle per line load.

Note: The higher the rotation angle per line load, the greater the local stress at the internal lap faces. Increasing the local stress at the internal lap faces will increase the early stage crack propagation rate and consequently reduce lap joint fatigue life.

Increasing the sheet thickness in the lap joint configuration, increases the eccentricity of the applied load, however, this increase in sheet thickness is accompanied by an increase in sheet stiffness. This increase in lap joint stiffness reduces the susceptibility of the joint to rotate per line load, improving fatigue properties.

Conversely, the introduction of an interfacial gap between the sheets increases the eccentricity of the applied load, whilst the sheet stiffness remains the same; hence the lap joint is more susceptible to rotation per line load, lowering fatigue properties.

Weld width, although not covered by the model, has already been seen to have an effect on lap joint fatigue properties, see section 5.8.1, and will be covered in section 5.13.

The modulus of elasticity also plays a fundamental roll in the prediction of lap joint rotation. Since the modulus of elasticity is the same for stainless steel and mild steel (190GPa), the model predicts that the respective similar metal lap joints would rotate to the same extent per line load.

5.12.1 Experimental Rotation Comparison

As stated in section 3.4.4, the rotation angles of both similar and dissimilar metal laser welded lap joints were determined experimentally. Since the model by Nordberg can only be used to predict the rotation angles of similar thickness joints, comparison with the experimental dissimilar thickness lap joint rotation angles could not be carried out. The graph below compares the experimental rotation angles with those predicted by the model for a 1mm similar metal stainless steel lap joint (1mm 2101).

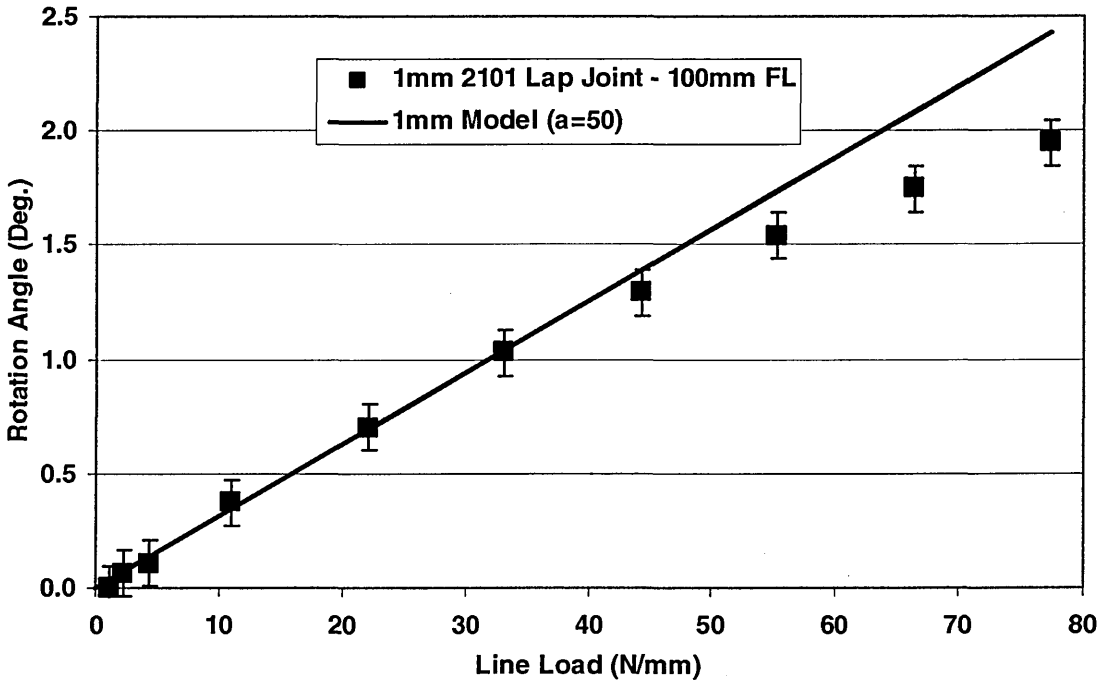

Graph 57 1mm 2101 similar metal lap joint experimental and predicted rotation comparison

Hence, it can be seen that the model predicts the rotation angle per line load range of a 1mm similar thickness laser welded lap joint quite accurately up to a maximum of 40 N/mm upon which the experimental rotation deviates from the linear. This may be attributed to the sample slipping in the jaws of the fatigue machine. As previously mentioned, the model does not take into account the effects of weld width, which might also explain the increasing discrepancy between the experimental and predicted rotation results.

Unfortunately, this was the only joint for which the comparison between experimental and predicted rotation angles could be made, as this was the only similar thickness lap joint produced during this investigation and the model cannot predict the rotation angles of dissimilar thickness joints.

However, a comparison between the experimental rotation angles of the similar and dissimilar thickness joints can be made and can be seen below in Graph 58.

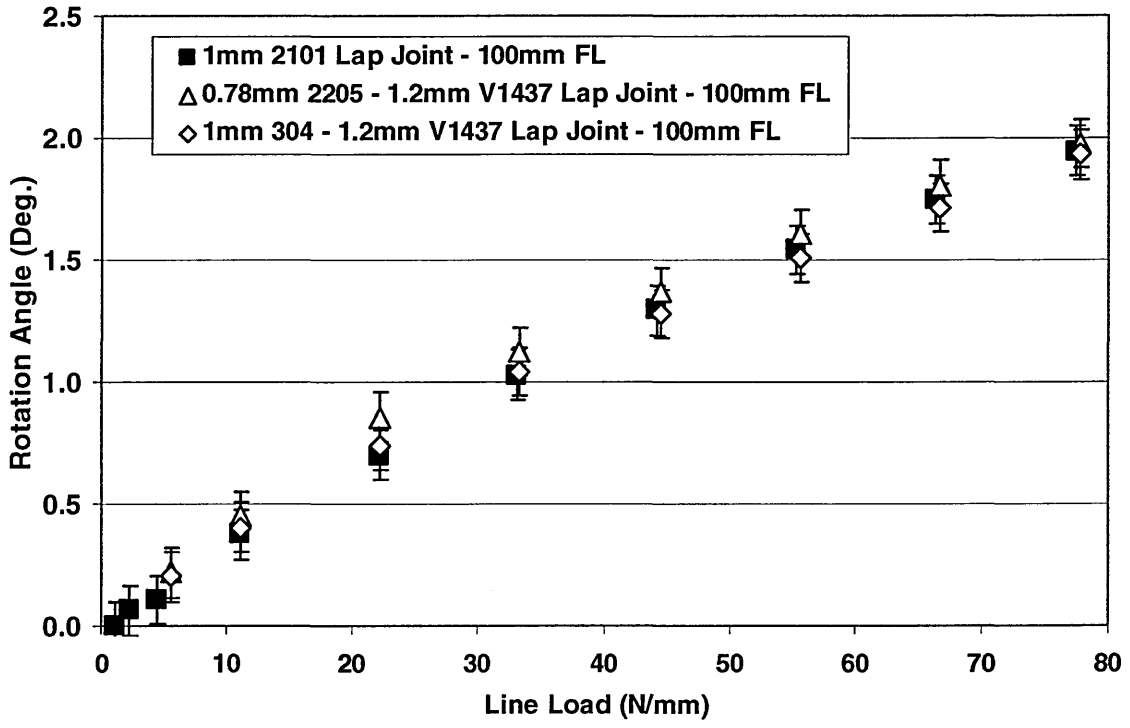

Graph 58 Comparison of experimental rotation angles per line load for similar and dissimilar metal laser welded lap joints

It can be seen that the experimental rotation angles for the three joints are effectively the same when the estimated errors are taken into account. This was the reason for not comparing the rotation angles for both configurations of the respective dissimilar thickness joints and attempting to characterise the effects of weld width on the rotation angles. Again when the estimated error of the rotation and weld width was taken into account, no trends could be identified. It can also be seen that the rotation angles above 40N/mm also appear to deviate from the linear, which may have been due to the sample slipping in the jaws during the test.

These experimental rotation angles were linked to the line load by inserting a linear trend line, which intercepted zero. This relationship was used to plot rotation angle against cycles to failure for the joints in question and can be seen in Graph 59 below.

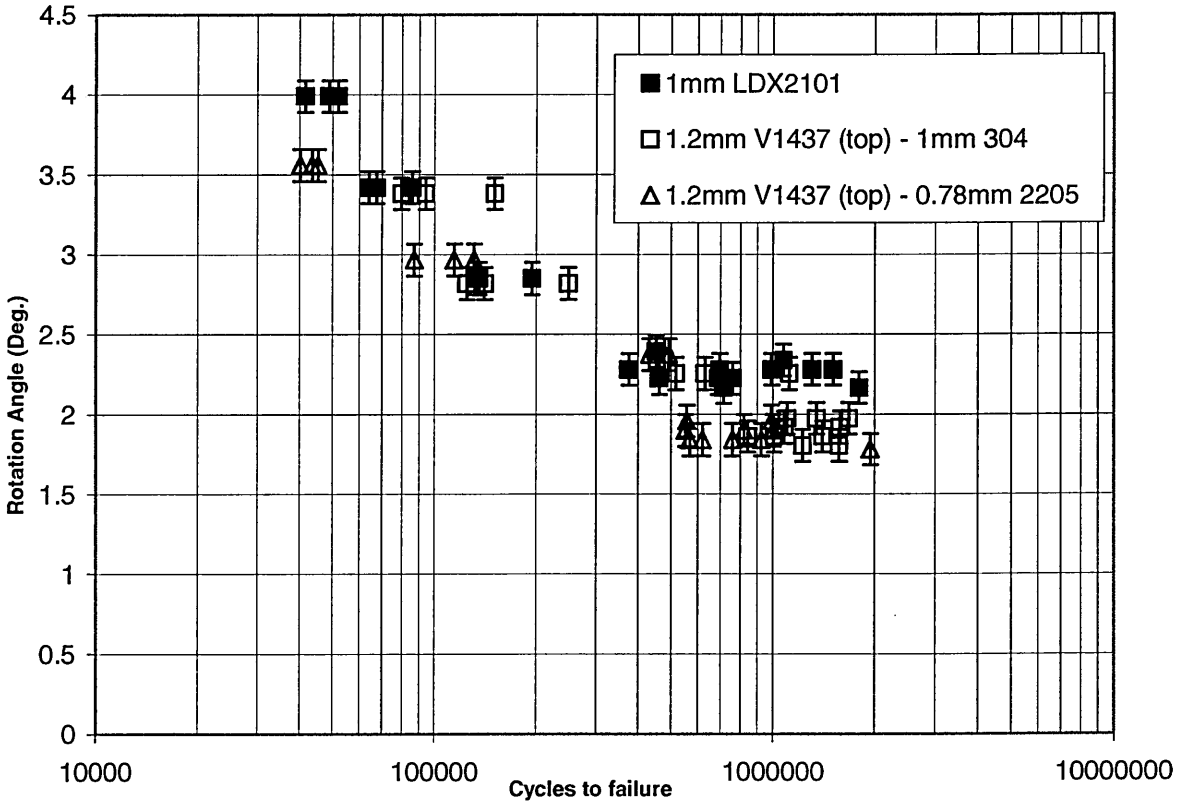

Graph 59 Relationship between rotation angle and cycles to failure

It can be seen that increasing the rotation angle reduces the cycles to failure.

It is worth mentioning that the configurations of the laser welds produced during this investigation all possessed similar:

- Sheet thickness or average sheet thickness for the dissimilar thickness joints
- Weld widths
- Interfacial gap
- Elastic Modulus

Since the joints all possessed a similar average sheet thickness, one would expect the stiffness of the joints to be comparable. Furthermore, due to the nature of the oscillating

weld widths, when the tolerance or scatter is taken into account, the differences in weld width between joints are relatively small.

This is reflected in the fatigue properties of the joints, which only show trends in the mean fatigue line load ranges at $2x10^6$ cycles when one standard deviation is used. Should two standard deviations be used, differences or trends between the joints are removed or, at most, are very weak.

Thus, the factors affecting joint rotation have been identified and will now be discussed with comparisons of the fatigue properties from this investigation with those from previous research.

The predicted rotation angles from the model produced by Nordberg and McCann have been used in the following discussions to predict the rotation angles of the joints, with the aim being to link them to the fatigue properties.

5.13 Factors Controlling Lap Joint Rotation

The factors identified as controlling the extent to which a joint will rotate per line load are:

- Sheet thickness
- Interfacial gap
- Weld width
- Elastic Modulus

Before these are discussed in more detail, it is worth mentioning that if the fatigue properties of similar and dissimilar metal laser welded lap joints are controlled by these geometric factors, then lap joints that possess the same sheet thickness, interfacial gap and weld width should rotate to the same extent per line load, providing the elastic modulus of the materials is the same. This should result in similar or comparable fatigue properties. This will be discussed in the following section.

5.13.1 Similar Geometry & Rotation Angle

It can be seen from Graph 60, that the two dissimilar metal laser welded lap joint fatigue properties are very similar. Both joints were produced consecutively with the Rofin 2kW CO_2 laser welder. The same welding parameters were used and both lap joints possessed a similar weld width between the sheets (~1.4mm ±0.05mm). It can be seen that the statistically valid mean fatigue line load ranges for the joints are within 2 N/mm of each other. When the standard deviations are taken into account, 4.3 N/mm for the 2205 and 3.7 N/mm for the 2101 dissimilar metal lap joints, both joints exhibited the same fatigue properties. It should be noted that both dissimilar metal laser welded lap joints did not possess an interfacial gap.

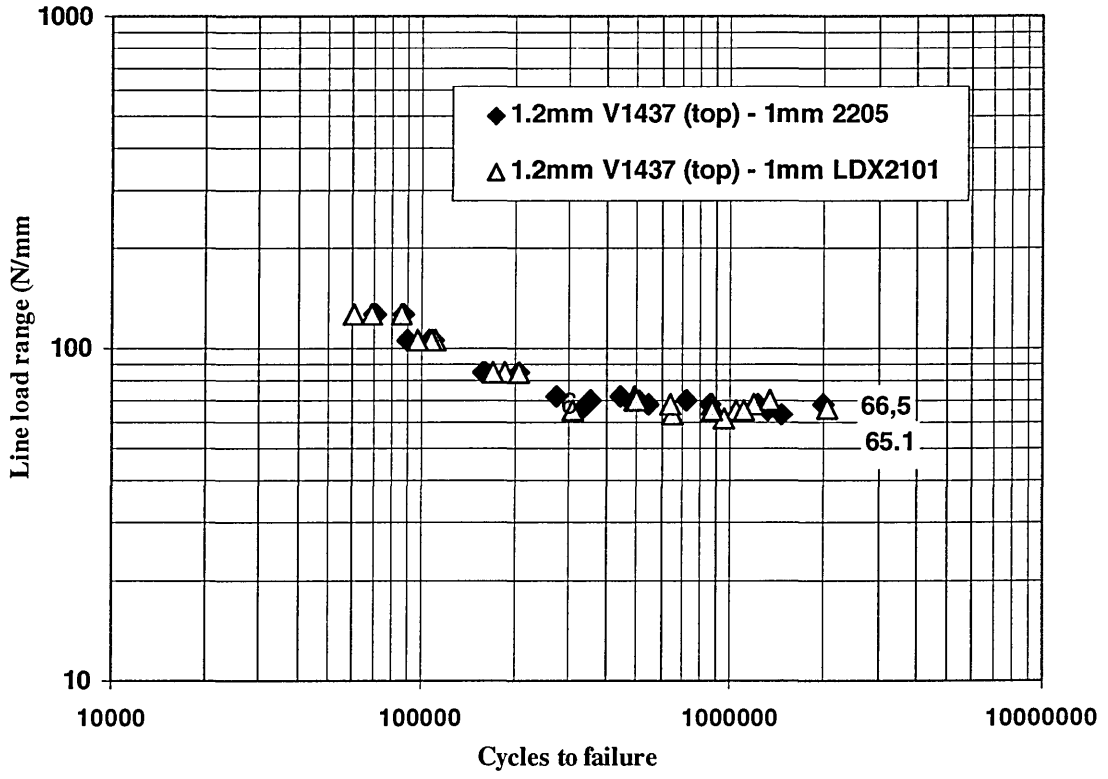

Graph 60 Dissimilar metal lap joint fatigue property comparison 1.2mm V1437 (top) – 1mm 2205 & 1mm 2101

Thus, with the same average sheet thickness, weld width and no interfacial gap, the joints would rotate to the same degree per line load, producing similar fatigue properties.

Graph 61 compares the fatigue properties of three dissimilar metal lap joints, 1.2mm V1437 (top) – 1mm 304, 2205 and 2101 respectively. Again, the joints have the same average sheet thickness, no interfacial gap and the same weld width, see Table 20.

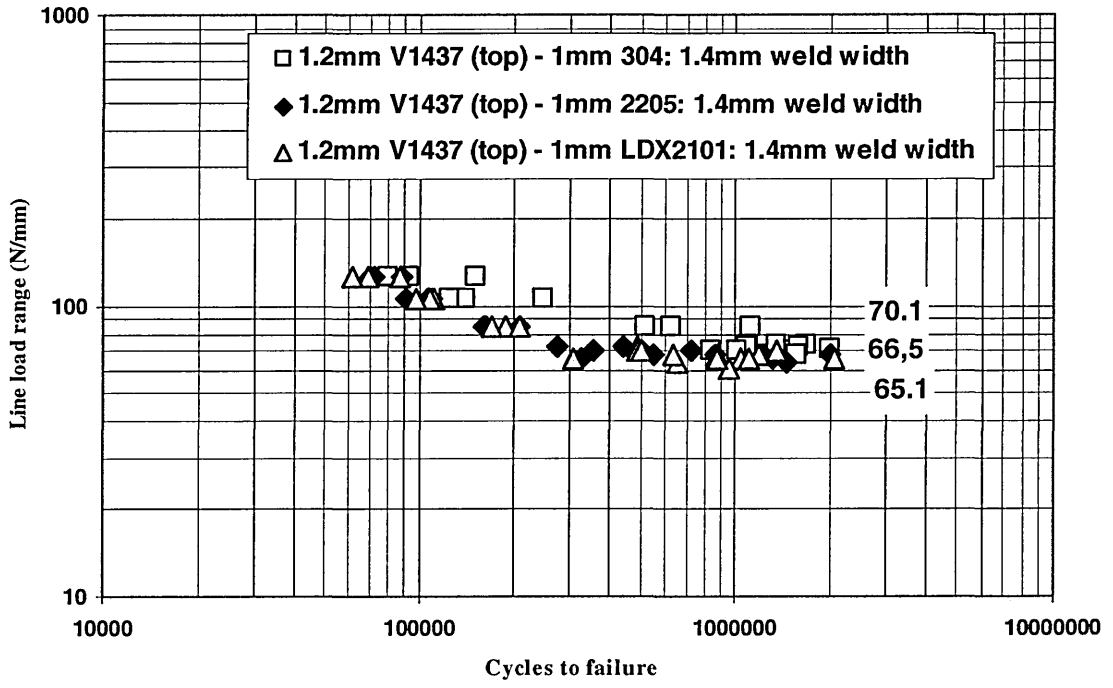

Graph 61 Dissimilar metal lap joint fatigue comparison with equal applied bending moment

It can be seen that the fatigue properties of the three dissimilar metal lap joints are very similar; although the 1.2mm V1437 (top) – 1mm 304 was produced with a different laser welder to the other two joints. Hence, laser welded lap joints with differing base material properties possess the same fatigue properties if the average sheet thickness, interfacial gap and weld width are the same, or more importantly, the rotation and consequently the local stress at the internal lap faces is the same. As previously mentioned, the fatigue failures occurred randomly; hence, the early fatigue crack growth rate of the material at the internal lap faces is also the same.

5.13.2 Effect of Sheet Thickness

The following graph compares results from this investigation with those produced by Linder et al, showing the effects of increasing the sheet thickness of one or both sheets in the lap joint configuration. The joints do not possess an interfacial gap.

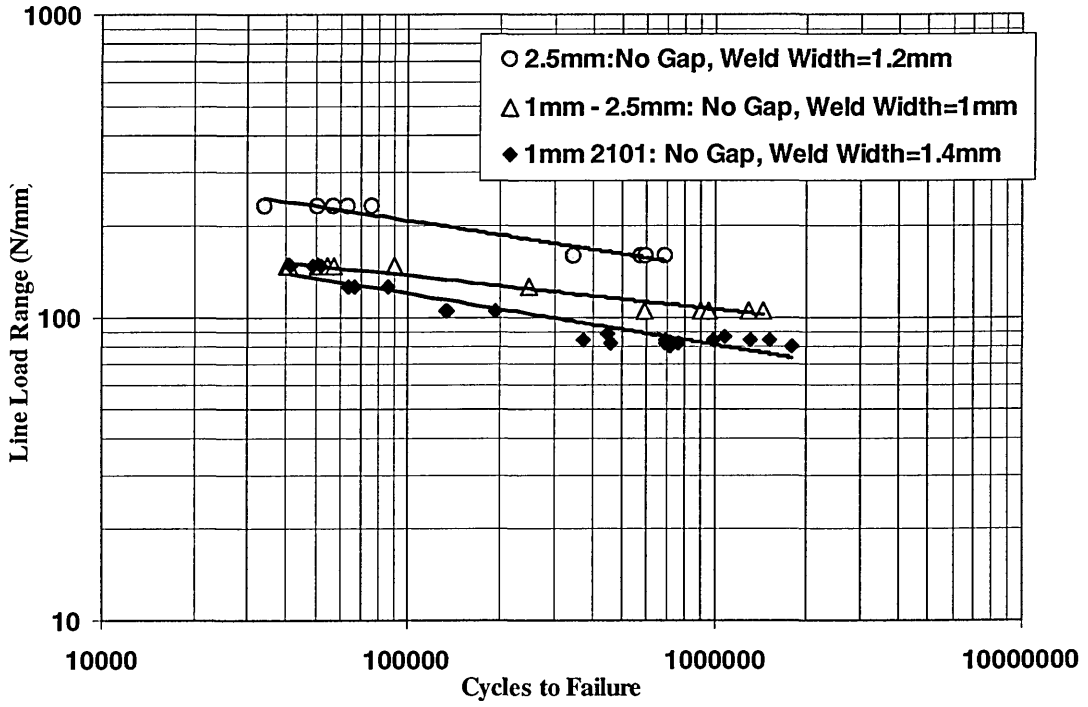

Graph 62 Comparison of fatigue results between joints with large differences in stiffness[70]

It can be seen that increasing the sheet thickness of one of the sheets results in an improvement of the fatigue properties. Increasing the sheet thickness of both sheets further improves the fatigue properties of the joints.

The rotation angles per line load have been predicted using the model of Nordberg and McCann. For the dissimilar thickness joint, the average sheet thickness has been used to predict the rotation angles.

The model predicts that as the sheet thickness increases, the stiffness of the lap joint increases and is consequently less susceptible to rotate per line load.

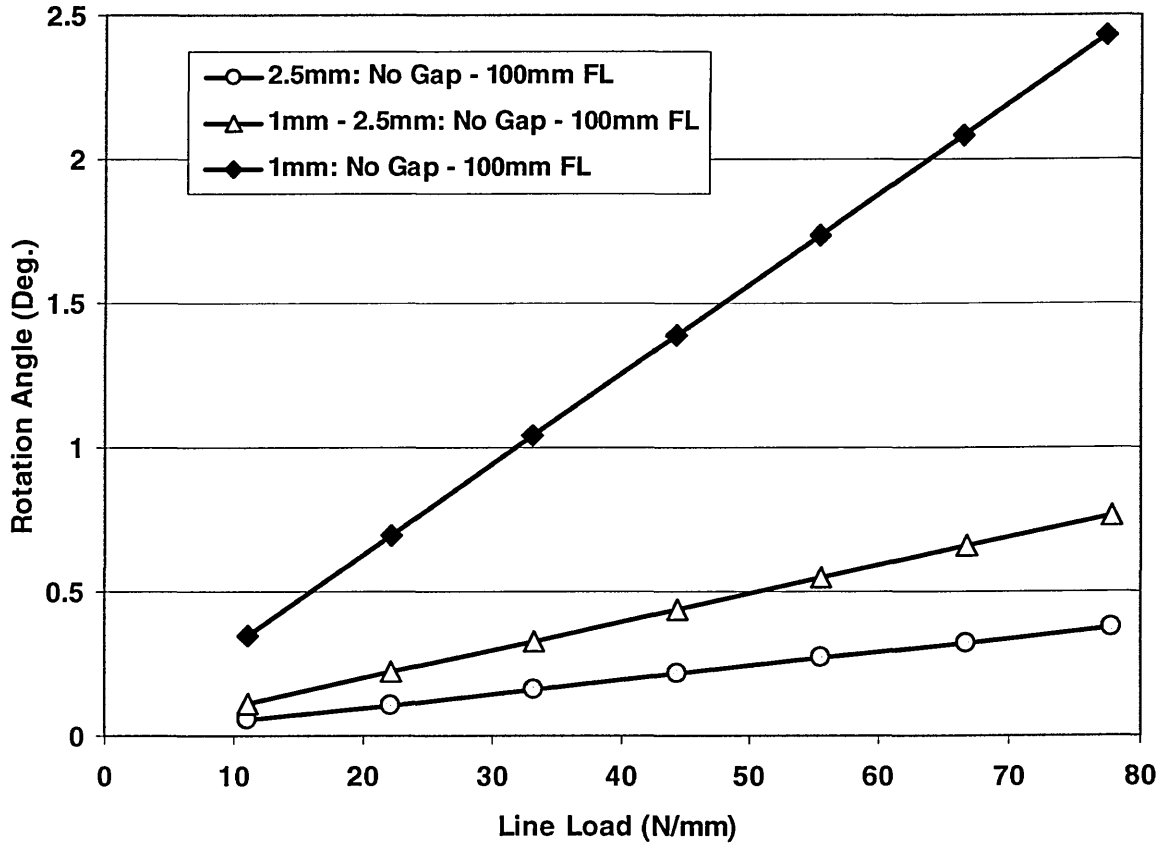

Graph 63 Effect of sheet thickness on the predicted rotation angles of similar and dissimilar thickness laser welded lap joints

This shows that increasing the sheet thickness of even one sheet in the lap joint configuration will increase the stiffness of the joint. This will reduce the rotation angle per line load, reducing the local stress at the internal lap face and consequently the early crack growth rate, improving the fatigue properties.

5.13.3 Effect of Interfacial Gap

The fatigue tests in Graph 64 below were conducted by Linder et al[70] and have been recalculated into the line load unit see below.

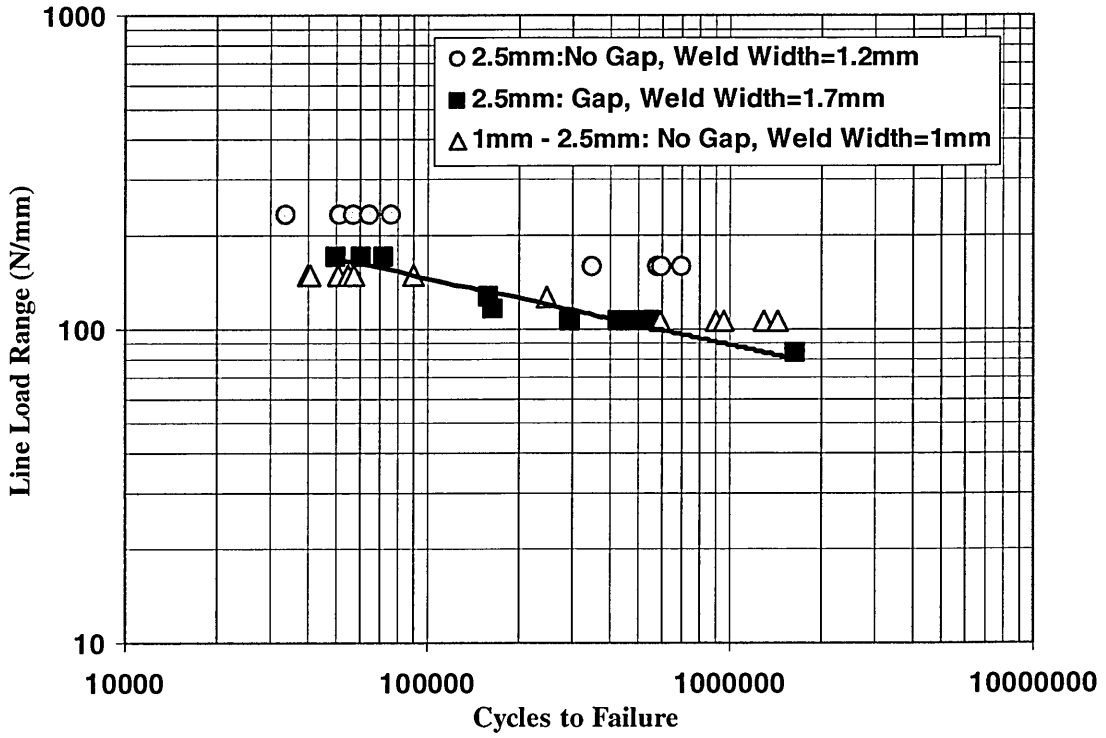

Graph 64 Linder: Line load range similar metal stainless steel fatigue properties – effect of sheet thickness and interfacial gap[70]

It can be seen that the fatigue properties of the 2.5mm lap joint with no gap are the highest. This was noted from the previous graph and was due to the increase in joint stiffness. However, the introduction of an interfacial gap to the 2.5mm lap joint produces a drastic reduction in the fatigue properties. The linear trendline shows the fatigue properties become lower than the dissimilar thickness joint at higher cycle failures. Hence, the introduction of an interfacial gap has overcome the effects of increased sheet stiffness and weld width.

The predicted rotation angles per line load for these joints can be seen in graph 63 on the following page.

As the actual interfacial gap for 2.5mm lap joint was not known, it has been estimated at 10% of the sheet thickness (0.25mm).

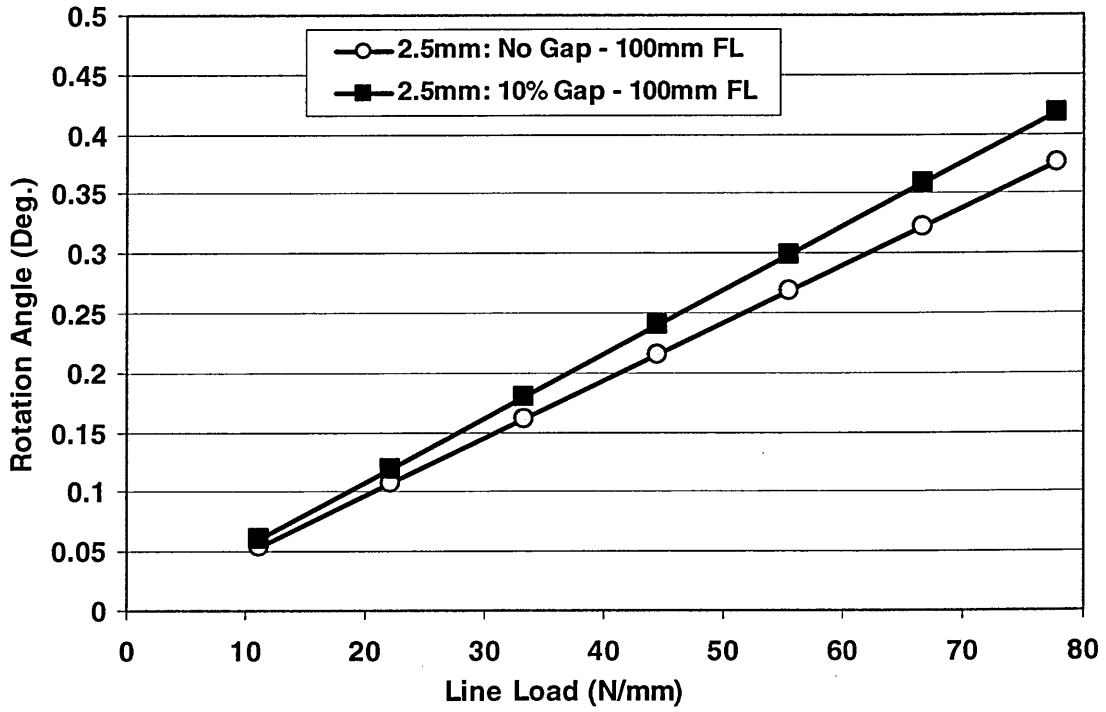

Graph 65 Effect of interfacial gap on the predicted rotation angles of similar thickness laser welded lap joints

Hence, it can be seen that the model predicts the presence of an interfacial gap will increase the rotation angle per line load. As previously stated, this is due to the increase in the eccentricity of the applied load.

This increase in rotation per line load can be seen to reduce the fatigue properties of the lap joint.

The effect of interfacial gap is also mentioned in the following section.

5.13.4 Effect of Weld Width

Section 5.8.1 states the initial dissimilar metal lap joints produced and tested showed that higher fatigue properties were achieved when the 1.2mm V1437 was at the top of the lap joint. This corresponded to an increase in weld width between the sheets and can be seen in Graph 55 and Graph 56 respectively.

A similar weld width trend has been found with the fatigue properties of similar metal laser welded stainless steel and carbon steel lap joints and can be seen respectively in Graph 66 and Graph 67 below. The results from the following two graphs are from Linder et al[70] (cold rolled SS2333 austenitic stainless steel) and have been recalculated and presented using the line load range unit.

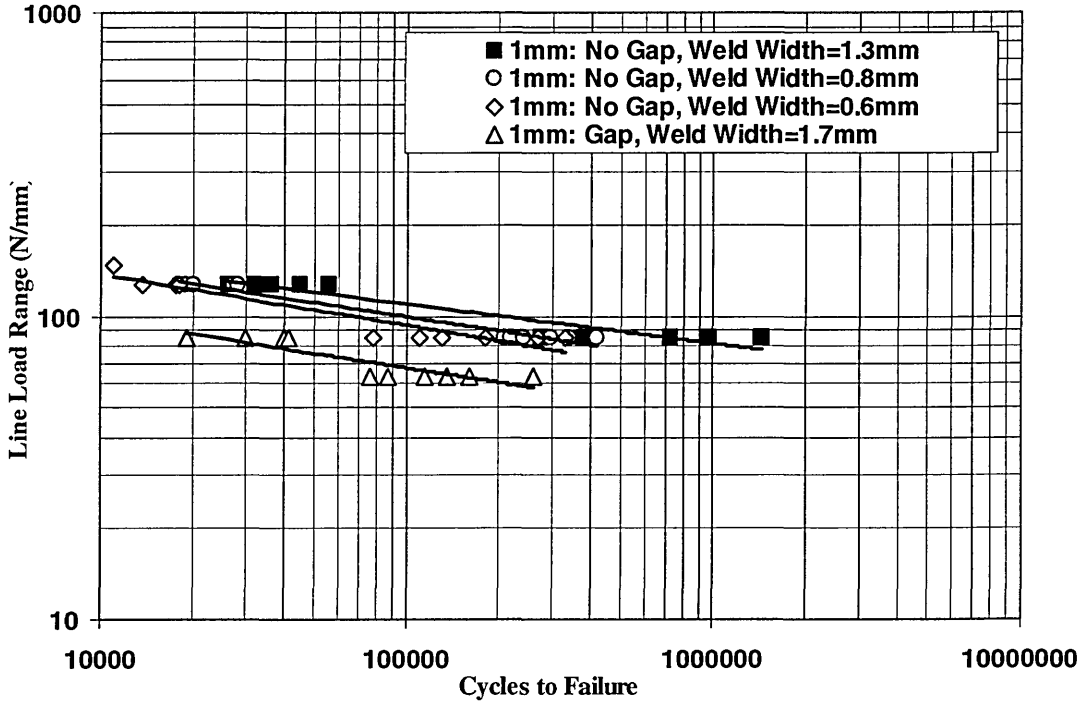

Graph 66 Linder: Line load range similar metal stainless steel lap joint fatigue properties – effect of interfacial gap and weld width

It can be seen that the laser welded lap joint with the lowest fatigue properties, although possessing the highest weld width, was the only joint to have an interfacial gap. Hence for the same sheet thickness (joint stiffness), the presence of an interfacial gap overcame

the effect of weld width, increasing the rotation of the joint per line load and reducing the fatigue properties.

It can also be seen that for the three remaining joints with no interfacial gap, increasing the weld width increased the fatigue properties of the joints by, it is proposed, reducing the rotation angle per line load range.

The following graph shows the similar metal carbon steel fatigue properties used for comparison by Linder et al. The fatigue properties have been recalculated into the line load range unit.

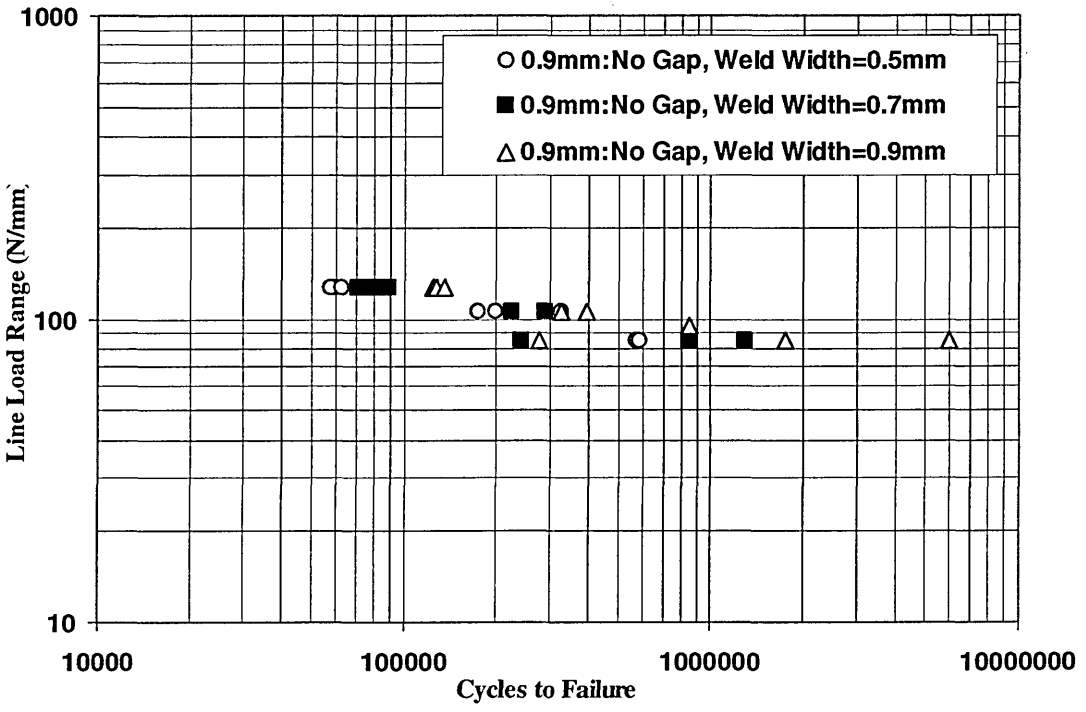

Graph 67 Linder: Similar metal carbon steel laser welded lap joint fatigue properties (0.9mm results from Linder et al)

Increasing the weld width between the sheets provides a slight increase in the cycles to failure for a given line load range by reducing the rotation angle per line load range. This reduces the local stress and early crack growth rate improving fatigue properties.

The lap joints in Graph 68 all possess the same average sheet thickness, this allowed the fatigue properties of the 1mm 2101 similar metal lap joint fatigue properties to be compared with the 1.2mm V1437 – 0.78mm 2205 (both configurations), with an average sheet thickness of 0.99mm.

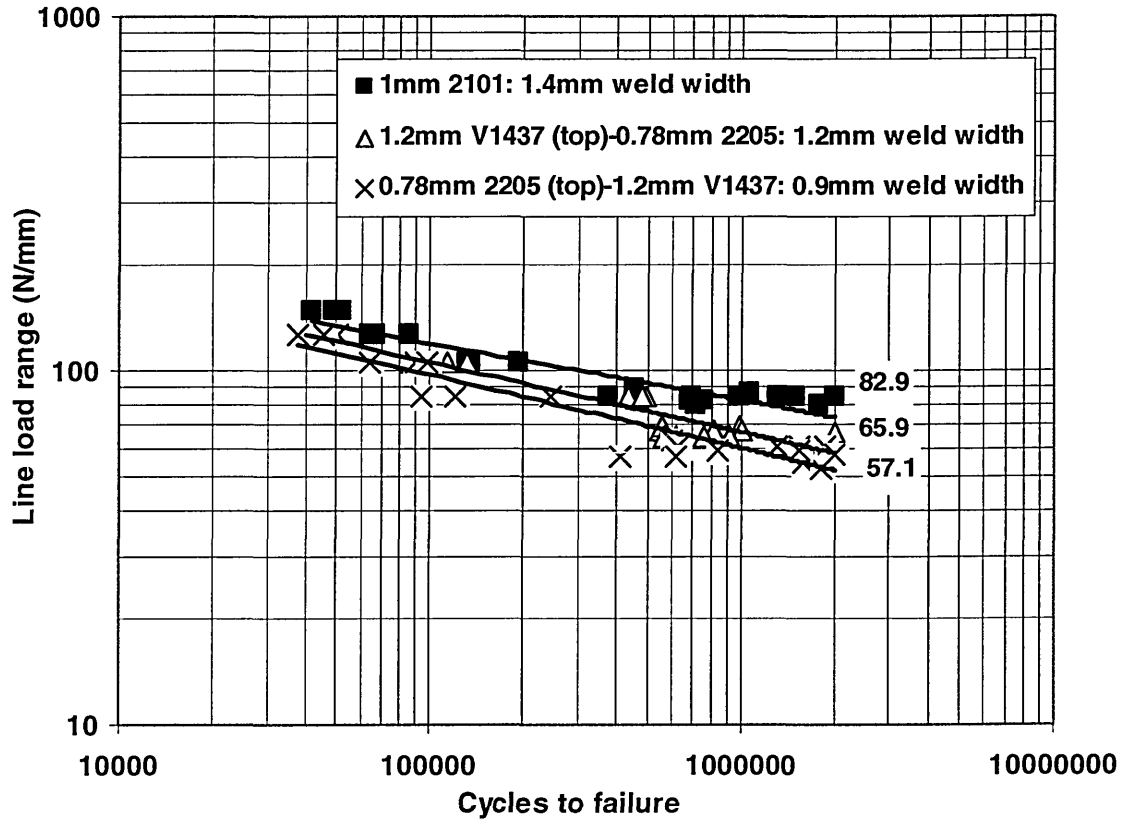

Graph 68 Effect of sheet thickness on lap joint fatigue properties (similar joint stiffness

It can be seen that the 1mm 2101 similar metal laser welded lap joint possessed higher fatigue properties than both the 1.2mm V1437 – 0.78mm 2205 dissimilar metal lap joints. The respective mean fatigue line load ranges ($2x10^6$ cycles) can be seen on Graph 68, as can the weld widths. This shows that for the same average sheet thickness and consequently a similar joint stiffness, increasing the laser weld width produced an improvement in the fatigue properties of the joints. Unfortunately, the effect of weld width could not be characterised using the model by Nordberg and McCann.

5.13.5 Young's Modulus

In order to illustrate the affect of elastic modulus on the predicted rotation angles, it was necessary to find a material that had a significantly different modulus to that of steel or stainless steel. As previously stated, the aluminium alloys are currently the largest alternative to zinc-coated mild steel in the automotive sector. The Young's modulus of aluminium is also much lower than that of steel or stainless steel and in the following rotation predictions a value of 69.5GPa has been used.

This material was selected to allow comparison and correlation of predicted rotation angles with lap joint fatigue properties.

The graph below compares the predicted rotation angles of a 3mm aluminium lap joint with that of a 3mm steel/stainless steel lap joint.

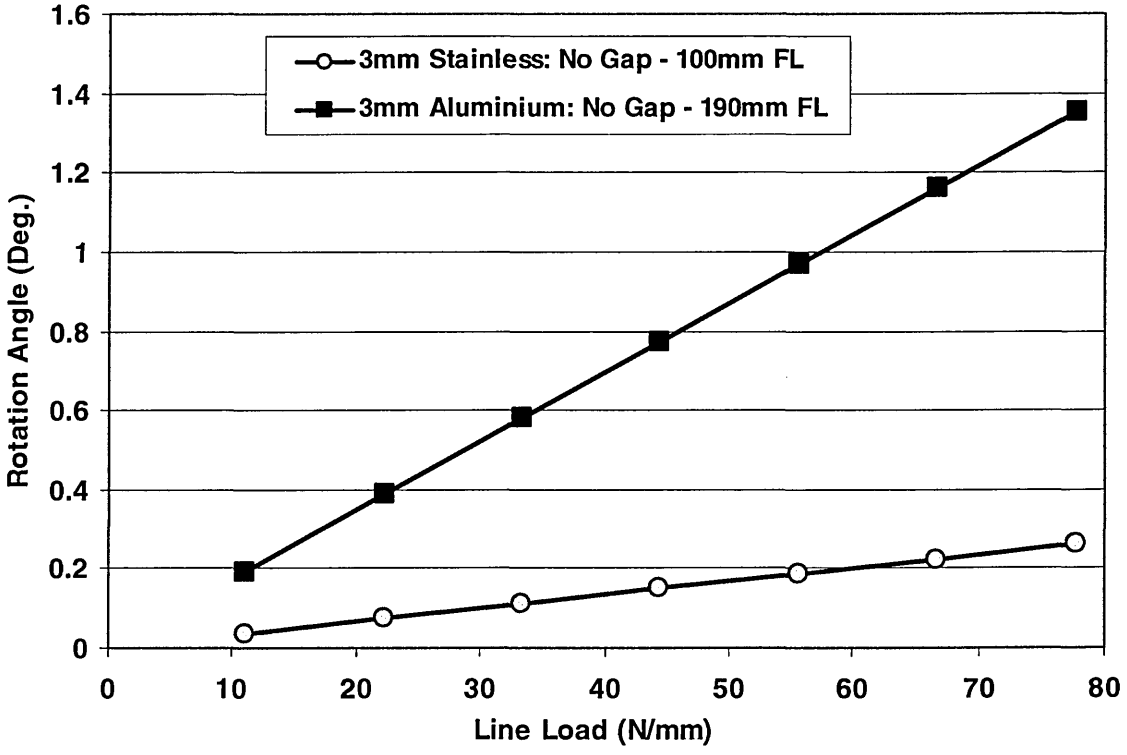

Graph 69 Comparison of predicted rotation angles for aluminium and steel laser welded lap joints

It can be seen that the predicted rotation angles for aluminium laser welded lap joints are far higher than those of the comparative steel lap joints.

This would suggest that a similar thickness laser welded lap joint fabricated using aluminium would rotate more than a comparable thickness steel, stainless steel or indeed a dissimilar metal (steel / stainless steel) lap joint. The fatigue properties of these joints can be seen in the following graph, which compares the line load lap joint fatigue properties of 3mm aluminium laser welded lap joint with a 3mm stainless steel laser welded lap joint and a 1mm 2101 stainless steel lap joint.

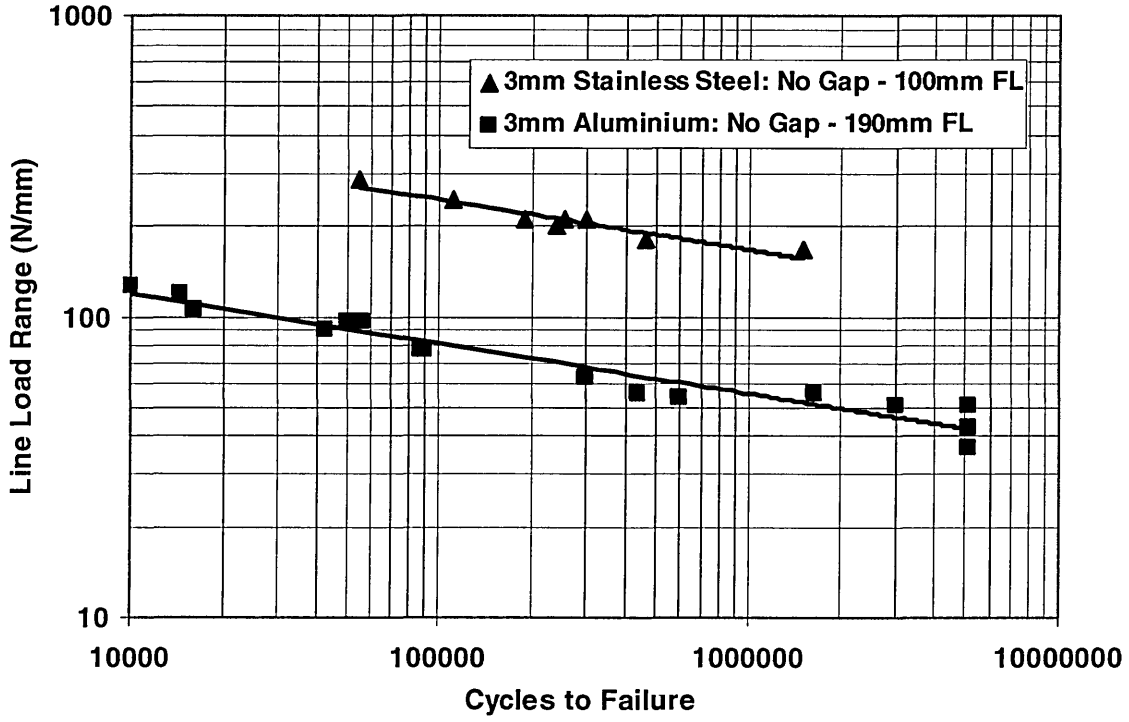

Graph 70 Lap joint fatigue comparison between 3mm aluminium lap joint and 1mm and 3mm stainless steel lap joints

Hence, it can be seen that the 3mm aluminium lap joint possessed the lowest fatigue properties.

This supports the evidence that lap joint fatigue properties are controlled by geometry, which in turn, determines the extent to which the lap joint will rotate per line load. This affects the local stress and consequently the early crack growth rate. It should be noted that the aluminium weld microstructure would also have an affect.

5.13.6 Partial Penetration and Double Laser Welds

This also explains why no reduction in fatigue properties was seen with partial penetration laser welding and also the presence of porosity in the weld bead. As stated, if partial penetration laser welds possess the same weld width between the sheets, then the joint stiffness would not be affected, thus the rotation angle per line load would not change and the fatigue properties would not be affected. It is also unlikely that the presence of porosity within the weld bead would affect the stiffness of the lap joint and consequently the fatigue properties.

On the other hand, if the porosity is present at the edge of the weld, this would effectively reduce the weld width perhaps increasing rotation, but more importantly increasing the local stress and affect the early stage fatigue crack growth, drastically reducing the fatigue properties.

The introduction of double laser welds may behave in a similar manner to a very wide weld and reduce rotation per line load range, which would increase in fatigue properties over single laser welds.

The rotation angle may also be used to explain why Wray[57] found no change in fatigue properties for the four different grades of resistance spot welded duplex stainless steel. The joints possessed the same sheet thickness and were welded with the same nugget diameter, hence it is proposed that the rotation per line load range and consequently the local stress would be the comparable for the four joints, see Graph 10.

5.13.7 Removal of Joint Rotation

For comparative purposes, the final laser weld configuration selected during this investigation was a dissimilar metal butt joint. Clearly, the butt joint configuration results in alignment of the applied load, thus, the joint does not rotate during fatigue loading. Removal of the lap joint and the stress concentration significantly improves the fatigue properties of dissimilar metal joints.

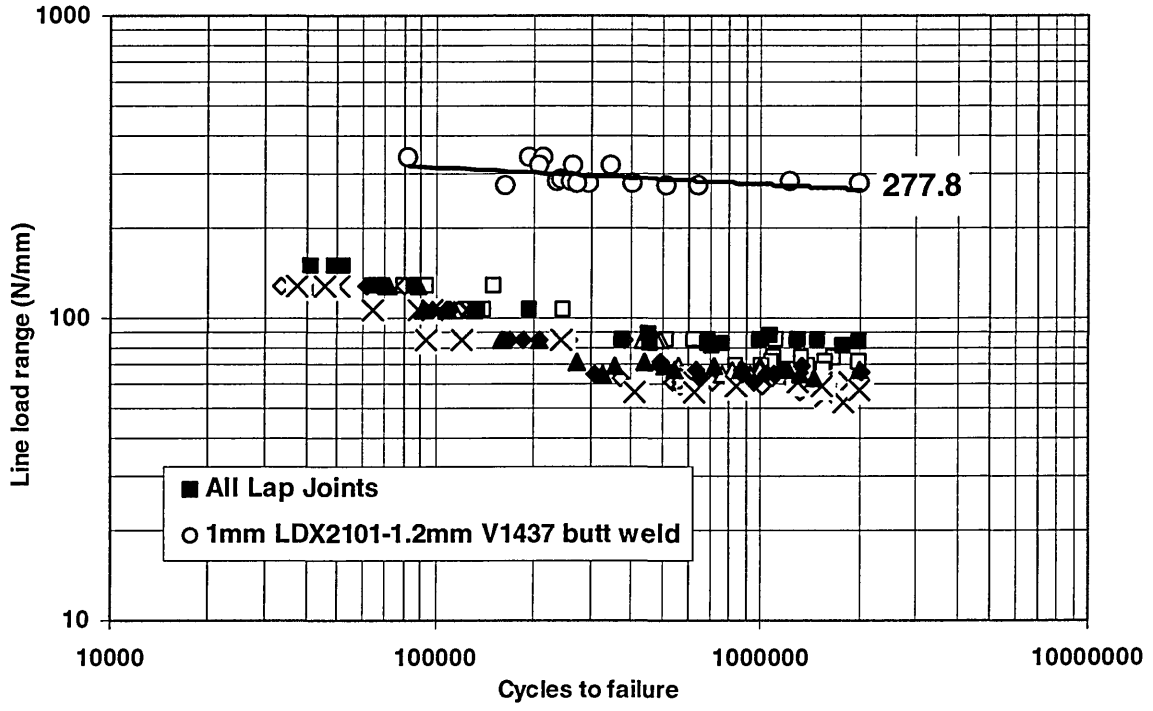

Graph 71 Laser welded lap and butt joint fatigue property comparison

It can be seen from Graph 71, that the dissimilar metal butt joint fatigue properties are far higher than the similar and dissimilar metal laser welded lap joints. The staircase produced was statistically valid, however the increment was increased from 0.1kN to 0.2kN, to produce three active levels. The S-N curve was only conducted at two load levels (317 and 338 N/mm) as when testing commenced on the third (358 N/mm) plastic deformation of the 1.2mm V1437 occurred. Fatigue failure was observed in weld bead and in the HAZ, between the weld and both parent materials (see Image 39 to Image 41).

5.14 Spot Weld Fatigue Comparison

The fatigue properties of dissimilar metal laser welded (LBW) lap joints were compared to dissimilar metal resistance spot welded (RSW) joints as this is currently the most widely used, highest production joining technique in the automotive industry and thus the benchmark for comparison.

The following graph compares 1mm 304 (Marples[38]) and 1mm 2101 (Wray[72]) resistance spot welded lap joint fatigue properties with 1mm 2101 laser welded lap joint fatigue properties. The spot weld pitch spacing used to calculate the line load unit was 17mm, see Equation 13.

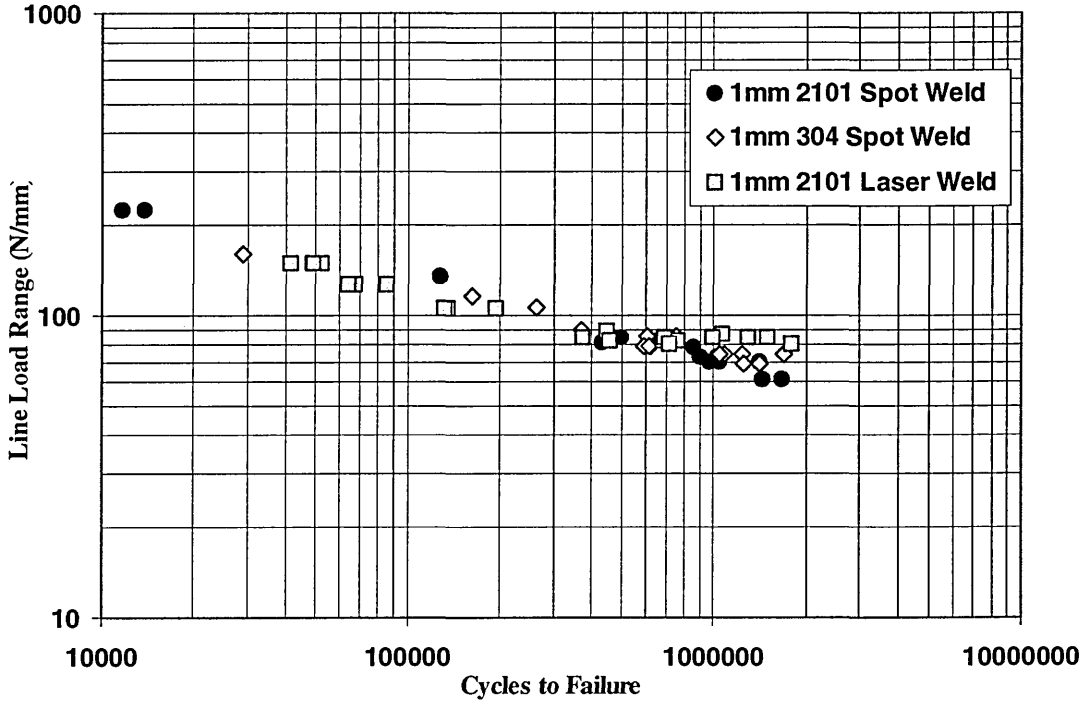

Graph 72 Fatigue property comparison for 1mm 304 RSW and 1mm 2101 LBW similar metal lap joints

It can be seen that the laser welded lap joint fatigue properties are very similar to the resistance spot welded lap joint fatigue properties, although the base material properties of the 1mm 2101 are much higher than the 1mm 304. As stated, the laser welded lap shear properties are independent of base material properties and are a product of the joint geometry. Thus, similar laser welded and spot welded fatigue properties are

achieved with the same sheet thickness joint. The 1mm 304 spot welded fatigue properties are the same as the 1mm 2101 spot welded fatigue properties, suggesting that spot welded fatigue properties are independent of base material properties and are also controlled by rotation.

A similar trend can be seen between the dissimilar metal laser and spot welded lap joints (Marples[38]). The pitch spacing used to calculate the resistance spot welded line load unit was 18.4mm, see Equation 13, for dissimilar metal lap joints the average sheet thickness was used for "t".

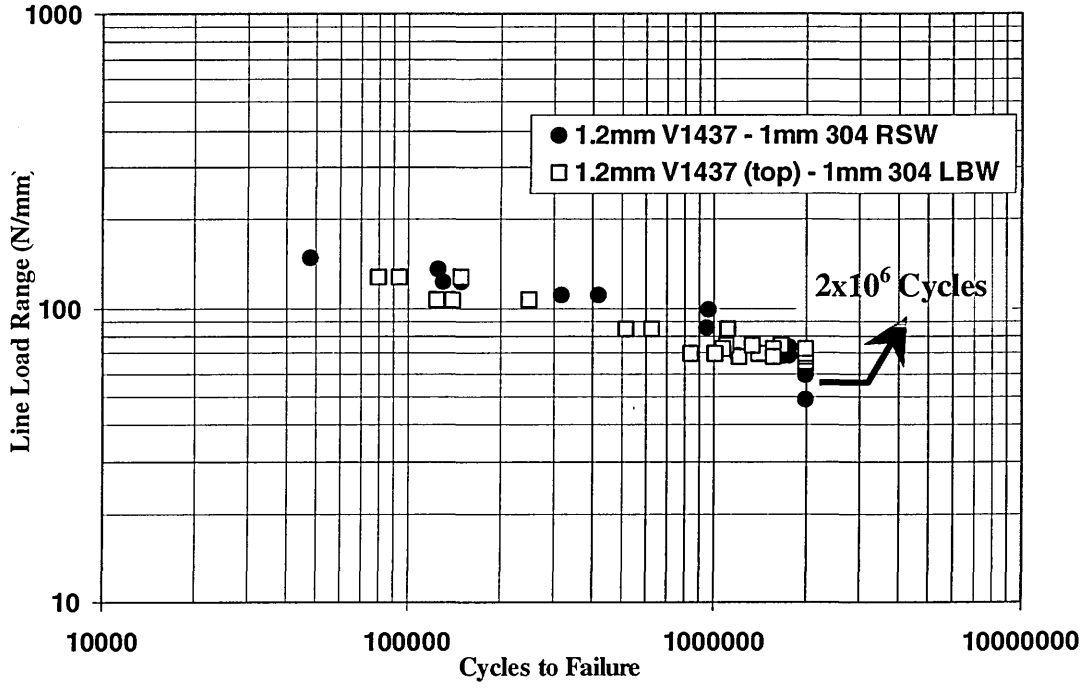

Graph 73 Fatigue property comparison for 1mm 304 – 1.2mm V1437 RSW and 1mm 304 – 1.2mm V1437 LBW dissimilar metal lap joints

It can be seen that dissimilar metal resistance spot welded and laser welded lap joint fatigue properties are very similar, with no significant improvement being achieved by the continuous laser welded lap joint.

6 *Conclusions*

- The original guidelines for laser welding zinc-coated mild steel, which state that the introduction of methods to allow zinc degasification of the internal lap face are not required for zinc-coatings of <5μm appear to be incorrect. A single zinc-coating thickness of 6.14μm at the internal lap face of the dissimilar metal joints was sufficient to produce porosity and blowholes in the respective weld beads when no zinc evacuation methods were employed.

- The problems caused by zinc vapour at the internal lap face of dissimilar metal lap joints may be overcome without the use of additional equipment or processes such as shims between the sheets.

  Increasing the heat input of the process by reducing the welding speed and defocusing the laser beam, provided sufficient time for the zinc vapour at the internal lap face to escape through the molten weld pool. This not only removed the problems with internal and surface porosity (blow holes), but also allowed adequate suppression of the plasma formed.

- No detrimental effect of liquid metal embrittlement of austenitic stainless steel by molten zinc was evident. The diffusion of the zinc into the 1mm 304 was not observed to affect either the lap shear or lap joint fatigue properties of the dissimilar metal lap joints.

- Reducing the welding speed did not improve the homogeneity of dissimilar metal butt joints. On the contrary, the range of compositions found in the weld bead increased as welding speed was reduced (more inhomogeneous).

  Reducing laser welding speed produces a more uniform weld bead shape (butt joint), with an average reduction in weld bead microhardness.

- The effects of Marangoni flow did control dilution and stirring in the laser welded butt joint. The effects are clearly characterised by the chromium and nickel speed maps further substantiating the mathematical and FE models from current literature.

  The material at the top and bottom of the lap joint configuration greatly affect the composition of the lap joint weld bead; the dilution and composition range being shifted towards the base material from the top of the lap joint (mild steel/stainless steel grade).

- The thermal properties of the respective materials control the shape of the lap joint weld bead. A more uniform weld bead is achieved when the V1437 is at the top of the lap joint compared to a 'top-heavy' weld bead shape when the respective stainless steel is at the top of the lap joint.

  The result being that a wider weld width between the sheets is achieved when the V1437 is at the top of the lap joint for a fixed set of laser welding parameters.

- The predicted structure (Schaeffler diagram) of the dissimilar metal laser welded butt and lap joints is martensite, which is corroborated by the high weld bead microhardness.

- Similar metal stainless steel lap shear properties were between 89 - 98% of the parent material tensile strength. The elongation to failure was lower due to the weld bead not contributing to plastic deformation. Both lap shear and fatigue failure occurred at the edge of the weld in the HAZ.

  The "non optimised" 1.2mm V1437 similar metal lap shear properties were 87% of the parent material tensile strength with failure occurring in the HAZ.

  Dissimilar metal laser welded lap shear properties with greater than 100% weld efficiency were achieved with the 1mm 304, 2205, 2101 and 0.78mm 2205 to 1.2mm V1437 (failure occurred in the parent material of the V1437).

- Joint configuration (material at the top and bottom of the lap) and weld width did not affect the lap shear properties

Fatigue Conclusions

- It is possible to produce dissimilar metal laser welded butt and lap joints between two materials with large parent material tensile property differences without fatigue failure occurring preferentially in the material with lower properties. Lap joint fatigue failure occurred randomly in both respective materials; in some cases failure occurred in both materials for the same applied line load range.

- Both similar and dissimilar metal lap joint fatigue properties are controlled by:
  1. The severity of the local stress at the internal lap face.
  2. The early crack growth rate of the material at the internal lap face.
- The extent of the local stress is directly linked to the applied load and rotation angle.
- Since the rotation is symmetrical, both materials rotate to the same extent; hence the local stress is the same at the internal lap face of both similar and dissimilar metal and thickness lap joints.

- The model produced by Nordberg and McCann for predicting rotation angles per line load appears to be accurate up to 40N/mm with regard to the 1mm 2101 similar metal lap joint.
- The model correctly predicts the effects of sheet thickness, interfacial gap and elastic modulus, when compared with similar and dissimilar metal fatigue properties.

- The laser weld microhardness, composition and martensitic structure had no effect on the fatigue properties of dissimilar metal lap joints. That is, the early stage crack growth rate of the materials at the internal lap faces were similar for the range of joints produced, promoting random fatigue failure.
- The extent to which a joint would rotate per line load was controlled by:
    1. Sheet thickness
    2. Interfacial gap
    3. Weld width
    4. Elastic modulus

- Increasing the sheet thickness of one sheet, although increasing the eccentricity of the applied load, would increase lap joint stiffness, reducing the joints susceptibility to rotation and improving the fatigue properties.

- The introduction of an interfacial gap increases the eccentricity of the applied load and increases the joints susceptibility to rotation due to no increase in stiffness. Thus, the fatigue properties are reduced.

- Increasing the weld width between the sheets improves lap joint stiffness, thus the susceptibility of the joint to rotate is reduced, improving fatigue properties.

- Lap joints produced with a lower modulus of elasticity appear to rotate more per line load and consequently have lower fatigue properties (Aluminium Alloys).

- Dissimilar metal lap joint fatigue failure occurred in the HAZ, weld bead, and HAZ/weld bead interface; thus, the propagating fatigue crack has no preference for microstructure.

- Fatigue cracks were present in both materials for both 1mm 2101 and 2205 to 1.2mm V1437 lap joint configurations. The observed fatigue crack angles were the same.

- 1mm 2101 similar metal lap joint fatigue crack propagation occurred at an angle of 75° to the sheet surface. In comparison, 1mm 2101 – 1.2mm V1437 and 1mm 2101 – 1.2mm V1437 fatigue crack angles were 65°.

- The fatigue cracks were found to exist intermittently along a transverse section of a lap joint, thus supporting the hypothesis proposed by Linder et al of multiple fatigue cracks.

- Dissimilar metal laser welded butt joint fatigue properties were far superior to the lap joint fatigue properties as no rotation of the joint occurred.
  Dissimilar metal butt joint fatigue failure occurred randomly in either the stainless steel or zinc-coated mild steel HAZ interface.

- The use of the line load range (N/mm) unit for assessing and comparing lap joint fatigue properties allows a far wider comparison of fatigue properties than other units used to compare fatigue properties.

6.1.1 Integrating Stainless Steel into Existing Automotive Design

The future seems bright for the integration of austenitic and duplex stainless steel into existing automotive design.

The use of stainless steel offers distinct advantages over the largest currently used alternative to zinc-coated steels, the aluminium alloys. The use of special welding techniques to improve the weldability and increase the performance of aluminium laser welds is not required for the production of high quality stainless steel laser welds. The fatigue properties of similar metal aluminium lap joints are also considerably lower than a like thickness similar metal stainless steel joint.

The major disadvantages of dissimilar metal lap joints between stainless steel and zinc-coated mild steel, for example, the high hardness of the weld bead and dilution of Cr and Ni in the weld bead does not affect the fatigue properties of the respective lap joints.

The problems with increasing the galvanic effect and consequent higher rate of zinc removal in the dissimilar metal joints would be negligible as the joints would be subjected to the standard automotive painting systems. This being possible as the stainless steel does not require the use of additional pre-treatments and reached the required standard in scab tests, etc.

The problems of liquid metal embrittlement of austenitic stainless steel by molten zinc have not been seen during this investigation.

With new, more cost effective grades being produced, such as the 2101 duplex stainless steels, which contain significantly lower Ni contents compared to standard duplex grades, the integration of stainless steel into existing automotive design becomes more attractive and cost effective.

With grades of stainless steel being produced with R_m values in the order of 1000MPa the scope for weight reduction is larger than ever and obviously reduces the cost of integration further. For example, a dissimilar metal lap joint between 0.5mm, 1000MPa stainless steel and 1.2mm V1437 would fail in the parent material of the 1.2mm V1437 (lap shear). Thus, the estimated weight savings of up to 40% could be realised. This would allow the automotive manufacturers to meet the current legislations for reducing vehicle emissions, which stated that the development of engine technology and reductions in friction etc would not be enough.

Although, the production of stainless steel dissimilar metal lap joints with zinc-coated mild steel produced no improvement in fatigue properties compared to the standard zinc-coated mild steel lap joints (as lap joint fatigue properties are independent of base material properties), this may allow the existing design criteria to be used.

7 *Further Work*

Further clarification linking the effects of joint rotation to the fatigue properties of similar and dissimilar metal laser welded lap joints is required. A range of joint configurations comparing sheet thickness, weld width and interfacial gap need to be completed to characterise the angles of rotation and the respective fatigue properties.

Question: Does an increase in weld width increase joint stiffness and reduce the rotation angle therefore improving fatigue properties?

Since lap joint fatigue properties are geometry dependent, if the rotation angle could be accurately predicted using a model similar to that produced by Nordberg and McCann it may be possible to link the rotation angle to the fatigue properties. In the case of dissimilar thickness lap joints, the use of FE analysis may be used to predict the rotation angle, with the aim being to link them to the experimental fatigue properties.

Question: What is the effect of the free length on the rotation angle?

This may allow the fatigue properties to be predicted and hence reduce the time consuming fatigue testing programs, especially the determination of mean fatigue properties at pre-assigned cycle lives (staircase method). The use of FE analysis may also allow the clarification of the weld width variable with regard to rotation and consequently fatigue properties.

The effect of the elastic modulus on the rotation angles and consequent lap joint fatigue properties needs to be investigated; more specifically, the characterisation of the rotation angle of a dissimilar metal aluminium/steel lap joint.

Question: Would the rotation angle be equal in both sheets?

Would fatigue failure occur randomly in either material?

8.1 Trumpf 5kW – Fatigue Results (Staircase & S-N Curve)

FATIGUE TESTING, STAIRCASE METHOD

Product: LASER WELD	Grade: 304 (top) – V1457	Nom. Dimension: 1mm – 1·2mm	Testing No.	Tested by	Date: 20/08/01
Special material specifications: TENSION / TENSION R=0·05 (LAP JOINT)					
Testing machine: INSTRON	Type of loading: SINUSOIDAL	Stress level interval, d, [N/mm2]: 0·1kN	Number of specimen: >20 TESTS @ 50Hz		

Specimen no.		1	2	3	4	5	6	7	8	9	10	11	12	13	14	15	16	17	18	19	20	21	22	23	24	26	27	28	29	30	31	32	33	34	35	36	37	38	39	40	Number of run-outs	Number of failures f_i	$i * f_i$	$i^2 * f_i$
Total Stress N/mm²	Step No ,i																											6	k	2		5	k	2		4	k	2						
3	4	*														*																												
2·9	3		*						*		*							*									X	X	X		X	X	X		X	X	X						
2·8	2			*				O		O		*		O		O			*		*																							
2·7	1				*	*	O		O				*		O					O																								
2·6	0					O																O																						
Number of cycles *10³		373 393	709 592	1845 583	1571 899	2763652	3001174	2077272	1252548	2291921	535 436	1014 140	3033513	2064499	2785335	1083417	1928509	563 023	3751273	1463136	1313268	2864943				39 180	80 169	32 562		118 362	117 438	116 942		250 534	259 126	382 445				Σ=F	Σ=A	Σ=B

Statistical calculations:

Mean fatigue strength = X, standard deviation = s
P_0 = Total stress for step 0 (i=0)

[ ] = Failure
O = Runout

$X = P_0 + d\,(A/F - 1/2) =$ _____ (_____ - 1 / 2) = _____ [N/mm²]

If $(F*B - A^2)/F^2 =$ _____ >0.3 and <1.2

$S = 1.620 * d\,\{(F*B - A^2)/F^2 + 0.029\} =$ _____ [N/mm²]

NOTE	

FATIGUE TESTING, STAIRCASE METHOD

Product	Grade	Nom. Dimension	Testing No.	Tested by	Date
LASER WELD	304 – V1437 (top)	1mm – 1.2mm			29/07/01

Special material specifications: TENSION / TENSION R = 0.05 (LAP JOINT)

Testing machine	Type of loading	Stress level interval, d, [N/mm2]	Number of specimen
INSTRON	SINUSOIDAL	0.1 kN	> 20 TESTS @ 50 Hz

Specimen no.	1	2	3	4	5	6	7	8	9	10	11	12	13	14	15	16	17	18	19	20	21	22	23	24	26	27	28	29	30	31	32	33	34	35	36	37	38	39	40	Number of run-outs	Number of failures f_i	$i * f_i$	$i^2 * f_i$
Total Stress N/mm² / Step No ,i																											6	K	2		5	K	2		4	K	2						
3.5 / 4																											X	X	X		X	X	X		X	X	X						
3.4 / 3																																											
3.3 / 2																																											
3.2 / 1																																											
3.1 / 0																																											
Number of cycles *10³	4644 806	1222068	2921903	2012556	13989999	2044848	2231467	2045545	1100 681	2004019	1341087	1081 885	840932	2024 806	2197 245	2635008	1672 364	1575 611	1006 677	1563 888							150 308	79 888	94 078		140 611	124 771	248 598		516 284	629 919	1116 026				Σ=F	Σ=A	Σ=B

Statistical calculations:

Mean fatigue strength = X, standard deviation = s
P_0 = Total stress for step 0 (i=0)

X = Failure
O = Runout

$X = P_0 + d\,(A/F - 1/2) =$ _____ (_____ - 1 / 2) = _____ [N/mm²]

If $(F*B - A^2)/F^2 =$ _____ >0.3 and <1.2

$S = 1.620 * d\,\{(F*B - A^2)/F^2 + 0.029\} =$ _____ [N/mm²]

NOTE

FATIGUE TESTING, STAIRCASE METHOD

Product: LASER WELD	Grade: 2205 – V1437(top)	Nom. Dimension: 0.78mm – 1.2mm	Testing No.	Tested by	Date: 31/07/01
Special material specifications: TENSION / TENSION R = 0.05 (LAP JOINT)					
Testing machine: DARTEC	Type of loading: SINUSOIDAL	Stress level interval, d, [N/mm2]: 0.1kN	Number of specimen: > 20 TESTS @ 50Hz		

Specimen no.	1	2	3	4	5	6	7	8	9	10	11	12	13	14	15	16	17	18	19	20	21	22	23	24	26	27	28	29	30	31	32	33	34	35	36	37	38	39	40	Number of run-outs	Number of failures f_i	$i * f_i$	$i^2 * f_i$
Total Stress N/mm² / Step No ,i																											6	k	2		5	k	2		4	k	2						
3.3 / 4								*																			X	X	X		X	X	X		X	X	X						
3.2 / 3		*					O		*						*																												
3.1 / 2			*			O				*			O			*																												
3 / 1				O	O						O			O			*		*	O																							
2.9 / 0												O	O					O			O	O																						
Number of cycles *10³	821 064	759 436	1938 339	3 322 559	2012 650	2 198 680	2045 425	989 860	551 869	618 243	4 341 829	2008 213	2 318 425	557 709	1000 779	567 957	2116 079	925 385	2 258 572	2 028 772	10000 000						45 270	43 435	40 169		87 110	114 302	130 695		492 929	432 242	439 304			Σ=F	Σ=A	Σ=B

Statistical calculations:

Mean fatigue strength = X, standard deviation = s
P_0 = Total stress for step 0 (i=0)

X = Failure
O = Runout

$X = P_0 + d\,(A/F - 1/2) =$ _____ (_____ - 1 / 2) = _____ [N/mm²]

If $(F*B - A^2)/F^2 =$ _____ >0.3 and <1.2

$S = 1.620 * d\,\{(F*B - A^2)/F^2 + 0.029\} =$ _____ [N/mm²]

NOTE	

FATIGUE TESTING, STAIRCASE METHOD

Product	Grade	Nom. Dimension	Testing No.	Tested by	Date
LASER WELD	2205(top)-V1437	0·78mm-1·2mm			20/08/01

Special material specifications: TENSION / TENSION R=0·05 (LAP JOINT)

Testing machine	Type of loading	Stress level interval, d, [N/mm2]	Number of specimen
DARTEC	SINUSOIDAL	0·1kN	>20 tests @ 50Hz

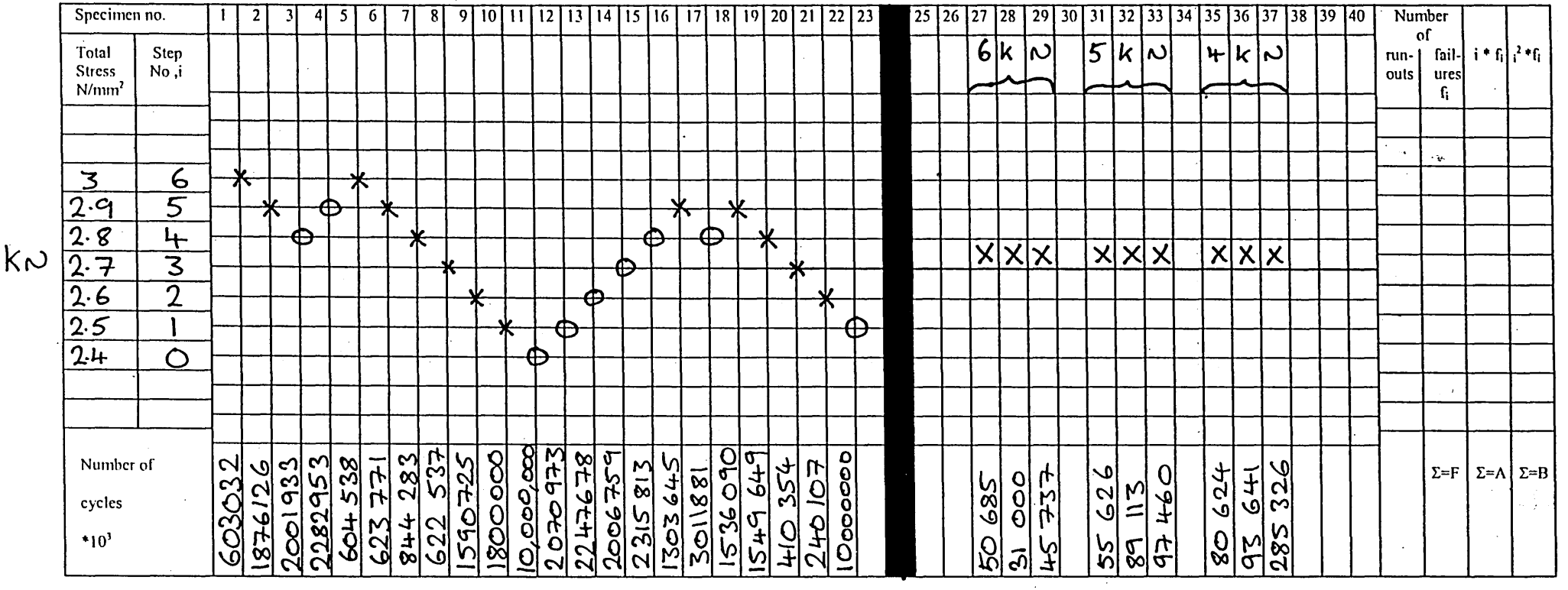

Statistical calculations:

Mean fatigue strength = X, standard deviation = s
P_0 = Total stress for step 0 (i=0)

[ ] = Failure
O = Runout

$X = P_0 + d\,(A/F - 1/2) =$ _____ (——— - 1 / 2) = _____ [N/mm²]

If $(F*B - A^2)/F^2 =$ _____ >0.3 and <1.2

$S = 1.620 * d\,\{(F*B - A^2)/F^2 + 0.029\} =$ _____ [N/mm²]

NOTE	

8.2 Rofin-Sinar 2kW – Fatigue Results (Staircase & S-N Curve)

FATIGUE TESTING, STAIRCASE METHOD

Product	Grade	Nom. Dimension	Testing No.	Tested by	Date
LASER WELD	2101 – V1437	1mm – 1·2mm			

Special material specifications: TENSION / TENSION R = 0.05 (BUTT JOINT).

Testing machine	Type of loading	Stress level interval, d, [N/mm2]	Number of specimen
INSTRON	SINUSOIDAL	0.2kN	> 20 TESTS @ 25Hz

Specimen no.	1	2	3	4	5	6	7	8	9	10	11	12	13	14	15	16	17	18	19	20	21	22	23	24	26	27	28	29	30	31	32	33	34	35	36	37	38	39	40	Number of run-outs	Number of failures f_i	$i * f_i$	$i^2 * f_i$
Total Stress N/mm² / Step No ,i																											16 k N				15 k N												
13·8																																											
13·6 4										*																																	
13·4 3	*										*																X	X	X		X	X	X										
13·2 2		*		*				O	O			*																															
13 1			O		*		O			O			*		*		O																											
12·8 0						O								O		O		O	O																									
Number of cycles *10³	237096	298112	2030144	401789	1641445	2030569	2066356	2028745	2251473	2445990	2604430	2720237	5164770	2475623	6431574	2038643	5000001	2004937	1221996	2013865							1938844	2150440	830005		209818	348562	263502										

Statistical calculations:

Mean fatigue strength = X, standard deviation = s
P_o = Total stress for step 0 (i=0)

X = Failure
O = Runout

$X = P_o + d\,(A/F - 1/2) =$ _____ (-------- - 1 / 2) = _____ [N/mm²]

If $(F*B - A^2)/F^2 =$ _____ >0.3 and <1.2

$S = 1.620 * d\,\{(F*B - A^2)/F^2 + 0.029\} =$ _____ [N/mm²]

NOTE	

FATIGUE TESTING, STAIRCASE METHOD

Product	Grade	Nom. Dimension	Testing No.	Tested by	Date
LASER WELD	2205 – V1437(top)	mm – 1.2mm			

Special material specifications: TENSION / TENSION R = 0.05 (LAP JOINT)

Testing machine	Type of loading	Stress level interval, d, [N/mm2]	Number of specimen
DARTEC	SINUSOIDAL	0.1kN	> 20 TEST @ 50 Hz

Specimen no.	1	2	3	4	5	6	7	8	9	10	11	12	13	14	15	16	17	18	19	20	21	22	23	24	26	27	28	29	30	31	32	33	34	35	36	37	38	39	40	Number of run-outs	Number of failures f_i	$i * f_i$	$i^2 * f_i$
Total Stress N/mm² / Step No ,i																											6	k	2		5	k	2		4	k	2						
3.4 / 6	X																																										
3.3 / 5		X		X					X																		X	X	X		X	X	X		X	X	X						
3.2 / 4			O		X		O			X																																
3.1 / 3						O		O			X	X																															
3 / 2									X				X																														
2.9 / 1										X				X																													
2.8 / 0											O				X	O	O																											
												O	X					O	O	X																								
Number of cycles *10³	489307	1346400	2987672	4907718	8723781	3089612	4883930	4999918	1183334	2087764	2011768	1034192	650422	952104	2684276	2043000	2110089	2278411	635081	874373	2040099	1096704					86398	69088	61079		110694	107496	97002		187481	169967	207921			Σ=F	Σ=A	Σ=B

Statistical calculations:

Mean fatigue strength = X, standard deviation = s
P_0 = Total stress for step 0 (i=0)

U = Failure
O = Runout

$X = P_0 + d\,(A/F - 1/2) =$ _____ (-------- - 1 / 2) = _____ [N/mm²]

If $(F*B - A^2)/F^2 =$ _____ >0.3 and <1.2

$S = 1.620 * d\,\{(F*B - A^2)/F^2 + 0.029\} =$ _____ [N/mm²]

NOTE	

FATIGUE TESTING, STAIRCASE METHOD

Product	Grade	Nom. Dimension	Testing No.	Tested by	Date
LASER WELD	2101 – VL457(top)	1mm – 1.2mm			

Special material specifications: TENSION / TENSION R = 0.05 (LAP JOINT)

Testing machine	Type of loading	Stress level interval, d, [N/mm2]	Number of specimen
DARTEC	SINUSOIDAL	0.1kN	>20 TESTS @ 50Hz.

Specimen no.	1	2	3	4	5	6	7	8	9	10	11	12	13	14	15	16	17	18	19	20	21	22	23	24	26	27	28	29	30	31	32	33	34	35	36	37	38	39	40	Number of run-outs	Number of failures f_i	$i * f_i$	$i^2 * f_i$
Total Stress N/mm² / Step No ,i																											6	k	2		5	k	2		4	k	2							
3.4 / 5	*		*																																									
3.3 / 4		O			*	*																*					X	X	X		X	X	X		X	X	X							
3.2 / 3					O		*	*				*						*		O			O																					
3.1 / 2									*	O	O		*				O		O																										
3 / 1														*	O	O																													
2.9 / 0																																													
Number of cycles *10³	44807	227308	273493	506070	322345	720627	1219603	788754	245150	2307452	861029	1320156	1456782	2001454	2014443	3356435	546175	2104560	2006886	3544458	2045553	2100441					71566	70345	88406		916073	107187	110039		158892	207540	161382				Σ=F	Σ=A	Σ=B

Statistical calculations:

Mean fatigue strength = X, standard deviation = s
P_0 = Total stress for step 0 (i=0)

□ = Failure
O = Runout

$X = P_0 + d\ (A/F - 1/2) =$ _____ (_____ - 1 / 2) = _____ [N/mm²]

If $(F*B - A^2)/F^2 =$ _____ >0.3 and <1.2

$S = 1.620 * d\ \{(F*B - A^2)/F^2 + 0.029\} =$ _____ [N/mm²]

NOTE	

FATIGUE TESTING, STAIRCASE METHOD

Product	Grade	Nom. Dimension	Testing No.	Tested by	Date
LASER WELD	2101 – 2101	1mm – 1mm			

Special material specifications: TENSION / TENSION R = 0.05 (LAP JOINT)

Testing machine	Type of loading	Stress level interval, d, [N/mm2]	Number of specimen
INSTRON	SINUSOIDAL	0.1kN	> 20 TESTS @ 50Hz

Specimen no.	1	2	3	4	5	6	7	8	9	10	11	12	13	14	15	16	17	18	19	20	21	22	23	24	26	27	28	29	30	31	32	33	34	35	36	37	38	39	40	Number of run-outs	Number of failures f_i	$i * f_i$	$i^2 * f_i$
Total Stress N/mm² / Step No ,i																											7 k 2				6 k 2				5 k 2							
4.2 / 5				*																							X	X	X		X	X	X		X	X	X					
4.1 / 4			O		*																																						
4 / 3		O				*						*		*		*		*																									
3.9 / 2	O						*	*		*	O		O		O		O		*																								
3.8 / 1									O											*		*																					
3.7 / 0																					O		*																					
Number of cycles *10³	3025490	2019017	2177028	450688	1073744	990309	759845	2118001	688380	2256297	2586303	1301524	2780114	1503188	2659574	695257	4160725	357362	461443	745078	3622453	1792054					52114	48988	41553		86006	67335	69352		194095	135002	132516			Σ=F	Σ=A	Σ=B

Statistical calculations:

Mean fatigue strength = X, standard deviation = s
P_0 = Total stress for step 0 (i=0)

X = = Failure
O = Runout

$X = P_0 + d\ (A/F - 1/2) =$ _____ (------- - 1 / 2) = _____ [N/mm²]

If $(F*B - A^2)/F^2 =$ _____ >0.3 and <1.2

$S = 1.620 * d\ \{(F*B - A^2)/F^2 + 0.029\} =$ _____ [N/mm²]

NOTE	

8.3 Lap Joint Rotation Results

The following appendix contains the experimentally determined lap joint maximum rotation angles as a function of line load range for the following joints.

1mm 304 – 1.2mm V1437 (top) dissimilar metal lap joint

0.78mm 2205 – 1.2mm V1437 (top) dissimilar metal lap joint

1mm 304 – 1.2mm V1437 (top) dissimilar metal lap joint

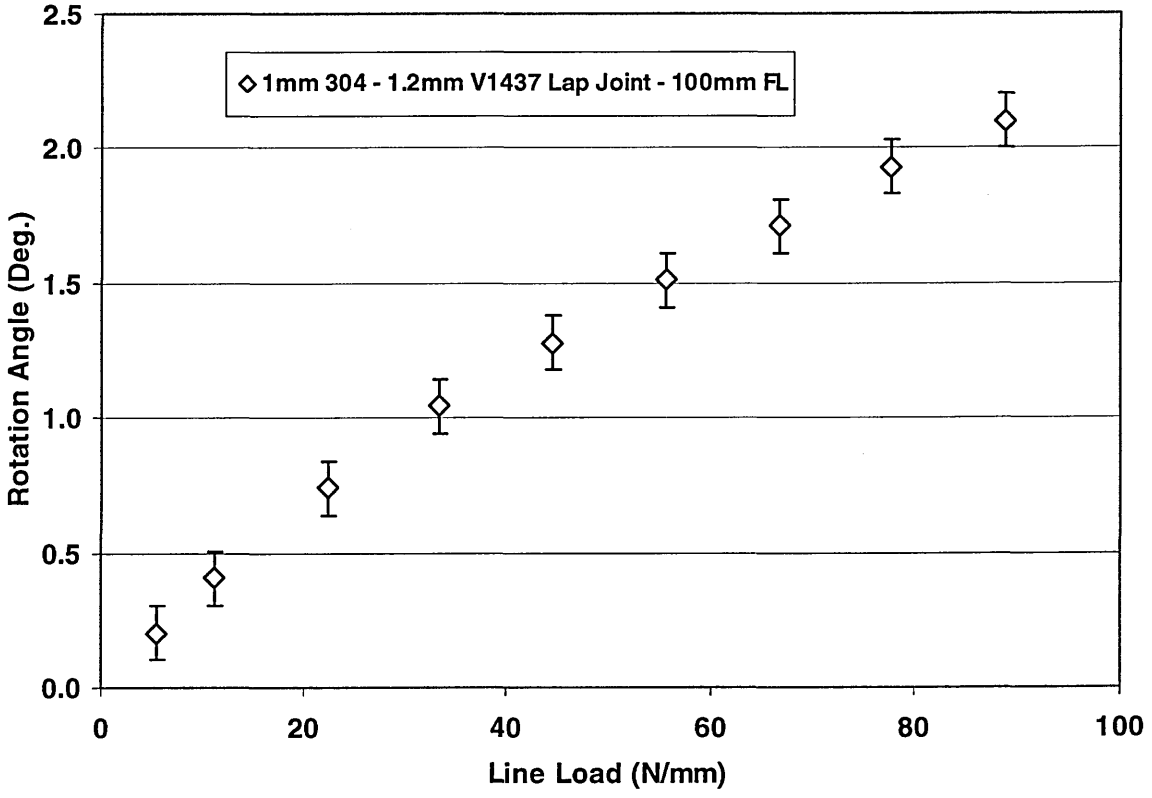

Graph 74 1mm 304 – 1.2mm V1437 (top) lap joint rotation angle per line load

0.78mm 2205 – 1.2mm V1437 (top) dissimilar metal lap joint

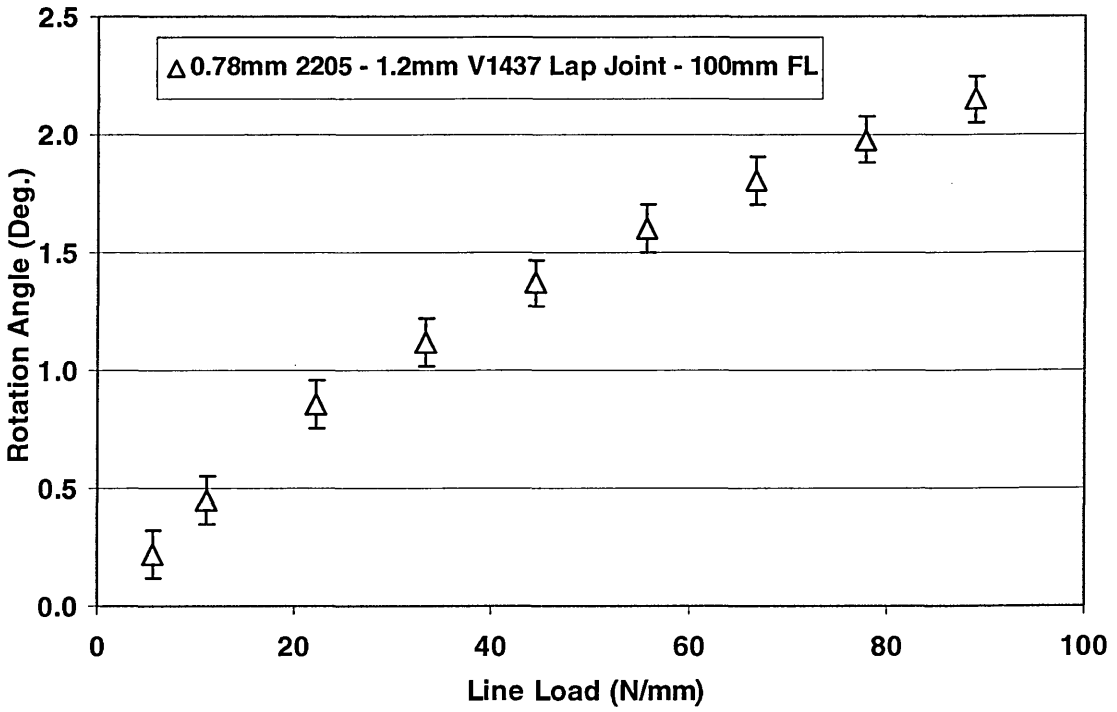

Graph 75 0.78mm 2205 – 1.2mm V1437 (top) lap joint rotation angle per line load

8.4 Butt Joint Composition

Parameter set 2 (P2):1mm 304 – 1.2mm V1437

The following speed maps were produced using a Philips XL40 SEM.

1mm 304

1.2mm V1437

Image 53 Secondary electron image from parameter set 2: 1mm 304 – 1.2mm V1437 butt joint

1mm 304

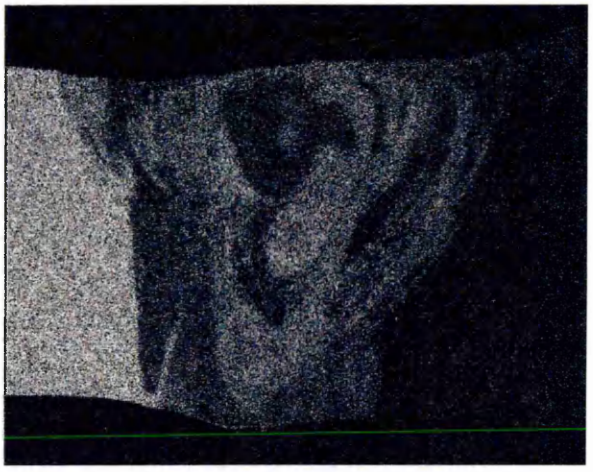

1.2mm V1437

Image 54 Speed map for Cr from parameter set 2: 1mm 304 – 1.2mm V1437 butt joint

1mm 304

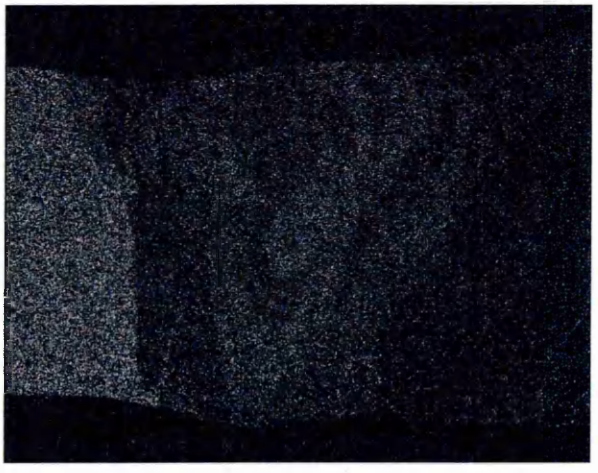

1.2mm V1437

Image 55 Speed map for Ni from parameter set 2: 1mm 304 – 1.2mm V1437 butt joint

The two graphs below show the approximate percentages of Chromium and Nickel within the weld bead. **P2 = 3.5m/min**

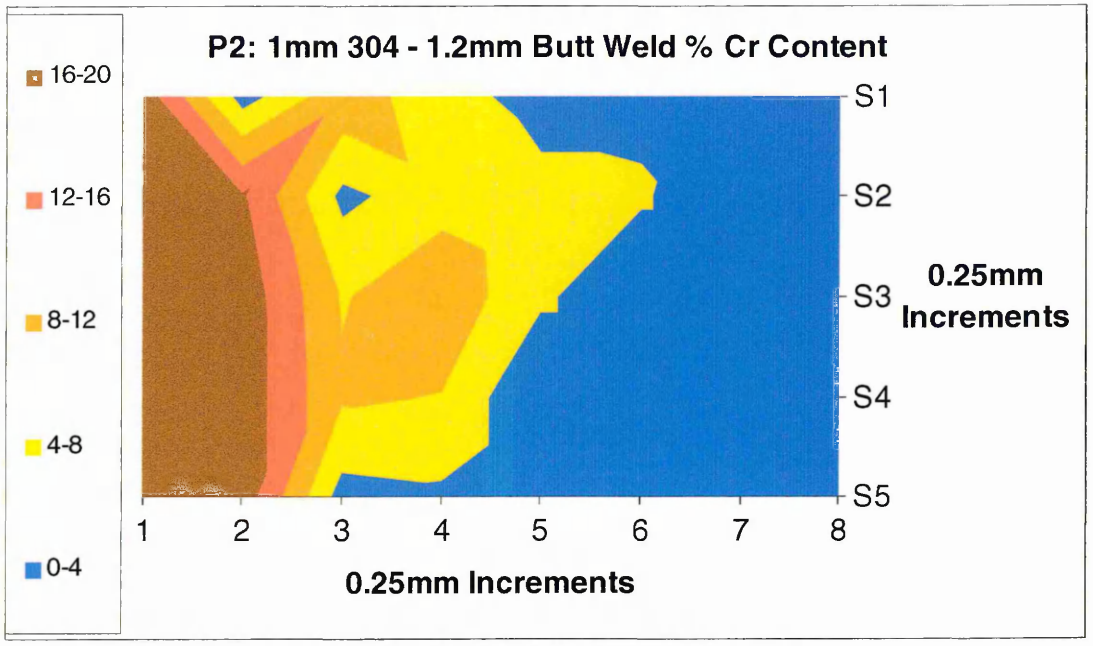

Graph 76 Weld bead % Chromium content from parameter set 2: 1mm 304 – 1.2mm V1437 butt joint

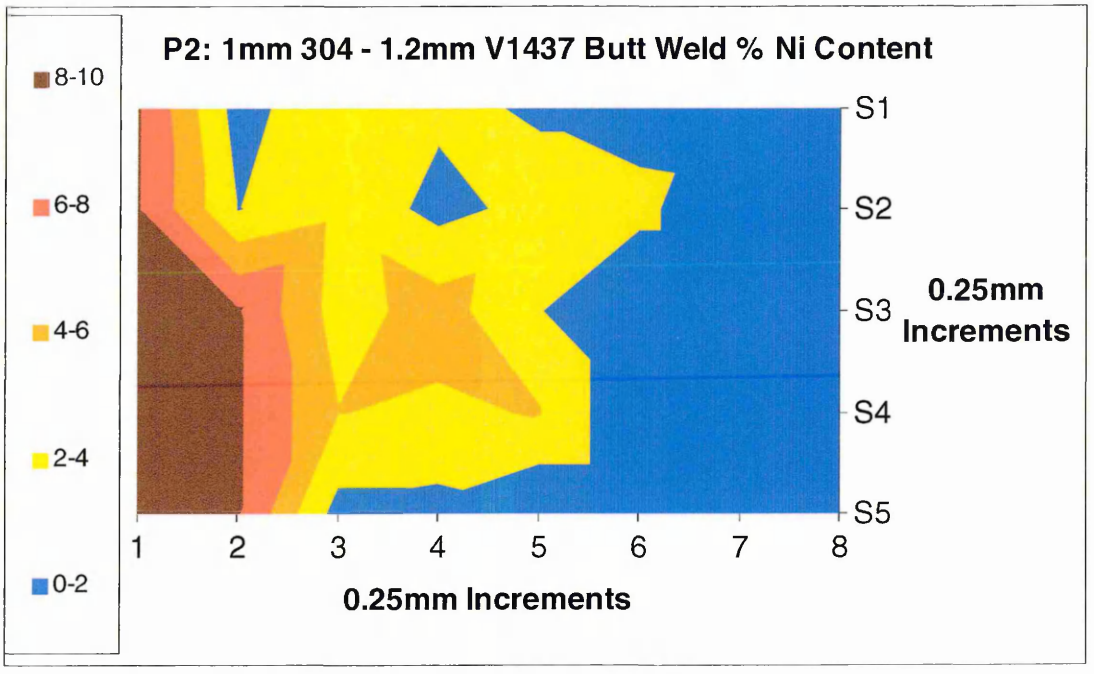

Graph 77 Weld bead % Nickel content from parameter set 2: 1mm 304 – 1.2mm V1437 butt joint

The data used to produce the weld bead composition graphs was then used to predict the dilution and phases present in the laser weld bead. The range of compositions found in the weld bead can be seen on the modified Schaeffler diagram below.

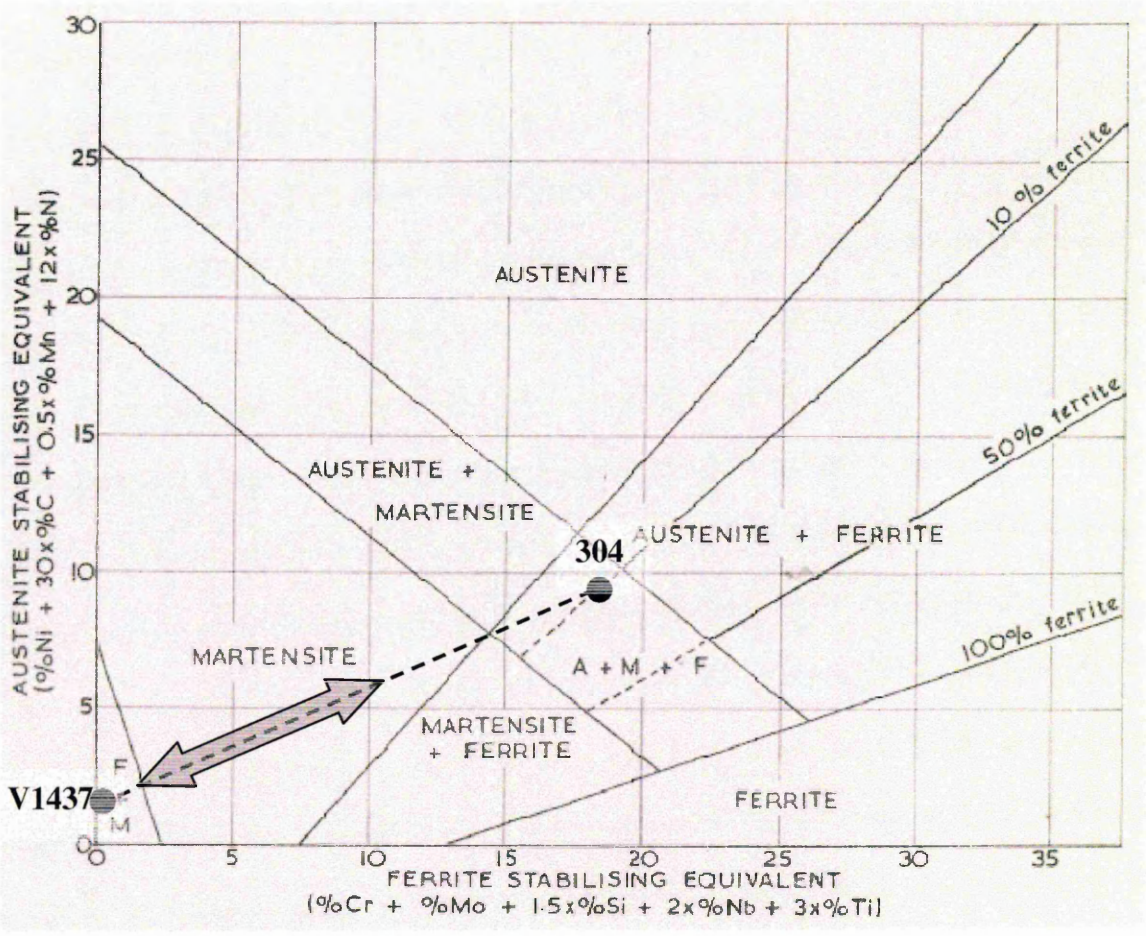

Figure 70 Shows the predicted weld bead composition for the 3.5m/min 1.2mm V1437 – 1mm 304 butt weld

Hence, the predicted weld bead microstructure would be martensite.

Parameter set 3 (P3):1mm 304 – 1.2mm V1437

The following speed maps were produced using a Philips XL40 scanning electron microscope.

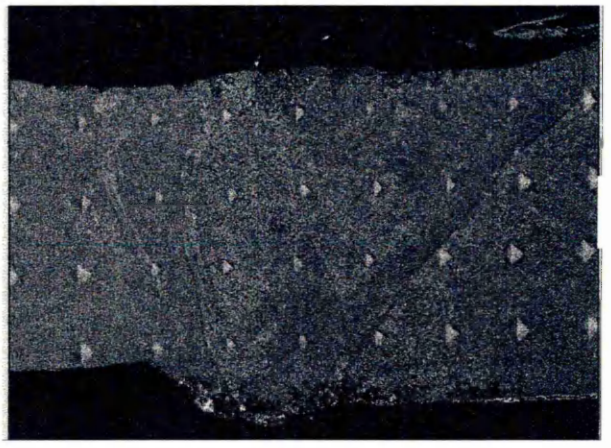

Image 56 Secondary electron image from parameter set 3: 1mm 304 – 1.2mm V1437 butt joint

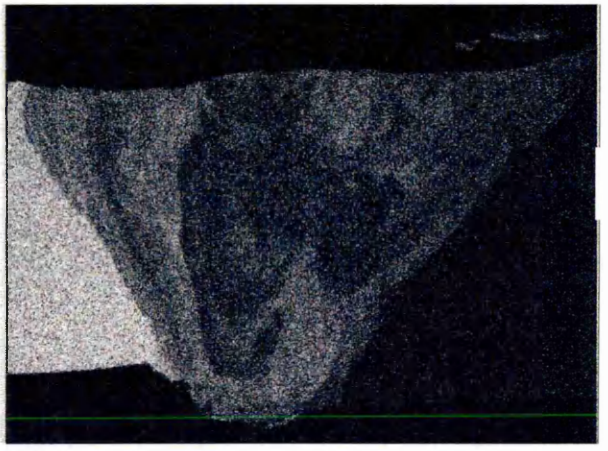

Image 57 Speed map for Cr from parameter set 3: 1mm 304 – 1.2mm V1437 butt joint

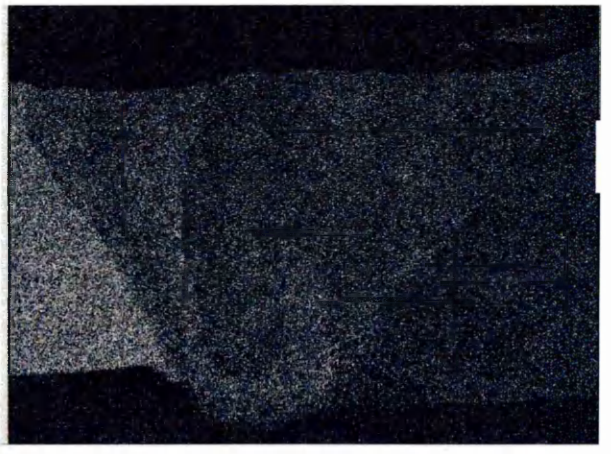

Image 58 Speed map for Ni from parameter set 3: 1mm 304 – 1.2mm V1437 butt joint

The two graphs below show the approximate percentages of Chromium and Nickel within the weld bead. **P3 = 3.0m/min**

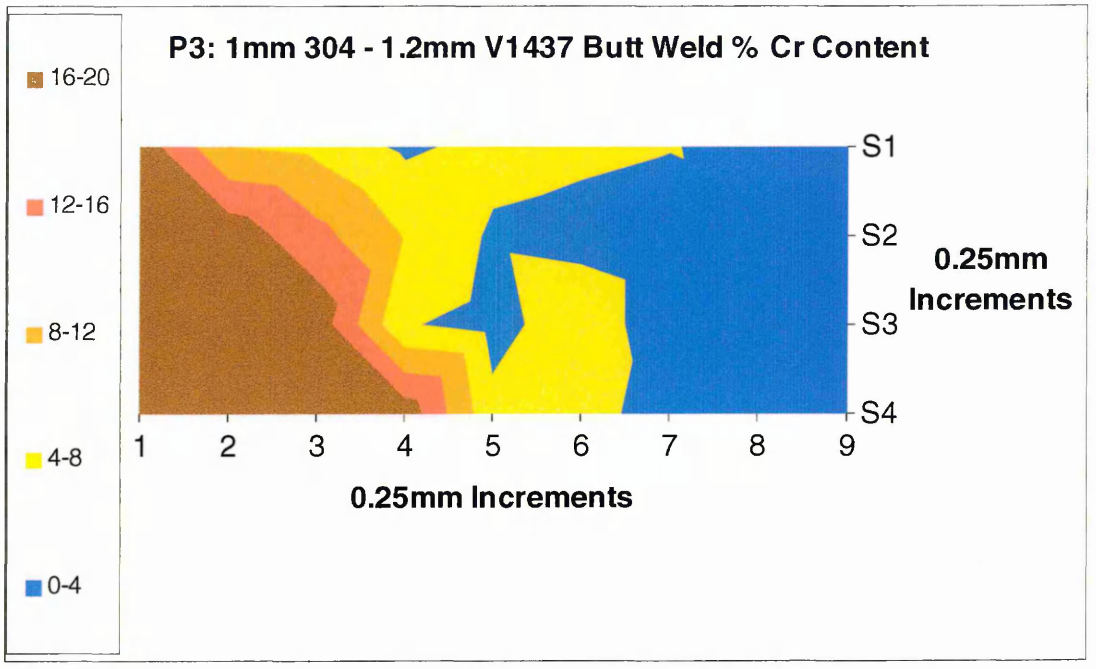

Graph 78 Weld bead % Chromium content from parameter set 3: 1mm 304 – 1.2mm V1437 butt joint

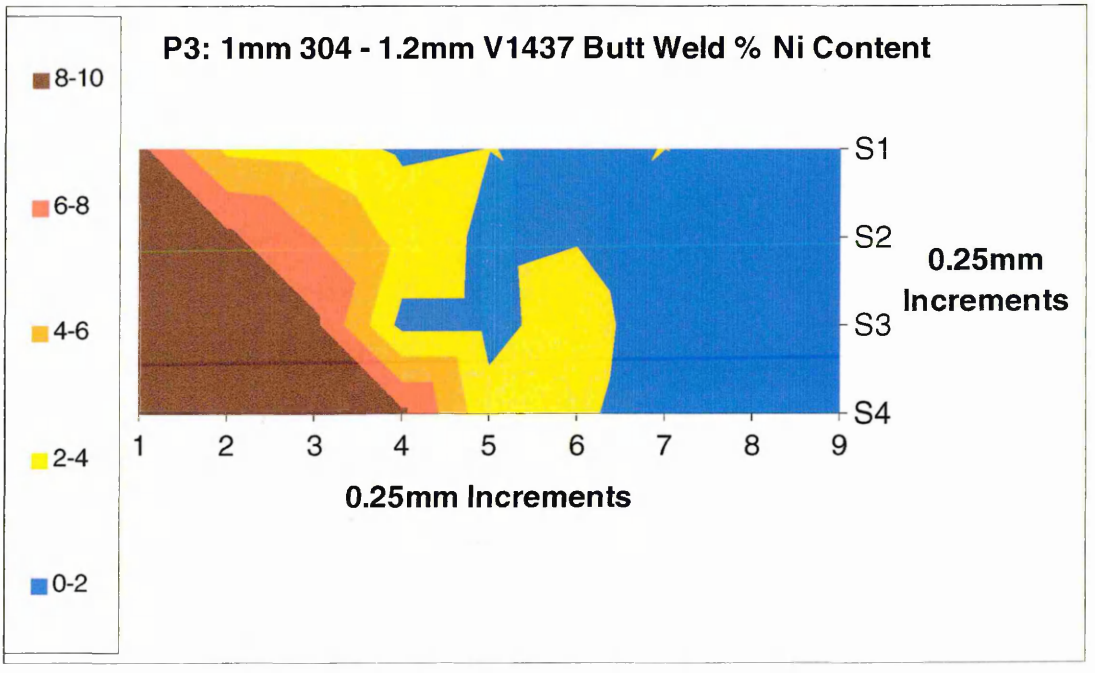

Graph 79 Weld bead % Nickel content from parameter set 3: 1mm 304 – 1.2mm V1437 butt joint

The data used to produce the weld bead composition graphs was then used to predict the dilution and phases present in the laser weld bead. The range of compositions found in the weld bead can be seen on the modified Schaeffler diagram below.

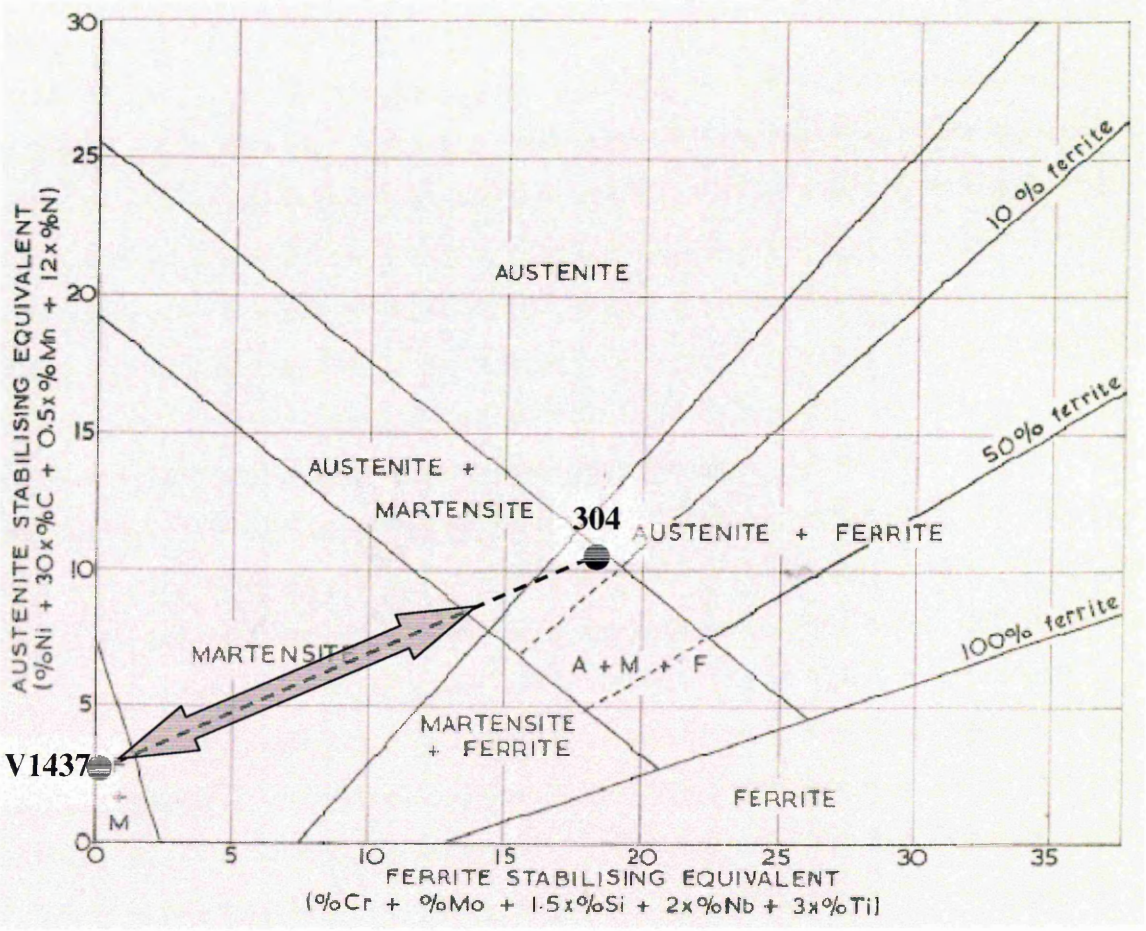

Figure 71 Shows the predicted weld bead composition for the 3m/min 1.2mm V1437 – 1mm 304 butt weld

Hence, the predicted weld bead microstructure would be predominantly martensitic with small quantities of austenite and ferrite present.

Parameter set 1 (P1):0.78mm 2205 – 1.2mm V1437

The following speed maps were produced using a Philips XL40 SEM.

0.78mm 2205

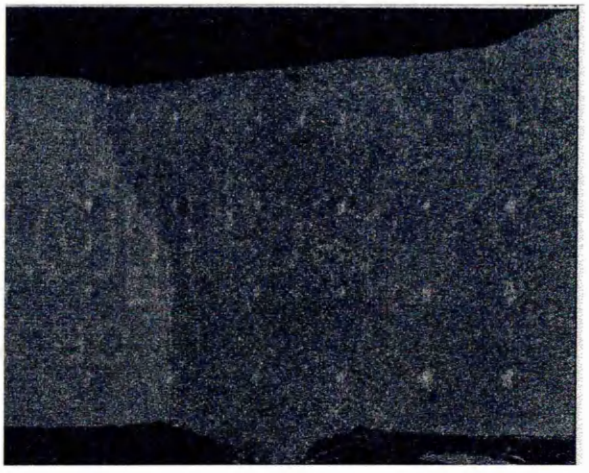

1.2mm V1437

Image 59 Secondary electron image from parameter set 1: 0.78mm 2205 – 1.2mm V1437 butt joint

0.78mm 2205

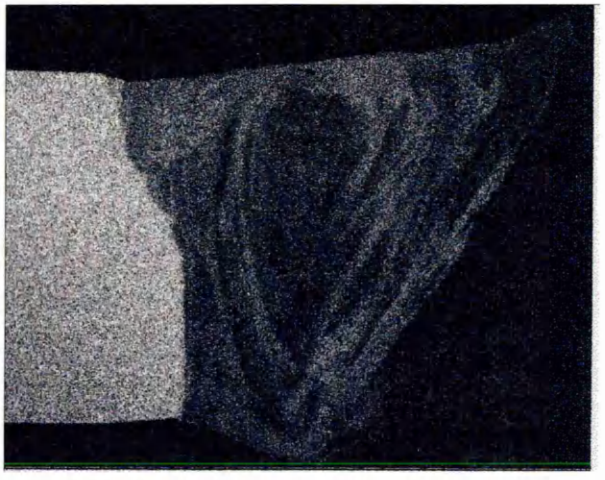

1.2mm V1437

Image 60 Speed map for Cr from parameter set 1: 0.78mm 2205 – 1.2mm V1437 butt joint

0.78mm 2205

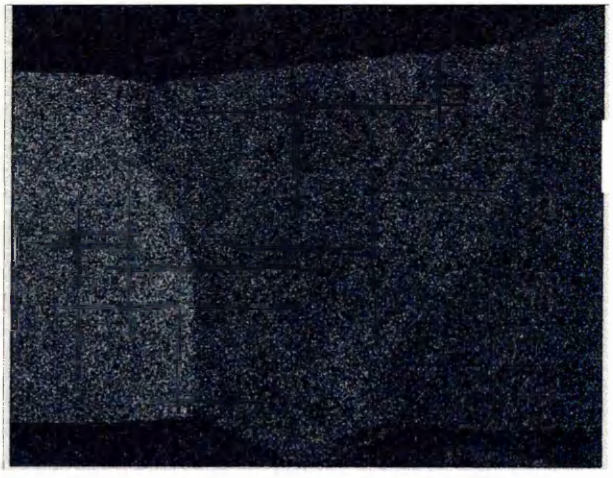

1.2mm V1437

Image 61 Speed map for Ni from parameter set 1: 0.78mm 2205 – 1.2mm V1437 butt joint

The two graphs below show the approximate percentages of Chromium and Nickel within the weld bead. **P1 = 4.0m/min**

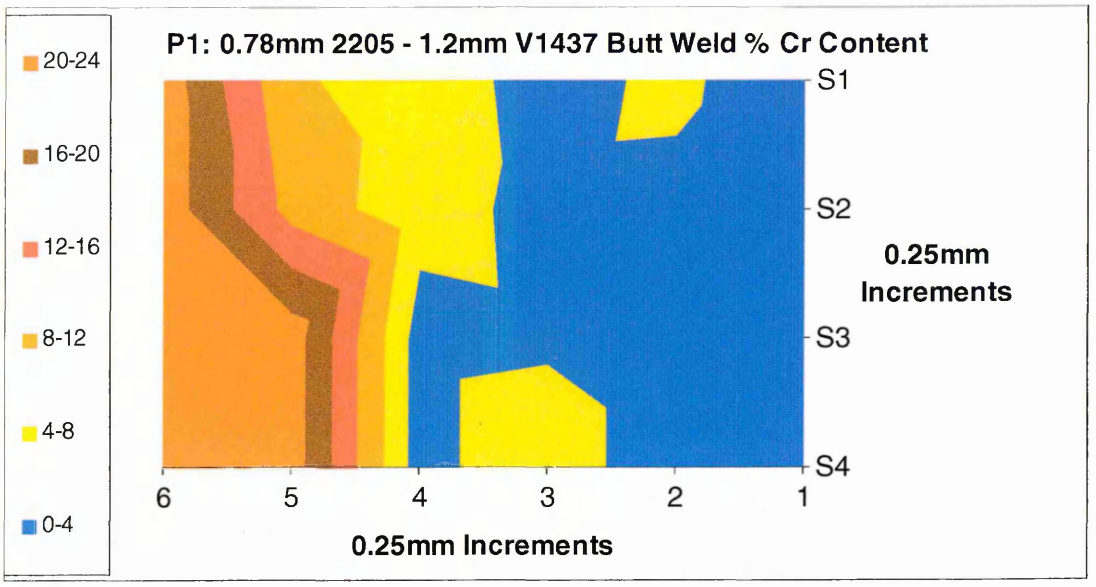

Graph 80 Weld bead % Chromium content from parameter set 1: 0.78mm 2205 – 1.2mm V1437 butt joint

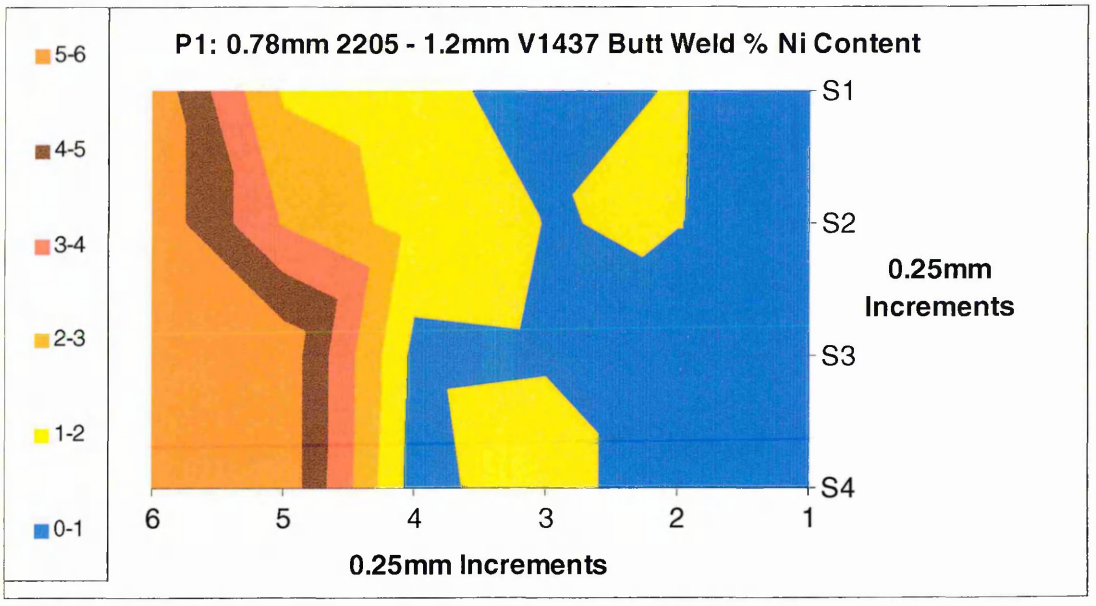

Graph 81 Weld bead % Nickel content from parameter set 1: 0.78mm 2205 – 1.2mm V1437 butt joint

The data used to produce the weld bead composition graphs was then used to predict the dilution and phases present in the laser weld bead. The range of compositions found in the weld bead can be seen on the modified Schaeffler diagram below.

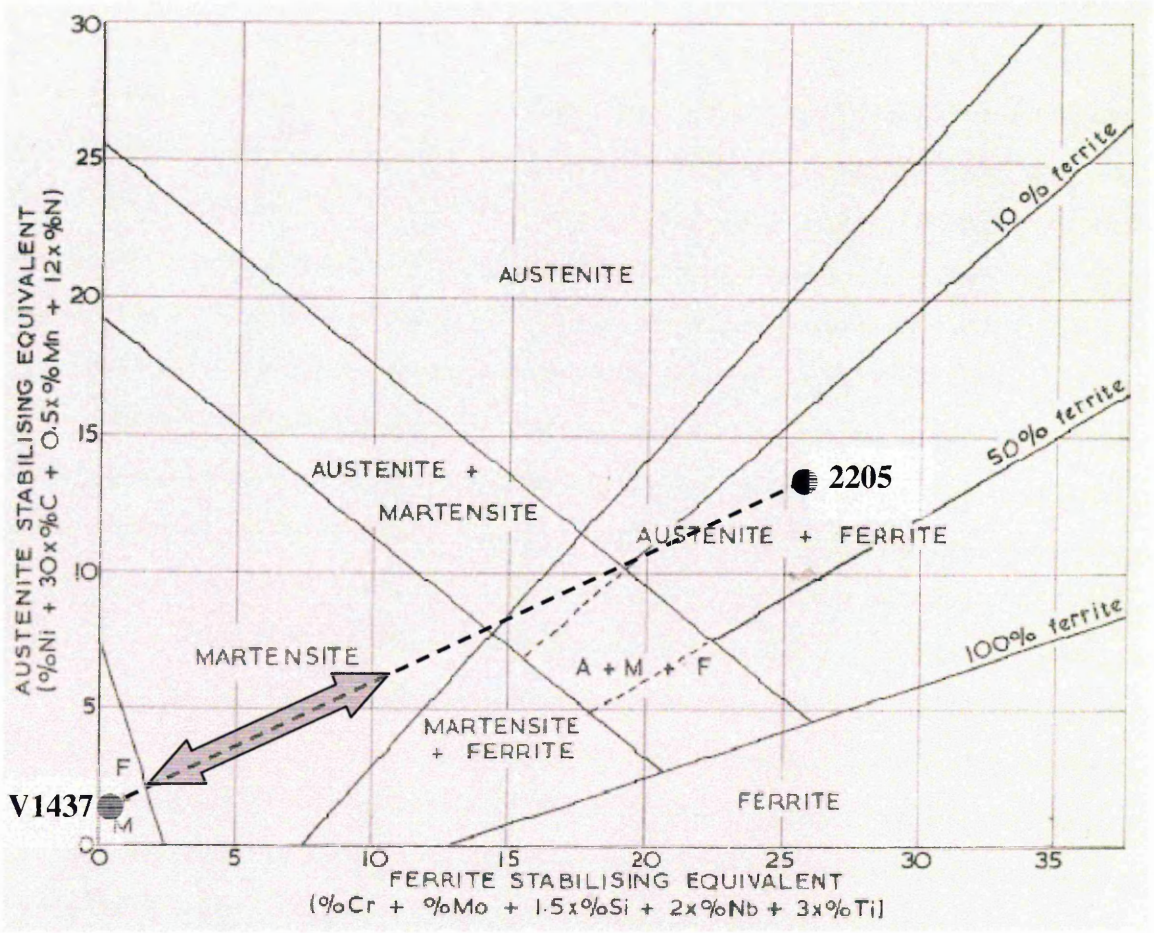

Figure 72 Shows the predicted weld bead composition for the 4m/min 1.2mm V1437 – 0.78mm 2205 butt weld

Hence, the predicted weld bead microstructure would be martensite.

Parameter set 2 (P2):0.78mm 2205 – 1.2mm V1437

The following speed maps were produced using a Philips XL40 SEM.

0.78mm 2205

1.2mm V1437

Image 62 Secondary electron image from parameter set 2: 0.78mm 2205 – 1.2mm V1437 butt joint

0.78mm 2205

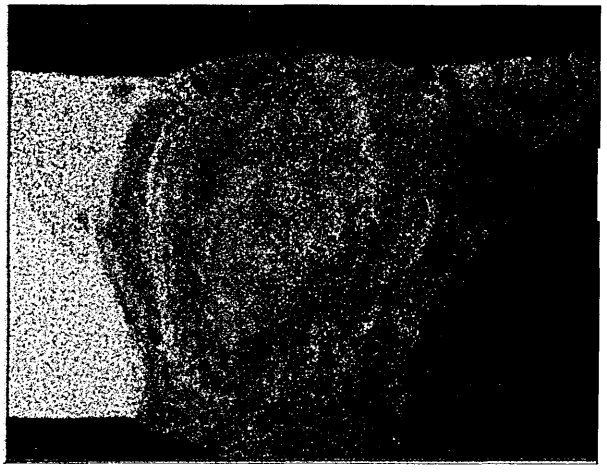

1.2mm V1437

Image 63 Speed map for Cr from parameter set 2: 0.78mm 2205 – 1.2mm V1437 butt joint

0.78mm 2205

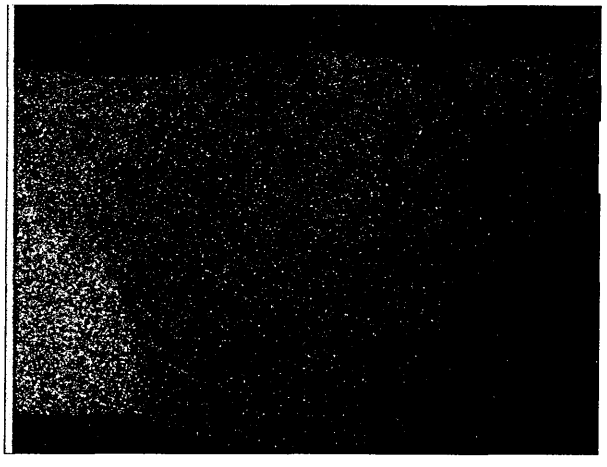

1.2mm V1437

Image 64 Speed map for Ni from parameter set 2: 0.78mm 2205 – 1.2mm V1437 butt joint

The two graphs below show the approximate percentages of Chromium and Nickel within the weld bead. **P2 = 3.5m/min**

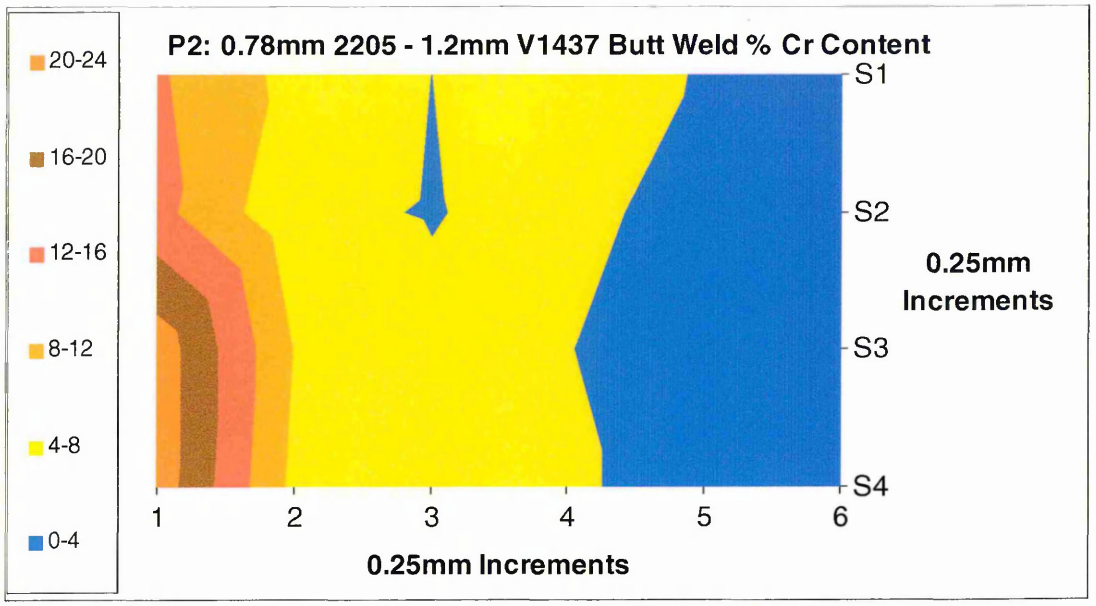

Graph 82 Weld bead % Chromium content from parameter set 2: 0.78mm 2205 – 1.2mm V1437 butt joint

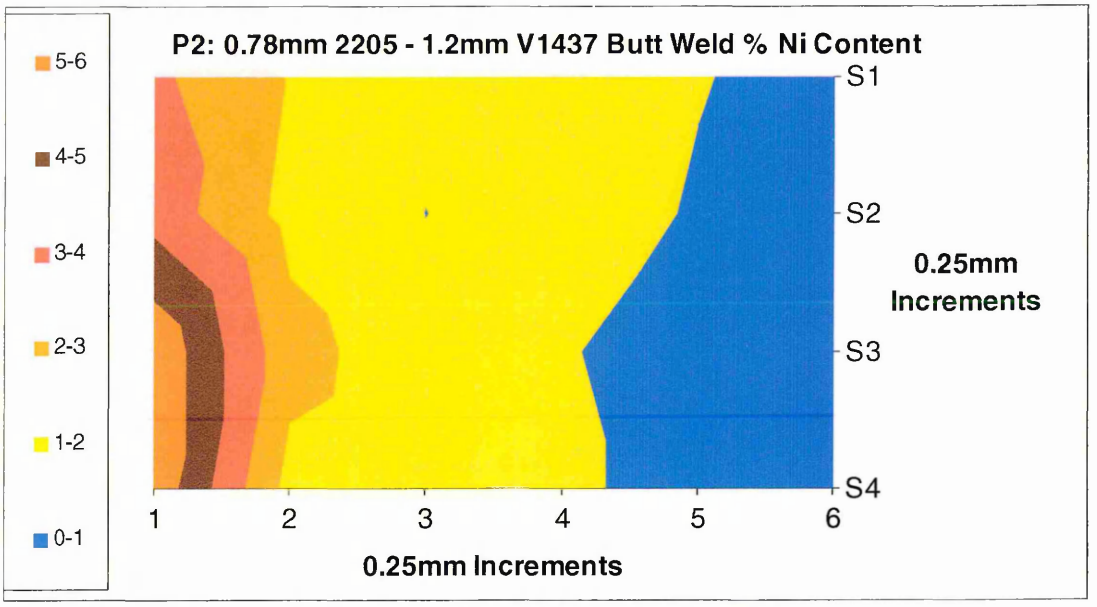

Graph 83 Weld bead % Nickel content from parameter set 2: 0.78mm 2205 – 1.2mm V1437 butt joint

The data used to produce the weld bead composition graphs was then used to predict the dilution and phases present in the laser weld bead. The range of compositions found in the weld bead can be seen on the modified Schaeffler diagram below.

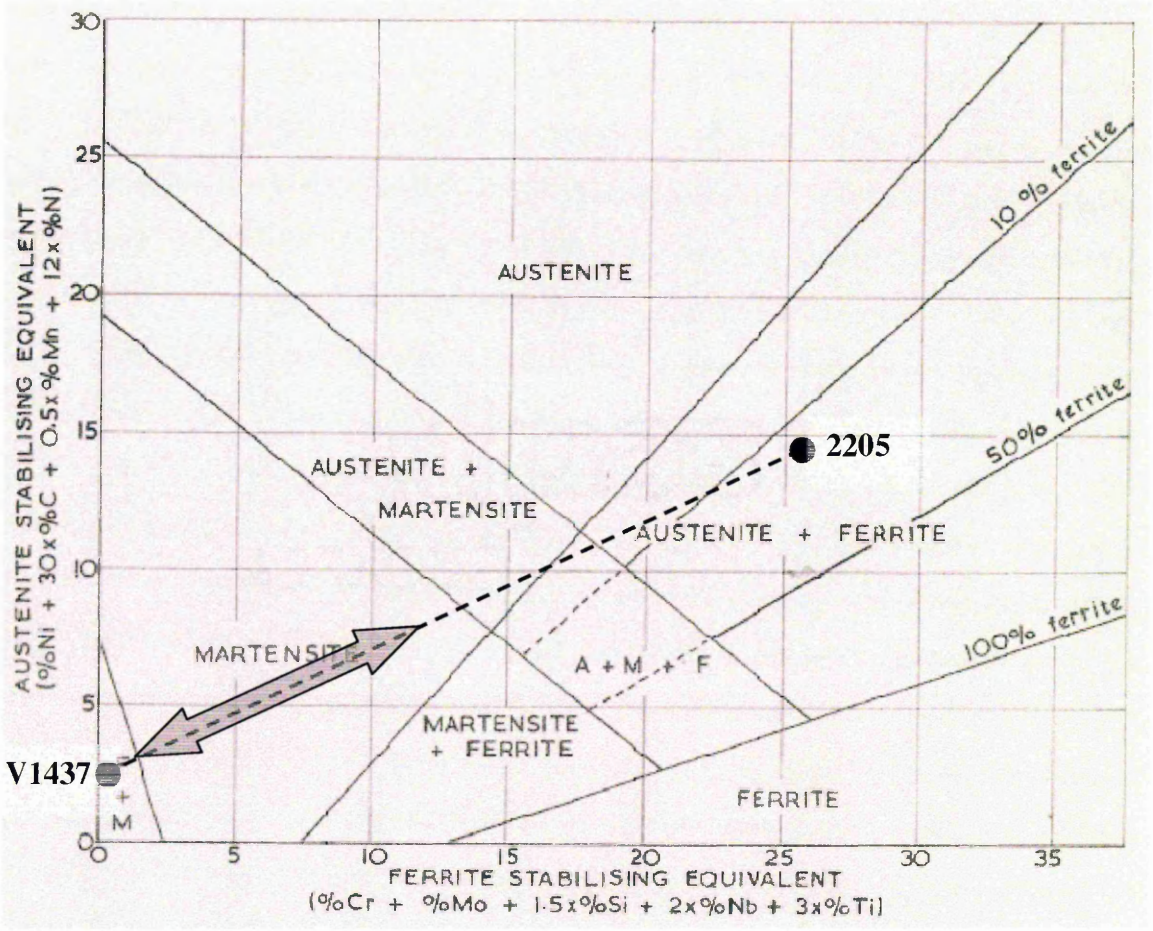

Figure 73 Shows the predicted weld bead composition for the 3.5m/min 1.2mm V1437 – 0.78mm 2205 butt weld

Hence, the predicted weld bead microstructure would be martensite.

Parameter set 3 (P3):0.78mm 2205 – 1.2mm V1437

The following speed maps were produced using a Philips XL40 SEM.

0.78mm 2205

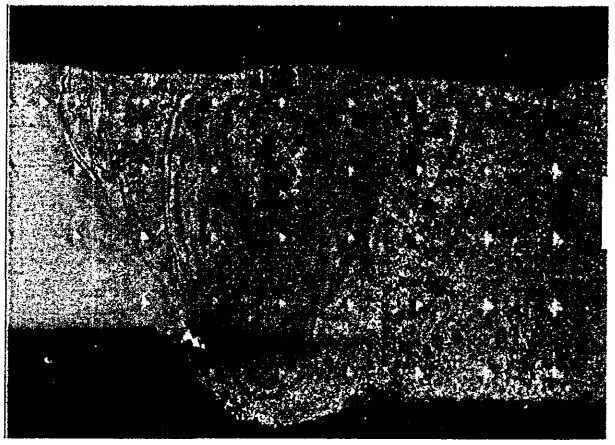

1.2mm V1437

Image 65 Secondary electron image from parameter set 3: 0.78mm 2205 – 1.2mm V1437 butt joint

0.78mm 2205

1.2mm V1437

Image 66 Speed map for Cr from parameter set 3: 0.78mm 2205 – 1.2mm V1437 butt joint

0.78mm 2205

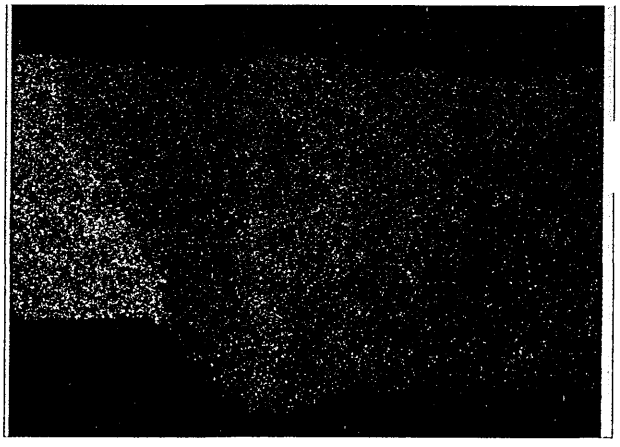

1.2mm V1437

Image 67 Speed map for Ni from parameter set 3: 0.78mm 2205 – 1.2mm V1437 butt joint

The two graphs below show the approximate percentages of Chromium and Nickel within the weld bead. **P3 = 3.0m/min**

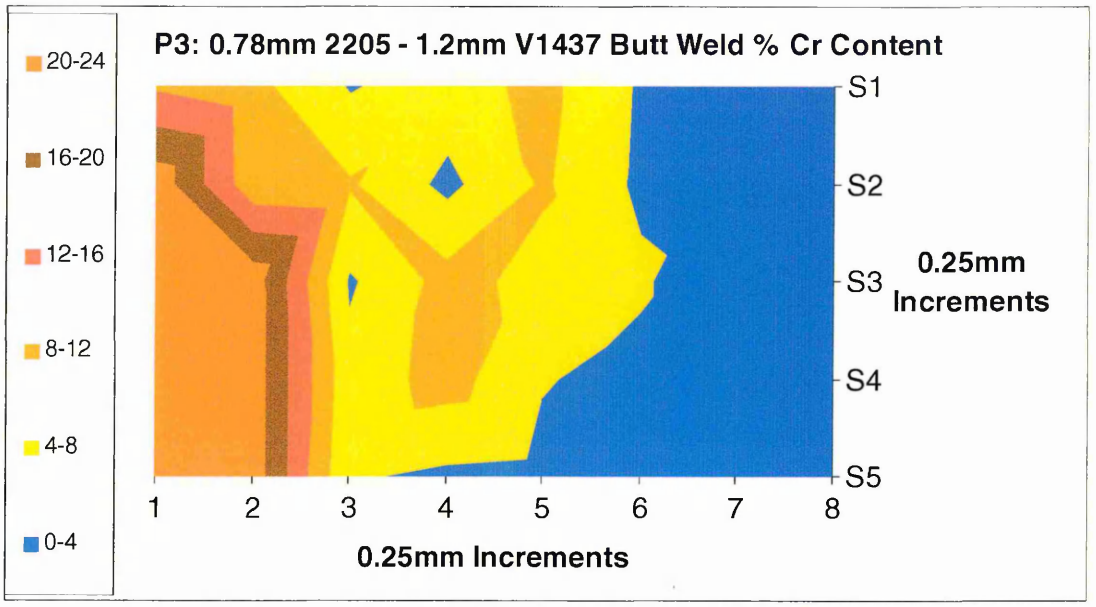

Graph 84 Weld bead % Chromium content from parameter set 3: 0.78mm 2205 – 1.2mm V1437 butt joint

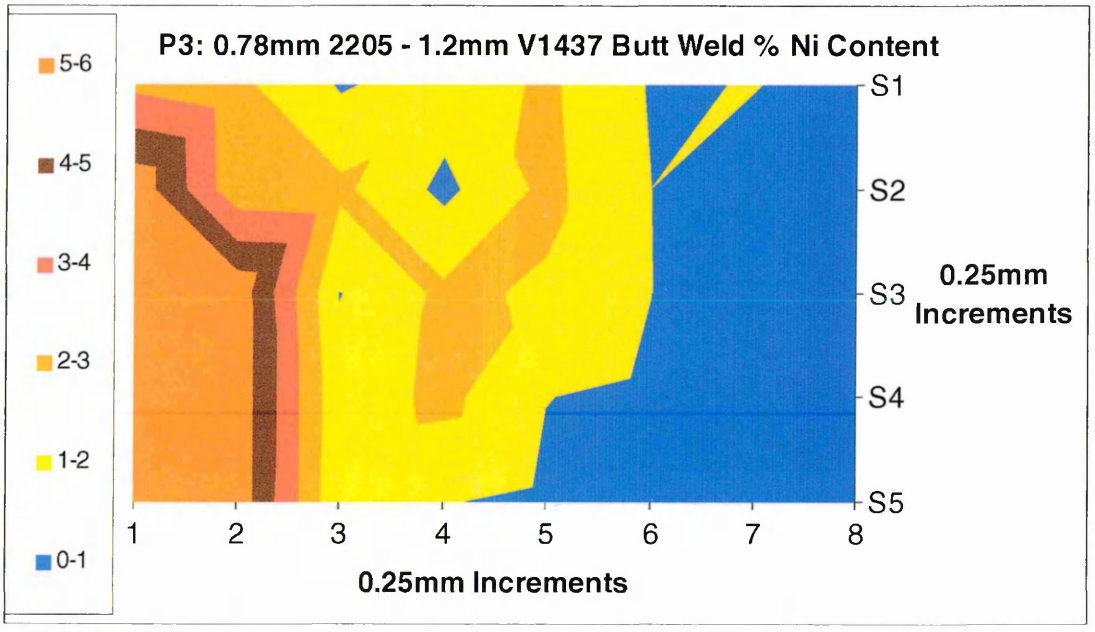

Graph 85 Weld bead % Nickel content from parameter set 3: 0.78mm 2205 – 1.2mm V1437 butt joint

The data used to produce the weld bead composition graphs was then used to predict the dilution and phases present in the laser weld bead. The range of compositions found in the weld bead can be seen on the modified Schaeffler diagram below.

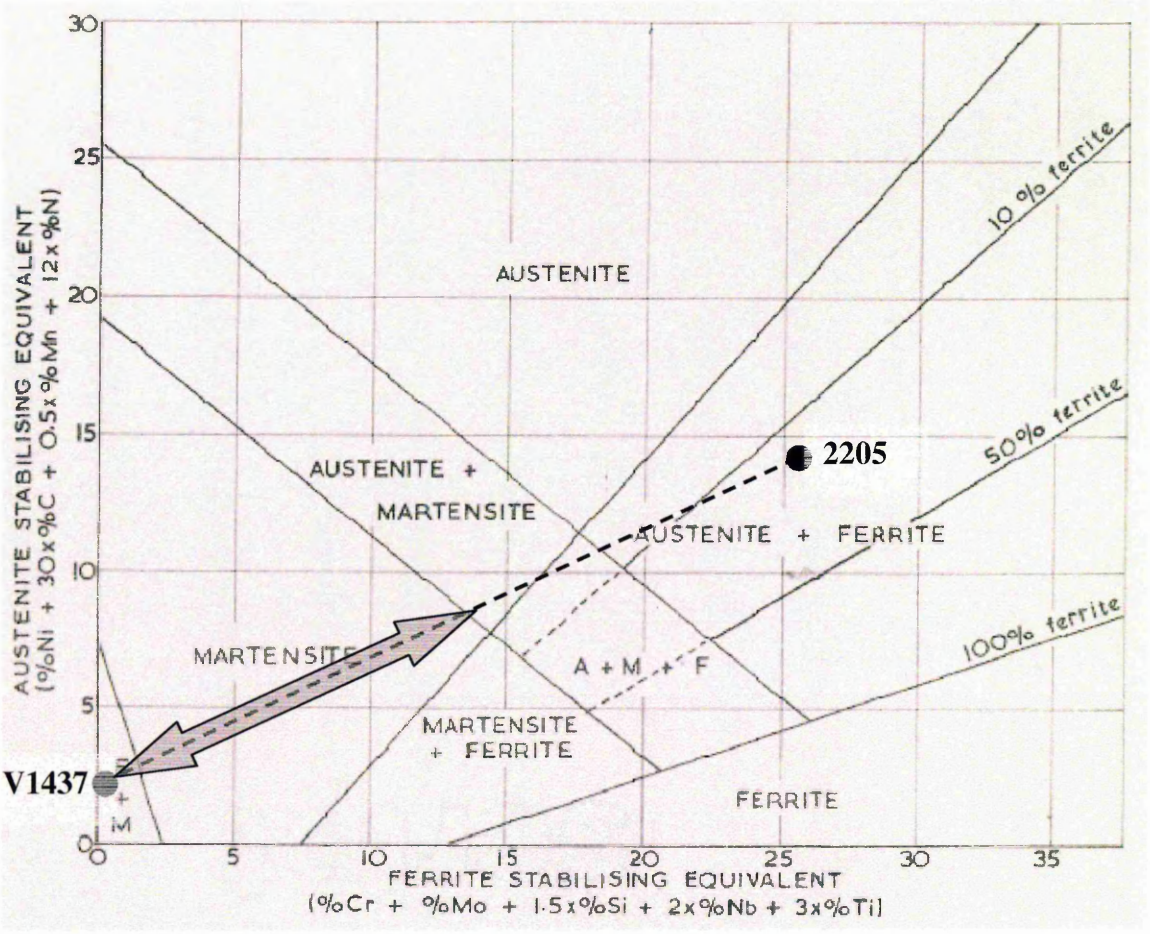

Figure 74 Shows the predicted weld bead composition for the 3m/min 1.2mm V1437 – 0.78mm 2205 butt weld

Hence, the predicted weld bead microstructure would be predominantly martensitic with a small quantity of austenite and ferrite.

8.5 Lap Joint Composition

1.2mm V1437 (top) – 1mm 304

The two graphs below show the approximate percentages of Chromium and Nickel within the weld bead.

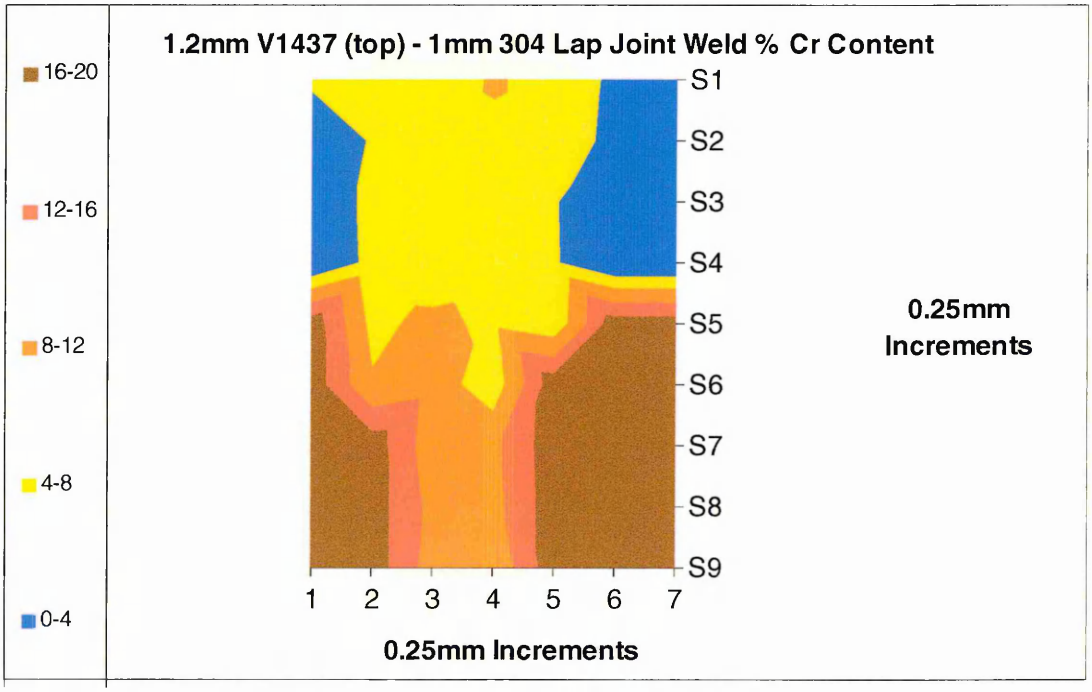

Graph 86 Weld bead % Chromium content: 1.2mm V1437 (top) – 1mm 304 lap joint

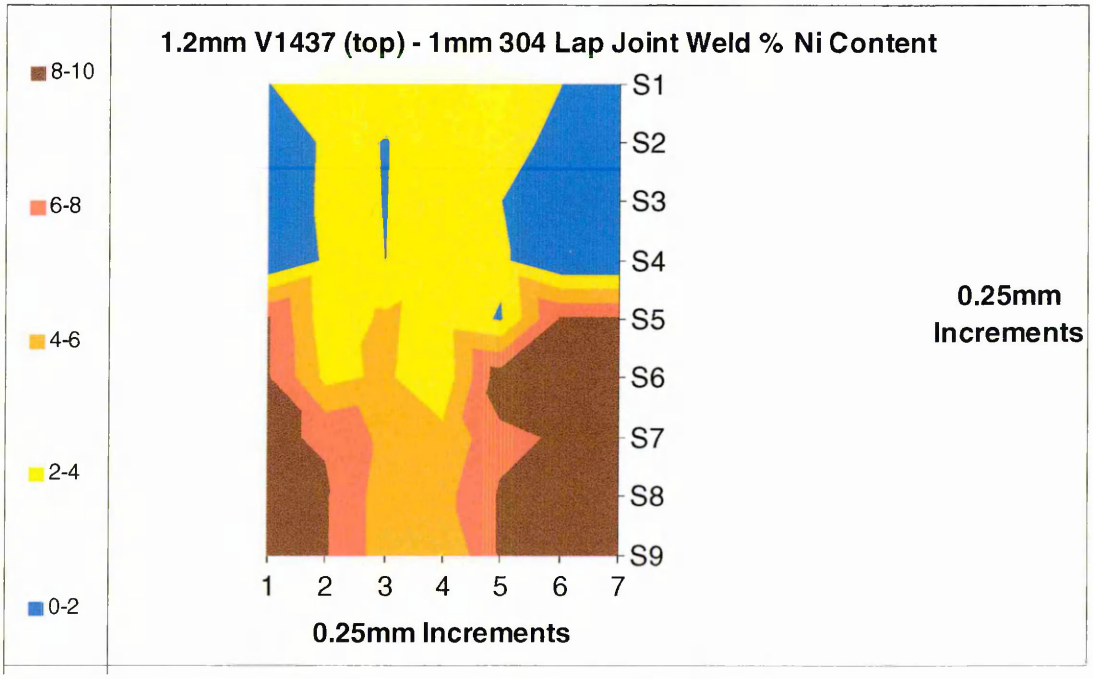

Graph 87 Weld bead % Nickel content: 1.2mm V1437 (top) – 1mm 304 lap joint

The data used to produce the weld bead composition graphs was then used to predict the dilution and phases present in the laser weld bead. The range of compositions found in the weld bead can be seen on the modified Schaeffler diagram below.

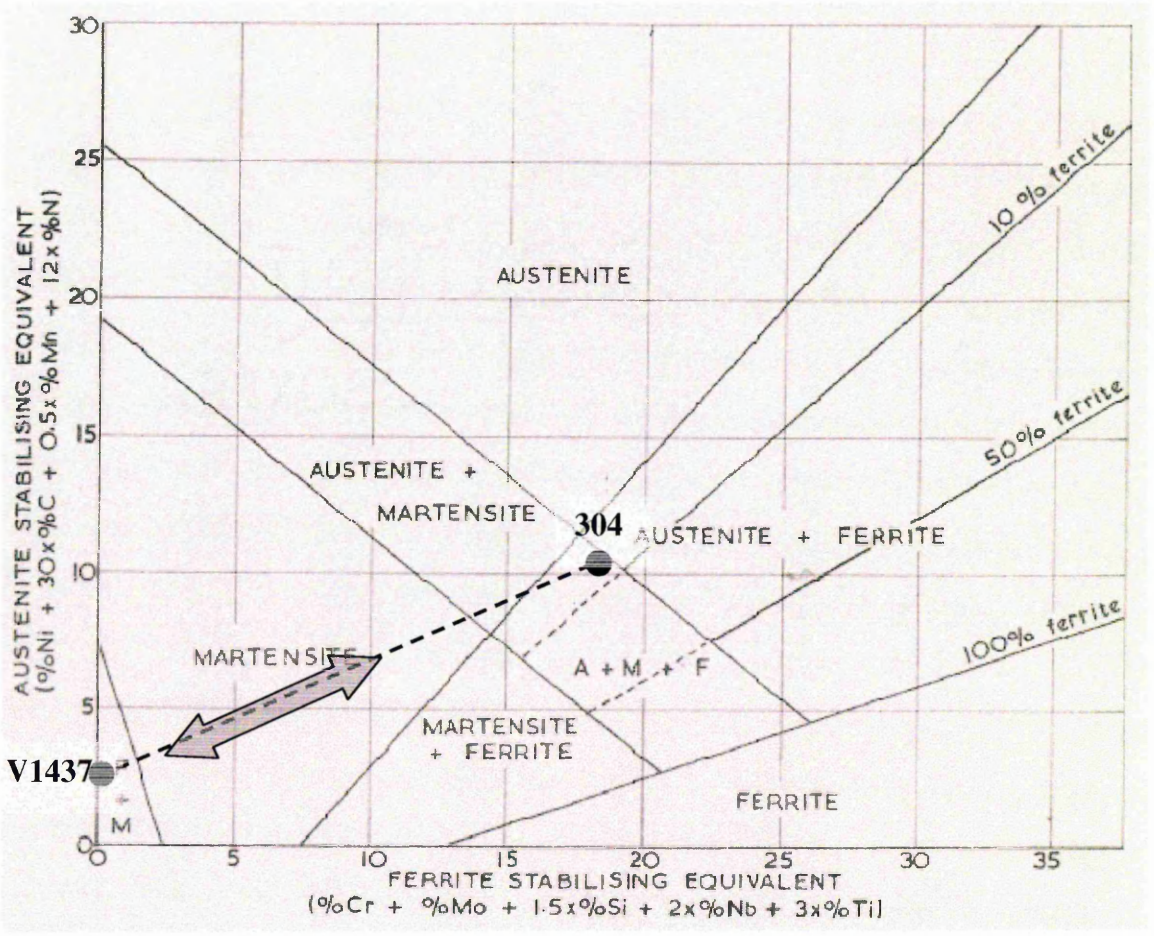

Figure 75 Shows the predicted weld bead composition for the 1.2mm V1437 - 1mm 304 (top) lap joint

Hence, the predicted weld bead microstructure would be martensite.

0.78mm 2205 (top) – 1.2mm V1437

The two graphs below show the approximate percentages of Chromium and Nickel within the weld bead.

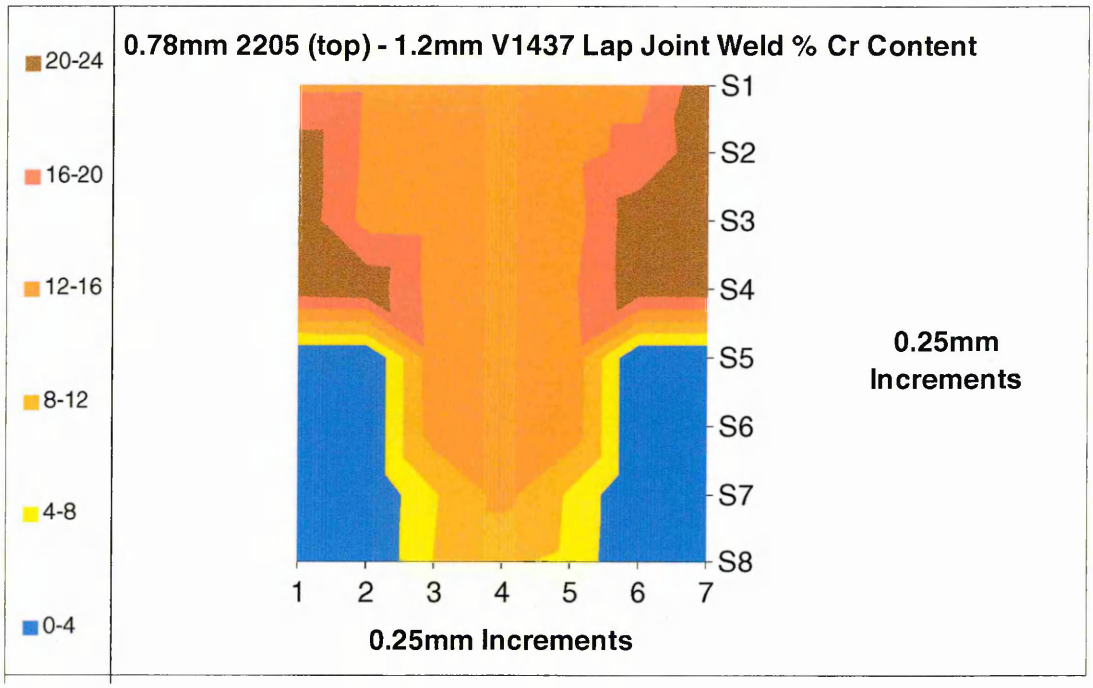

Graph 88 Weld bead % Chromium content: 0.78mm 2205 (top) – 1.2mm V1437 lap joint

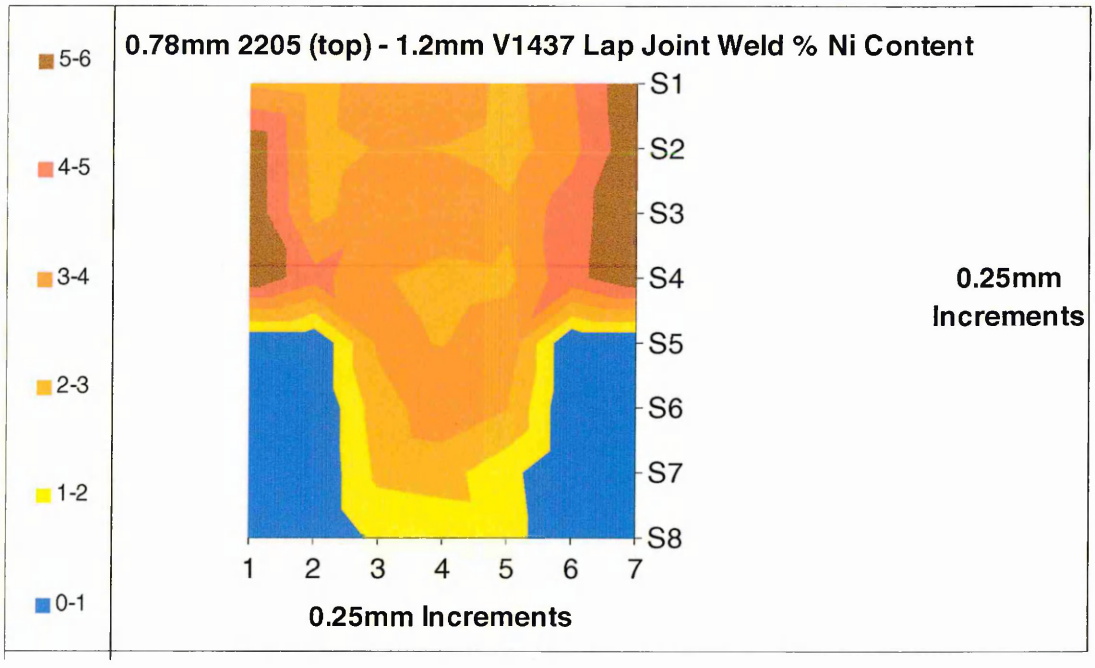

Graph 89 Weld bead % Nickel content: 0.78mm 2205 (top) – 1.2mm V1437 lap joint

The data used to produce the weld bead composition graphs was then used to predict the dilution and phases present in the laser weld bead. The range of compositions found in the weld bead can be seen on the modified Schaeffler diagram below.

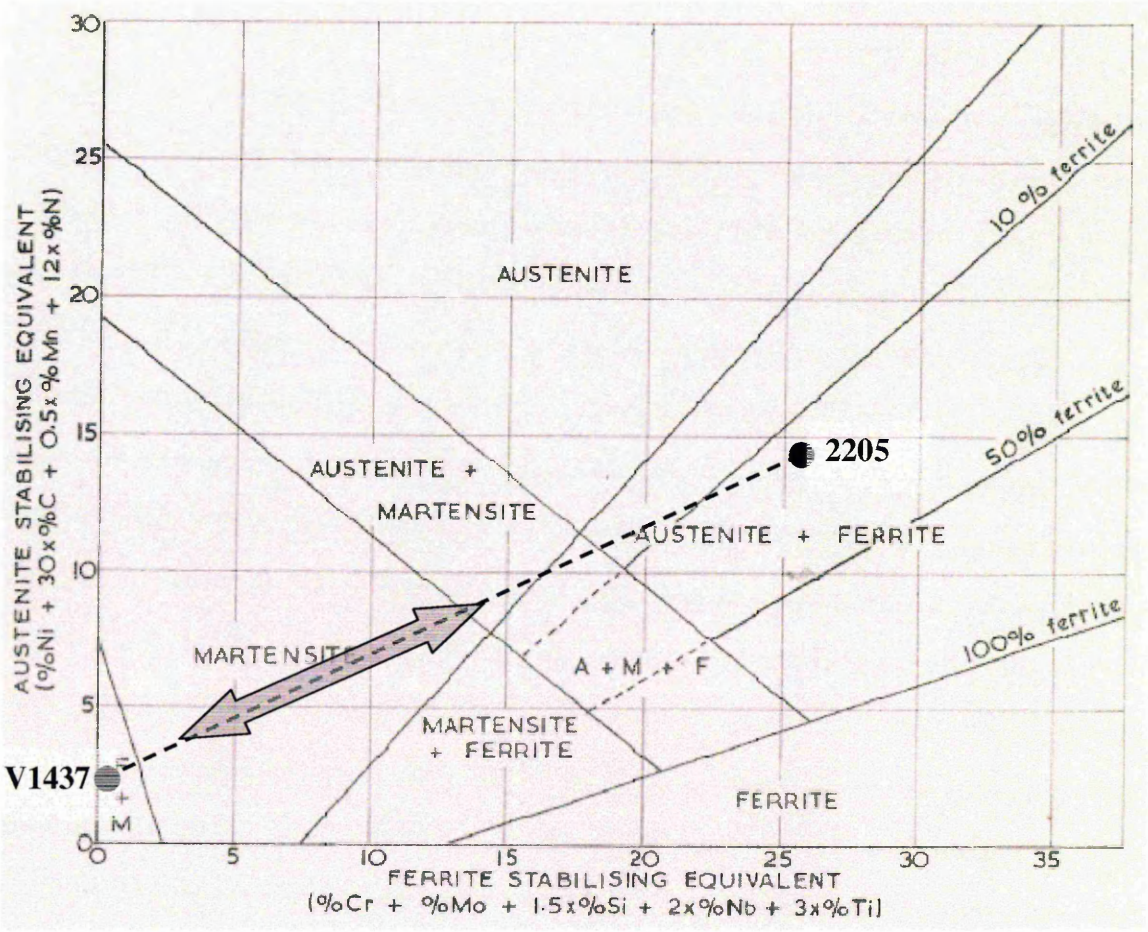

Figure 76 Shows the predicted weld bead composition for the 1.2mm V1437 (top) – 0.78mm 2205 lap joint

Hence, the predicted weld bead microstructure would be martensitic with a small quantity of austenite present.

1.2mm V1437 (top) – 0.78mm 2205

The two graphs below show the approximate percentages of Chromium and Nickel within the weld bead.

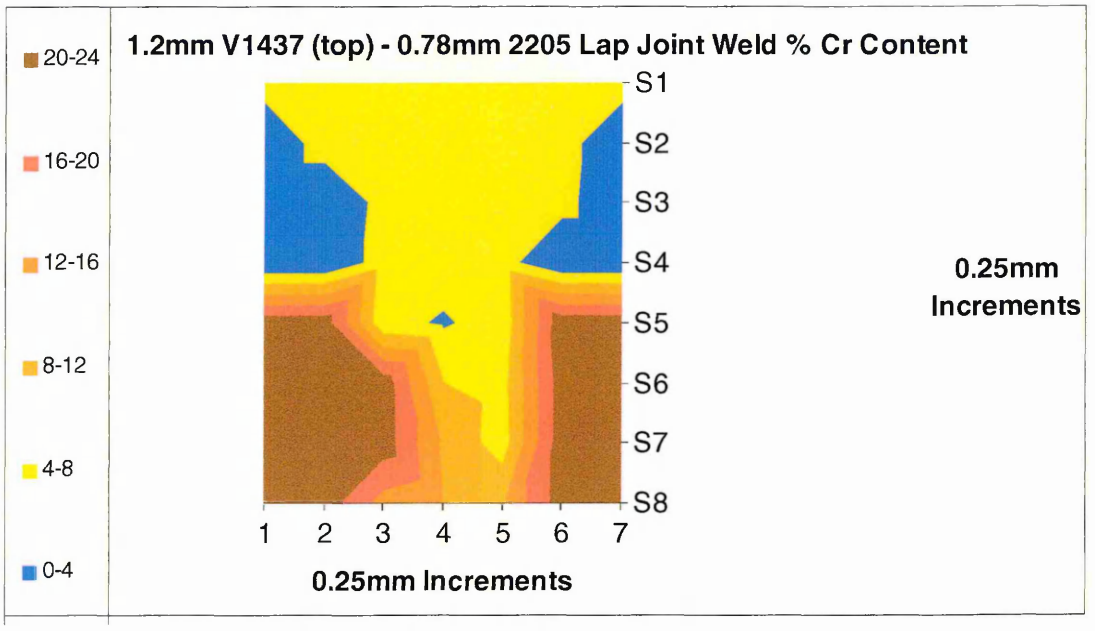

Graph 90 Weld bead % Chromium content: 1.2mm V1437 (top) – 0.78mm 2205 lap joint

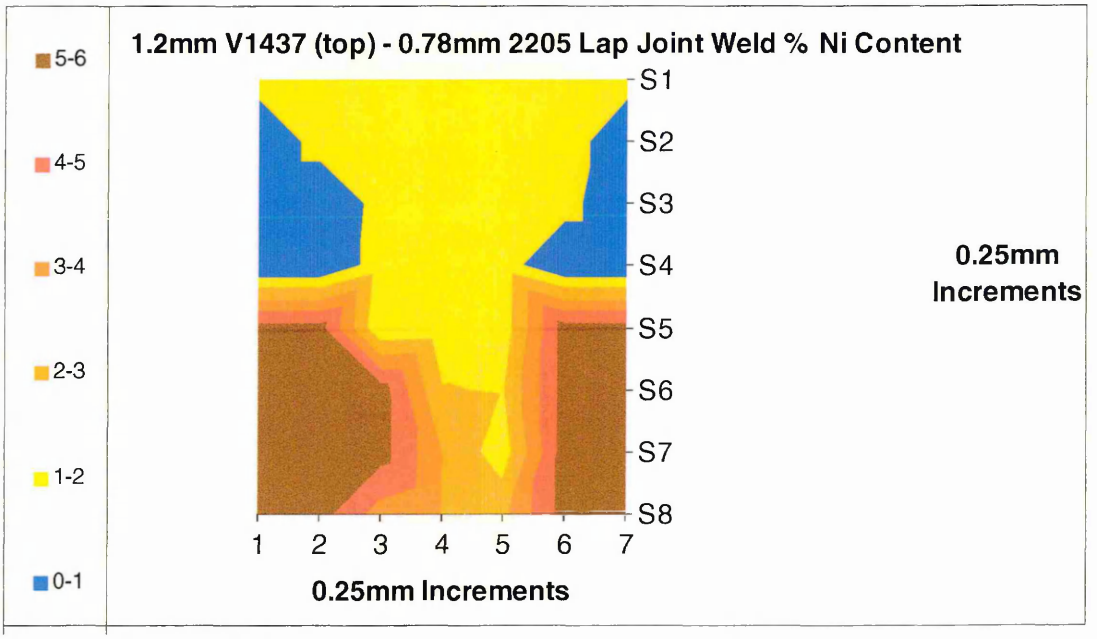

Graph 91 Weld bead % Nickel content: 1.2mm V1437 (top) – 1.2mm V1437 lap joint

The data used to produce the weld bead composition graphs was then used to predict the dilution and phases present in the laser weld bead. The range of compositions found in the weld bead can be seen on the modified Schaeffler diagram below.

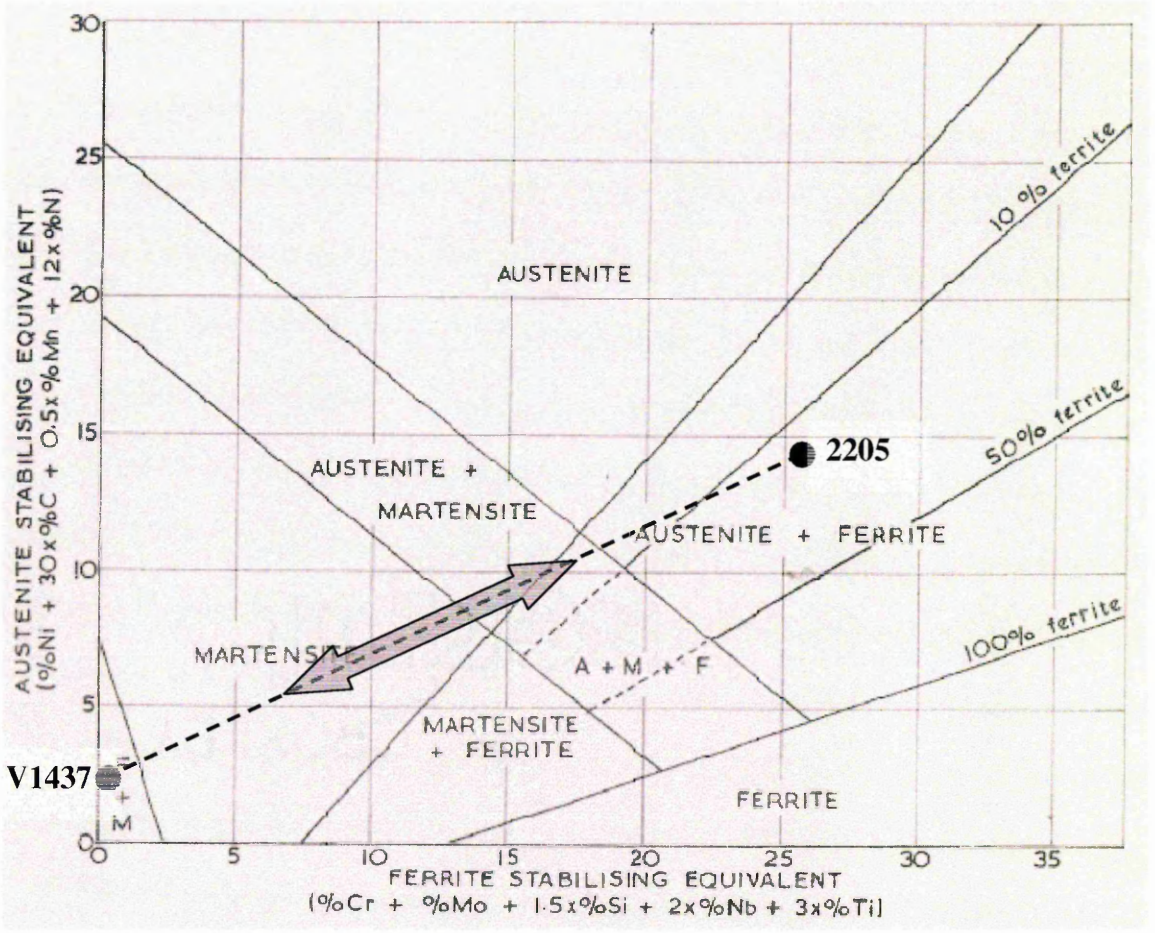

Figure 77 Shows the predicted weld bead composition for the 0.78mm 2205 (top) - 1.2mm V1437 lap joint

Hence, the predicted weld bead microstructure would be predominantly martensitic with a large portion of austenite present.